

A Design Tool for Timber Gridshells

The Development of a Grid Generation Tool

MSc Thesis by M.H. Toussaint
May 2007

Delft University of Technology
Faculty of Civil Engineering and Geosciences
Section of Structural and Building Engineering
Structural Design Lab

Master's thesis

A Design Tool for Timber Gridshells

The Development of a Grid Generation Tool

Submitted in partial fulfilment of the
requirements for the degree of

MASTER OF SCIENCE

in

CIVIL ENGINEERING

by

M.H. Toussaint

born 02-03-1980
in Naaldwijk, The Netherlands

Delft University of Technology
Faculty of Civil Engineering and Geosciences
Section of Structural and Building Engineering
Structural Design Lab

Preface

This report describes the result of my Master's thesis project. This project is the completion of my MSc study in Building Engineering at Delft Technical University, faculty Civil Engineering and Geosciences. The subject of the Master's thesis is the development of a (conceptual) design tool to determine the geometry of a gridshell structure. The research was performed at the Structural Design Lab from January 2006 to April 2007. One of the research topics of the SDL is innovative and accessible use of ICT in design. This thesis is part of this.

I would like to thank all members of my graduation committee for their contribution to this report, and for their comments and advices during our meetings. I would also like to thank Mr R. Harris (Buro Happold) for his quick reaction to questions that I put to him through email. Next, I would like to thank my fellow students in room 0.72 for their support and all the pleasant coffee breaks. Furthermore I would like to thank my family and friends who have been supportive and contributed to this report, especial Riny Toussaint who checked parts of this report on spelling and grammar errors. I also want to thank my parents for supporting me throughout my study period. Finally special thanks go to Azahara van Bergen for her daily support and encouragements.

Matthijs Toussaint
's-Gravenhage, May 2007

Graduation committee:
Prof. Ir. L.A.G. Wagemans
Ir. J.L. Coenders
Dr. Ir. J.W.G van de Kuilen
Dr. Ir. P.C.J Hoogenboom

Table of contents

Preface	i
Abstract	vii
1 Introduction.....	1
1.1 Introduction to the problem	1
1.2 Problem definition and thesis goal.....	3
1.3 Research questions.....	4
2 Timber shell structures.....	7
2.1 Introduction.....	7
2.2 Use of timber through history.....	7
2.3 Shells in theory	16
2.4 Examples of timber shells.....	21
2.5 Timber shells in practice: field research.....	29
3 Timber gridshells.....	35
3.1 Introduction.....	35
3.2 Structural principles of the gridshell	36
3.3 Gridshell example projects	50
3.4 Comparison of the gridshells	66
4 Form finding	69
4.1 Introduction.....	69
4.2 Form finding techniques.....	69
5 Grid generation tool for arbitrary surfaces.....	81
5.1 Introduction.....	81
5.2 Tool development set-up	82
5.3 Shape analysis	83
6 Development of the grid generation tool.....	87
6.1 Introduction.....	87
6.2 Proposed method	89
6.3 Assumptions and starting points	92
6.4 The gridshell design tool	93
6.5 Results compared with reality by physical modelling.....	117

7	Members in bending	121
7.1	Introduction.....	121
7.2	Stresses induced by the formation process	122
7.3	Interaction between the laths.....	143
7.4	Curvature and RD-forces.....	150
7.5	Conclusions	170
8	Conclusions and recommendations.....	173
8.1	Introduction.....	173
8.2	Conclusions	173
8.3	Recommendations.....	174
8.4	Evaluation of the gridshell design tool	175
	References	179
	List of symbols.....	183
	Appendices.....	185
	Appendix 1: Determination of the maximum bending radius.....	187
	Appendix 2: GenerativeComponents.....	192
	Appendix 3: Proof of $R \gg$ mesh size.....	197
	Appendix 4: Problems encountered in developing the grid generation tool.....	199
	Appendix 5: Physical modelling.....	203
	Appendix 6: Contact information.....	223

Abstract

In the last few years the timber gridshell has gained popularity. Recently two gridshells were constructed: the Weald and Downland gridshell in 2002 and the Savill Garden gridshell in 2006. These structures are examples from which the benefits of timber gridshells become apparent. A gridshell can display elegance and style, with its slender ribs curved into shape. It is also a sustainable structure, as the use of material is small, due to the shell behaviour. Also the timber can source from sustainable resources. Despite the advantages of the timber gridshell and the interest in sustainable engineering and free form architecture, the gridshell is not used very often. What can be seen as an important reason for this is the fact that the design process for a free form gridshell is rather complicated. An iterative design process is used to determine the grid geometry, which is only known to a few people. Main goal of this Master's thesis is a study into the application of a design tool based on the geometrical properties of the grid of a grid shell, i.e. equal distance between the nodes on the quadrangle grid.

The gridshell structure is a structure built with long slender laths. The laths are positioned in a flat quadrangle mat with one or more layers in two directions. This mat is then pushed and pulled into the desired shape by bending the laths and deforming the quadrangle meshes into rhombic shapes. When the desired shape is achieved, the laths are attached to edge supports and the structure is stiffened by diagonal bracing or applying a continuous layer on top of the laths. Timber is outstandingly suitable for this kind of building method. It is lightweight compared to its strength and can be bent and twisted relatively easy.

Timber has always been used in structures by mankind. It was not until the twentieth century for timber to be used in large scale shell structures. In 1975 the first large scale timber gridshell was finished. This structure is the Multihalle in Mannheim. The structure can be seen as true pioneers work. The geometry of the structure was determined by physical form finding and it was constructed by pushing up the flat mat of laths by aid of scaffolding towers and fork lifts.

More recently the Weald and Downland Gridshell and the Savill Garden gridshell were constructed. The former was constructed by lowering down the flat mat into shape on a special movable scaffolding. The latter was constructed by simply laying out the grid on a pre-shaped formwork. The gridshells were designed by aid of a computer form finding technique.

The gridshell design tool has been set up to generate a gridshell grid on an arbitrary surface. The method used to generate the gridshell geometry uses two spheres to determine the intersection points of the gridshell laths. If the two spheres are positioned in such a way that their midpoints are located on the surface and that the two spheres are intersecting, there will be two intersection points between the two spheres and the surface. Together with the sphere midpoints, these four points form a mesh in the gridshell grid. A script has been created to execute this determination of points in a sequence which locates all possible intersection points on the surface.

The sequence starts from start-off sections, interpolated on the surface. This implies that the correctness of the grid is dependent on the correctness of these start-off sections. Although the results of the grid generation tool look promising, further testing is advised to prove this.

The design tool has been set up having the possibility to check the curve angles of the generated grid. From these angles the bending stresses can be calculated and checked if the bending or torsion stress criteria are exceeded. If this is the case, the checked element is given a colour. The generated structure can be checked visually for stress levels exceeding the stress criteria.

The design tool has been tested on a surface consisting of two semi-spherical parts connected by an anti-clastic part. The resulting grid was used to construct a physical model to check the computer model on reality. Deviations were found in shape and geometry between the two models, but also similar effects were found. Therefore the conclusion must be that the design tool creates a grid which is correct. Form finding is needed to adjust the shape to a surface that complies with the shape that will be formed by the grid in reality. This form finding can be performed manually using the results of the physical model. The results also show that (semi-) spherical surfaces are hard to create by means of a gridshell structure. The laths have to bend and scissor too much to comply with the curvature. These kinds of surfaces should be avoided.

In the construction of a gridshell the laths are bent into the desired shape on internal supports. If this shape is not equal to the equilibrium bending position of the lath, the lath will deflect toward this equilibrium position when the internal supports are removed. This results in an undesired change of geometry and stress level. This behaviour was analysed with a single lath. The structural analysis software GSA was used for this. A maximum deviation of 23% was found in the stress level. This can lead to breakages if this is unaccounted for.

The formation process of a gridshell results in bending and torsion stresses in the members. After relaxation of the timber, a residual stress level remains in the structure. This stress has to be accounted for in structural analysis. The stress levels can be derived from the curve angles in the structure. These angles are part of the output of the gridshell design tool and can therefore easily be utilised. First it has been tested if the formation bending stresses can be implemented as a load case in GSA. For a single lath this method gets accurate results but in a 3D structure the results are less usable. The bending stresses had better be used as a superposition load with other load cases that are analysed in GSA, like wind and snow loads. The stress levels can be added to the stress levels resulting from the GSA-analysis, after applying a reduction factor which takes the timber relaxation into account.

It has been found that a complex stress distribution is present in a 3D structure, while the stress levels resulting from the curve angles show a more continuous stress distribution. The laths interact with each other when bent into shape, resulting in a combination of bending, torsion and axial force. When edge disturbances are neglected, a deviation of approximately 10% is found between the stress levels resulting from analysis and the stresses calculated by using the curve angles. The conclusion of this analysis is that the calculated stress levels can be used for analysis. However, to get safe results, the reduction factor should not be taken too low. More research is desired to verify the use of the curve angles to determine stress levels and to determine a safe reduction factor.

Introduction



This chapter is the introduction to the problem analysed in this Master's thesis. First the scope of the subject of the thesis will be introduced and an introduction to the problem will be displayed in Section 1.1. In Section 1.2 the research problem will be defined, together with the main goal of the thesis. Finally, in Section 1.3 the main goal of the thesis will be translated into research questions, which will be guidelines in this thesis.

1.1 Introduction to the problem

One main characteristic of a shell is its large span to thickness ratio. By nature a shell uses a very efficient way of diverting forces to a support structure, which is called shell action. This makes it possible to create large spans with little material. This principle is also used by nature itself, shown in examples like soap bubbles, sea shells and bird eggs. A shell structure can show elegance and efficiency when designed correctly.

Since ancient times shell structures are used by mankind. One of the first types of shells used by mankind is the dome. Before domes, large spans were hard to create and columns were needed to support a roof. Stone domes structures were first seen in Roman civilisation, which constructed semi spherical domes. One example is the Pantheon in Rome, built in 125 AD. Parallel to this, in Persia domes also developed. Pendentives were first used here, which enabled the dome to be supported by four columns. One of the largest dome achievements by the Byzantine Empire is the Hagia Sofia (537 AD) in Constantinople, the modern Istanbul¹. Until the twentieth century, domes can be characterized as weighty structures. Thick walls were needed to resist the horizontal forces resulting from the heavy stone dome. This changed with the rapid development of computer technology, after World War II. Shell theory was already known, but with the computer it became possible to derive and verify solutions for very slender shells with large spans. This enabled engineers to create very thin shells with large spans. Especially in the fifties and sixties, quite a lot of large span shells were built. The concrete shells by Heinz Isler are excellent examples of efficient shell behaviour (Figure 1.2). Also timber proved itself to be very suitable for shell structures, especially in hypar shells (Figure 1.3). Timber shells lack the need for an expensive casing, which is needed for concrete shells.

Timber also proved to be very useful for free form architecture. With a system of long continuous timber laths, a free form lattice shell can be built. Such structure is known as a gridshell. The shape of gridshell is obtained by bending and deforming a flat mat of timber laths. When the quadrangle mat of laths is deformed in the desired shape, the laths can be pinned to an edge construction and stiffened with diagonal bracing. This way, a 3D shell structure is created out of 2D base, with only the natural behaviour of the timber. This construction method was first used on a large scale in 1975 at the Multihalle Mannheim gridshell.

¹ <http://litestraboen.blogspot.com/2007/01/domes.html> accessed 15-03-2007



Figure 1.1: Pantheon in Rome²



Figure 1.2: Shell structure by Heinz Isler³



Figure 1.3: Timber hyper shell in Dortmund (Holzbau Konstruktionen)



Figure 1.4: Weald & Downland gridshell⁴

Unfortunately, increasing labour costs made the construction of shells too expensive compared to conventional concepts in the last few decades. This caused the interest in shell structures to diminish. However, the rise of free form architecture and the interest in sustainable buildings has renewed the interest in shells in timber. This was acknowledged by the completion of the Weald and Downland gridshell in 2002, and the Savill Garden gridshell in 2006. These structures display style and elegance and were built with timber from sustainable sources. They combine architecture and sustainable engineering in well thought-out designs.

The structures mentioned above are the only large-scale timber gridshells existing today. Despite the advantages in appearance and sustainability, the gridshell is not used very often. The fact that the design process is quite complicated, probably is an important factor in this. A gridshell is designed by means of an iterative design process which is little transparent and the existing gridshells are all designed by only a few people. To increase the use of the gridshell system, the knowledge on gridshell design should be spread and the design process made more transparent. This thesis is meant to be part of this.

² http://www.nazionaleroma.it/english/where_We_Are/surroundings/rome_pantheon.html accessed 13-02-2006

³ <http://staff.bath.ac.uk/abscjkw/OrganicForms/HistoryPictures/HeinzIsler.jpg> accessed 19-03-2007

⁴ <http://www.wealddown.co.uk/downland-gridshell.htm> accessed 18-12-2005

1.2 **Problem definition and thesis goal**

Timber gridshell structures are not often used, despite the advantages. The complicated design process is considered the main problem in gridshell design. The largest problem in this design process is the determination of the geometry of the structure. During construction the gridshell lattice is bent and deformed, approximating the desired shape. The geometry of the shape, which is dependent on the bending behaviour of the material, is not known in advance. To be able to predict the structural behaviour of the gridshell, the design model should be an accurate approximation of the outcome of the construction sequence. An iterative process which takes the bending behaviour into account is needed to do this. This design process is little transparent and without knowledge of the subject this is a huge obstacle.

The problem in the design process can possibly be solved by introducing a different method to determine the grid geometry. This method should be more accessible and transparent. The proposed method in this thesis is based on the geometrical properties of a gridshell grid, which is the equal distance between nodes. The bending behaviour of the material can be implemented as a boundary condition to which the geometry has to comply. This method can be implemented in a design tool. By basing this design tool on commercially available software, the tool is kept accessible. The tool should be usable as a plug-in for anybody who purchases this software.

A goal of this thesis is to implement the proposed method in a conceptual design tool. To verify the results of this tool, a study is needed into the bending behaviour of the grid members. This can be summarised into the main goal of this thesis, which is:

A study into the applicability of a geometrical design tool to the design process of a timber gridshell

1.3 Research questions

The main goal stated in the previous section can be split into two subjects: the implementation of the proposed method into a conceptual design tool and the study into the bending behaviour of the members of a gridshell. The first part can be researched by the following research questions and sub-questions:

1. *Is the proposed geometrical model suitable for determination of the gridshell geometry for an arbitrary surface?*

a) Which free form gridshells exist today and what are their characteristics?

This question is researched in Chapter 2, 3 and 4. Chapter 2 will give an insight into the development of timber structures through history and an overview of timber shell structures. In Chapter 3 existing gridshells will be studied and compared. Chapter 4 will give an overview of form finding techniques, by which the geometry of free form structures is determined.

b) How can the proposed geometrical method be used to create the gridshell structure?

This question leads to the development of the actual design tool. The proposed method will be implemented in a tool which can generate the grid of a gridshell. This process will be displayed in Chapter 5 and 6. First, in Chapter 5 the proposed grid generation method will be further specified. In Chapter 6 the set-up of the actual design tool will be explained and the resulting geometry will be displayed.

c) To what extent is reality approximated by the proposed method?

To answer this question, the results of the design tool should be verified in a real structure. This is attempted by creating a physical model of a gridshell, which models the physical behaviour of the structure. The physical modelling will be compared with the computer model. This can be found in Section 6.5.

To be able to analyse and assess the results of the design tool, more knowledge is needed of the bending behaviour of the gridshell members during construction. This leads to the second research question and sub-questions:

2. *What stresses occur during the process of bending the gridshell into shape?*

- a) *What stresses occur in a slender member which is bent into shape over internal supports?*

The members of a gridshell are bent into shape while supported by internal supports. The bending results in bending stresses, but what happens when the internal supports are removed after construction? This process will be analysed by modelling the process step by step in Chapter 7.

- b) *Can the formation stresses be deduced from the curvatures which are determined by the geometrical design tool?*

To structurally analyse the formation process, the stresses resulting from the formation process should be known. If these can be deduced from the generated grid geometry, it should be possible to implement these as a load case in the structural analysis of a grid shell. This will be researched in Chapter 7.

Timber shell structures



2.1 Introduction

In this chapter an overview is displayed of the use of timber in shell structures. As an introduction to this, the use of timber through history is investigated in Section 2.2. To be able to assess structures as shells the different definitions of a shell and a general overview of shell theory will be displayed in Section 2.3. After this, in Section 2.4 some illustrative examples of existing timber shell structures will be presented to give an overview of possibilities in timber construction. The chapter will be finalized with the display of the field research executed in different timber shell subjects by the author.

2.2 Use of timber through history

Wood is one of the oldest building materials known to mankind. The oldest known wooden artefacts date back some 14000 years, and probably wood is used in structures since the ancestors of modern mankind started to build shelters⁵. Because of the perishability of wood, not much is known about those ancient times. Only archaeological reconstruction can provide some information about what might have been. Remains of dwellings in Central Europe from around 3000 BC show us that round wood was used as the main construction material in those days (Kuklik, cited in Thelandersson & Larsen, 2003, p.1). A lot of timber structures also disappeared when the use of steel became common. Either they were replaced by steel, or simply rotted away because maintenance wasn't considered important anymore (Yeomans, 1999).

The history of the use of timber can be studied by looking at the remaining examples. The oldest examples of timber structures still remaining date from the middle ages. In Western Europe some 14th century structures still remain. Also in Scandinavia, where wood has always been a resource widely available, some medieval buildings still remain. The oldest Scandinavian building is the Borgund church in Norway, which was built in the twelfth century. Some parts of Asia also have a long tradition of timber construction. In Japan, some seventh century structures still remain (Thelandersson & Larsen, 2003). The largest all wood historical building in the world also stands in Japan: the Diabutsu-Den at the Todai-ji temple in Nara (Figure 2.1). The current building, measuring 57x50m and 47m high, was built in 1709 and houses world's largest bronze statue of Buddha. The original, even greater building dated from 749, but it was destroyed by fire⁶.

⁵ <http://www.arplus.com/broch/articles/araug05pdfs/araug05reviewsP103.pdf> accessed 26-01-2006

⁶ <http://web-japan.org/atlas/historical/his13.html> accessed 15-01-2006

Figure 2.1: Diabutsu-Den, Nara, Japan⁷

Studying the development of timber as structural material in Western Europe, four periods can be distinguished. In the Middle Ages wood was the main construction material and some fine examples of all wood buildings still remain today. In the 16th to 18th century, brick came into use and timber was mainly used in roof structures. With the development of iron in the 19th century, timber connections were improved with iron elements and laminated timber was introduced. In the 20th century, mass produced connectors and engineered timber such as Glulam, made the timber construction to what it is today (Ross, 2002).

2.2.1 The middle ages

In the middle ages, timber was the main building material. Lacking tension capacity, stone was only applicable in compressive structures, like arches and domes. Therefore it was only used in prestigious buildings. Timber was universal for roofs and framed structures. The most common frame type was the cruck structure, used in houses and barns. One of the oldest remaining examples is the Leigh Court barn near Worcester, UK and was built around 1325 (Horn, 1973) (Figure 2.2 and Figure 2.3). Loads are mainly transmitted through contact pressure in the joints, with triangulation for stability. The joints were obviously critical elements. Joints could become quite complicated and remaining examples show carpentry was a true skill.



Figure 2.2: Leigh Court barn (Horn 1973)



Figure 2.3: Inside Leigh Court barn (Horn 1973)

⁷ <http://www.taleofgenji.org/todaiji.html> accessed 15-01-2006

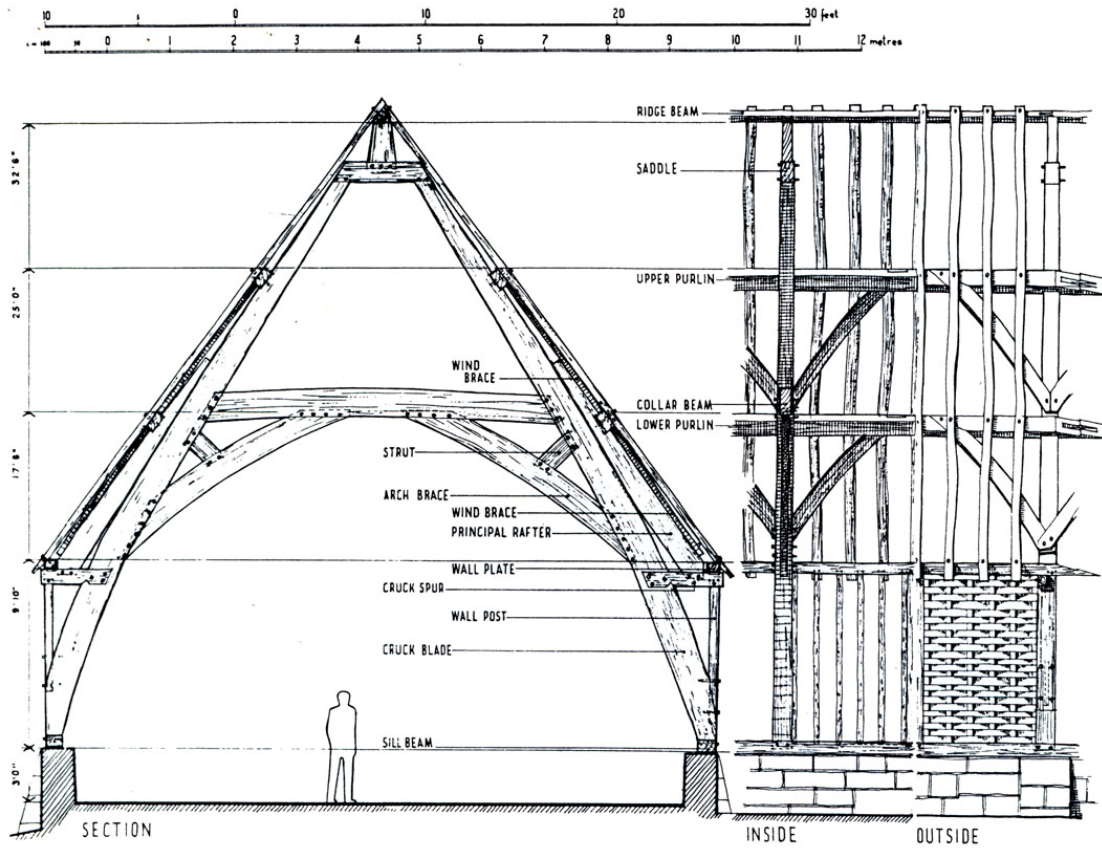


Figure 2.4: Schematic drawing of the Leigh Court barn (Horn 1973)

The most common joints in the middle ages were:

- The tennon joint, which is in compression only (Figure 2.5a)
- The lap joint, which has small tension capacity (Figure 2.5b-c)
- The scarf joint, to extend members. The joint was placed in a non critical section in the length of the beam. A variety of locking methods was used. (Figure 2.5d-g)
- The post head and tie beam joint, which deals with the critical point where the roof truss sits on a post. Tension capacity was needed, to support the reaction force of the tie beam. (Figure 2.5h)

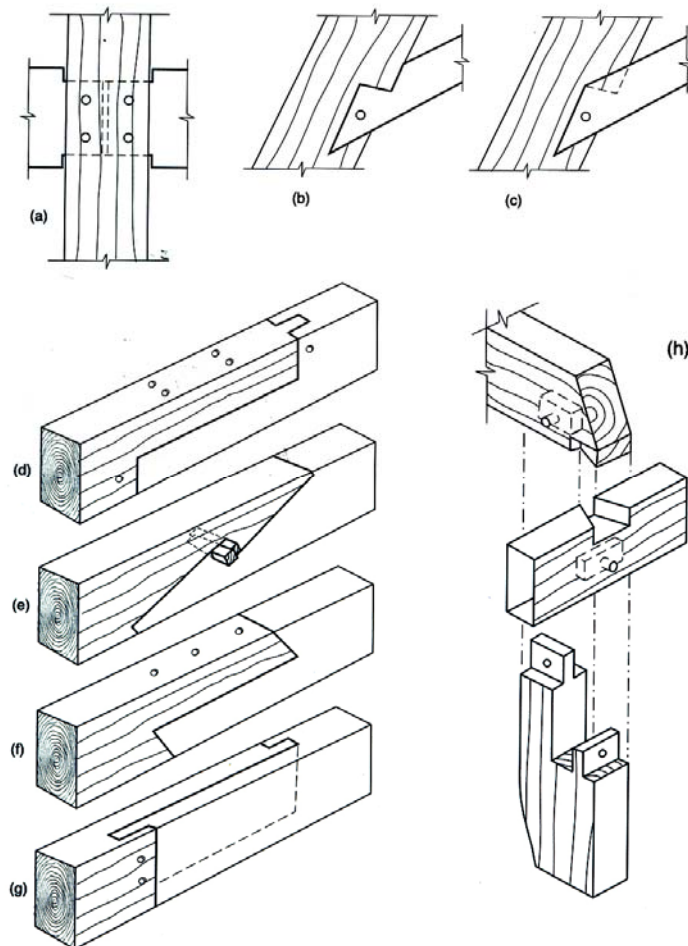


Figure 2.5: Common joints (Ross 2002)

The best known Western-Europe example is probably Westminster Hall in London (Figure 2.6). It is considered a true masterpiece in timber engineering from those times. The original building was built in the 11th century and was reconstructed in 1395. The roof spans 20,5m and is 72m long and is of hammer-beam type. The main rafters are supported by Crown, Queen and Hammer posts. The Hammer post rests on the braced Hammer beam, which is in tension and resists the outward thrust of the main rafter (Figure 2.7). Of course the flow of forces in such a complicated structure is dependent on a lot of factors like support deflections and connection stiffness. There was an ongoing discussion on whether the loads are brought down by the great arch, or directly by the main rafters to the wall head. This was ended by tests on a scale model and numerical models. It proved that almost all of the vertical dead weight is supported by the corbels, and the load is brought down by combined action of the hammer post and the great arch. The major horizontal thrust is resisted by the walls, halfway between the corbel and the wall head. Also the Hammer beam was proved to be in tension and to relieve the wall head of horizontal force (Courtenay & Mark, 1987).



Figure 2.6: Westminster Hall (Courtenay & Mark 1987)

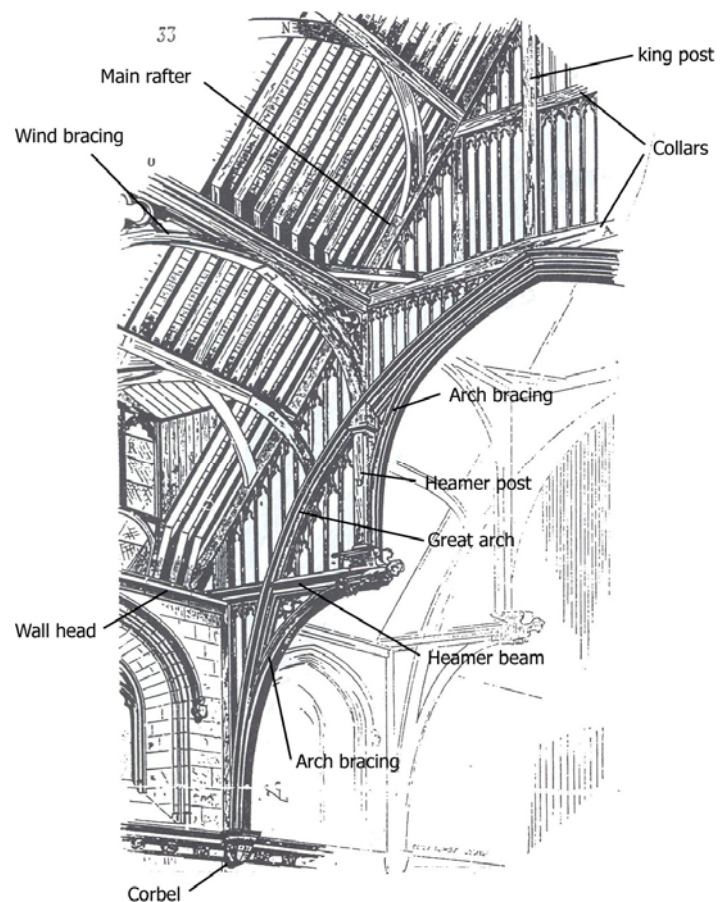


Figure 2.7: Drawing of Westminster Hall by Violett-le-Duc (Courtenay & Mark 1987)

2.2.2 Early modern period

The Renaissance brought a different architectural style, based on Greek and Roman buildings. In this new architecture, timber frames had no place. The use of brick became common and trusses came into use for the roof structure. The structure was hidden behind a plaster ceiling for architectural needs. Most common was the king post truss (Figure 2.8). Iron straps were introduced to reinforce the tension connection with the tie beam. Alternative roof shapes and truss configurations appeared, such as the queen post and multiple-bay trusses, as longer spans were attempted. (Ross, 2002)

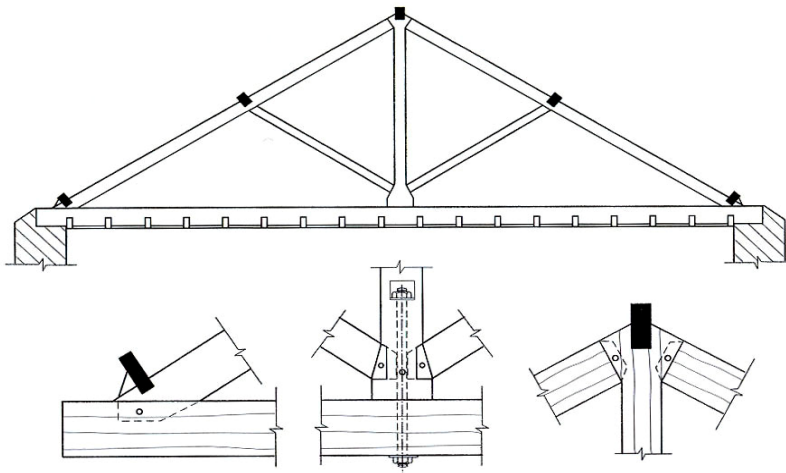


Figure 2.8: King post truss with iron strap connection (Ross 2002)

Quality and efficiency of the truss depended on the skills and knowledge of the carpenter, which he acquired from his master. Like in the Middle Ages this knowledge was transferred from master to apprentice only. In the 16th century the first carpenters' manuals were published. The earliest were mainly on measuring and face estimation though. It was not until the 18th century, for the first manual which dealt with geometry and construction properly to be written by Francis Price.

In the profession of carpentry, a transformation can be seen from carpentry as a craft activity to a production profession. If desired an architect could be hired to provide the designs, although knowledge on construction was still provided by the carpenter. If a more modest building was required, a tradesman capable of building in the required style could be hired. As new architectural forms were introduced and planning, construction and decorative forms became more sophisticated, it became more common to hire an architect. (Yeomans, 1986) Another development took place in the theory of structures and material properties. The first significant effort in the theory of elasticity was undertaken by Galileo (1564-1642). Robert Hooke (1635-1703) formulated his famous law and Petrus von Musschenbroek (1692-1761) performed the first major series of tests on various species of timber, to determine the strength properties of the material (Booth, 1964).

The first structural method for large span arches in timber was invented by the French architect Philibert de l'Orme (1515-1577). In 1561, he announced his invention of a composite timber member, composed of two or three planks on its side and sawn off radially, then joined together with wooden pegs at several points. The longitudinal sides of the planks were cut to an arch shape. This method used considerably less material than conventional methods and large spans were possible. De l'Orme made designs for domes with spans up to 60m and he believed spans of 200-400m would be feasible. Despite the time-consuming production and poor stiffness due to the large amount of parts and joints, his methods were used until well in the nineteenth century. The largest dome using it was the dome roof of the Halle au Blé in Paris, spanning 41m and built in 1783 (Müller, 2000).

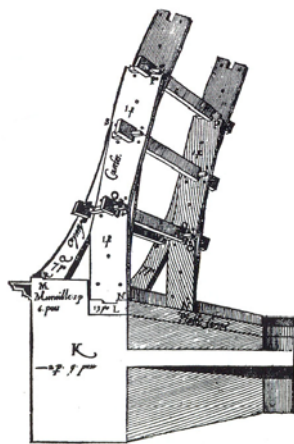


Figure 2.9: De l'Orme's composite member (Müller 2000)

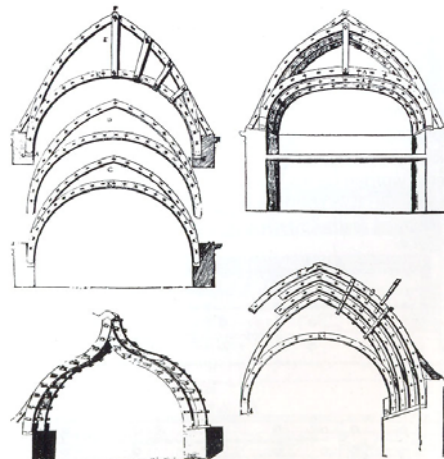


Figure 2.10: De l'Orme arch designs (Müller 2000)

2.2.3 Nineteenth century

In the nineteenth century, the industrial revolution brought radical changes in society and technology. Large industrial buildings were needed. Floors had to bear heavy loads, so large primary beams were used. Also the roof structures needed to span larger distances. Iron was increasingly used in strap connections to improve the tension connections. The industrial revolution brought machine driven saws and mass produced nails and bolts, which reduced costs dramatically and made assembly of trusses a lot easier. With the development of wrought iron, a construction material with high tension capacity was introduced. As the principles of statics became more clearly understood, the tie member was replaced by an iron rod more often (Ross, 2002).

To compete with steel, new methods for timber were searched. This led to the invention of laminated timber. Instead of using short pieces of wood like De l'Orme's method, the long length of the material was taken advantage of. Thin planks were bent into shape and then jointed together with clamping bolts and collars. At first, laminated timber was mainly used in bridges. Spans over 60m were already possible at the start of the century. Convinced of the advantages on De l'Orme's method, Armand Rose Emy (1771-1851) was one of the first engineers who used laminated timber in his designs for arched structures. His methods were widely adopted for military and factory buildings in France, with spans over 40m. Confident of his own method he even made designs for spans over 100m (Booth, 1971; Müller, 2000).

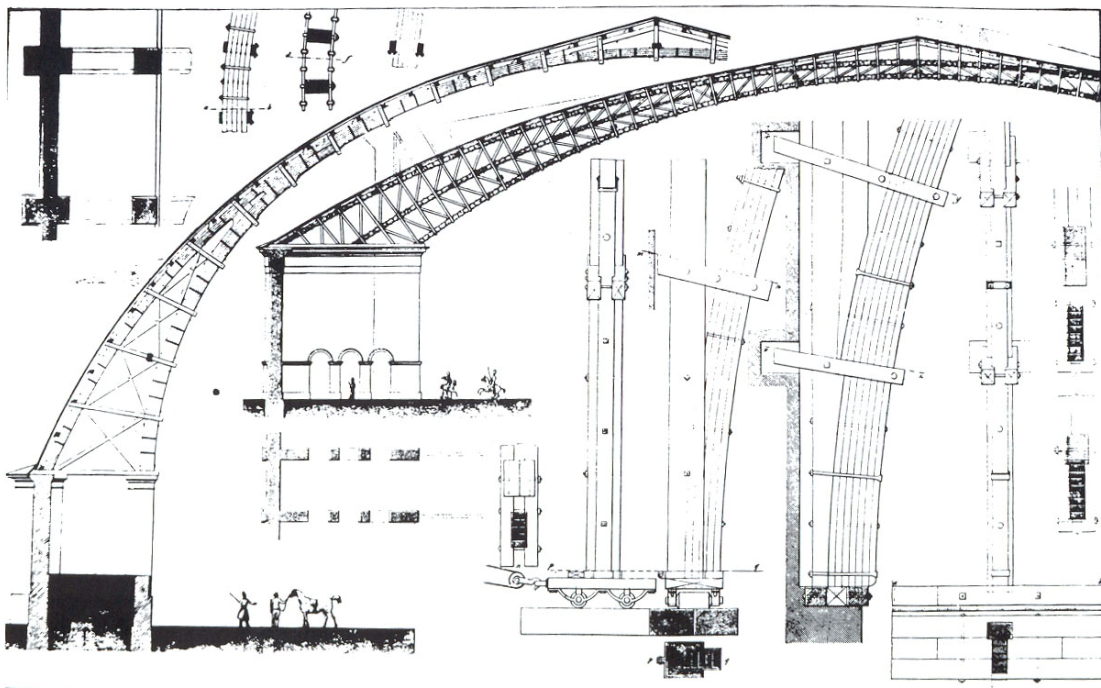


Figure 2.11: Designs for large halls by Emy (Müller 2000)

2.2.4 Twentieth century

In the first half of the last century, a wide range of mass produced connectors and shear connectors became available. The connections in trussed structures were further improved with these and possible spans became larger again.

At the start of the century, probably the first attempt to construct a lattice shell with a three dimensional load transfer was made. Around 1904, Fritz Zollinger (1880-1945) transformed De l'Orme's composite members in a three dimensional frame (Figure 2.12). By opening up the two parts of the member, he created a diamond shaped lattice. In this way a three dimensional curved structure was made. At each joint one plank was going trough. The connection was made with bolts (Figure 2.13). The system was no success. Lacking moment capacity in these joints, the structures showed large deflections. Later, the jointing system was improved and successfully used in Germany, see Section 2.4.1.



Figure 2.12: The Zollinger system (Müller 2000)

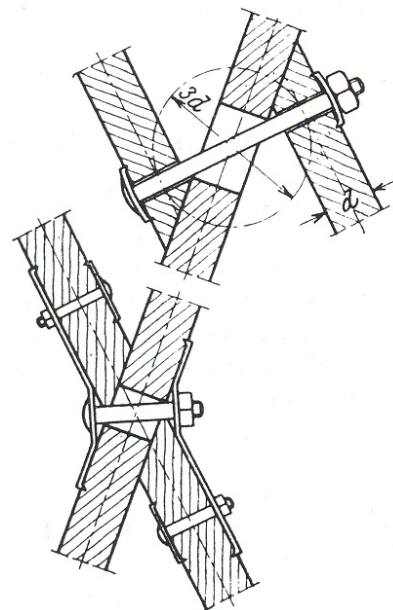


Figure 2.13: Node of the Zollinger system (Müller 2000)

Laminated timber was further developed in the twentieth century. Production techniques were enhanced and new glues were developed. In early glued laminated timber, organic glues were used. These perform well in dry conditions, but moisture degrades the glue. In the 1930s moisture resistant Phenol-formaldehyde glues were developed. While this glue needs heat for curing, it was difficult to produce large cross sections. Urea-formaldehyde glues, which were developed in the 1940s, cured with normal temperatures. From the 1950's, glued laminated beams became in general use in construction, with only transportation considerations limiting its dimensions (Ross, 2002).

The last few decades, production techniques improved by aid of computer technology. It is now possible to create complex curved shapes, with double curved Glulam beams. Timber is graded at high speed by automatic grading machines, and timber of high quality can be produced by extracting wood deficiencies and joining the pieces with advanced joining techniques. To illustrate the vast possibilities of modern timber construction some examples are shown in Section 2.4.

2.3 Shells in theory

2.3.1 Shell surfaces

The diversity of shell surfaces is vast. Any surface which is curved in one or more directions can be seen as a shell surface. One way of defining shell surfaces is by Gaussian curvature. Another is the way the surface is generated. Both are displayed here.

Gaussian Curvature

A shell can be described by curves. When looking at a point on a shell, different curves can be drawn on the surface through this point, which all have a different radius of curvature. The curves which have the minimum and maximum value of curvature are the principle curvatures κ_1 and κ_2 . The Gaussian curvature is the product of these two: $\kappa_g = \kappa_1 \cdot \kappa_2$ (Hoefakker & Blauwendraad 2005). Three different types of Gaussian curvature are defined, which are shown in Figure 2.14. A shell is typed by its type of Gaussian curvature. These types are:

- $\kappa_g < 0$: Principle curvatures are opposite. This is called an anti-clastic surface.
- $\kappa_g > 0$: Principle curvatures are of the same sign. This is called a clastic surface.
- $\kappa_g = 0$: At least one of the principle curvatures is zero. This results in a cylindrical surface or a plane when both κ_1 and κ_2 are zero.

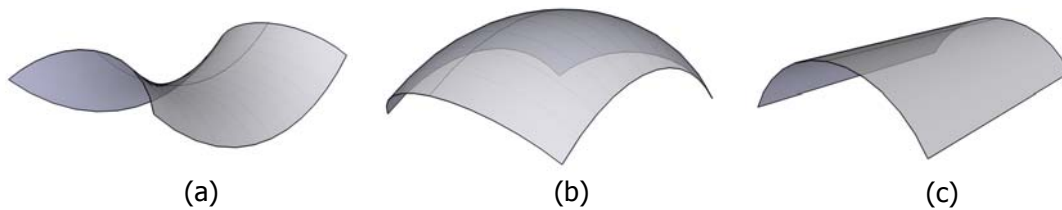


Figure 2.14: negative (a), positive (b) and zero Gaussian curvature (c) surfaces

Surface generation

Surface generation is the way the surface is created. Some of the different possibilities to do this will be displayed here:

- **Surface of revolution:** these surfaces are generated by revolving a curve around the axis of revolution. This curve is called a meridian curve. Examples are the cone, the dome and the hyperboloid, but also a cylinder is a surface of revolution.

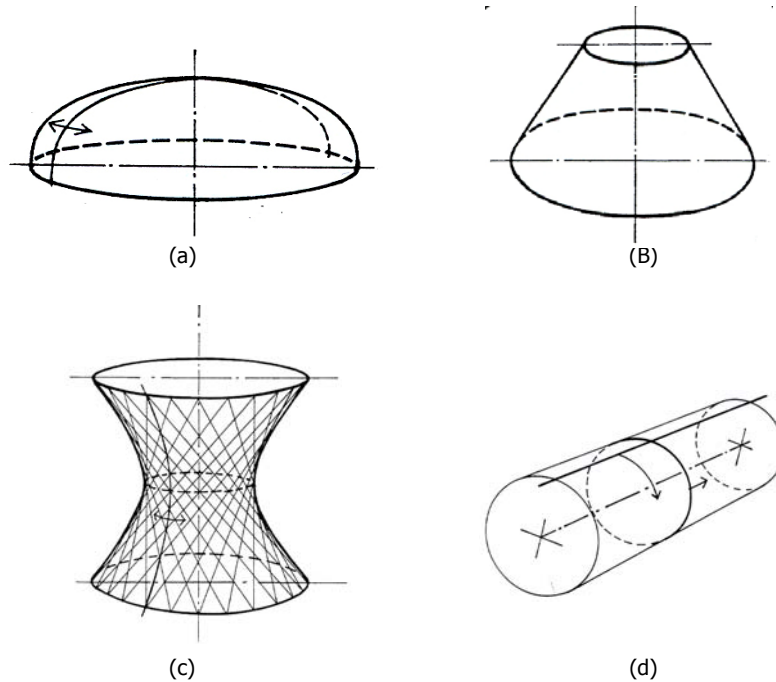


Figure 2.15: surfaces of revolution. Spherical shell (a), cone (b), hyperboloid (c), cylinder (d) (Pestman)

- **Surface of translation:** these surfaces are created by translating one plane curve along another, while keeping the sliding curve's orientation constant. The curve along which the other one slides is called the generator. When the generator is a straight line, the translation of a curve results in a cylindrical surface. Figure 2.16 shows examples of the surface of translation:

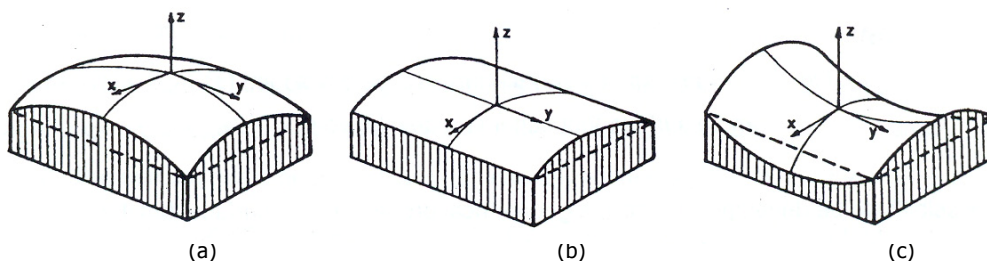


Figure 2.16: surfaces of translation. Elliptical paraboloid (a), cylindrical paraboloid (b), Hyperbolic paraboloid (c) (Hoefakker & Blaauwendraad 2005)

- Ruled surfaces: a ruled surface is generated by sliding the ends of a straight line along their own generating curve, keeping the straight line parallel to a prescribed direction. Examples are the conoid and the hyper. The hyper is a special case in this, because it can also be cut out of a hyperbolic paraboloid by four straight lines along the surface.

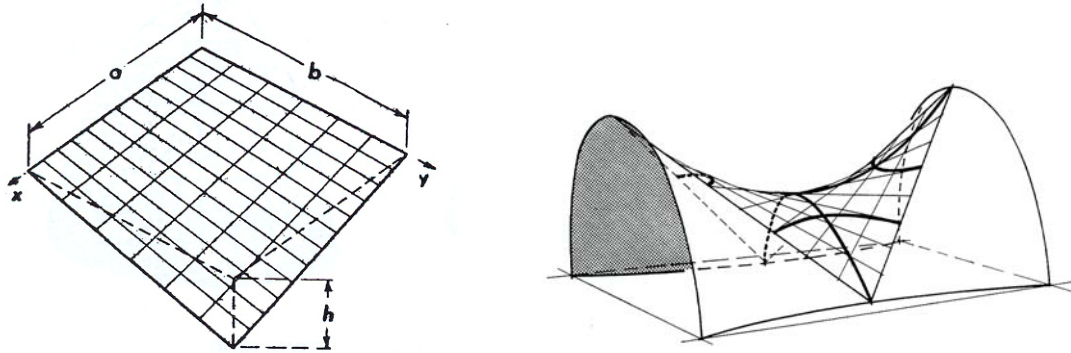


Figure 2.17: Hypar shell as a ruled surface (left) (Hoefakker & Blaauwendraad 2005) and as a part of a hyperbolic paraboloid (right) (Pestman)

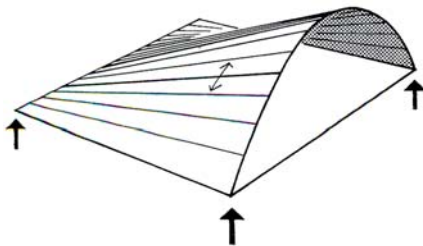


Figure 2.18: Conoid shell (Pestman)

2.3.2 General principles of shell theory

Shell structures have a few unique properties, which makes them interesting for designers and structural engineers. Shells can display elegance and lightness if designed correctly. With a minimum of material, large spans can be made. A shell can be recognized by its small thickness to span ratio. What makes this possible is the principle of membrane action, which is unique for shell structures.

The basic assumption of membrane theory is that in a distributed loaded thin shell only pure membrane stress fields are developed. In this stress field, only normal and in-plane shear stresses are developed, which are uniformly distributed over the cross section. Bending stresses are negligible small compared to the in-plane stresses. Due to the initial curvature a shell can resist in-plane forces as well as out-of-plane loads by membrane action. (Hoefakker & Blaauwendraad 2005).

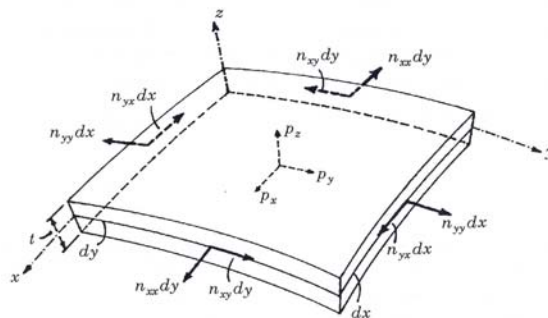


Figure 2.19: Stress resultants and load components on a shell element

However, in some cases membrane theory does not satisfy equilibrium and/or the displacement requirements anymore and bending theory is needed. Disturbance of membrane behaviour occurs when:

- boundary conditions and deformation constraints are not compatible with the requirements of a pure membrane stress field (Figure 2.20 b&c)
- the shell is loaded by a concentrated load (Figure 2.20 d)
- a change in shell geometry occurs (Figure 2.20 e)

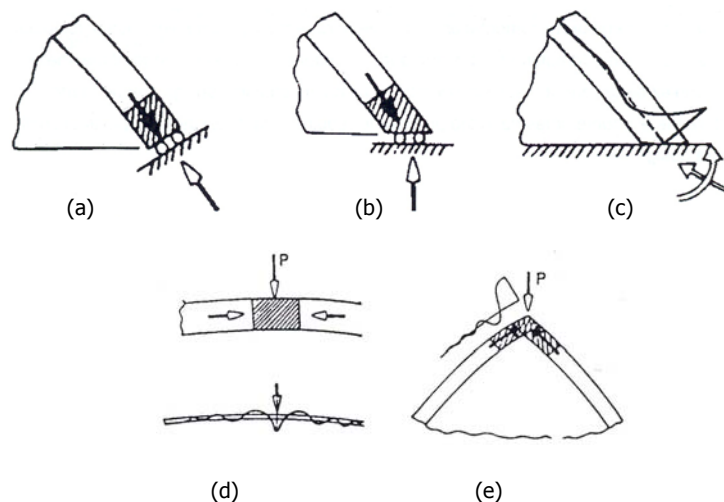


Figure 2.20: Membrane disturbances (Hoefakker & Blaauwendraad 2005)

To resist the forces that disturb the membrane behaviour of the shell, additional structural elements are needed. In a lot of shell structures ribs and/or edge beams are added, resulting in a structure where membrane action and bending behaviour is combined to resist load. True shells where the loads are resisted by membrane behaviour only are not seen very often. So if the definition of a shell depends on whether loads are transferred through membrane action or not only, probably a lot of structures which are considered to be shells are in fact not.

In timber, true shell behaviour is not seen very often. A lot of double curved timber structures consist of a lattice of ribs combined with one or more continuous layers of timber ply. This continuous layer provides interaction between the ribs and membrane action in a certain extend. The question if a timber shell is in fact a shell depends on in what extend a membrane stress field can develop in its surface.

In the next section examples of timber shells are given. If possible an answer will be provided to the question whether membrane action is present or not.

2.4 Examples of timber shells

To give an overview of the possibilities of modern timber construction for shell structures, some representative examples are presented in this section. Looking at the shell surfaces defined in Section 2.3, the next surfaces will be used in the examples:

- cylindrical shells: lattice barrel vaults
- spherical shells and domes: radial rib dome
 lattice dome
- Hypar shell
- Other: Suspended shells
 Gridshells

As stated in the previous section, it is uncertain if all these structures are in fact shells from a structural system point of view. When only the shape is concerned, the examples are all curved structures and therefore shells. Therefore these structures will be designated as shells and it is tried to answer the question whether shell action is present or not in the overview.

The gridshell, which is the structure concerned in this thesis, is also defined as a type of shell. Here another definition problem appears, as the words grid and lattice have the same meaning. In literacy, the terms point to the same kind of structures, although the term lattice shell points more often to structures with triangulated grids and gridshell to quadrangle grids. In this thesis a difference is added. The term lattice shell will be used to refer to ribbed shells, where rib members are connected to each other in the joints. This lattice can be combined with a structural continuous layer to provide membrane action. A gridshell is a different kind of structure. In a gridshell the ribs are continuous from support to support and connected to each other at the intersections. Stiffness is generally provided by triangulation. In Chapter 3, gridshells will be investigated.

2.4.1 Cylindrical lattice shell

After some less successful attempts to build a cylindrical lattice shell using the Zollinger system mentioned in Section 2.2.4, it was successfully used in 1989, in the roof of a sports hall in Berlin-Charlottenburg (Figure 2.21 and Figure 2.22). The diamond lattice shell is stiffened by diagonal sheeting, which provides in membrane action in a certain extend. The spacing between the ribs is 2m and the connections are made rigid using steel plates and pin joints. The horizontal support reaction is resisted by raised ties. Despite of this stiff system, four steel stiffening beams were added to be sure.

2.4.2 Radial rib dome

The radial rib dome is one of the earliest structural forms. Some nomadic tribes have used this system in their tents for centuries. The primary structural members are three pinned arch ribs (Figure 2.23). Ring purlins resist tangential membrane forces. Because of this geometry, the span of the purlins varies considerably, which is the main disadvantage of the radial rib dome. Also sheeting causes problems near the top because of this. Although not a dome, a good example of a radial ribbed construction is the ice rink in Davos, Switzerland, built in 1979-1980 (Figure 2.24 to Figure 2.26). Loads are carried by a heavy weight structure with members with a depth up to 1950mm, to be able to resist high snow loads. The sheeting does not provide membrane action.



Figure 2.21: Sports hall Berlin-Charlottenburg (Müller 2000)



Figure 2.22: Node of the barrel vault lattice (Müller 2000)

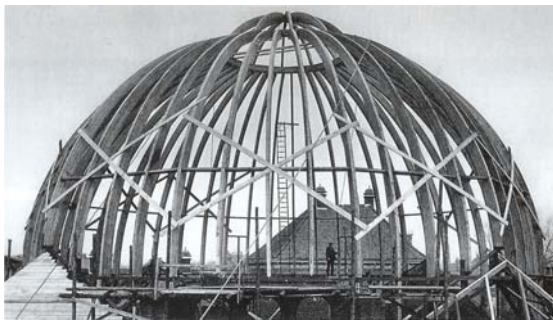


Figure 2.23: Radial rib dome (Müller 2000)



Figure 2.24: Davos ice rink (Müller 2000)



Figure 2.25: Davos ice rink under construction (Müller 2000)



Figure 2.26 Davos ice rink under construction (Müller 2000)

2.4.3 Lattice domes

In search of a structural form with identical members, the geodesic dome was developed. This dome is generated by projecting icosahedrons (20 sided three dimensional figure, composed of equilateral triangles) onto the enclosing sphere surface (Figure 2.27). The network can be separated into ten large triangles. This results in a system of hexagons with pentagons at the nodes of the large triangles.

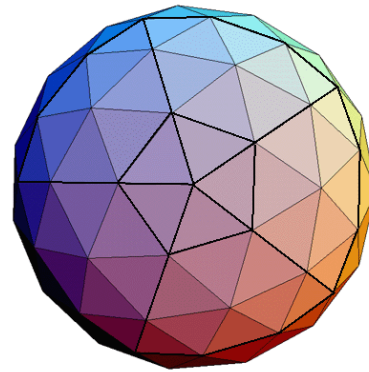


Figure 2.27: Geodesic sphere⁸

The main problem with the geodesic dome is the irregular edge lengths. This causes design problems at the supports, when building a geodesic dome that is not hemispherical.

To overcome this edge problem, the ensphere dome was developed. This is a combination of the hexagonal and triangular dome. The outer ring of the triangular dome is used, to avoid irregular edge lengths. The other rings are formed as a hexagonal dome, with ribs parallel in three axes. One of the largest ensphere domes is the Tacoma dome in Washington with a span of 160m (Figure 2.28-Figure 2.31). Primary members are glued Douglas fir and measure 170-220mm wide and 750mm deep. The sheeting is made of Douglas fir planks of 50mm depth. The dome is supported on a pre-stressed concrete beam. Only two months were needed to erect the dome.

Another fine example of the lattice shell is the roof of the thermal baths in Bad Sulza (1990) (Figure 2.32 to Figure 2.34). It consists of two intersecting domes on an irregular plan. It is supported by concrete columns and edge arches, which are curved in two directions. The ribs are continuous over two bays and are connected with hard wood dowels. Steel plates were placed on top of the joints to secure the members during construction. The sheeting is arranged diagonally in two directions and is nailed and glued to provide membrane action and interaction between the members.

⁸ <http://www.skymind.com/~ocrow/dome/dometop.gif> accessed 07-03-2007

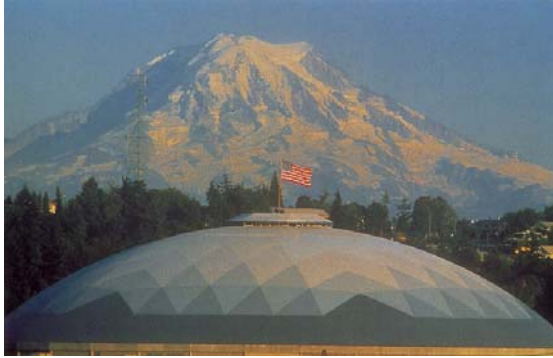


Figure 2.28: Tacoma dome (Müller 2000)



Figure 2.29: Tacoma dome under construction (Müller 2000)

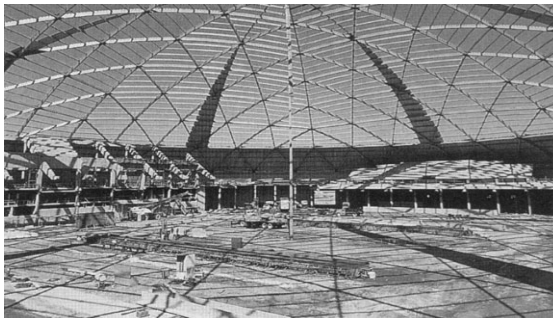


Figure 2.30: Tacoma dome under construction (Müller 2000)



Figure 2.31: Tacoma dome under construction (Müller 2000)



Figure 2.32: Bad Sulza inside (Müller 2000)

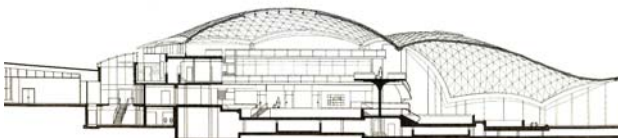


Figure 2.33: Bad Sulza vertical section (Müller 2000)



Figure 2.34: Bad Sulza roof structure (Müller 2000)

2.4.4 Suspended shells

A different kind of structure is the suspended shell. Here, loads are transferred to the supports through tension forces instead of compression. To provide stiffness against wind suction and to achieve the necessary pre stress, the form of the shell has to be curved in two directions. Tents are a good example of suspended structures. In timber it is the suspended lattice shell.

The largest suspended shell built in timber, is the roof over a waste plant in Vienna (Figure 2.35). The plant was built in 1982 and consists of 48 radial ribs suspended from a reinforced concrete tower of 67,35m high. The overall diameter is 170,6 m. A double layer of boards has been nailed in two directions to provide membrane action and extra stability. It was built by assembling the ribs in pairs with purlins and one layer of cladding on the ground (Figure 2.36). After hoisting the ribs into place, the remaining cladding was installed.



Figure 2.35: Waste plant in Vienna (Müller 2000)

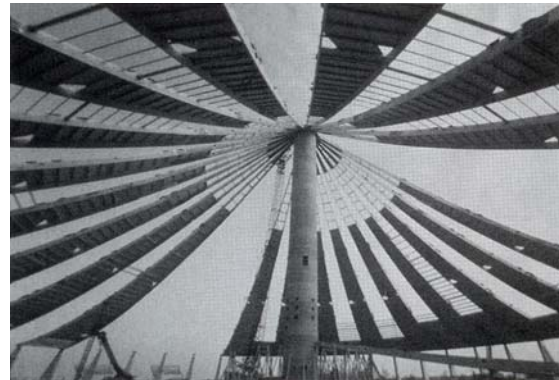


Figure 2.36: Waste plant under construction (Müller 2000)

A well known suspended lattice shell is the roof of brine baths at Bad Dürkheim (Figure 2.37). It was designed by Geier and Geier in collaboration with the engineers Wenzel, Frense and Barthel, and built in 1987. It is designed with the computer program EASY, which is a program used for form finding membrane structures. The roof is hanged from five tension rings, supported by tree-like columns between 9.1 and 11.5m high (Figure 2.39). The lattice has been constructed of double curved and sometimes twisted Glulam ribs with two layers of diagonal sheeting to link the ribs. The meridian ribs, measuring 200x205mm, are suspended from ring to ring, or ring to perimeter arch and follow the catenary line. Following the primary stress trajectories, these are primary loaded in tension. The annular ribs are 80x80 or 120x140mm with 800mm spacing.

The tension rings and perimeter arches were designed as box section in such way that the ribs can be pinned between the box panels (Figure 2.38). The corners of the arches are supported by large cast steel bearings (Figure 2.41), mainly to resist horizontal forces. The deadweight of the arches is supported by the façade.

Of course for such a structure, a price has to be paid. The extra work during planning and assembly was considerable. Now, finished and famous, the extra expense weighs out the extra costs, as it mostly does in any one-off special structure with high aesthetics.



Figure 2.37: Bad Dürreim (Müller 2000)



Figure 2.38: Box section under construction (Müller 2000)



Figure 2.39: Tree columns (Müller 2000)



Figure 2.40: Bad Dürreim under construction⁹



Figure 2.41: Cast steel bearing (Müller 2000)

⁹ <http://www.burgbacher.de> accessed 20-01-2006

2.4.5 Hypar shells

Quite successful as a timber shell is the hypar. A hypar is double curved surface and it is a part of a hyperbolic parabolic shell, described by hyperbolas and parabolas. It can also be defined as a ruled surface, according to Section 2.3 and generated by straight lines on the surface.

Big advantage of the hypar shell is the constant stress in the material along the surface. This is because a (distributed) vertical load on a hypar shell is transmitted through shear forces only. Consider a small element of a hypar shell (Figure 2.42). Because of the torsion of the surface, the shear forces along the edges of the element result in a vertical component. This resultant is in equilibrium with the vertical load. The shear forces are constant along the descriptive straight lines. At the edges the forces are absorbed by the edge beam and transmitted to the supports (Pestman).

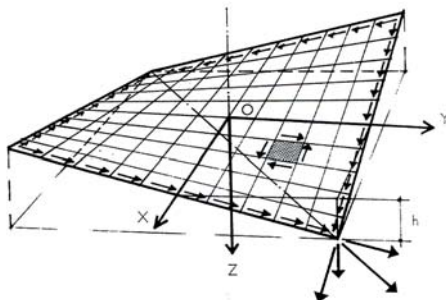


Figure 2.42: A small element with shear forces along the edges. The edge beam transmits the forces to the supports (Pestman)

In construction the timber hypar is mostly built up out of several layers of timber in different directions to provide membrane action, and edge beams of laminated timber. By combining several hypars, larger roofs can be created. A beautiful example is the expo roof in Hannover, built for the EXPO 2000 (Figure 2.43 and Figure 2.44). The roof consists of ten canopies of 39x39m carried by 18 m. high towers. Each canopy consists of four prefabricated shell segment supported by cantilever arms. A two layered sheeting of boards is fixed at an angle to the ribs and provides bracing of the shell. The boards are attached at a spacing of 100 mm for transparency and ventilation of the timber. Also the synthetic roof cover is attached 50 mm clear of the lattice for ventilation.



Figure 2.43: Exporoof Hannover (D), (source unknown)

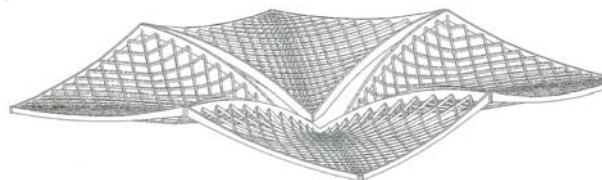


Figure 2.44: Perspective view of one element of 39x39m. in the Exporoof canopy(Müller, 2000)

2.5 Timber shells in practice: field research

Not all knowledge can be found in books. Practical experience can be an important source of information in any field of science. To get an insight in the field of practice in timber engineering, three companies that could provide relevant information on timber shells were visited. First Luning adviesburo, a consulting firm specialized in technical timber structures was visited. Second, Heko Spanten was visited, who produces laminated timber structures. Third visit was to Van Drenth Buighout. This company does not produce structural timber, but their production techniques for curved timber elements could be interesting for curved timber shells. The following sections report on these visits.

2.5.1 Luning adviesburo voor technische houtconstructies B.V.

Luning adviesburo in Doetinchem (NL) is a consulting agency specialized in technical timber structures. Geodesic domes is one of their specialties, as they have developed their own node system. Figure 2.45 shows a project designed by Luning, a geodesic dome under construction for the planetarium in Artis zoo in Amsterdam.



Figure 2.45: Geodesic dome by Luning (GeoDomeDesign)

In a conversation with Mr. Luning, some problems with timber shell structures were discussed. The first subject discussed was that true shells should be made of isotropic material to generate true membrane action. Timber is not an isotropic material. When designing a timber shell, this should be taken into account. This problem rises for instance when designing edge connections. As an example the hypar shell which was built for the Bundesgartenschau of 1970 in Dortmund was discussed (Figure 2.46). When using timber as membrane skin, different layers will be applied in different directions. The stresses will pass different layers of wood in different directions, so stresses parallel to the grain in one layer will be rolling stresses perpendicular to the grain in the next, which is a much weaker direction. Such detailing problems are typical for shells with a stressed timber skin. Attention has to be paid which stress is transmitted to which layer of wood and in which direction to the grain.

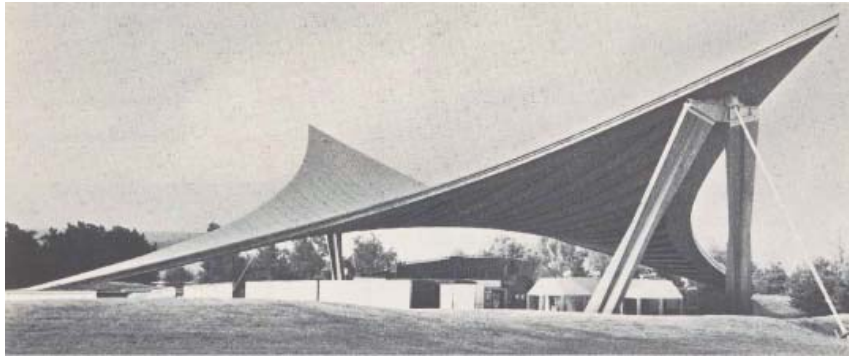


Figure 2.46: Hypar shell, Bundesgartenschau Dortmund 1970 (Holzbau Konstruktionen)

When timber is used as a membrane skin another problem arises. The swelling and shrinkage of the timber due to moisture content will cause the stressed skin to change in length. As a shell such as this hypar is statically undetermined, these changes will cause undesired stresses in the structure. This should be taken into account in the design. According to Mr. Luning, with the Dortmund hypar this movement is compensated by the flexibility of the anchor cables.

With respect to glued joints, attention has to be paid to the production process. The quality of the glued joint is dependent on this, because errors can not be corrected. Especially when gluing on site, moist, dirt and temperature are factors that should be watched closely. Another point of attention should be moist in the service state. Glued joints are not allowed to be degradable by moist so the right type of glue has to be picked for each application.

When discussing the Weald and Downland gridshell, the question rose whether the shrinkage of the green oak after construction wasn't a problem. The bolts in the nodes probably had to be re-tightened after a while.

A "new" type of wood was discussed: acetylated wood. The treatment method of acetylation has been studied as early as the 1930's. In the past twenty years this research has been intensified and only recently, the process has become economically available.

Most traditional treatment methods use toxics such as oil, arsenics, ammonia or metal compounds to impregnate the cell walls of the wood. Non-toxic methods like thermal modification change the appearance of the wood and weaken it, making the method unsuitable for most applications.

Acetylation treatment lacks all these disadvantages. The process uses acetyl, which is derived from vinegar, to physically alter the molecular structure of the wood. No toxic chemicals are used for this. The acetyl, being only made out of carbon, hydrogen and oxygen, is bonded to the free hydroxyls in the wood, which are naturally present in its structure. The research demonstrated that the physical alteration of the wood improves various material properties considerably¹⁰:

- durability: class 5 durability softwood can be improved to class 1
- dimensional stability: swelling and shrinkage is reduced to 70-80% compared to untreated wood
- Decay resistance: acetylated wood is largely fungi and insect repellent. Wood-eating insects are unable to digest acetylated wood.
- Hardness: an increase of 30% in hardness can be reached
- Retention of colour: acetylation improves the stability of wood colours when exposed to day light, ensuring consistent aesthetics

¹⁰ <http://www.titanwood.com/> accessed 06-04-2006

Furthermore the treatment has no negative impact on strength properties of the material and on the appearance. Acetylated timber can easily compete with tropical hard wood, as the durability is the same or even better. At the same time, fast growing wood such as beech can be used, which is much cheaper than tropical hard wood.

2.5.2 Heko Spanten, Ede

The company Heko Spanten in Ede (NL) is specialized in fabricating laminated timber frames, girders and columns. They are capable of creating cross sections of any desired size, straight or curved, with only transportation dimensions as limitation. Figure 2.47 shows an example project. The parts for complete projects can be pre fabricated and can be delivered ready for assembly, e.g. making slots and drilling holes can be done in the factory (Figure 2.48). Straight beams are produced in a large straight press (Figure 2.49). Curved beams are produced in a press which can be adjusted to fit the desired curvature (Figure 2.50). Also curvature perpendicular to the main direction is possible, although limited to the height of the press.



Figure 2.47: Tree centre, Baarn (NL)¹¹



Figure 2.48: Heko Spanten factory hall.



Figure 2.49: Straight laminated beam in press.



Figure 2.50: Adjustable curved press.

¹¹ http://www.bomencentrumnederland.nl/?page=hetpaviljoen_fotos accessed 06-04-2006

2.5.3 Van Drenth Buighout:

Van Drenth Buighout in Culemborg (NL) is part of Van Drenth Groep. This company fabricates curved laminated elements, mainly for the furniture industry (Figure 2.51 and Figure 2.52). Also rotary die shells are made for the packaging industry. These half circle shells are used for stanching package shapes out of large sheets of paper or cardboard.

In its factory, half fabricates are made such as back- and armrests, seats and complete chair seating. Either these can be delivered finished or unfinished for further processing such as applying furnishing.

The timber mainly used is beech which has good properties for the production process. Also other species can be used as the client desires, or different outer layers can be applied to only give a different look. The standard size of the laminates used is 2m wide and 0.7 to 4mm thick. Standard thickness is 2mm, which gives a bending radius appropriate for most applications. The maximum width is 2.6m, which is limited by the suppliers and the presses used in the factory.

The products are made by pressing stacks of laminates into moulds. First the laminates are stacked in the right order and glue is applied on every laminate (Figure 2.53). The stack is pressed into shape in its mould and heated (Figure 2.54). The result is a curved timber shell (Figure 2.55). It is possible to create a cross section of every desired thickness. This is limited by cost-effectiveness, as for large cross sections production time becomes considerable large. For every mm of thickness 1 minute of heating time is needed.

The glue used is Kaurit 325, which is urea formaldehyde resin glue, with a hardener. During pressing, heat is needed for proper bonding of the glue and laminates. Also high frequency heating is used.

For every different shape a different mould is needed. As every client wants his own different shape, this results in a lot of different moulds in stock (Figure 2.56). The moulds are made of timber mostly. Also aluminium is used for products produced in very high numbers. The production of a simple timber mould with single curvature costs approximately 2000 to 3000 euro. This is why this production technique is only cost-effective for mass production.

After pressing, the product is further processed. The desired shape is milled out of the raw product and holes are drilled by a 5 axial CNC machine, which makes it possible to approach the product from every side and under every angle. For smaller number of products, sawing, drilling and sanding is performed by hand.

There is little known about the structural value of these products. Should this technique be applied for structural elements, first the behaviour of the adhesive used should be known. If this behaviour is unsatisfactory, a different adhesive should be applied. Secondly, there is a problem of cracking. With double curved elements, cracking can occur in the layers (Figure 2.57). As the stack of laminates is pressed into its mould, the layers are not only bent, but also deformed into shape. If it is a non-structural element which is furnished later on this is not a problem. When it is a structural element, it is a problem as the cracking degrades the strength of the element. Especially for the outer layers this is a problem, as stresses due to bending are the highest in these layers. Because of the cracks, these outer layers will not act as part of the structural section anymore.



Figure 2.51: Armrests



Figure 2.52: Curved elements in stock



Figure 2.53: Glue is applied on laminates



Figure 2.54: stack of laminates¹²



Figure 2.55: End result (Van Drenth Groep)



Figure 2.56: Mould in store



Figure 2.57: Cracks in upper layer.

¹² <http://www.vandrenthgroep.nl/leaflet> accessed 04-04-2006

Timber gridshells



3.1 Introduction

As the interest in free form architecture has seen a mayor increase in the last decades, also the interest in timber gridshells increased. With a timber grid, a double curved shape can be created fairly easy, as will be explained later, and a few elegant examples of this exist today. The first large scale gridshell structure was built in 1975 in Mannheim, Germany, which is described in Section 3.3. Some 30 years later the building is still in use, an acknowledgement of the success of the structure as it was designed for only one winter and one summer (Burkhardt et al 1978). Despite the success of the Mannheim gridshell, gridshells were not used very often anymore. At universities experimental gridshells were built by students, but not on a large scale. An increase of labour costs made gridshells only less popular, as the construction process is rather labour intensive, and so was the design process.

The process of designing and form finding a gridshell is not straight forward (Harris & Kelly, 2002). An iterative process is needed to find a smooth surface which is possible to create from a flat mat of laths. In this design process, mayor developments took place in the past few decades. As computer aided design methods improved dramatically it became possible to use the computer in this iterative design process. 25 years after the construction of the Mannheim gridshell, computer technology helped developing the gridshell at the Weald and Downland open air Museum in Sussex, UK (see Section 3.3.2). Also the latest construction and gluing techniques were used in the construction process. The Weald and Downland gridshell is a perfect example of what is possible in timber gridshells with today's modern technologies. Also from the point of view of sustainability the structure can be seen as an example. Use of material is minimized by using a shell and timber is a sustainable material which can be obtained from environmentally sustainable sources.

The benefit of timber gridshells becomes apparent in the construction stage. Complex forms can be shaped relatively easy (Harris & Kelly, 2002). This is achieved by laying out a flat mat of continuous timber laths in two directions. After connecting the laths at the intersections using a pin connection, the grid can be deformed by bending the laths and deforming the quadrangles of the maze into rhombic shapes. If the required shape is reached, the laths are fixed to the edge boundaries and the nodes are tightened. To keep construction easy, this method can only be used with a material which is light, can be bent without too much effort and has enough capacity to resist the loads after construction. Here, the properties of timber are taken full advantage of, as timber is a light weight material and can be bent relatively easy, with enough strength to resist loads and bending moments.

With use of modern technologies, the gridshell has become an efficient and environmentally sustainable structure. Despite this, there seems to be a reluctance to use it more often. Possible reason could be that the design process is considered complicated. The gridshells that have been built were designed on basis of experience and with time consuming design processes. Other possible reason could be that difficulties are encountered in forming the double curved shape from an initial flat mat of laths (Kelly et al, 2001). If the possibilities and advantages of a gridshell are unknown, a more conventional structure is quickly chosen.

In this chapter the principles of the gridshell will be investigated. First the structural principles of the gridshell will be explained in Section 3.2. The topics shell behaviour, stiffness and strength will be analysed and the bending behaviour of a gridshell element will be investigated by determining the method to calculate the maximum bending and torsion stresses. To learn from existing buildings, Section 3.3 displays examples of existing gridshells. In these examples, the characteristics of each gridshell will be displayed, as well as design and construction methods. The gridshells will be compared by their characteristics in Section 3.4.

3.2 Structural principles of the gridshell

The gridshell structural system is based on the use of continuous laths which are pinned at their intersections. From an initial flat mat of laths, the structure is shaped by bending the laths and deforming the mat by deforming the quadrangles of the mat to rhombic shapes (Figure 3.1). After the shape is formed, the nodes are tightened and the structure is stiffened by diagonal bracing.

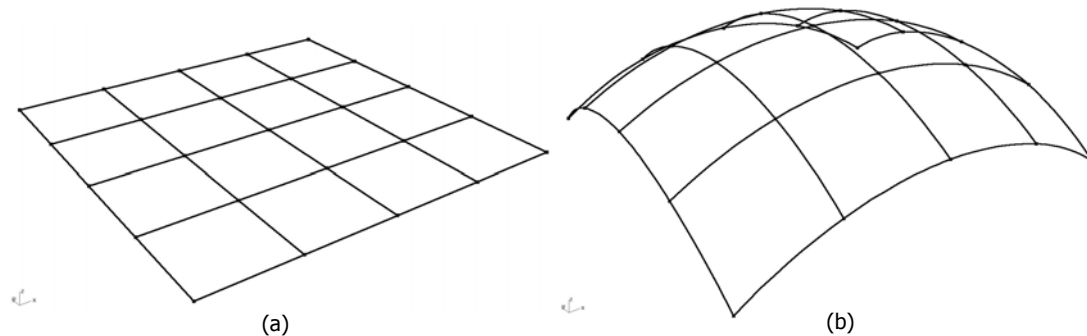


Figure 3.1: A flat mat of laths (a) is deformed to a spherical structure (b), by bending the laths and deforming the quadrangles of the mat to rhombic shapes.

This building method creates a rather complex structural system of bent laths working together to resist loads. The general behaviour of the system is analysed in this section. First shell behaviour is analysed. In Section 3.2.2 the structural strength and stiffness is analysed. After this the moment capacity of the laths is reviewed in Section 3.2.3. In Section 3.2.4 it is determined how the stresses in an element can be determined by using the curve angle of a member, and how these stresses should be checked on ultimate stress criteria.

3.2.1 Shell action

The definition gridshell suggests that is a gridshell structure is in fact a shell. This is incorrect as will be explained here. For a continuous shell a distributed load results in shear and normal stresses (Figure 3.2), as explained in Section 2.3.2. This creates a rather rigid system as every element of the continuous surface is locked in by the internal stresses and transfers these to the neighbouring elements.

With a gridshell, one could say shell behaviour is imitated by the system of continuous members. For a gridshell, the continuous layer is discretized by transferring all material of the shell element into the edges. The result is a system of four laths joined in the nodes, which can only transmit forces in the direction of the laths and can resist out of plane bending. The (distributed) normal stress in the continuous shell element is transferred to the edges too, which results in normal forces on the laths (Figure 3.3). The normal stresses that are present in the shell element are now accounted for.

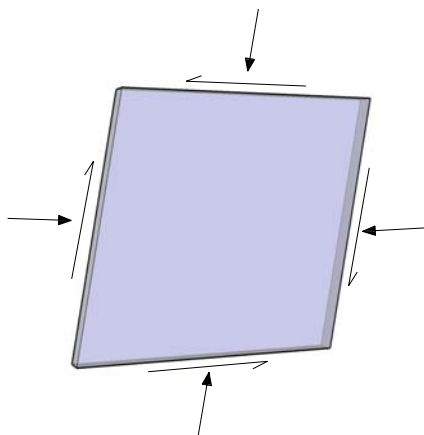


Figure 3.2: Continuous and gridshell elements

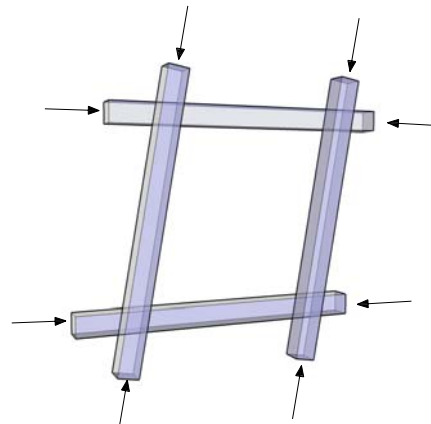


Figure 3.3: Gridshell element with normal forces

Without additional measures, a gridshell structure can be seen as a series of slender parallel arches, which work together to resist the applied loads. When shell action is desired the shear forces that were present in the shell element should be accounted for by the gridshell element. By linking the laths diagonally, diagonal stiffness is introduced in the gridshell and the shear forces can be transmitted from one edge of the gridshell element to the opposite one. The laths will work together and the gridshell will perform more as a continuous shell.

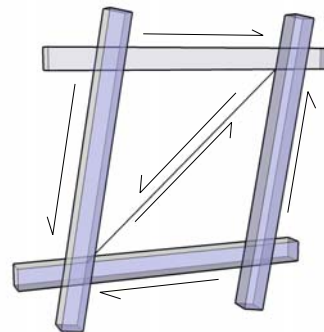


Figure 3.4: Gridshell element with diagonal bracing

Diagonal stiffness can be provided in several ways:

- Rigid joints
- Cross ties
- Rigid cross bracing
- A continuous layer

Triangulation of the grid, either by applying cross ties or bracings is realized quite easy. By applying rigid bracings, the structural behaviour of the grid would be comparable with a continuous shell. It is also possible to create diagonal stiffness by applying a continuous layer on top of the laths of the structure. This provides structural stiffness and cladding of the structure in the meantime. Bracing with cross ties leaves the option to vary the diagonal stiffness by altering the pre stress, thickness or the material of the ties (Burkhardt et al 1978).

Diagonal stiffness provided by rigid joints is less easy to realize. Rigid connections transfer shear forces through bending moment to the supports. This can be achieved either with connectors or gluing of the joints. Timber connectors such as dowel type fasteners or connector plates always have a certain rotation capacity which decreases the moment resistance and thus the stiffness of the structure. Gluing can provide good moment connection, but complicates the construction process as gluing conditions have to be optimized to guarantee the quality of the joint.

3.2.2 Stiffness and strength of the gridshell

As stated in the previous section, diagonal bracing is needed to provide diagonal stiffness to the structure. If diagonal bracing is omitted, the gridshell is a series of slender arches, resisting a load together. When this is compared with a continuous shell, a load on such structure can be transmitted to the supports in a direct line to the supports, which keeps deflections small. With a gridshell, the load cannot be transmitted directly but activates the laths, which deflect to a position in which there is equilibrium of forces (Happold & Liddell 1975). The load is transmitted through normal forces and bending moments.

When a gridshell is left unbraced the stiffness of the structure depends on the ability of the laths to deflect to an equilibrium position and thus on the stiffness of the laths. The ultimate deflection capacity is dependent on the ultimate moment capacity of the material used. This ultimate moment capacity is dependent on ultimate stress level f_u of the material. When elastic behaviour is assumed, the material collapses as f_u is exceeded. In a pin supported curved element an asymmetric load results in a combination of normal and bending stresses. The combination of these stresses determines the actual stress level. Due to normal force F_N the normal stress level is σ_n . The bending stresses σ_m due to moment M can increase until f_u is reached (Figure 3.5). This increase is the moment capacity. As the normal load increases, less stress capacity is left and the moment capacity of the cross section decreases.

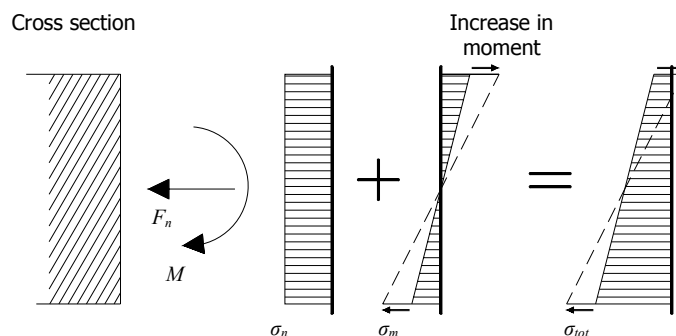


Figure 3.5: Combination of normal and bending stress; $\sigma_n + \sigma_m \leq f_u$

When the laths in a gridshell are already loaded by a high compressive load, little stress capacity is left for the structure to resist moment stress, i.e. deflect to equilibrium. This behaviour can be seen as a decrease of structural stiffness and is typical for compression structures. In contrast with this, tension structures only stiffen as loads are increased (Burkhardt et al 1978). Figure 3.6 shows the load-deflection curve of a continuous shell, a

gridshell and a tension net under disturbance load. The continuous shell has a much higher collapse load than the gridshell. As stated before, in a continuous shell the normal forces can be transmitted through the entire surface instead of just a few laths. An increase of load has less effect on the stress distribution and therefore the ultimate load capacity is higher.

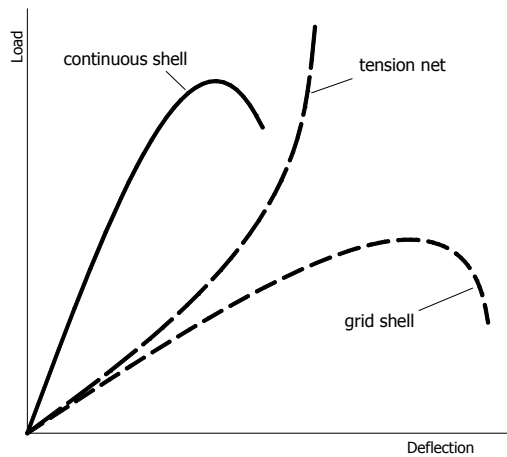


Figure 3.6: load-deflection diagram (Burkhardt et al 1978)

3.2.3 Moment capacity of the cross section

In Section 3.2.2 it was found that the load resistance of a gridshell is dependent on the moment capacity of the cross section of the grid. The out-of-plane moment capacity can be improved greatly by increasing the moment of inertia (I) of the members. This can be established by increasing the height of the structural members. Applying one or more additional layers of laths in each direction is an effective method to do this. Installing shear blocks between the layers will provide composite action of the layers, which will further increase I .

The disadvantage of applying a double layer of laths is that it complicates the construction process. On top of the scissoring of the laths, the laths of the outer layer must be able to slip relative to the laths of the inner layer when the laths are bent into shape. Figure 3.7 shows this slip for two laths of equal length. Of course this movement must also be possible in the joints. To be able to tolerate these two movements, the joints need to be very loosely connected during construction. If tightened too much, twisting and bending of the laths can prevent the layers from slipping and scissoring, which could result in breakage of the laths. With the Mannheim gridshell and the Weald & Downland gridshell different solutions for this problem are used, which will be discussed in Section 3.3.1.4 and 3.3.2.5 respectively.

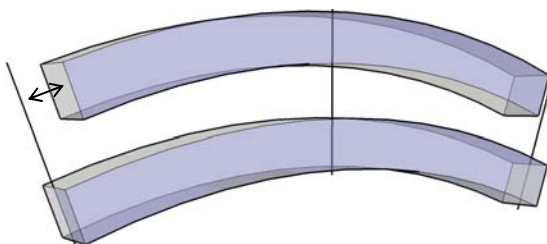


Figure 3.7: Slip of the laths. Two laths of equal length are bent to the same radius. Fixed in the middle, the outer edges move relative to each other.

3.2.4 Bending behaviour of an element

The shape of a gridshell is created by applying a large deflection to the system of laths. The laths are bent and twisted to shape the mat of laths to the desired shape. The possibility to bend and twist makes it possible to create this shape, but also puts restrictions on the shape. The laths can only bend to a curvature in which the ultimate stress level is reached. In this section, it is explained how the maximum curvature and torsion angle can be determined. First the maximum curvature is calculated using the ultimate bending stress of a material in Section 3.2.4.1. Next, in Section 3.2.4.2 the design bending stress which should be used for design purposes is modified using Eurocode5. Section 3.2.4.3 reviews the maximum torsion angle. Finally, the combinations of stresses occurring in a bent and twisted member are investigated.

3.2.4.1 Maximum curvature

The maximum curvature of a timber member depends on the maximum bending strength f_m and the modulus of elasticity E_θ . An increasing f_m leads to a decreasing bending radius. A stronger piece of timber can be bent further prior to failure than a weaker piece, but a larger bending strength also implies a larger modulus of elasticity. This means the bending radius does not decrease proportionally to the increase of moment, e.g. a larger moment or force is needed to bend a strong piece of timber to the same radius of a weaker one. This can be reviewed using simple mechanical analysis.

To analyse bending behaviour, a segment of a member shown in Figure 3.8 is considered. The member is subjected to a bending moment, which results in internal stresses and a bending curvature.

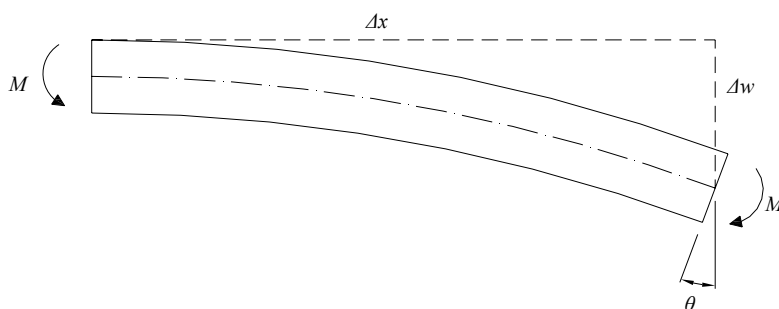


Figure 3.8: Bending member

The bending moment due to the curvature can be calculated as:

$$M = EI\kappa \quad (3.1)$$

Where

$$I = \frac{1}{12}bh^3 \quad (3.2)$$

and

$$\kappa = \frac{1}{R} \quad (3.3)$$

With:

- M = bending moment;
- E = modulus of elasticity;
- I = moment of inertia;
- κ = curvature of the beam;
- b = width of the member;
- h = height of the member;
- R = radius of curvature.

The bending stress in the outer fibres of a member can be calculated with:

$$\sigma_m = \frac{M}{W} = \frac{M}{\frac{1}{6}bh^2} \quad (3.4)$$

With:

- σ_m = bending stress;
- W = moment of resistance.

The formula above can now be rewritten as:

$$\frac{\frac{1}{12}Ebh^3}{R} = \frac{1}{6}bh^2\sigma_m \quad (3.5)$$

Replacing σ_m by the maximum bending stress of the material f_b , this leads to:

$$R_{\max} = \frac{Eh}{2f_m} \quad (3.6)$$

The maximum bending radius of a timber member is thus dependent on the maximum bending stress of the material and its moment of elasticity. When a high curvature is desired, e.g. a small bending radius, timber with a small E/f_m ratio should be selected. This can be achieved by selecting the timber with the desired properties by strength grading. For example, in the Weald and Downland gridshell oak was used, which has a low E/f_m ratio by nature. Also a high timber grade was achieved by selecting timber by strict requirements such as limiting grain slope and avoiding knots (Harris & Kelly 2002) (see Section 3.3.2.4)

The derivation made above can be found more extensively in Appendix 1: Determination of the maximum bending radius. Also an analysis of the maximum bending radius related to the strength class material properties can be found here.

For design purposes, the design value of the ultimate stress capacity should be used. The design bending strength value can be determined according to Eurocode5 with:

$$f_{m,d} = \frac{k_{mod} f_{m,k}}{\gamma_M} \quad (3.7)$$

Where:

- $f_{m,k}$ = the characteristic bending strength
- k_{mod} = the modification factor which takes into account the influence of load duration, service class and material type
- γ_m = the partial factor for material properties

Values for k_{mod} and γ_m can be found in Eurocode5. The bending stress due to the construction process can be seen as a medium term load (1 week to 6 months). For medium term loads $k_{mod} = 0.8$ can be used. For the partial factor for material properties, $\gamma_m = 1.3$ is recommended for solid timber.

3.2.4.2 Curved timber and moment capacity

Curving a beam induces bending stresses in the material. The distribution of these stresses in a curved or tapered beam is non-linear (Blass et al, 1995). This has an effect on the maximum bending stress and should be taken into account when designing such a beam. Additionally the bending stress causes radial stresses perpendicular to the grain.

For design purposes, the maximum bending stress of a curved beam can be calculated approximately with simple bending theory, modifying M/W with a shape factor k_r , which depends on the ratio between the height of the cross section and the radius of curvature. This factor takes into account the strength reduction due to bending of the laminates during production (Blumer, 1975, 1979 referenced in Blass et al, 1995). This also can be found in Eurocode5 part 1-1, Section 6.4.3. According to the Eurocode this theory applies for glued laminated timber and LVL only. The theory is based on the theory of thin anisotropic plates, taking into account the influence of stresses perpendicular to the grain. It is not known if taking this influence into account gives correct results when members that are not built up out of thin layers are concerned, but are strongly curved. However with a gridshell the effect of a non-linear stress distribution is present due to the strong curvature in combination of bending stresses. Therefore the factor k_r is still applied to take into account this effect.

The non-linear bending stress distribution can be illustrated by a small section in bending. Based on Navier's theory of elasticity, the strain of the outer fibres of a curved beam is smaller than the strain of the inner fibres. To regain equilibrium of forces the neutral line has to shift down and according to Hooke's law and the maximum bending stress $|\sigma_o|$ in the outer fibres is smaller than the maximum bending stress in the inner fibres $|\sigma_i|$. (Blass, 1995).

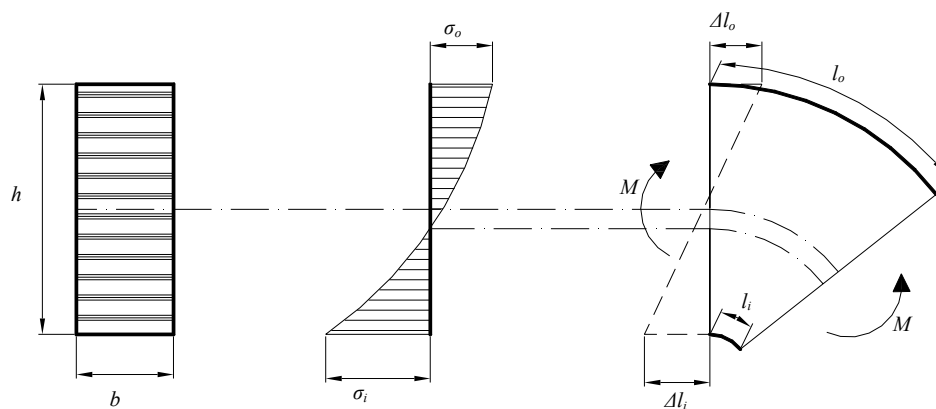


Figure 3.9: Distribution of bending stresses in a curved beam (Blass et al, 1995)

According to Eurocode5 the design bending stress in the apex zone of the curved beam (Figure 3.10) should be calculated by:

$$\sigma_{m,d} = k_l \frac{6M_{ap,d}}{bh_{ap}^2} \quad (3.8)$$

With:

$$k_l = k_1 + k_2 \left(\frac{h_{ap}}{R} \right) + k_3 \left(\frac{h_{ap}}{R} \right)^2 + k_4 \left(\frac{h_{ap}}{R} \right)^3 \quad (3.9)$$

$\sigma_{m,d}$ = the design bending stress;
 $M_{ap,d}$ = the design moment in the apex zone
 h_{ap} = height of the beam in the apex zone
 b = width of the beam

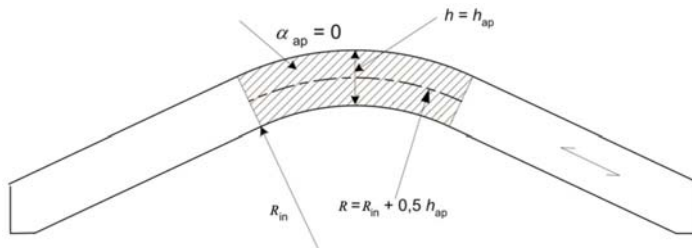


Figure 3.10: Curved beam with its apex zone (Eurocode5)

Factors k_1 to k_4 depend on α_{ap} , which is the angle of taper in the beam. This angle is zero in case of a curved beam. The factors become:

$$\begin{aligned} k_1 &= 1 \\ k_2 &= 0.35 \\ k_3 &= 0.6 \\ k_4 &= 6 \end{aligned}$$

For a beam of 50x50mm bent to the maximum curvature, the factor k_l is 1.0013. When $h_{ap} \ll r$ the influence of the curvature on the design bending strength becomes small. The effect is therefore neglected in this thesis. Also the additional stress perpendicular to the grain is related to the angle of curvature and can be neglected due to the small factor h_{ap}/r .

For verification of the failure condition of bending, Eurocode5 also applies a reduction factor k_r to take into account the bending stresses in the laminates of curved glued laminated timber due to production. A curved glued laminated beam is produced by bending the laminates and then gluing them together. The stresses due to this bending reduce in time due to plastic deformation and relaxation, but still have to be taken into account when verifying the failure condition. By applying the reduction factor it is recognized that the laminates are in a stressed condition, but these stresses are not equal to the full stress induced in the production process (Harris, R., pers. comm., 22 dec. 2006). This effect also counts for the laths of a gridshell, where relaxation reduces the bending stresses which were caused by bending in the formation process. By applying factor k_r these reduced bending stresses can be taken into account.

The failure condition due to bending can now be verified with:

$$\sigma_{m,d} \leq k_r f_{m,d} \quad (3.10)$$

With:

$$k_r = \begin{cases} 1 & \text{for } \frac{R_{in}}{t} \geq 240 \\ 0.76 + 0.001 \frac{R_{in}}{t} & \text{for } \frac{R_{in}}{t} < 240 \end{cases} \quad (3.11)$$

$\sigma_{m,d}$ = the design bending stress
 $f_{m,d}$ = the design bending strength
 t = the design bending stress
 R_{in} = the inside radius of a beam

When a lath of 10m in length and a cross section of 50x50mm and timber grade D30 is considered and this lath is bent to its minimum bending radius k_r becomes:

$$R = c * h = 167 * 50 = 8350$$

(for values of constant c , see Appendix 1: Determination of the maximum bending radius)

$$\frac{R_{in}}{t} = \frac{8350 - 25}{50} = 166.5 < 240$$

$$k_r = 0.76 + 0.001 \frac{R_{in}}{t} = 0.9265$$

3.2.4.3 Torsion

The maximum torsion stresses occur in the middle of the edges of a member. According to Eurocode5 the following expression needs to be satisfied:

$$\tau_{tor,d} \leq k_{shape} f_{v,d} \quad (3.12)$$

With

$$k_{shape} = \min \begin{cases} 1 + 0.15 \frac{h}{b} \\ 2.0 \end{cases} \quad \text{for rectangular cross sections}$$

- $\tau_{tor,d}$ = the design torsion stress;
- $f_{v,d}$ = the design shear strength;
- k_{shape} = factor depending on the shape of the cross section;
- h = the larger cross-sectional dimension;
- b = the smaller cross-sectional dimension.

A general formula for the maximum torsion stress and torsion angle for a circular rod is:

$$\tau_{max} = \frac{Tz}{I_p} \quad (3.13)$$

And

$$\theta_t = \frac{Tl}{KG} \quad (3.14)$$

With

- T = the torsion moment
- I_p = the polar moment of inertia
- G = the shear modulus
- l = the length of the member
- θ_t = the angle of torsion

According to Young and Budynas (2002) these formula can be modified to calculate the maximum torsion moment and torsion angle in a member with a solid rectangular cross section (Figure 3.11). This maximum stress occurs at the midpoint of each side. With the modifications τ_{max} and θ_t can be calculated with:

$$\tau_{\max} = \frac{3T}{8ab^2} \left[1 + 0.6095 \left(\frac{b}{a} \right) + 0.8865 \left(\frac{b}{a} \right)^2 - 1.8023 \left(\frac{b}{a} \right)^3 + 0.9100 \left(\frac{b}{a} \right)^4 \right] \quad (3.15)$$

for $a \geq b$

$$\theta_t = \frac{Tl}{KG} \quad (3.16)$$

With:

$$K = ab^3 \left[\frac{16}{3} - 3.36 \frac{b}{a} \left(1 - \frac{b^4}{12a^4} \right) \right]$$

for $a \geq b$

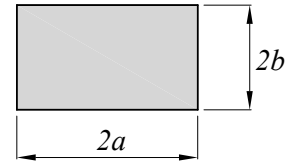


Figure 3.11: Rectangular cross section

The maximum shear strength f_v can be used in equation 3.15 to calculate a maximum torsion moment T . This can then be used to calculate the maximum torsion angle $\theta_{t,\max}$ with equation 3.16.

3.2.4.4 Combination of stresses

When a gridshell is bent in shape, the laths are subjected to bending moment in two directions, torsion and shear forces in two directions. This deformation can be seen as an ultimate limit state deformation, as these stresses are present in the shaping process as a maximum. After construction, relaxation of the timber takes place and part of the formation stresses will disappear. It is estimated that the formation stresses will decrease to 0,5 of the initial stress level. This half will remain present in the material as a residual stress level. It is needed to take this residual stresses into account in structural analysis.

To check the stress combination in the construction phase for failure conditions, a criterion which combines all stress combinations is desired. Guidelines exist for only for certain combinations of stresses. A criterion for the combination of stresses in a gridshell is set-up here using existing combination criteria.

First, the available stress combination criteria available are stated.

According to Eurocode5 a member bent in two directions in ultimate limit state should satisfy the following condition:

$$\frac{\sigma_{m,y,d}}{f_{m,y,d}} + k_m \frac{\sigma_{m,z,d}}{f_{m,z,d}} \leq 1 \quad (3.17)$$

$$k_m \frac{\sigma_{m,y,d}}{f_{m,y,d}} + \frac{\sigma_{m,z,d}}{f_{m,z,d}} \leq 1 \quad (3.18)$$

With:

k_m = factor which makes allowance for re-distribution of stresses and the effect of inhomogeneities of the material in a cross section. For solid timber, glued laminated timber and LVL, k_m is 0,7 for rectangular sections.

$\sigma_{m,y/z,d}$ = the design bending stress in the y or z direction;

$f_{m,y/z,d}$ = the design bending strength in the y or z direction.

These criteria are valid for cases without buckling or tilting. It is assumed that no buckling or tilting occurs, as elements in a grid shell are relatively short (0,5-1m) The criteria for the combination of bending and tension or compression can be stated as:

$$\frac{\sigma_{t/c,0,d}}{f_{t/c,0,d}} + \frac{\sigma_{m,y,d}}{f_{m,y,d}} + k_m \frac{\sigma_{m,z,d}}{f_{m,z,d}} \leq 1 \quad (3.19)$$

$$\frac{\sigma_{t/c,0,d}}{f_{t/c,0,d}} + k_m \frac{\sigma_{m,y,d}}{f_{m,y,d}} + \frac{\sigma_{m,z,d}}{f_{m,z,d}} \leq 1 \quad (3.20)$$

With:

$\sigma_{c/t,0,d}$ = the design compression/tension stress parallel to the grain;

$f_{c/t,0,d}$ = the design compression/tension strength parallel to the grain.

Eurocode5 does not provide guidance for the combination of shear and torsion stresses. The following criterion is given by Möhler and Hemmer (1977, cit. Blass et al (1995)):

$$\frac{\tau_{tor,d}}{f_{tor,d}} + \left(\frac{\tau_{xy,d}}{f_{v,d}} \right)^2 \leq 1 \quad (3.21)$$

With:

$\tau_{xy,d}$ = the design shear stress;

Furthermore, timber can be checked on a combination of stresses with the stress criterion of Norris (1964, cit. Van de Kuilen & De Vries, 2005)

$$\left(\frac{\sigma_{m,d}}{f_{m,d}} \right)^2 + \left(\frac{\tau_{v,d}}{f_{v,d}} \right)^2 + \left(\frac{\sigma_{c/t,90,d}}{f_{c/t,90,d}} \right)^2 \leq 1 \quad (3.22)$$

Where:

$\sigma_{c/t,90,d}$ = the design compression/tension stress perpendicular to the grain;

$f_{c/t,90,d}$ = the design compression/tension strength perpendicular to the grain.

The last part of this formula takes into account the stress perpendicular to the grain for timber sawn angular to the grain. This is not the case in a gridshell and can be left out.

Based on the criterion on Norris, the following criterion for the combination of bending, shear/torsion and tension/compression can be stated:

$$\left(\frac{\sigma_{m,d}}{f_{m,d}} \right)^2 + \left(\frac{\tau_{v,d}}{f_{v,d}} \right)^2 + \left(\frac{\sigma_{c/t,0,d}}{f_{c/t,0,d}} \right)^2 \leq 1 \quad (3.23)$$

in which:

$$\sigma_{m,d} = \sigma_{m,y,d} + \sigma_{m,z,d}$$

$$\tau_{v,d} = \tau_{xy,d} + \tau_{tor,d}$$

This criterion is quite conservative, because reduction factors have been left out. However, the timber needs to have enough stress capacity for resisting different loads during the lifetime of the building, on top of the (diminished) stresses resulting from the formation process. For a first analysis, the criterion gives a satisfying approximation. Further investigation is desired to determine if a more accurate criterion can be used.

3.3 Gridshell example projects

3.3.1 Multihalle Mannheim

3.3.1.1 Background

Every two years a garden exhibition is held in one of the major cities in the Federal Republic of Germany. In 1970 it was decided that this Bundesgartenschau of 1975 was to be held in Mannheim (Happold & Liddell 1975). A master plan was developed for the area of Herzogenried park, where the festivities would take place. The plan included a large covered space, where a variety of activities could take place. The winning design for this space was the gridshell of Frei Otto and Ove Arup & Partners as structural engineers. Otto, famous for his structures of tension nets, uses hanging models for his designs. Also the Multihalle of Mannheim was designed with hanging models.

The complex consists of a multi-purpose hall, where a range of activities can take place, such as exhibitions, flower shows, entertainment, concerts, theatre, sports activities, etc. In a second smaller hall a restaurant is situated. The halls are connected by a covered link. Figure 3.12 shows an aerial view of the complex. Figure 3.13 shows an inside picture (Burkhardt et al 1978)



Figure 3.12: Aerial view of the Multihalle (Burkhardt et al 1978)



Figure 3.13: Inside view of the Multihalle (Burkhardt et al 1978)

3.3.1.2 The roof

The Multihalle lies as an artificial hill in its surroundings. The gridshell is designed in such way that the shape continues the hilly landscape of the garden. The enclosed building area of 3600 m² is air conditioned and it is covered with PVC coated fabric. The grid has a maximum longitudinal span of 85m. It is built up out of a double layered mat of laths of Hemlock Pine. This performed best in test with respect to shrinkage and creep. It was also selected for its straight grain and availability in long lengths. The laths have a cross section of 50x50mm and are spaced on 500mm. Approximately 72000m of lath was used to construct the shell. The grid is supported by four different edge supports: concrete foundations, cables, laminated timber beams and arches. Diagonal stability is improved by applying cross ties. Pairs of 6mm cables are spaced at 4,5m in both directions.

After completion the roof was tested by loading it to 1,7 times the design load. This was applied by hanging dust bins filled with 90 l. of water on every ninth node. Deflections stayed well under the calculated deflection, proving the gridshell a safe structure.

3.3.1.3 Structural modelling and analysis

Physical modelling

The initial form finding of the gridshell was entirely performed with physical modelling. At first, a wire model was made of the preliminary design. A second hanging model was made using the system line of the structure, to determine the initial data on node coordinates (Figure 3.14). This model had to be very accurate as an error will be enlarged when transferring the data on a full scale construction. Other methods of form finding, i.e. drawing and computing the coordinates were considered, but these appeared not to be better. To correctly compute the coordinates, input data was needed on form behaviour of the grid, but this was not available. Also the number of iterative steps to calculate the coordinates would be numerous and time consuming.

The model was made of rings and links (Figure 3.15). Although these were machine manufactured, the sizes of the elements were not exact, due to tolerances in the manufacturing process and wearing of the tools, so it was impossible to rule out all imperfections. One of every 3 laths was modelled. In the model a mesh was used of 15mm, which represented 1,5m in the full scale structure. The intermediate nodes would be interpolated afterwards. The model was set up on a marble plate, so inaccuracies due to shrinkage or distortion of the base of the model was ruled out.

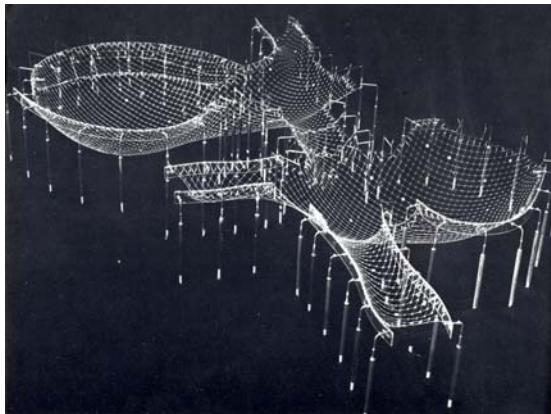


Figure 3.14: Hanging model (Burkhardt et al 1978)

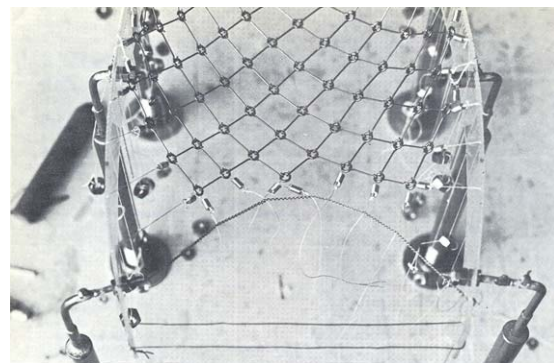


Figure 3.15: Detail of the model (Burkhardt et al 1978)

Computer form finding

The coordinates of the nodes were determined by taking stereo photographs of the model. With these coordinates, the structure could be analysed by computer calculations. Because of inaccuracies of the model, not all members of the hanging model were in tension. To correct this, the correct geometry was calculated using the force density method. The intermediate results of the iterative steps were analysed. Deviations of a medium force smaller than 15% were considered non critical. When larger deviations occurred, adjustments were made in geometry. From this calculated suspended net, the data needed for production and erection was derived (Burkhardt et al 1978).

Structural analysis

When Ove Arup & Partners started with their designs, very little reference material was available. Only three much smaller gridshells were built before. Initial studies were performed to determine the design load and hand calculations on shell buckling were made. Structural design was started before the final geometry was finished. To gain knowledge on behaviour of gridshells, tests on a working model of the Essen gridshell were executed. The results showed that lath size had to be increased to enhance buckling resistance, to 100x100mm. This would give problems however with forming the shell, as more force is needed to bend the laths with a bigger cross section. Also the contract was already let and a lath size of 50x50mm was agreed. Decided was to apply a double layered mat, so bending flexibility was maintained during construction. After applying shear blocks between the layers, sufficient out of plane bending strength will be provided.

Design loading was determined by using wind and snowfall records in the area and by wind tunnel testing on a 1:200 scale model. This way, the design could be fully optimized, instead of just using normative average loading values. Also tests were carried out on the nodes and to investigate stress relaxation of the timber.

To determine a collapse load, tests were executed on a model of the gridshell. To correctly model the full size structure, dimensional analysis was used, which means scaling the factors that govern the behaviour of the physical system. Perspex members were used to model the grid. One model member represented six double layer members on full scale (Figure 3.16). The model was tested by hanging 100mm nails on the nodes and dial gauges were used to measure the deflections (Figure 3.17).

The test results were compared with the results of computer calculations. The collapse load determined by the tests was $2,8 \text{ kN/m}^2$. The calculations gave a value slightly over 1 kN/m^2 . This difference occurs because the model does not scale the shear deformation of the full scale structure. This shear resistance is largely controlled by the individual slip per unit of force of the joints. The Perspex model corresponds to a full size structure with a very high value of joint stiffness, thus resulting in a high collapse load.

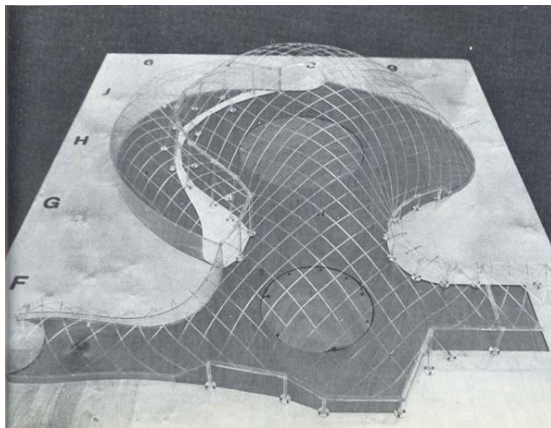


Figure 3.16: Test model (Burkhardt et al 1978)

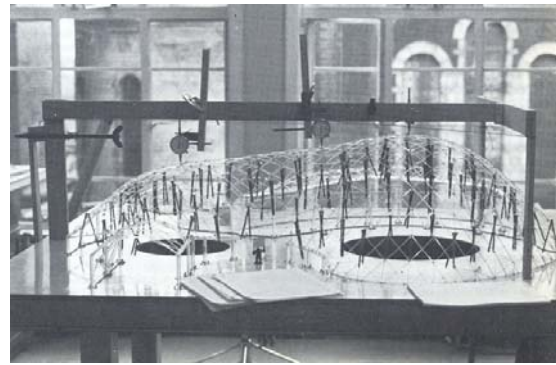


Figure 3.17: Tests on the model (Burkhardt et al 1978)

3.3.1.4 Connection details

Typical node joint

The laths are bolted together in the nodes. To provide slipping of the outer layers during erection, these layers have slotted holes. After erection, shear resistance is needed, so the bolts are tightened to provide sufficient friction. Testing indicated that tension in the bolts would decrease in time, due to shrinkage of the timber. To prevent this, spring washers are applied (Figure 3.18 and Figure 3.19).

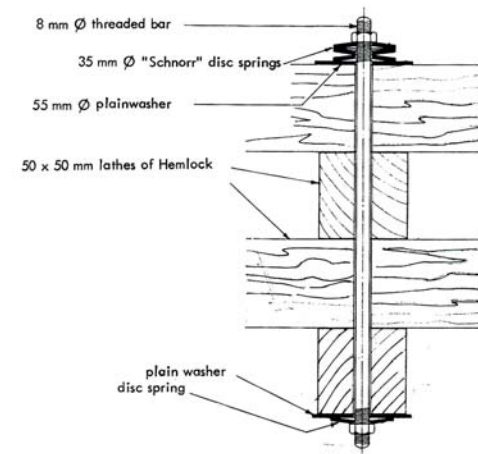


Figure 3.18: Typical node joint (Burkhardt et al 1978)



Figure 3.19: Photo of a typical node joint¹³

Joints in the laths

The laths are prefabricated into laths up to 40m by finger jointing. The joints used were 20mm with a 6mm root, to suit the machines of the factory. Quite a lot of joints broke during site handling and erection due to this short connection length. The laths were repaired by nailing 50x25mm lapping pieces to each side. This was also used to lengthen the laths into the required length.

Boundary connections

Four types of edge connections are used in the Multihalle (Figure 3.20). Originally, Frei Otto designed all boundaries on columns as cable edges. Cable edge supports are possible where boundary forces are more or less constant and where the change in angle of the boundary system line at the column is not so large that excessive support reactions are caused. These conditions were only met at parts of the restaurant. To connect the gridshell to the cable, it is first connected to a plywood board. This board also helps to cope with the differences in distributed lath forces and the cable reaction force. At the columns the cables are brought together (Figure 3.21).

Where cable supports could not be applied, edge beams are used. 60x500mm laminated timber beams are connected on either side of the grid. The laths are bolted to these beams. Also where the grid is connected to the concrete support, it is first connected to timber beams.

The timber beams are connected to the steel columns with steel plates. These plates are bolted to the beams and welded to the columns (Figure 3.23). The connection itself was simple, but the geometry was not as for every connection the angles were different. The cutting profile for the plates had to be determined accurately to provide production drawings. A special computer program was written for this task. Also the production drawings for the arches were produced by a specially written computer program.

At the valley between the Banana and the Multihalle a laminated timber beam is applied with a circular section. Steel connectors connect the grid to the valley beam (Figure 3.22).

¹³ http://www.kunst.uni-stuttgart.de/wendland/progetti/mannheim/mannheim_img accessed 20-01-2006

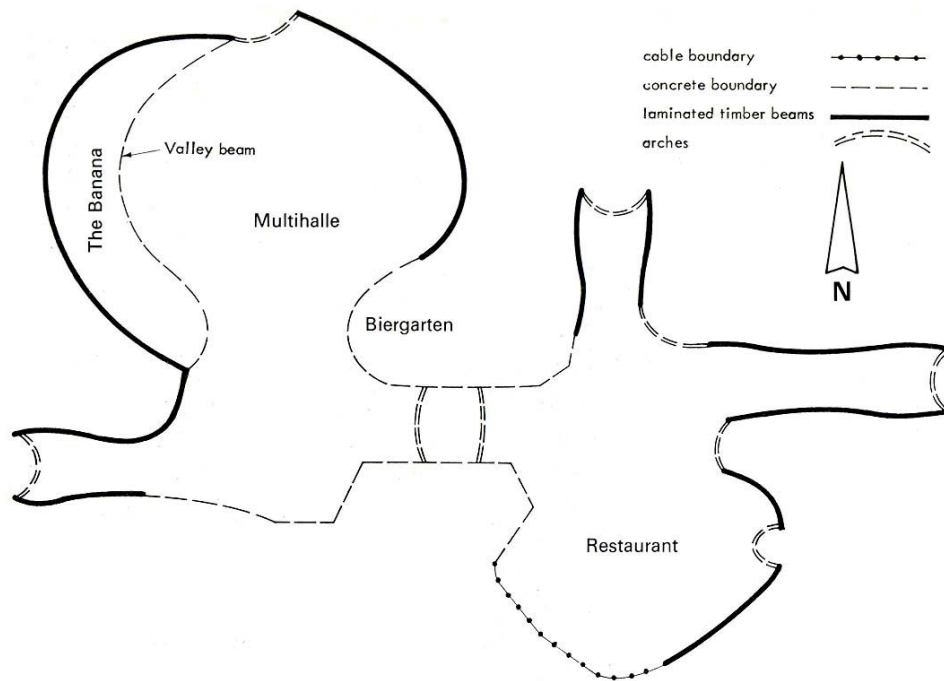


Figure 3.20: Edge layout (Burkhardt et al 1978)

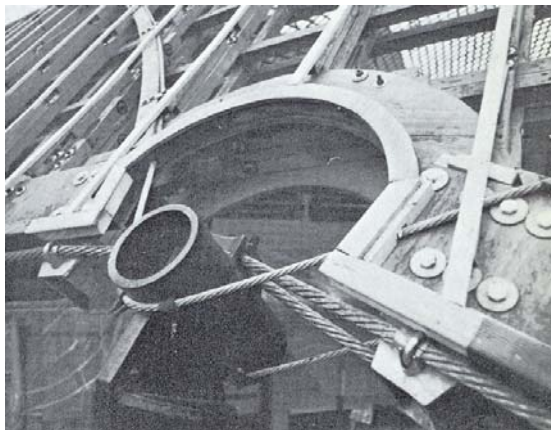


Figure 3.21: Cable edge connection (Burkhardt et al 1978)

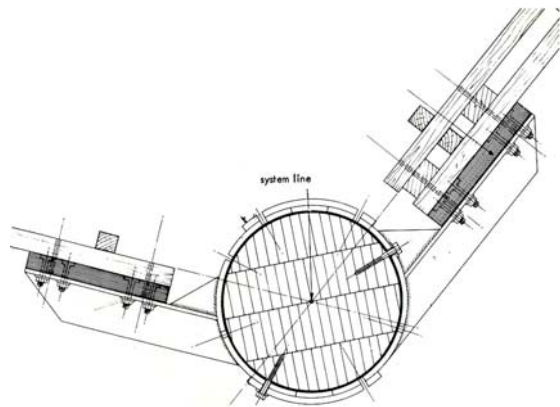


Figure 3.22: Valley beam connection (Burkhardt et al 1978)

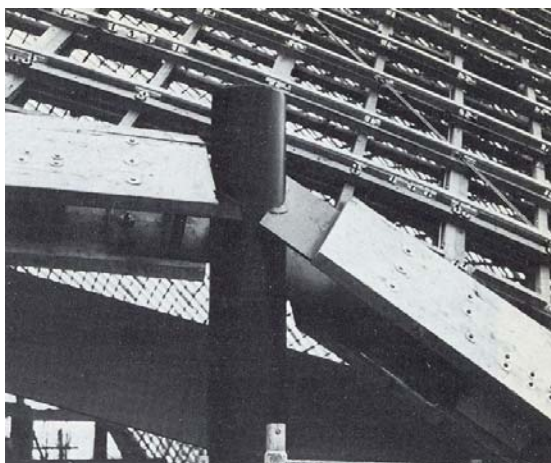


Figure 3.23: Edge column connection (Burkhardt et al 1978)

3.3.1.5 Assembly

As with the Essen gridshell, the Mannheim grid was supposed to be lifted into shape by cranes. Calculations however, showed that four 200 tonnes cranes were needed over a period of three weeks. The high costs of this forced the contractors to think of other options. Finally, the gridshell was erected by pushing up the lattice from underneath. Fork lifts were used to lift the scaffolding towers (Figure 3.25). By using these, the horizontal movement of the scaffolds as the shape of the lattice changed could be followed easily. To spread the forces on the grid, H-shaped timber spreaders were used. A ball joint between the scaffold and spreader provided rotation to fit the curve of the shell. To reduce costs, as few scaffolds as possible were used. This resulted in quiet long spans between the scaffolds. To eliminate low areas between the scaffolds, flying struts were used (Figure 3.26).

The PVC coated fabric is applied and fitted to the structure on site (Figure 3.27). It is made of sheets of the fabric, hot welded together, and attached to the grid with over 400.000 staples.

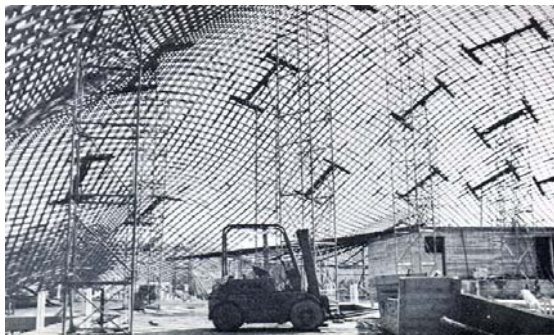


Figure 3.24: Under construction (Burkhardt et al 1978)

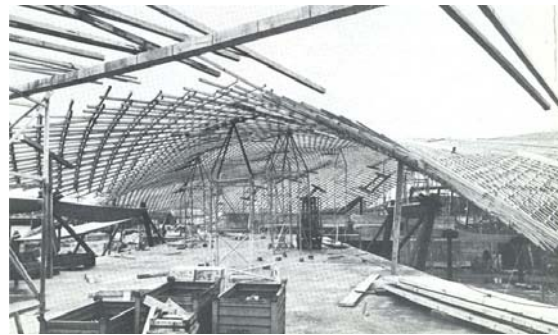


Figure 3.25: Scaffolding towers (Burkhardt et al 1978)

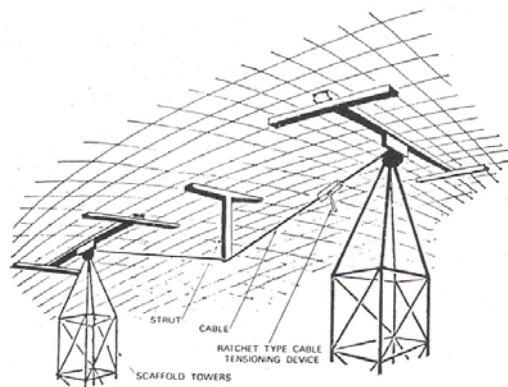


Figure 3.26: Intermediate strut (Burkhardt et al 1978)



Figure 3.27: Applying the roof skin (Burkhardt et al 1978)

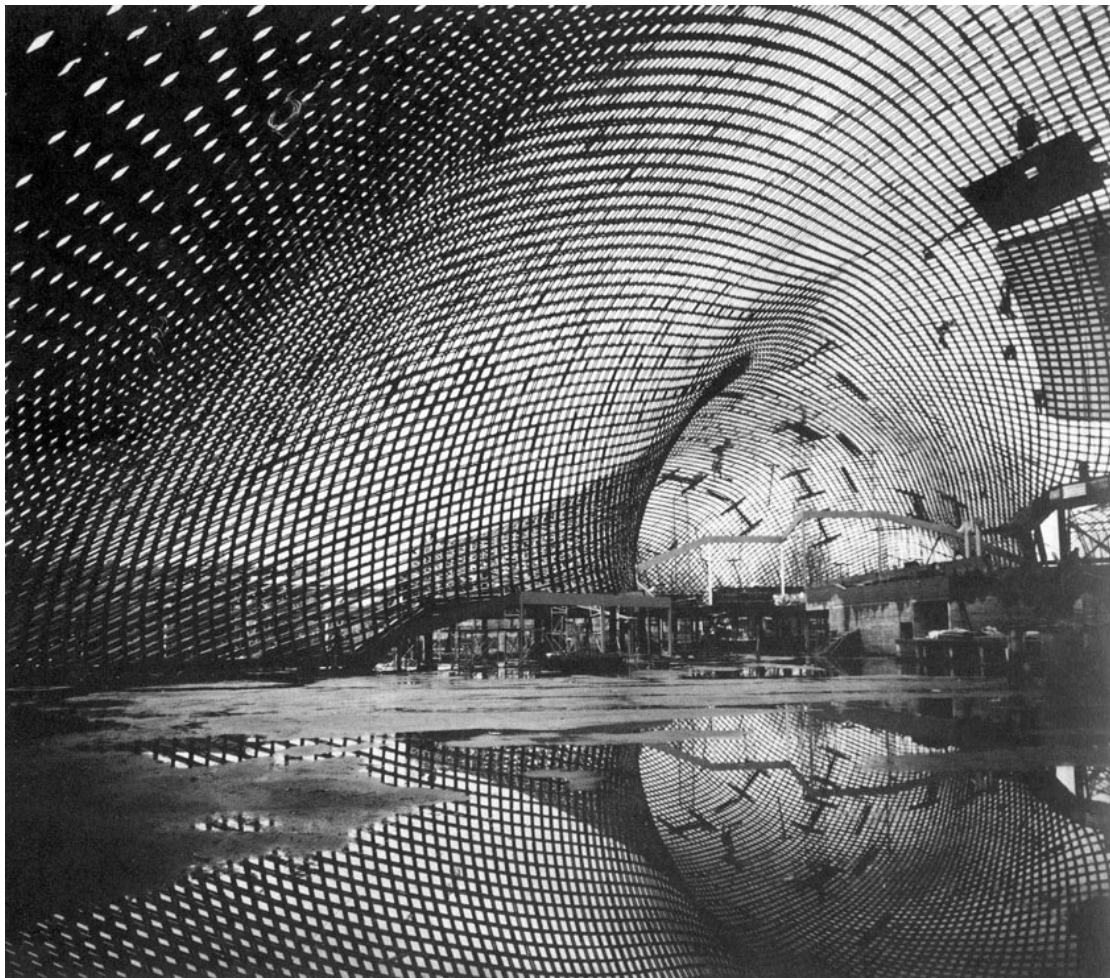


Figure 3.28: Interior (Wilhelm 1985)

3.3.2 Weald and Downland gridshell

3.3.2.1 Background

The Weald and Downland gridshell, shown in Figure 3.29 and Figure 3.30 is built at the Weald and Downland Open Air Museum in Singleton in the UK, and was finished in 2002. This museum has over 45 historical buildings from South East England, which have been rescued and rebuilt there. The museum needed a new building for study and practice of building conversation, especially the timber framing tradition in England. Also a new conservation store for collection items was needed. To extend the collection of timber structures into the 21st century, the new building should be an example for modern rural buildings. The result of the combination of skills of the architect Edward Cullinan Architects, the engineer Buro Happold and the carpenter, Green Oak Carpentry Company, truly is a display of modern craftsmanship (Harris & Kelly, 2002). The basement of the building is sunken into the hillside and houses the conservation store. The workshop is situated on the ground floor and is roofed by the gridshell. The roof has the shape of a triple-bulb hourglass, to mirror the rolling shapes of the West Sussex Downs.



Figure 3.29: The Weald & Downland gridshell¹⁴



Figure 3.30: Inside view of the gridshell¹⁴

3.3.2.2 The roof

The triple-bulb hourglass roof is 48m long and between 11-16m wide. It has an internal height of 7-10m. The roof is clad with Red Cedar boards and polycarbonate glazing. The grid is built up out of 50x35mm oak laths in four layers, like the gridshell in Mannheim, to provide good out of plane resistance. The laths have a spacing of 500mm in areas with high load, and 1000mm in other areas. Original designs were made with 500mm spacing for the whole structure. Careful examination of the forces and stresses by computer analysis lead to increasing of the spacing, which saved construction time and reduced costs significantly. Shear blocks are screwed between the different layers to provide composite action between the layers. To increase stability, diagonal bracing is applied. In the lower parts the bracing laths run in longitudinal direction, at the top in transverse direction. These also provide support for the cladding boards.

The cladding consists of polycarbonate glazing, which covers the upper part of the roof, and Western Red Cedar boards. This closed part is insulated with a multi-layered composite insulation material¹⁴

¹⁴ <http://www.wealldown.co.uk/downland-gridshell.htm> accessed 18-12-2005

3.3.2.3 Structural modelling and analysis

Physical modelling

Physical modelling involved an important part of the modelling process. It provided a lot of information on form, structure and construction of the shell. Scheme models of wire mesh were made to research the form. After this a larger 1:30 model using wood strips was built. This proved to be very instructive. The geometry of the model was used to determine the boundary conditions for the computer model. It also served as presentation model (Harris & Kelly 2002).

After this an accurate wire mesh model was made, to explore the formation of the shape and to determine self weight bending. Dimensional analysis was used to correctly model the full scale structure (Jensen 2000). A boundary template was used to determine if the correct shape was reached. Also internal scaffolding was modelled to approximate the formation procedure as good as possible. The wire mesh was loaded by hanging large steel nail on the nodes.

Main conclusion of the experiment was that the saddles would not form themselves under dead weight. External forces are needed to reach the final shape. As the lattice becomes more curved, larger forces are needed to stretch the lattice, so the initial lay out of the lattice should be already stretched instead of with square angles. It was also concluded that formation of the waists costs a lot of force when first a barrel shape is adopted. Formation of the valleys and tops should be formed simultaneously to prevent breakage of the laths.

Computer form finding

The geometry of the grid was obtained using a form finding technique called dynamic relaxation (see 4.2.2.2). This is an iterative process which modifies the desired shape by minimizing kinetic energy of the model as it is made to oscillate around an initial approximation of the shape. Numerous iterations are needed to create a smooth shape (Harris & Kelly 2002). The method is generally used to examine oscillations of a pure catenary shape to generate a final shape. The W&D gridshell however is not a purely catenary shape. It is not possible to create the saddles with a hanging chain model. The method had to be modified by including the bending stiffness of the laths, to correctly model the shape.

Structural analysis

The structure is analysed and designed in accordance with the Eurocode5, using timber grade D30 with a characteristic bending strength of 30N/mm^2 . Structural analysis was performed using the elastic analysis software STAAD Pro. Two methods were used. Dynamic relaxation was used for second order analysis of buckling instability. Using the STAAD model a deflection analysis to compare the deflected shape with the non-linear analysis under the same load. This proved that under working load the behaviour is elastic, with adequate factor of safety against buckling. Detailed stress checks were made using the information provided by the STAAD model.

It was also concluded that the shape of the grid enhanced the load bearing capacity. The waisting along the building improved the strength and stiffness against asymmetric loads (Harris & Kelly 2002).

3.3.2.4 Timber

Selection

A number of species of timber were considered for construction of the gridshell. Based on their properties and the results of a series of tests, oak was selected for the grid. This species performed best in the structural tests carried out at Bath University, with respect to bending behaviour. It proved to be stiffer than other species and has a considerably higher bending strength. Although it needs more force than other species to be bent it can achieve a smaller bending radius prior to failing. Also it showed a somewhat plastic failure mode, compared to more brittle timber. Additionally, oak has high natural durability, so no treatment would be necessary. Possible leakages will not lead to decay of the timber (R. Harris, pers. email comm. 14 March 2006).

Another reason is that oak is one of the most common used materials in the museum's collection of buildings and the species was readily available from sustainable sources in UK. Strangely enough, eventually the timber was sourced in Normandy, because better timber with a lower rejection rate was available there.

The main disadvantage of oak is that the direction of grain varies significantly, due to the growth characteristics. This was overcome by cutting out the defects and joining the pieces together to create laths of the required length. Selection was made on the following requirements (Harris & Kelly 2002):

- a maximum slope of grain of 1:10
- No dead knots or live knots. Only small pin knots were allowed, provided that they formed no more than 20% of the width of any face.
- No shakes or splits
- No sapwood (sapwood is not naturally durable and not resistant to infestations)

Lath production

Although tests indicated that the shell could be formed using dry oak, green oak was used. Green timber is easier to bend, thus making the forming process of the shell easier. One disadvantage of oak is its acidity, making it difficult to joint with adhesives. Using green oak only make this worse, also because of the moisture content of the green timber. After an adhesive was found which is not affected by this acidity and the moisture content, the use of it was no problem anymore.

In total, approximately 6000 linear meters of lath were needed. The average length of individual pieces was 0.6m so 10.000 finger joints were used in the structure. Laths of 6m length were made off site, using a special machine, to maximize the quality with a minimum wastage. The finger joints are hardly visible, so despite the amount the joints have minimal visual impact (Figure 3.31).

On site the laths were jointed into laths up to 37m long. Here, a scarf joint with a slope of 1:7 is used (Figure 3.32). The joints were made in a tunnel tent to avoid weather influences.

There is an interesting contrast between the two jointing techniques used. Finger jointing was the latest technology, while scarf jointing has been used for centuries.

The joints performed well during construction. There were approximately 145 breakages during forming. Almost all broken joints were finger joints. Main causes were (Harris & Kelly 2002):

- Pinching of the lattice on scaffold supports
- Tight curvature
- Tension build-up because restriction of the relative slipping between the layers
- Dry joints

Figure 3.31: Finger joint¹⁴Figure 3.32: Scarf joint¹⁴

3.3.2.5 Connection details

Typical node joint

For the connection between the laths a special connector was designed. It consists of three plates, connected with four bolts (Figure 3.33). The middle plate has a pin in the centre, keeping the connection into place. The outer layers can slide freely in their direction during shaping of the structure. Two of the four bolts can be used to connect the diagonal bracing. The connector proved to be very successful and has been patented.

Figure 3.33: Assembly of a typical node joint¹⁴

Edge connection

At the edges the gridshell is connected to the floor of the structure. The laths are bolted between two layers of plywood and connected to the floor beams. The floor and floor beams are cut into shape (Figure 3.34) and the first layer of plywood boarding is connected to the Glulam floor beams with angle brackets prior to the erection of the roof. Holes are drilled in the boarding aligned with the holes in the brackets. Figure 3.35 shows one of the positions of the brackets. After the grid is lowered, blocks are installed on this location to fix the sandwich structure firmly to the brackets on the inside (Figure 3.36). Also the gaps between the layers are filled up with timber where the grid overlaps the boarding to create a solid section four times the depth of a lath. The second layer of plywood is attached and the laths and plywood layers are bolted together (Figure 3.37). The whole sandwich is bolted to the brackets on the inside to create a rigid edge connection.



Figure 3.34: Floor and beams are cut into shape¹⁴



Figure 3.35: Location of the brackets¹⁴



Figure 3.36: Connection to the edge¹⁴



Figure 3.37: Edge detail¹⁴



Figure 3.38: Finished connection¹⁴



Figure 3.39: Flat mat of laths¹⁴



Figure 3.40: Start of lowering¹⁴



Figure 3.41: Adjustable jack¹⁴



Figure 3.42: Angled jacks¹⁴



Figure 3.43: Halfway down¹⁴



Figure 3.44: Completed form¹⁴

3.3.2.6 Assembly

Instead of pushing or lifting up the grid against gravity, the Weald and Downland gridshell was lowered into position. The flat grid of laths was laid out on a special scaffolding system at the level of the valleys of the shape. This scaffolding system used adjustable jacks to accurately alter the heights to form the shape of the gridshell.

The mat was laid out at a height of 7m. As concluded from the experiences of physical modelling, the mat was not laid out with 90° angles between the laths. 96° and 84° angles were used and the resulting mat was 47x25m (Kelly et al, 2001).

The process of lowering the grid was carefully monitored visually and with the information provided by scaffolding jacks system. The longitudinal centre line was used as a reference line, as this line was not to move transversely. The nodes on this line were painted white, to be able to visually check if the nodes remained on a straight line.

The scissoring and sliding of the laths was influenced with straps in plane of the grid. By tensioning the straps in the desired direction, the scissoring was stimulated. The strapping arrangement was continuously monitored. Failing of the lattice to scissor or of the laths to slide relatively to each other would lead to breakages so the process was observed carefully. After formation was finished, the valleys resembled the designs very well. The domes however appeared to be too low. Also the perimeter nodes around the domes were 300mm too low. Adjustments were made by pushing up the perimeter nodes using small jacks. The formation process was very successful. Observation was seen as the key control of the formation process. Potential problems could be isolated and dealt with continuously by observing the behaviour of the lattice.

3.3.3 Savill Garden gridshell

3.3.3.1 Background

Opened in June 2006, the Savill Garden visitors centre is the latest timber gridshell. The Savill Garden gridshell is the roof of the new visitor centre of The Royal Landscape. This park, which is part of Windsor Great Park near Windsor Castle in the UK needed a new visitors centre. Existing facilities were obsolete and scattered around the park. The Savill Garden visitors centre now forms the central gate to the Royal Landscape.

As a giant leaf the gridshell lies between the sloping surroundings. The gridshell itself forms the roof of the public part of the visitors centre, housing an information desk, shop, bar, restaurant and a banqueting hall. The slopes adjacent to the roof are actually the vegetated roof of different facilities like offices, stock, kitchen and toilets.

The building is designed by Glenn Howells Architects. For the engineering and realisation, the same companies as the Weald and Downland gridshell were contracted: Buro Happold and The Green Oak Carpentry. After years of preparation, the structure was built in three years, costing 8,3 million Euros. The careful preparation has resulted in a well thought design of the complex structure. The result is well recognized for its excellence in design and sustainability.

3.3.3.2 The roof

The roof is a symmetrical surface, formed by a central dome with a smaller dome on either side and ends pointing slightly upward. The roof is 98m in length, has a maximum of 28m in width and is 4,5 to 8,50m high¹⁵. The shape can be described by a sinusoidal wave in longitudinal direction and a parabola in transverse direction. The structure is a double layered grid of laths with a mesh size of 1m. The laths are 80mm wide and 50mm high. Shear blocks of 80 *120*300mm connect the two layers. This way a structural cross section with a height of 190mm is created.

To save costs, it was chosen to apply a continuous layer on top of the laths for diagonal stiffness, instead of diagonal bracing. Birch plywood is used for this, which also serves as a roof cover together with isolation and an aluminium rain cover.

Support construction is a circumferential waving steel tube, which is supported by steel angled columns. Timber laths are bolted to the edge tube, through laminated veneer lumber elements, provides strong connection with less support points.

3.3.3.3 Timber and assembly

Weeks of computing were needed to structurally model the structure. To find the right timber for the structure and to verify the results of the structural modelling, prototypes of different timbers species were tested. It was found that Larch was the most suitable for the structure. Larch is known for its natural strength and its natural durability¹⁶, which adds to the structure's environmental value. All modelling work paid off, as breakage only occurred twice during construction.

All timber used was FSC approved. 400 larch trees were carefully selected and processed into a total of 35km of laths. For this 11000 finger joints were used.

The laths are finger joined with water based PUR glue into 6m pieces. On site 35m laths were created. These laths were laid out onto a temporary frame and manoeuvred into exact position by hand, using laser measuring equipment and simple drainage tubes. In place, the laths are screwed together. The construction method is fairly simple, but it took a full year of labour with 20 craftsmen to construct the timber roof.

¹⁵ http://www.e-architect.co.uk/oxford/savill_building.htm accessed 10-04-2007

¹⁶ <http://www.scottishwood.co.uk/hardwoods.htm#Larch> accessed 10-04-2007



Figure 3.45: the Savill Garden gridshell (De Groot, 2007)



Figure 3.46: inside view of the roof structure (De Groot, 2007)

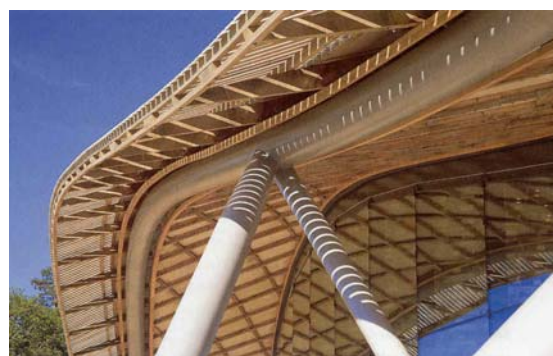


Figure 3.47: steel ring tube on angled columns (De Groot, 2007)



Figure 3.48: gridshell under construction (De Groot, 2007)



Figure 3.49: the gridshell under construction¹⁷

¹⁷ <http://www.greenoakcarpentry.co.uk/g-body-savill-garden-gridshell.htm> accessed 24-03-2007

3.4 Comparison of the gridshells

The almost 30 years that are between the constructions of first and latest two gridshells makes them differ in a lot of ways. Especially the aid of advanced computer techniques made the architectural and structural design and design process of the Weald and Downland gridshell and the Savill Garden gridshell a lot different. Advanced production and construction techniques made it possible to create a high quality building. The quality of the Mannheim gridshell lies maybe not in elegant construction solutions, but more in the fact that building it was true pioneers work and in the architectural design itself.

To compare the structures, the differences are displayed in Table 3.1. Also the strengths and weaknesses of these differences are stated. Apart from design methods, one of the main differences is found in the construction method. The mat of laths of Mannheim was pushed up, with Weald and Downland it was lowered, which proved to be more controllable and accurate than the method used with Mannheim. With the Savill Garden gridshell, construction was performed without deforming a mat of laths, but by manoeuvring every single lath into position.

The Savill Garden gridshell is probably built with the simplest methods of the three. On site, the laths were placed into position and simply screwed together. Also the problem of sliding layers was avoided by adding the different layers one by one. If this method is used, accurate data is needed on the positions of the laths and nodes. Because of the framework, not much room is left for on site adjustments.

The temporary framework is another downside of the building method, because this is probably partially once-off. But the method probably saves a lot of money, compared to the expensive adjustable scaffolding used with the Weald and Downland gridshell. Also manoeuvring every single lath into place and screwing them together are downsides, as it takes a lot of manual labour. On the other hand, the bolts and connectors used in the other gridshells also had to be placed by hand, and probably also had to be retightened due to shrinkage of the timber.

The simple building method probably also contributed to the low amount of breakages, which is two. In the Weald and Downland this was 145. During construction of the Mannheim gridshell there were numerous breakages, but no figure could be found.

The structures themselves differ most in means of stability. With Mannheim, stability is provided by steel cable bracing, which makes the stability dependent on the tension in the cables. Weald and Downland uses timber laths as rigid bracing. With the Savill Garden gridshell, again a different system was used: continuous sheeting providing shell action.

Construction costs can also be compared. The Weald and Downland has costed 1611€/m² gross internal floor area (Harris et al. 2003), with a total of 2,35 million Euro¹⁸. For the Savill Garden gridshell this is 3009€/m² gross internal floor area¹⁹, with a total of 7,05 million Euro²⁰, costing approximately twice as much as the Weald and Downland gridshell. The difference between the two structures can probably be explained by the 'luxurious' features, like the steel edge structure and a glass façade of 8m. high. The Savill Garden gridshell itself costed only 34,6% of this amount (1038€/m²). The Weald and Downland gridshell costed only 16% of its total amount of building costs per square meter (260€/m²). It is uncertain what causes this difference because no specification of the building costs could be found. It probably can be explained by the fact that the Savill Garden is approximately four times larger than the one in Weald and Downland, taking more time to construct and thus more labour costs. The costs for the Weald and Downland gridshell can be compared with the

¹⁸ <http://vs2.i-dat.org/unstructured02/eco2.html> accessed 09-04-2007

¹⁹ http://www.cnplus.co.uk/qweek/images/Savill_Gardens.pdf accessed 09-04-2007

²⁰ http://www.qweek.com/nav?page=qweek.contentspage&view_resource=5941138 accessed 09-04-2007

building costs of a typical building in medium costs range (Harris et al. 2003). This implies that the Savill Garden is a quite expensive building.

The Mannheim gridshell roof costed DM 3586000 (Burkhardt et al, 1978). Converted with the exchange rate of 2001²¹ this should be 1,83 million Euros. With 10500m² usable floor area this is 175€/m². The total building costs of the building per square meter were 435€/m² (DM850/m²). It is hard to compare the Mannheim gridshell with the latest two. Especially increased labour costs makes the figures differ. According to Burkhardt et al. (1978) the building could be built economically.

Table 3.1: comparison of the Mannheim and the Weald and Downland gridshells

	Mannheim	strength/weakness (+/-)	Weald&Downland	strength/weakness (+/-)	Savill Garden	strength/weakness (+/-)
Design	Mainly physical form finding	- labour intensive - less accurate	Combination of physical and computational form finding	+ high accuracy possible	unknown (assumably computational form finding)	
Broken laths	Pushed up with fork lift trucks	+ cheap - hard to control	Lowered down with special scaffolding	+ controllable - expensive	positioned lath by lath on formwork	+ simple + controllable - labour intensive
Stability	Cable bracing	+ easy to construct - stiffness depends on tension in ties	Ridged braces	- high accuracy needed + same type of connection as the grid	continuous layer	+ stiff system
Node connection	Slotted holes	- holes weaken the cross section	Special connector	+ works very good - development takes time and costs money	screwed	+ simple + cheap
Timber used	Air dry	+ strength and shape stays constant	Green	+ bending is easy - distortion and shrinkage possible due to drying - special glue needed	unknown	
Species	Hemlock Pine	+ straight grain	Oak	+ high bending strength + durable - irregular grain direction	Larch	+ strong + durable
Lath joint	Finger joint	- short weld length caused breakages	Finger joint by jointing machine	+ high quality	Finger joint with water based pur glue	
On site joint	Lap pieces	- holes weaken the cross section - stiffness is reduced	Scarf joint	+ continuous laths possible - on site gluing needed	unknown	
Broken laths	unknown		145 (mainly finger joints)		2	
Cladding	PVC coated fabric	+ translucent - on site welding of seams needed - requires accurate assembly for aesthetics	Western Red Cedar boards and polycarbonate glazing	+ insulation possible + daylight trough the roof	Continuous layer of Birch plywood	- no daylight possible + insulation possible
Building costs of the roof only	435 Euro per m ² of usable floor area		260 Euro per m ² of gross floor area		1038 Euro per m ² of gross floor area	

²¹ http://www.worldtrading.net/currency/old_converter.html accessed 10-04-2007

Form finding



4.1 Introduction

In free form architecture the search for the desired and optimal shape is always present. In general, the search for the optimal shape is called form finding. In architecture, the search is for an optimal shape with respect to the desired appearance or functionality of the enclosed space. Architectural form finding can be seen as shape finding with the optimum being rather subjective to the opinion of the architect. In structural design, the shape itself is not optimized, but the optimum is found in an optimal structural behaviour. The architectural and structural optima do not often have the same shape, which conflicts the interests of the architect and structural engineer. The art in designing is joining these interests in an early stage of the design process, combining them to create an overall optimum. For finding the optimal structural shape, different techniques can be used. In Section 4.2 these techniques will be elaborated.

4.2 Form finding techniques

Form finding can be applied on many subjects. In general, it is used to find an optimized solution to a problem, with respect to one or more criteria. To be able to solve it, the problem has to be defined in such way that these criteria can be optimized. Mathematically, this optimization can be performed in various ways. 'Classical' methods such as the LaGrange function, linear and non-linear programming, but also intelligent and adaptive models, which are part of Artificial Intelligence, can be seen as optimization methods. Coenders (2004) made an extensive overview of available methods.

Focussing on the optimization of structures, form finding is closely related to structural optimization. For instance, the optimization problem can be the structural behaviour of the structure, with a minimal use of material as optimization criteria. There are different techniques for finding this optimum. Physical modelling is the easiest method. With physical models, a quick insight in structural behaviour and form can be gained. High accuracy however is difficult to gain. More advanced computational methods are available to provide the accuracy necessary for further design and construction.

4.2.1 Physical modelling

With physical modelling the principles of nature are used to determine shapes. By evolution, nature has developed ways to transmit forces with minimal use energy and material. A spider's web, the shape of soap bubbles and radiolarians (oceanic organisms) are examples of structures by nature, highly efficient with respect to use of energy.



Figure 4.1: Structures by nature. A spider's web²², soap bubbles (Otto 1982) and a radiolarian²³

Back to structures of mankind, cable structures and fabric membranes are good examples of physical form finding. When loaded tension structures adapt to a unique shape which is not known in advance (Lewis 2003). The structure adopts itself to resist the load in an optimal way, minimizing the energy needed to resist the load. This behaviour can be modelled quite easy with flexible materials such as pantyhose fabric. Soap film is also very suitable to model tension fabric structures, as the soap film adopts the minimal energy surface between its rigid supports. Well known for using and exploring these techniques is Frei Otto and his Institut für Leichte Flächentragwerke (ILEK), which conducted a lot of research in structures in nature and form finding techniques. Otto used physical form finding in his designs, for instance the net roof of the Olympic stadium in Munich.

Compression structures can also be modelled physically. Soap bubbles and pneumatic membranes can be seen as the inverse of a compression shell. Arch structures can be modelled by threads or cables. Under a uniform load a cable structure adopts to the catenary line. Lacking moment capacity, there will be only pure tension in that cable. Made rigid and turned upside down this would become an arch structure with only pure compression. Antoni Gaudi used this principle in his famous designs, such as the Sagrada Familia in Barcelona (Figure 4.2). Gaudi used threads to model the columns and arches of his structures. Little weights hanged on the cables modelled the weight of building elements. Also with the Mannheim gridshell Otto used hanging models to form find the shape of the structure (see Section 3.3.1.3).

²² http://gallery.hd.org/_c/natural-science/spider-web-closeup-backlit-against-dark-sky-in-corner-of-door-frame-mono-1-DHD.jpg.html accessed 16-04-2007

²³ <http://www.cs.brown.edu/courses/cs024/imagesTechnology.html> accessed 16-04-2007

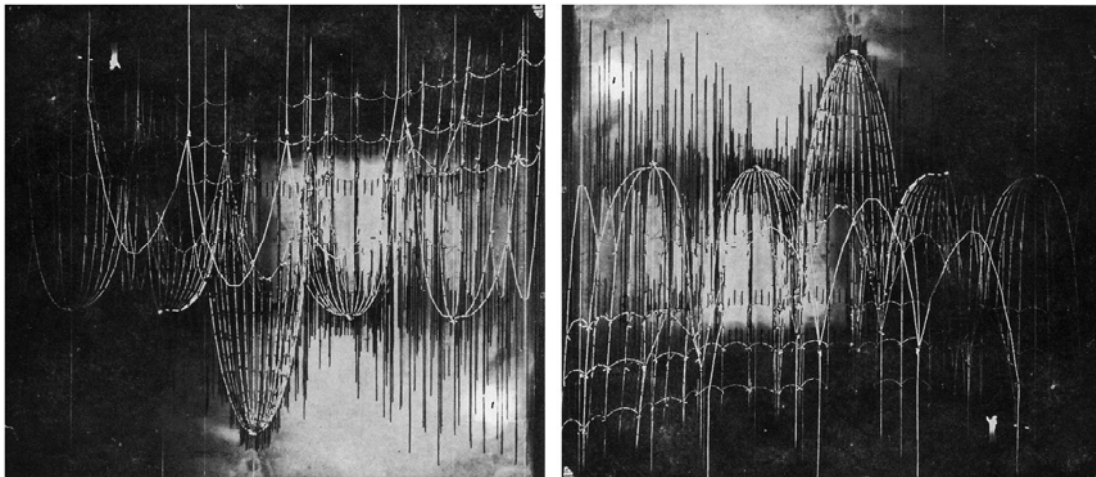


Figure 4.2: Hanging model by Gaudi and its inverse²⁴

The design methods used by for instance Gaudi and Otto can be seen as the oldest form of form finding. The geometry of a design is completely determined by physical models. The building of these models is very time consuming however. A change in design can not be passed through on the model easily. Nowadays, physical models are mainly used as physical representations of the design, a presentation model to other parties. The design is made with the aid of drawing and engineering software, in which changes can be made quickly. However, using physical modelling in the design stage can still play an important role in gaining better understanding of their design, especially with complicated designs with double curved surfaces.

²⁴ <http://staff.bath.ac.uk/abscjkw/OrganicForms/SlideShow/> accessed 4-5-2006

4.2.2 Computational form finding

Computational form finding is a numerical optimization process. With numerical optimization, an iterative calculation sequence is used to determine the optimum of a problem. In structural optimization, starting point of the optimization process is the initial shape of the structure, which does not comply with the desired optimization conditions. In the iterative form finding process, numerical algorithms describing mechanics of structures perform geometric adjustments of the structure, until static equilibrium is reached. The outcome of the form finding process is a computational model of the structure, describing its shape, stresses and deformations under load conditions by a set of numerical and graphical data (Lewis 2003). To reach the desired optimum, iterations steps can become quite numerous, especially when designs are complicated. Present-day computer technology makes it possible to make these calculations in a matter of minutes without much difficulty.

What makes numerical optimization especially useful for form finding is the possibility of solving non-linear problems in a relative easy way. When deflections get large, structures can display geometrically non-linear behaviour, which means the deflection is not linear with respect to its loadings. Tents and membrane structures are known for this behaviour. Non-linear problems are hard to solve with normal mechanics formulae, but it can be solved relatively easy with an iterative calculation process. Numerical optimization is an iterative process, which makes it suitable for form finding structures which display non-linear behaviour.

The two computational form finding techniques mainly used and developed over the last decades, are the force density method and the dynamic relaxation method. These methods are explained in the following sections.

4.2.2.1 Force density

The force density (FD) method allows you to generate shapes of tension structures that are in static equilibrium. It is a method that uses a linear system of equations to model static equilibrium of pre-tensioned cable net under prescribed force/length ratios. By assuming a constant ratio of force to length, non-linear system of equations becomes linear and can be solved. The next example is used to illustrate the principles of the FD method, which is reproduced from Lewis, 2003.

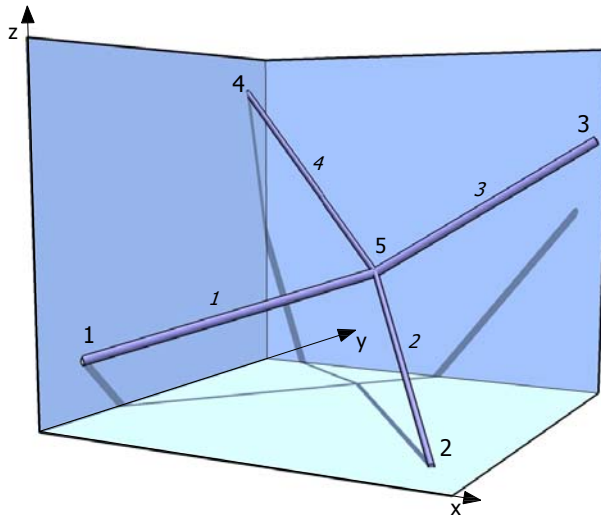


Figure 4.3: Structure with 4 members

Principles of the force density method

Figure 4.3 shows a structure of 5 nodes and 4 members, which can be seen as part of a larger structure such as a cable net. The equilibrium of forces at node 5 can be determined by resolving the tension forces T_m into x , y and z components ($m =$ member number). This is achieved by multiplying T_m by the direction cosines, defined as the ratios of the member lengths projected on the direction axes, to the actual lengths L_m . The directional force components can be defined as:

$$\begin{aligned}
 T_{m,x} &= \frac{T_m(x_i - x_k)}{L_m} \\
 T_{m,y} &= \frac{T_m(y_i - y_k)}{L_m} \\
 T_{m,z} &= \frac{T_m(z_i - z_k)}{L_m}
 \end{aligned} \tag{4.1}$$

Equilibrium of forces can be calculated by adding up the directional components, which should be equal to the external directional load vectors P_x , P_y , and P_z acting on node 5.

$$\begin{aligned}\frac{T_1(x_1 - x_5)}{L_1} + \frac{T_2(x_2 - x_5)}{L_2} + \frac{T_3(x_3 - x_5)}{L_3} + \frac{T_4(x_4 - x_5)}{L_4} &= P_x \\ \frac{T_1(y_1 - y_5)}{L_1} + \frac{T_2(y_2 - y_5)}{L_2} + \frac{T_3(y_3 - y_5)}{L_3} + \frac{T_4(y_4 - y_5)}{L_4} &= P_y \\ \frac{T_1(z_1 - z_5)}{L_1} + \frac{T_2(z_2 - z_5)}{L_2} + \frac{T_3(z_3 - z_5)}{L_3} + \frac{T_4(z_4 - z_5)}{L_4} &= P_z\end{aligned}\quad (4.2)$$

In the above system of equations, the member lengths L_m are non linear. By introducing a constant tension coefficient q_m , the force density, which is defined as the ratio T_m/L_m , the system becomes linear:

$$\begin{aligned}q_1(x_1 - x_5) + q_2(x_2 - x_5) + q_3(x_3 - x_5) + q_4(x_4 - x_5) &= P_x \\ q_1(y_1 - y_5) + q_2(y_2 - y_5) + q_3(y_3 - y_5) + q_4(y_4 - y_5) &= P_y \\ q_1(z_1 - z_5) + q_2(z_2 - z_5) + q_3(z_3 - z_5) + q_4(z_4 - z_5) &= P_z\end{aligned}\quad (4.3)$$

This linear system of three equations has three unknowns, the coordinates x_5 , y_5 and z_5 , and can therefore be solved. Notice that if the force density q_m has a constant value for all members, the calculated coordinate system is independent of q_m . If a change in configuration of the network is desired, different values for q_m can be defined for each member.

Using of the force density method

With the FD method the initial shape of cable nets and membranes can generated with only the boundary coordinates and the force densities to be specified. In the example only four members were used. The system of equations can be expanded for larger structures, but of course the system of equations becomes larger with an increasing number of nodes and members. Matrix notation and calculation are used to keep the system manageable. The method has developed into a non-linear FD method, which makes it possible to implement other requirements than only the boundary conditions, such as constant mesh width or constant pre-stress, making it a versatile design method for tension structures (Lewis 2003). One software package using FD in which this is possible is the programme EASY, in which complete tension structures can be designed and calculated. The package is not limited to fabric membranes only. The package also includes an application for calculating element with bending resistance, EasyBeam. The roof of Bad Dür rheim (Section 2.4.4) was designed and engineered using this application.

4.2.2.2 Dynamic relaxation

In dynamic relaxation, form finding is performed by a pseudo-dynamic process, which can be explained as follows. The mass of the structure is lumped in the nodes and oscillate around the initial position under influence of the out-of-balance forces. Due to artificial damping, the masses come to rest in an equilibrium position (Lewis 2003). In its original form, the iterative process uses viscous damping, where the movement of the nodes is damped by damping coefficients in its formulae. The alternative process with 'kinetic damping' proved to be more stable and to converge more rapidly when dealing with large displacements. This procedure traces the motion of the structure. When a peak in total kinetic energy is detected, all velocities are set to zero and calculations are restarted with the current geometry. The energy peaks generally decrease and the process is repeated until all vibrations have been dissipated and static equilibrium is reached (Barnes 1999).

Computation procedure

The computation procedure includes the following steps (Barnes 1999):

First, the resultant force for node i is calculated with Newton's second law for every direction. For simplicity, only the x -direction is stated here:

$$R_{ix}^t = M_i V_{ix}^t \quad (4.4)$$

where

R_{ix}^t = resultant force for node i

M_i = lumped mass at node i

V_{ix}^t = acceleration of node i

The acceleration at time t can be approximated with 4.5:

$$V_{ix}^t = \frac{V_{ix}^{t+\Delta t/2} - V_{ix}^{t-\Delta t/2}}{\Delta t} \quad (4.5)$$

where

V_{ix}^t = acceleration at node i

$V_{ix}^{t\pm\Delta t/2}$ = speed of node i at $(t \pm \Delta t / 2)$

Substituted equation 4.5 into 4.4 the velocity at $(t + \Delta t / 2)$ can be found:

$$V_{ix}^{t+\Delta t/2} = V_{ix}^{t-\Delta t/2} + \frac{\Delta t}{M_i} \cdot R_{ix}^t \quad (4.6)$$

The geometry can then be updated to time $(t + \Delta t)$:

$$x_i^{t+\Delta t} = x_i^t + \Delta t \cdot V_{ix}^{t+\Delta t/2} \quad (4.7)$$

Now the geometry is completely updated and the kinetic energy (KE) at $(t + \Delta t / 2)$ can be determined. If the current KE is larger than the previous KE (at $t - \Delta t / 2$) the system returns to 4.6 after calculating the new link forces and its resultant by:

$$R_{ix}^{t+\Delta t} = P_{ix}^{t+\Delta t} + \sum \left(\frac{T}{l} \right)_m^{t+\Delta t} \cdot (x_j - x_i)^{t+\Delta t} \quad (4.8)$$

where

$P_{ix}^{t+\Delta t}$ = updated link force acting on node i

T_m = tension in link m connecting nodes i and j

l_m = length of link m

$\sum \left(\frac{T}{l} \right)_m^{t+\Delta t}$ = summation over all links m connecting to i

If the current KE is less than the previous KE a peak in KE has occurred somewhere between $(t - 3\Delta t / 2)$ and $(t + \Delta t / 2)$. The process is then restarted at 4.4 with all velocities set to zero, after correcting the geometry. Because the peak occurred some time before $(t + \Delta t / 2)$ the current geometry, which is set to $x_i^{t+\Delta t}$, has to be corrected to a more exact position corresponding with the KE peak time t^* (Figure 4.4).

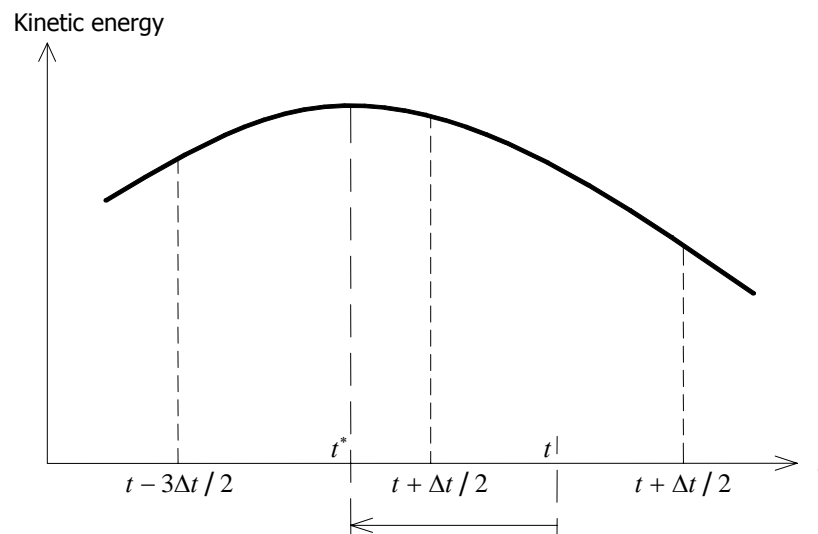


Figure 4.4: Graph of peak in kinetic energy

In equation 4.8 the term $\sum \left(\frac{T}{l}\right)^{t+\Delta t}$ can be seen as the nodal stiffness S_i . S_i can be

adjusted to the appropriate stiffness for different structures. In the example above, S_i is the geodetic stiffness of a tension structure. For cable net structures the elastic stiffness can be added and S becomes:

$$S_i = \sum \left(\frac{EA}{l} + g \frac{T}{l} \right)_m \quad (4.9)$$

where g is a factor for allowing the geometric stiffness to increase due to large change of length of the links during analysis.

For form finding structures where bending stiffness is present, S_i should include the bending stiffness of connecting beam links:

$$S_i = \sum \frac{2EI}{l^3} \quad (4.10)$$

What is easily forgotten is the nodal forces resulting from the bending of the laths. The continuous laths are initially straight and bent into shape. This results in moment in the laths and shear forces s_i acting on the nodes, normal to the chord between the nodes. In next figure, two subsequent links in a gridshell are considered:

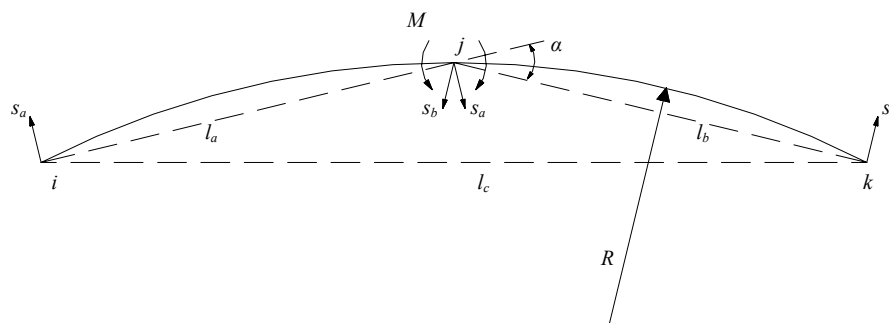


Figure 4.5: Moment and shear forces in laths

If the bending radius R and moment M are calculated with:

$$R = \frac{l_c}{2 \sin \alpha} \quad M = \frac{EI}{R}$$

with E assumed constant.

The shear forces s_a and s_b at j thus are:

$$s_a = \frac{2EI g \sin \alpha}{l_a g_c} \quad s_b = \frac{2EI g \sin \alpha}{l_b g_c}$$

For further elaboration on DR we refer to Barnes, 1999.



Figure 4.6: Computer image of the British Museum Great Court roof Image by C.J.K. Williams²⁴

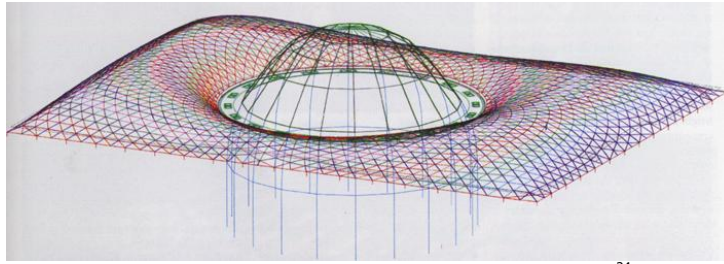


Figure 4.7: British Museum Great Court Image by C.J.K. Williams²⁴

Evaluation of the dynamic relaxation method

Big advantage of DR over matrix methods like force density, is that no matrix manipulations are needed, therefore saving computer CPU time. Although more iterations are needed to reach equilibrium, the iterations take little CPU time, still resulting in less total CPU time compared to matrix methods. Furthermore dynamic relaxation shows high numerical stability and is capable of providing solutions to highly non-linear problems. This makes dynamic relaxation widely recognized as very successful for modelling pre-stressed cable nets and membranes (Lewis 2003).

Good example of application of DR is the British Museum Great Court roof (Figure 4.6 and Figure 4.7), designed by Chris Williams. Williams is known for writing his own small mathematical software applications for his designs. Figure 4.8 shows the results of one of his (simpler) DR programs.

Besides from writing your own software, one software application in which it is possible to apply DR is Oasys GSA, which is a frame and finite element programme. Also a DR form finding module called GsRelax is implemented.

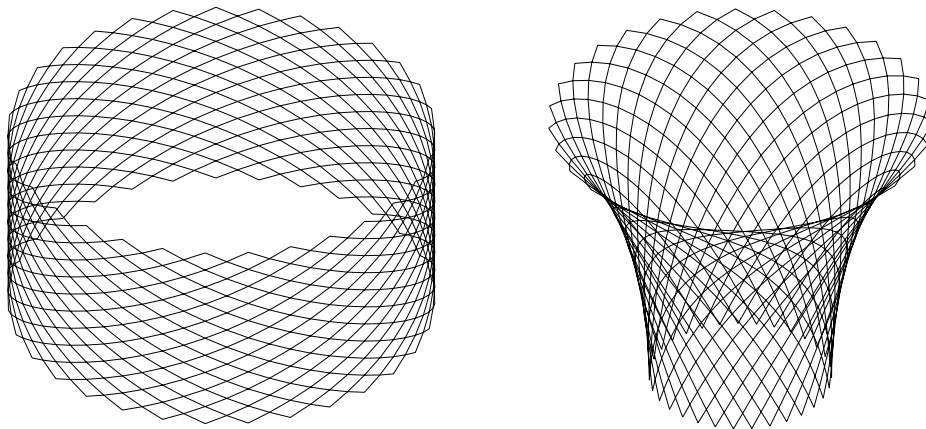


Figure 4.8: Dynamic relaxation of a basketball net. Left: initial net. Right: loaded net adjusted by dynamic relaxation. Image and software by C.J.K. Williams²⁴

Grid generation tool for arbitrary surfaces



5.1 Introduction

As stated in Section 3.1, the gridshell structure is not used very often. One of the reasons is the difficult design process. When designing a gridshell, the major problem is developing the grid geometry. If any structural analysis is to be performed on a structure, data is needed on position of the joints and length of the elements. The distance between two nodes in a gridshell is constant, so only the locations of the joints have to be calculated. The problem is that there is no standard design tool which can generate such a grid on an arbitrary surface. With former gridshell projects, the grid itself is was determined either by physical form finding, used to design the Mannheim gridshell (Burkhardt et al. (eds) 1978), or by an iterative form finding process, which involves numerous iterations to develop a smooth shape. This was performed for the Weald & Downland gridshell (Harris & Kelly, 2002). The process is based on dynamic relaxation techniques and mathematical expressions describing the starting grid of the geometry. One can understand that setting up such a process can become quite complicated. First, the form finding has to be implemented, which takes into account the physical properties of the material. Second, the surface has to be described mathematically, which can be quite difficult when it concerns a free form surface.

Making the gridshell design method better accessible would stimulate the use of the gridshell. It would make research into the feasibility of these structures for arbitrary free form surface designs easier and it would contribute to the usability of the method for a larger number of engineers.

One way of increasing the method's accessibility is providing a grid generation tool based on commercially available software. With this tool it should possible to generate a grid on an arbitrary surface, so creating the geometry of the grid would no longer be a problem. For this Master's thesis research it is attempted to create a first prototype of such a design tool. The results will be analysed with structural analysis and physical modelling.

In this chapter, the set-up for the tool development will be displayed in Section 5.2. Furthermore, the shape that will be used to test the design tool will be described and analysed in Section 5.3.

5.2 Tool development set-up

The development of the grid generation tool consists of the following parts: First the tool itself is developed. The tool development consists of the following parts:

- To develop and test the grid generation tool a shape is needed. The shape which is used is analysed in Section 5.3.
- In Section 6.2 the grid generation technique which is used will be explained.
- The grid generation technique is implemented in a usable grid generation tool, based on commercially available software. Section 6.4 describes the structure of the tool that has been developed.
- The output of the tool should be usable in third party software for structural analysis. The tool is set up to generate a text output with all relevant data, which can be processed further.
- The tool is tested by generating a grid on test case surfaces. The main test case surface is described in Section 5.3. Also an eggoid shaped surface is used. The result are be used to review the generation method. The result can be found in Section 6.4.2.
- The generation tool is set up to perform a curvature check on the generated grid. This curvature check is based on the maximum curve and torsion angles determined in 3.2.4.1. This addition to the tool is described in Section 6.4.1.5. Results with the curvature check can be found in Section 6.4.5.

The grid generation tool is reviewed by using the results in a few studies:

- A physical model is constructed with the case study shape to globally verify results. If the geometry of the generated grid is correct, it should be possible to construct a physical model with corresponding geometry. Also a conceptual model of the eggoid is built Section 6.5 discusses the results of the physical modelling.
- A study is performed into the bending stresses that occur in a structure that is bent into shape. First a single lath under different loads is analysed. Second, a 3D structure is analysed. In these studies, it is tried to relate the bending curvature to the stress levels that occur in the structure. The structural analysis software GSA²⁵ will be used for this. This study is displayed in Chapter 7.

After the studies have been performed and the result analysed, the gridshell design tool will be reviewed and conclusions can be drawn. In in Chapter 8, conclusions and recommendations for enhancement of the tool will be presented and the Gridshell design tool will be reviewed.

²⁵ Oasys GSA® by Oasys Limited

5.3 Shape analysis

The architectural design that will be used to test the design tool is shown in Figure 5.1 and Figure 5.2. This model is a design for a large hall²⁶. The dimensions of the building are approximately 40x60 m. large enough for a variety of functions, such as a wellness centre, an exhibition hall or a tennis court. The surface of the design consists of two clastic parts: a (partial) sphere and a ruled surface, a hyperbolic entrance and two connecting anti-clastic parts. The model is a poly surface, i.e. a surface built out of different elements, and can be viewed and modified in the program Rhinoceros²⁷. It is not a requirement to keep this shape as it is. Modifications are allowed when delaying difficulties in the study process are expected or experienced, or to optimize the shape structurally. However the concept of the shape is to be maintained.

The shape used is not very challenging from a contemporary architectural point of view. The shape is comparable with the shape of the Mannheim gridshell. However, from a structural point of view it has interesting aspects such as the double curvature and the anti-clastic area, which is rather flat. Analyzing the surface curvature, a plot of the Gaussian curvature can be made. This plot shows in which extend the surface is smooth with continuous curvature. Looking at Figure 5.3 some remarks can be made. As can be seen, there are some sudden changes of colour, indicating rapid change of curvature or discontinuities in the surface. At the edges of the different parts of the surface, disturbances are clearly visible. These probably were created by the software's routines when joining the different parts of the surface together. In the right part of the structure there is also an unexpected change of curvature takes place, indicated by the sharp change of colour. The discontinuities become better visible when curvature plots of section AA' and BB' are made (Figure 5.4 and Figure 5.5). The discontinuities show themselves as sharp jumps in the graph.

The tubular entrance shows a colourful pallet, indicating a rapid change of curvature. The rapid change to a much stronger curvature is likely to give problems from a structural point of view. The laths of the grid have to be able to follow the curvature. Possibly the entrance can be better implemented with an edge structure between the main structure and entrance. Therefore this part of the surface is simplified for further analysis. The entrance is replaced by a smooth surface as can be seen in Figure 5.6.

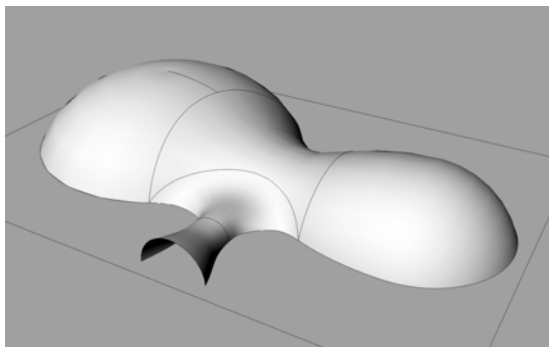


Figure 5.1: Rhino model perspective view

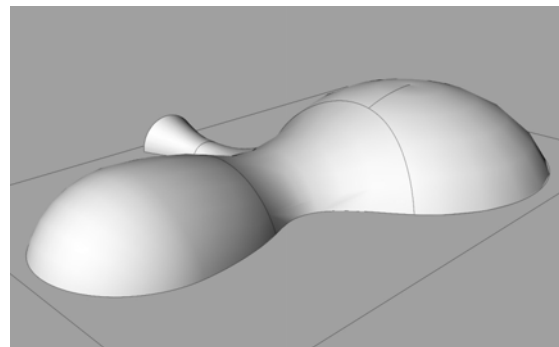


Figure 5.2 Rhino model perspective view back

²⁶ Model provided by Prof. Ir. L.A.G. Wagemans

²⁷ Rhinoceros® NURBS modeller for Windows by R. McNeal & Associates, version 3.0 SR4

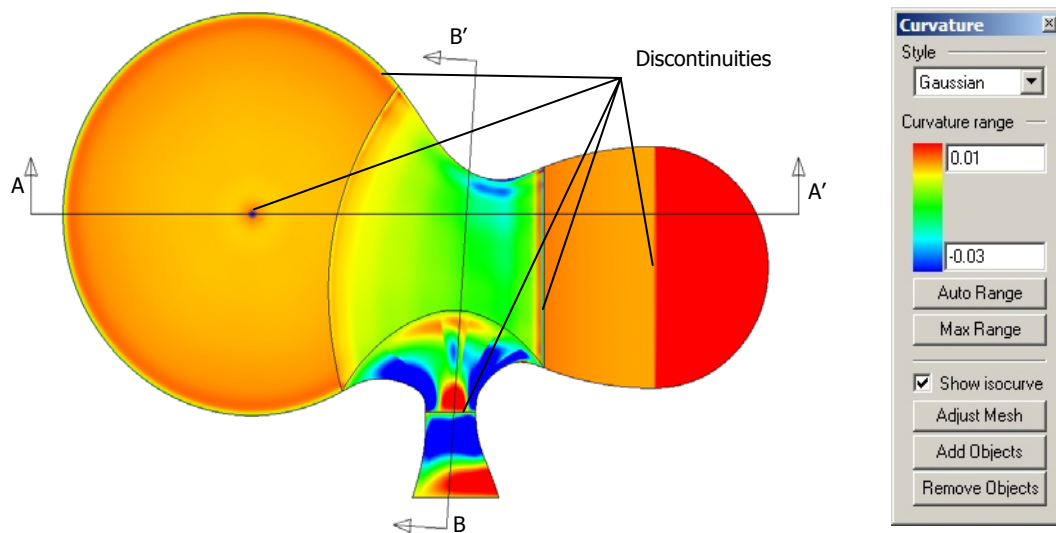


Figure 5.3: Gaussian curvature plotted on the surface

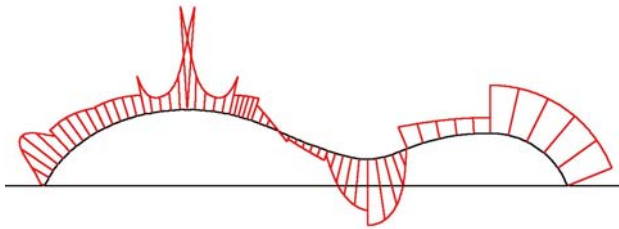


Figure 5.4: Curvature plot of section AA'

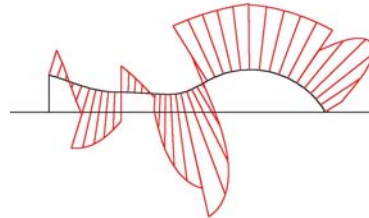


Figure 5.5: Curvature plot of section BB'

To avoid problems, the surface should be optimized to a smoother surface. Now the tubular entrance is deleted from the surface, this becomes relatively easy to do in Rhino. First a number of longitudinal sections have to be extracted from the surface. The surface can then be recreated by lofting a surface through the sections. The result is a more continuous NURBS surface (Figure 5.8). This surface can be further smoothed by editing its control points.

An interesting question rises whether the gridshell method is also applicable on a more modern design. In contemporary free form designs a development can be seen from dome like shape like Mannheim, to a shape where the curve bends inward at the lower part of the structure, to touch the ground at an angle larger than 90° (Figure 5.9 and Figure 5.10). The shape bending inwards is a challenging shape from a structural point of view because it results in large bending moments in the elbow of the structure. Apart from the structural feasibility of a gridshell with such a shape, the question raises whether it is geometrically possible to create such shape with the gridshell method. The laths have to be able to bend and scissor enough to create the surface. In Section 6 it is attempted to physically model an eggoid shape with a gridshell.

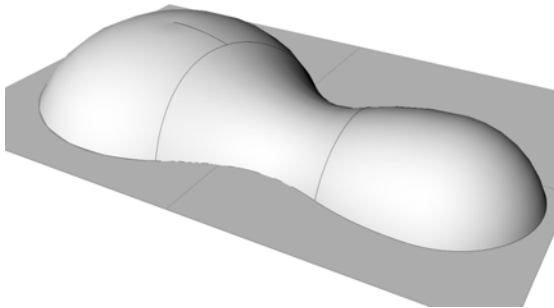


Figure 5.6: Model without entrance

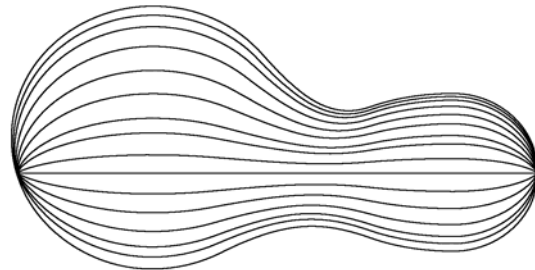


Figure 5.7: Longitudinal sections

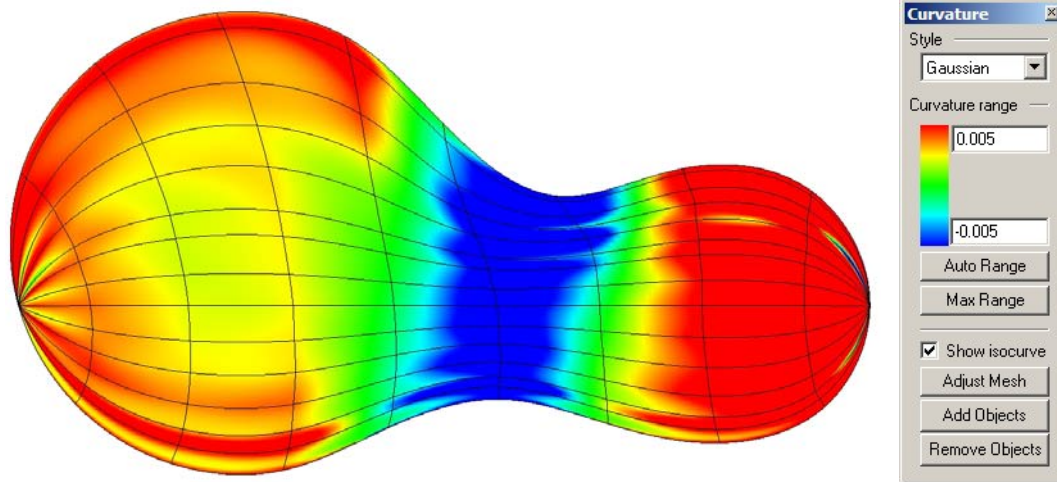


Figure 5.8: Lofted surface with Gaussian curvature analysis plot



Figure 5.9: Example of free form design: The BMW Bubble by Bernhard Franken, Frankfurt²⁸



Figure 5.10: Example of free form design: WEB van Noord Holland by Kas Oosterhuis (Boer & Oosterhuis, 2002)

²⁸ <http://www.e-architekt.cz/index.php?PId=1232&KatId=90> accessed 17-10-2006

Development of the grid generation tool



6.1 Introduction

As stated before, there is no software was found which can generate a grid on a surface with elements of equal length. Some standard grid generation methods available in software tools like Rhinoceros are:

- Points by UV-coordinates (Figure 6.1)
- Point projection in z-direction (Figure 6.2)
- Line projection (Figure 6.3)
- Surface meshing into polygons (Figure 6.4)

As can be seen, none of these methods create a grid with equal mesh edge length. Projection methods disregard any distance between points and simply create the projection of a point or line by shifting them in z-direction and locating the intersection position with the surface. Meshing techniques create the best approximation of the surface with a maximum allowed polygon size, shape and/or number. Also UV projection does not take length into account, but uses a parameter along the surface. As standard grid generation methods do not provide the desired grid, a different approach is needed. One approach is creating the grid with a graphical method by hand. This option is investigated here.

The chapter starts with displaying and explaining the proposed grid generation method on which the design tool will be based in Section 6.2. In Section 6.3, the assumptions and starting points for the development of the tool will be displayed. Next, the actual design tool will be displayed and reviewed in Section 6.4. In this section the set-up of the scripts that are created for the design tool will be explained. Also results are presented for the grid generated on the test surface. In Section 6.5 these results will be compared with a physical model of the structure.

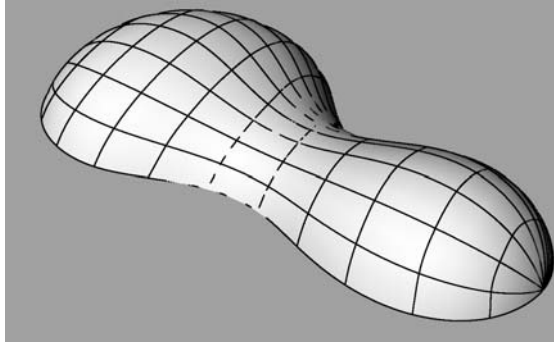


Figure 6.1: Line grid by UV coordinates

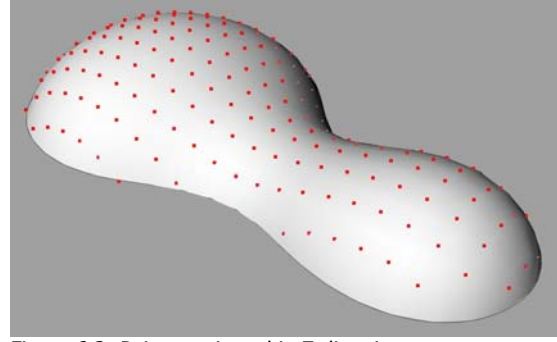


Figure 6.2: Points projected in Z-direction

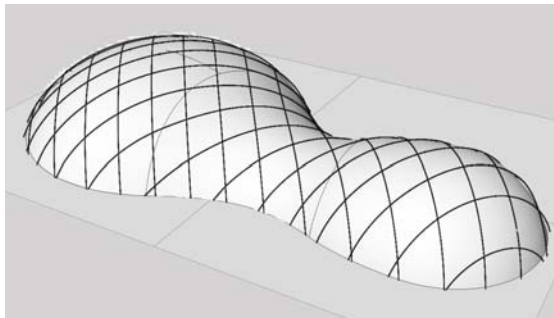


Figure 6.3: Lines projected on a surface

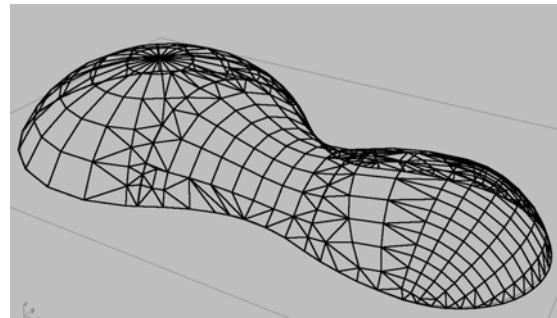


Figure 6.4: Meshed surface

6.2 Proposed method

When point 1, 2 and 3 are located on an arbitrary surface (Figure 6.5,) with equal distance x to each other, a fourth point on the surface can be defined by locating the intersection point between the surface and two spheres with radius x and their centre points at point 2 and 3. With an intermediate step of creating section curves of the spheres and the surface, point 4 is located on the intersection point of these curves. The distance from point 2 and 3 to point 4 is now equal to x .

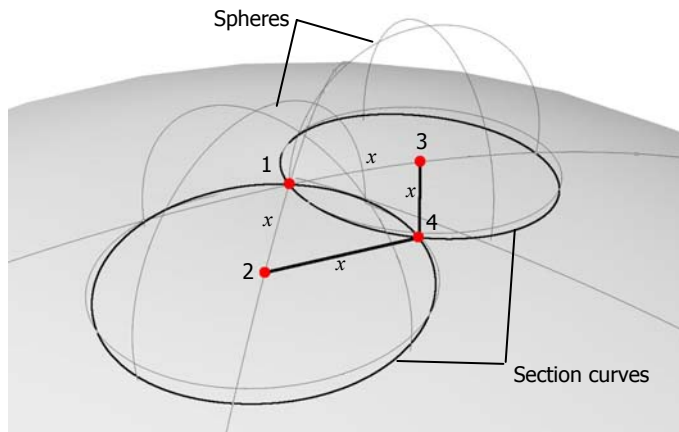


Figure 6.5: Locating a point with equal distance to the two outer points by aid of two spheres

By repeating this point location sequence until all points on the surface are located, a grid suitable for a gridshell is created. It should be possible to perform this repetition of steps in a 3D modelling tool. By using a third party software package, it is possible to use the already made features of the package to do this and there is no need to program the 3D model yourself.

Two software applications are selected in which running the series of steps should be possible. The package in which it was first attempted to create a grid-generation tool is GenerativeComponents²⁹ (GC). This is a parametric associative design system, where standard features can be used to setup the series of steps. The parametric associative character of the tool has high potential, allowing the user to adjust his design by changing just a few parameters. However difficulties were encountered in an early stage of developing the tool. The software was still a beta version at the time of use and no user's guide was available. Either a flawed set-up of the model or bugs in the software made it unable to determine the desired surfaces and intersections. A different method might have been more successful. The experiences with the development of the grid generation tool with GC and the problems encountered are described in Appendix 1: Determination of the maximum bending radius.

²⁹ GenerativeComponents® by Bentley Systems, version 8.9.0.0 Beta

Second application used is Rhinoceros (Rhino). Rhino is a 3D NURBS modeller in which complex 3D models can be created. Almost any 3D surface can be modelled. It is also possible to run command scripts to execute series of commands automatically. Rhino provides a plug-in for creating scripts, known as RhinoScript³⁰. RhinoScript exposes the internal working of Rhino, enabling the user to implement specific Rhino commands and it provides support for VBScript. VBScript, which is short for Microsoft Visual Basic Scripting Edition, is a variation on the Visual Basic programming language³¹.

For grid generation with the sphere method described above, a script will be used to execute the process of locating the intersection points on the surface. The following steps will be processed in Rhino by the script:

- Creating sections (Figure 6.6): the user is asked to create sections by picking points in the top view. These sections are used as the base of the grid generation. The use of these sections will be further elaborated in Section 6.3.
- Split sections: The grid generation will start at the intersection of the two sections. Therefore these are split at the intersection point (point 1).
- Divide by length (Figure 6.7): The sections are divided by the specified length. This length is equal to the desired mesh size.
- Create two spheres with radius equal to the mesh size at the first two points (point 2 and 3, Figure 6.8).
- Create intersection curves of the spheres with the surface (Figure 6.9).
- Create intersection point (point 4) of these two curves. This point will be one of the next points to create the next intersection point (Figure 6.9).

By repeating this sequence of creating spheres and intersections at point 5 and 4, point 6 can be located (Figure 6.10 and Figure 6.11). This sequence is repeated until all possible intersection points are located on the surface. After this, the points can be connected, to create the structure.

One difficulty to overcome in the scripting tool, is creating continuous laths. A gridshell structure is built with continuous laths in two directions and the laths are connected together at each intersection with free rotation around the node's z -axis. When the structure is to be implemented in a structural analysis program, the data on the geometry of the structure should be correct, i.e. it must be known which element is connected to which node and this must be correct for the entire structure.

The fact that rotation around the node's z -axis must be accommodated in the model means that the elements in different directions cannot be connected to the same node in the computer model.

The separation of the elements and associated nodes is created by using the sections as the main directions. First, all created nodes are copied. Two different sets of nodes are created this way: the originals and the copies. The separation between the directions is created by connecting the elements in one direction to one set of nodes and the elements in the other direction to the other set of nodes. This is further elaborated in Section 6.4.1.2.

³⁰ RhinoScript plugin help file

³¹ <http://en.wikipedia.org/wiki/Vbscript> accessed 19-02-2007

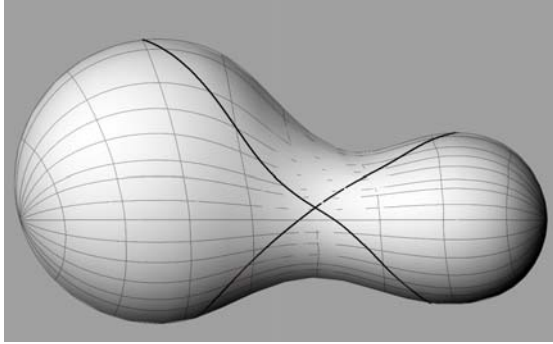


Figure 6.6: Creating sections

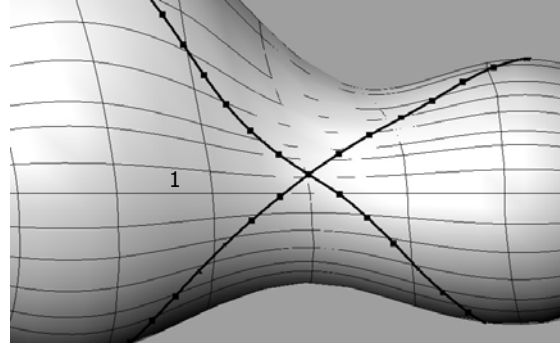


Figure 6.7: Sections are divided by length

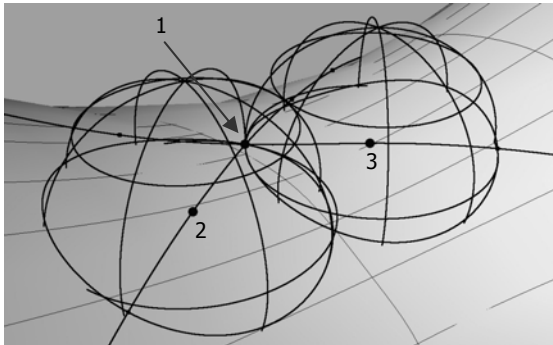


Figure 6.8: Spheres and intersections created

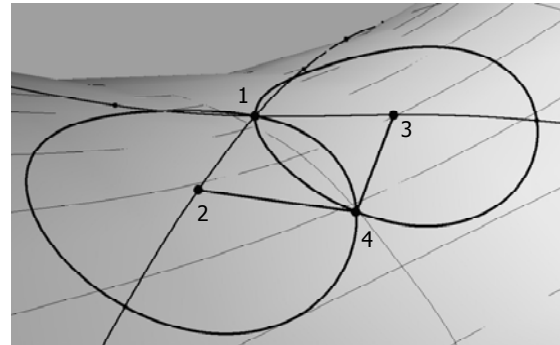


Figure 6.9: intersection point located

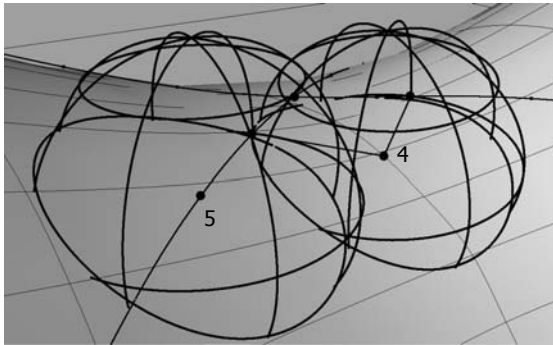


Figure 6.10: Spheres are created at point 5 and 4

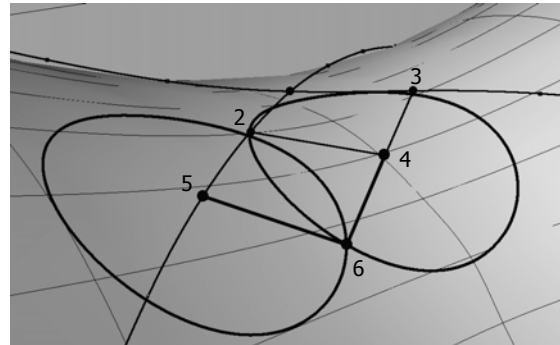


Figure 6.11: Point 6 is created at the intersection of the intersection curves

6.3 Assumptions and starting points

For the grid generation technique to work properly, a few assumptions have to be made:

- Line elements between the points are created as straight lines. These lines should follow the surface, as in real the timber is curved as well. The difference in length between the curved element and the straight line is neglected, based on the fact that radius of curvature \gg element length (see Appendix 3: Proof of $R \gg$ mesh size).
- The sections from which the grid generation takes off have such a shape that it can be approximated by curving and twisting a lath.
- Rhino is able to create and locate sections and section points with the necessary accuracy.

The sections from which the generation takes off are necessary as basis for the generation. The sections are used as basic directions for the grid and the first points will be located on this curve. The correctness of the grid depends on the correctness of the sections. The curve of the section should be curved in such manner that the lath is can follow this curve by bending and twisting.

Rhino has the function "InterpCrvOnSrf", which interpolates a curve on a surface between or through the desired points. It creates a curve running smoothly over the surface. It is assumed that these curves approximate the needed section curves and are usable for the grid generation.

Furthermore, the global and local axes of the members are shown in Figure 6.12. The local x -axis of a member points in the direction of the member. Its z -axis is pointing upward, in the positive direction of the global z -axis. The local y -axis is orthogonal to the local z - and x -axes

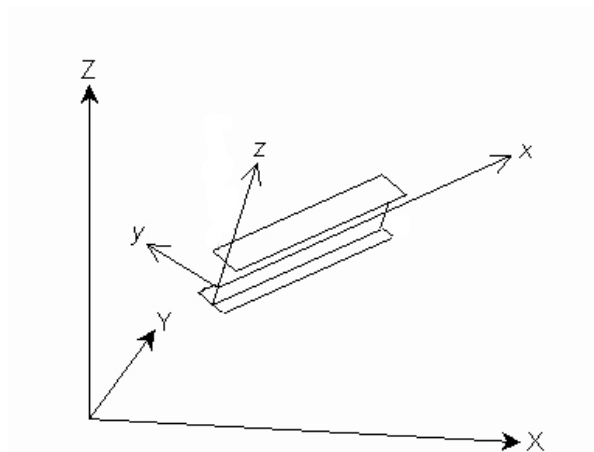


Figure 6.12: global and local axes of the members³²

³² OASYS GSA helpfile

6.4 The gridshell design tool

In this section the gridshell design tool is described, along with the results. The gridshell design tool is set up in such way that different sub-tools are used for different tasks. The main tool is the grid generation tool itself, which generates the grid on the surface pointed by the user. The script which is executed when running this tool is described in Section 6.4.1. The results are presented in Section 6.4.2. Some of the problems encountered while developing this script can be found in Appendix 4: Problems encountered in developing the grid generation tool.

A second tool can be used to trim the structure to a desired height. The script for this tool is described in Section 6.4.3. Finally, an output has to be generated when the generated grid is to be used for further structural analysis. A third tool is created for this, which extracts all information needed from the model. This can be found in Section 6.4.4.

Rhino provides the possibility to create a custom toolbars and buttons. A gridshell toolbar as shown in Figure 6.13 can be created as a graphical representation of the gridshell design tool. The three buttons represent the different tools.



Figure 6.13: Toolbar with buttons for the CreateGrid, TrimStructure and ExportStructure tools

6.4.1 Grid generation script

In this section the process in the script is elaborated. Flow charts are used for this.

Figure 6.14 shows a flow chart of the script's main structure. A subroutine is indicated with a diamond shape. The rectangles with rounded corners represent one or more commands that are executed. A Boolean operation is represented by a six cornered polygon.

The main structure of the tool starts with an input subroutine, in which the user is asked for the required input, after which the grid generation takes place. This consists of the generation of the grid of points, connection of the points with lines and if desired the check of the curvature and torsion angles. The different subroutines are discussed more detailed in the next sections.

The result of the script is a series of points and elements. When the geometry is found correct, a second script described in Section 6.4.4 can be executed to generate text output which can be used in a structural analysis package.

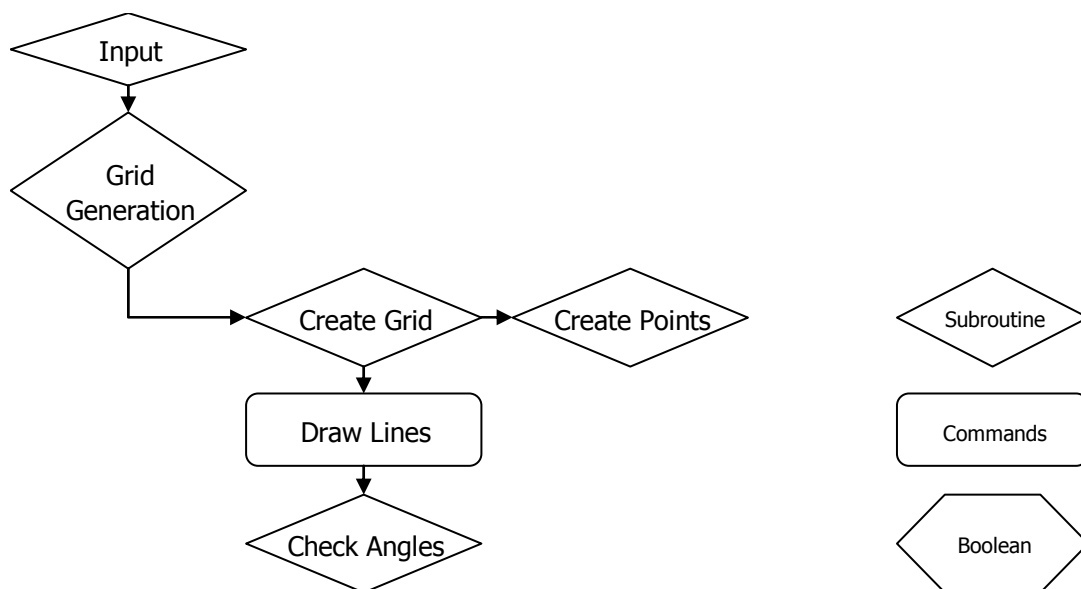


Figure 6.14: Flow chart of the script's main structure

The script is created with a main loop, which enables the user to exit without error messages. This is possible every time a message box appears. This happens when user input is required. The user has the option to click "Cancel", which exits the main loop. By default it is also possible to exit a script in Rhino by pressing the escape key. With this script this is needed several times before the script exits entirely.

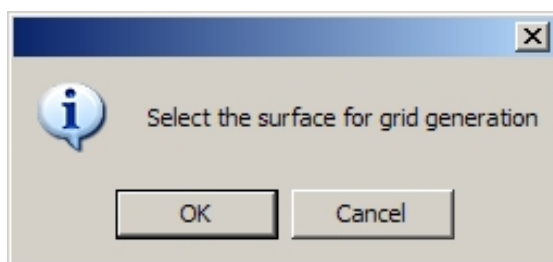


Figure 6.15: text box with options OK and CANCEL

6.4.1.1 Input

The grid generation tool starts with statements which ask the user for input. This sequence is shown in the flow chart below:

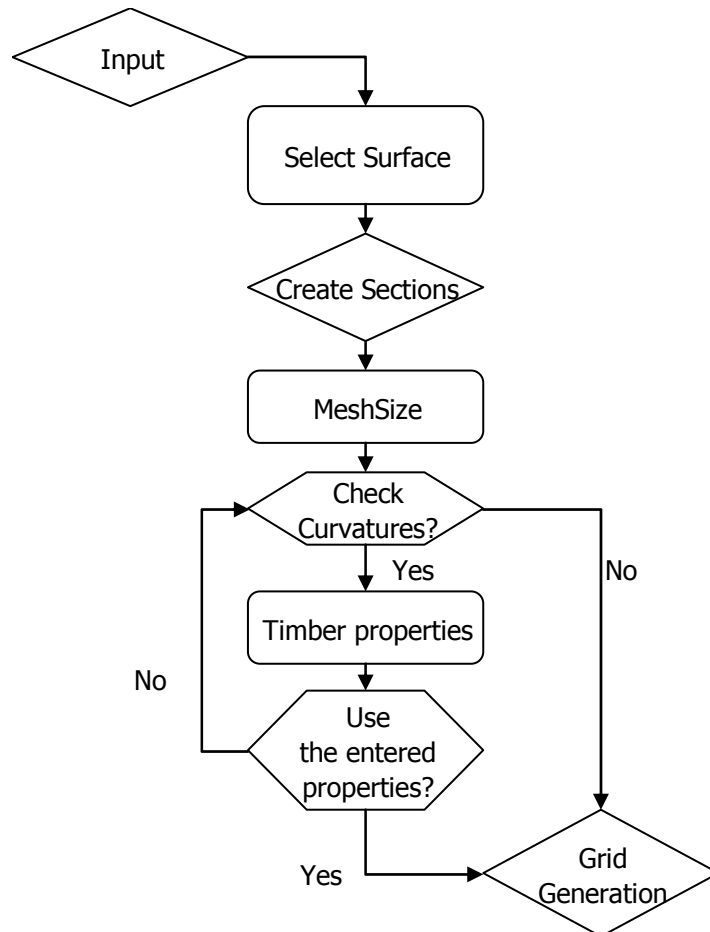


Figure 6.16: Flow chart input section

The input routine starts with asking the user to select the surface which will be used for grid generation. After this the user is asked to create the sections. This Create Section subroutine is shown in Figure 6.17. It exists of:

- Creating two sections
- Asking the user if the sections should be used. If NO is selected, new sections can be created
- The sections are split at their intersection points. There is no RhinoScript command for this, so the user is prompted to do this manually by following the command line instructions. There are now four section parts.
- If a section's start point is below its end point the section is flipped. If this is omitted, it can occur that the generation starts at the bottom of the structure. This will lead to failure of the grid generation.

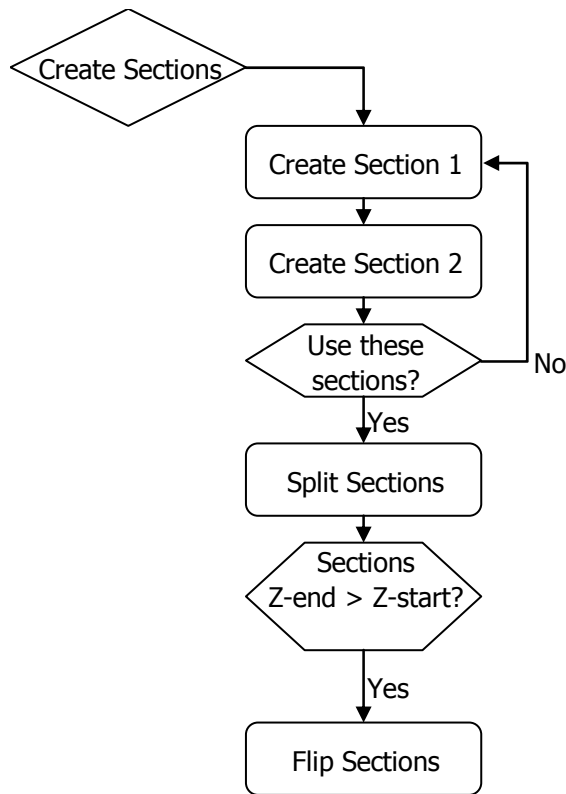


Figure 6.17: Create Sections subroutine

After creating the sections, the user is asked for the desired mesh size and if it is needed to check the curvatures in text boxes (Figure 6.18). The latter is asked because checking the curvatures consumes quite a lot of time. If YES is clicked, input is required on the material properties of the timber. The following input is required:

- Height of the timber laths $h_{timber,i}$
- Width of the timber laths $w_{timber,i}$
- E-modulus of the timber;
- Shear modulus of the timber;
- Bending strength of the timber;
- Shear strength of the timber;
- Modification factors k_{mod} and γ_m .

For every input a text box appears, such as shown in Figure 6.19. When all material properties are known, the maximum angles of curvature and torsion are calculated. The angles of curvature determined in the curvature check have to be equal or smaller than these values. The maximum angles are calculated according to Section 3.2.4.

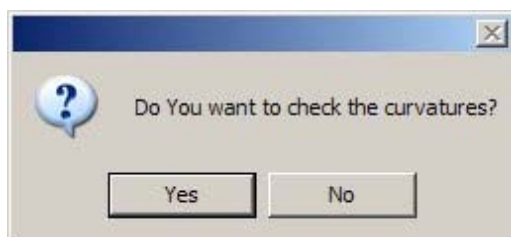


Figure 6.18: Text box Check Curvatures?

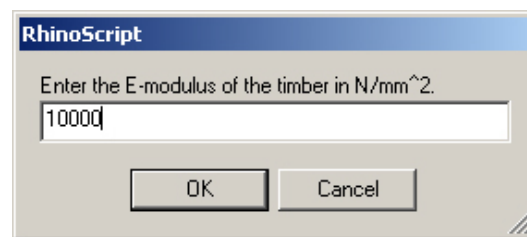


Figure 6.19: String input message box

6.4.1.2 Grid Generation

Figure 6.20 shows the flow chart of the grid generation sequence. The actual grid generation is split into the subroutine "Create Grid" which generates the node points and the part which connections of the nodes in different directions.

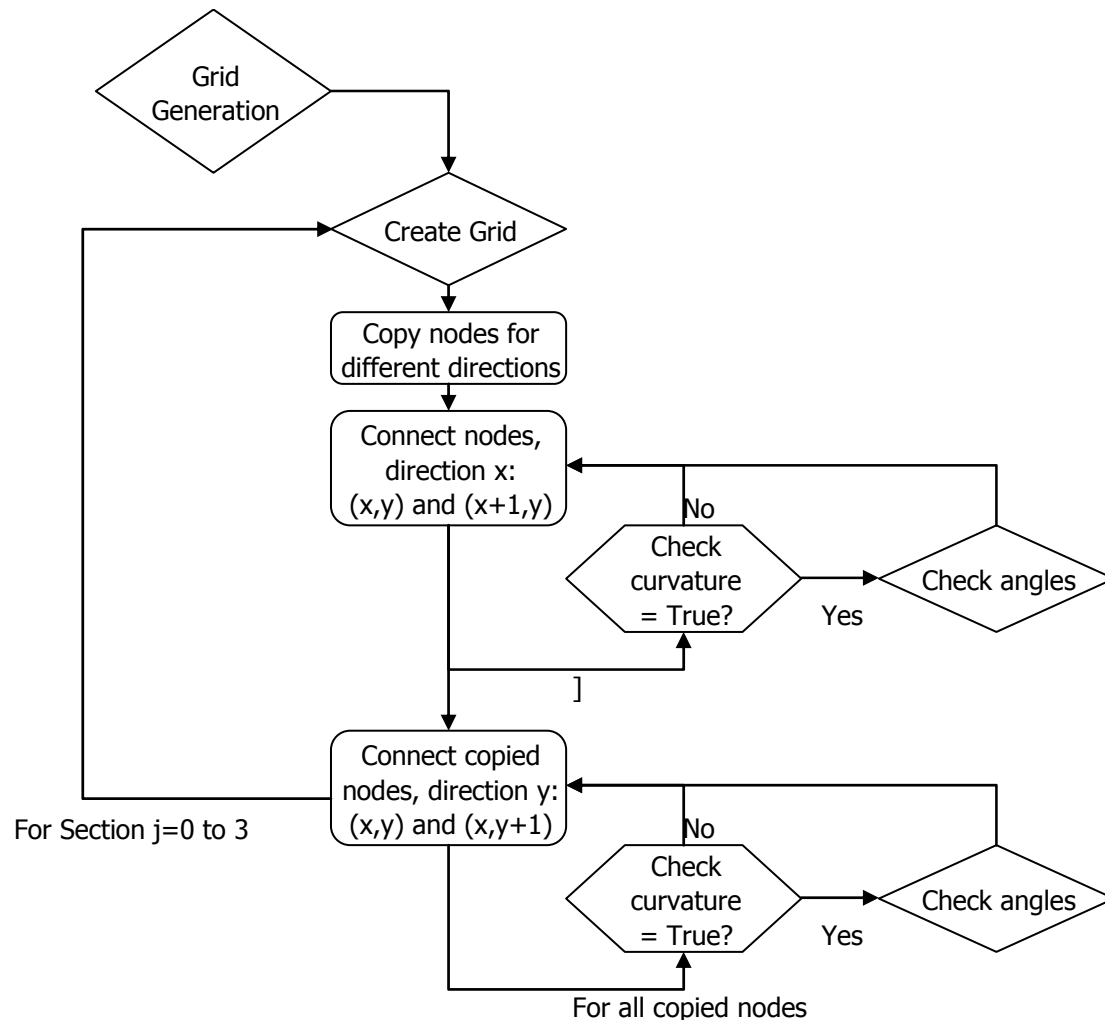


Figure 6.20: Flow chart Grid Generation sequence

The global directions in which the elements of the grid are drawn are indicated by the sections (Figure 6.21). The sections also divide the surface into quadrants. The grid generation is executed quadrant for quadrant between two subsequent sections, starting with section 0 and 1. First the subroutine "Create Grid" creates an array of points (Figure 6.22). The subroutine "Create Grid" is described in the next section. When all nodes are created, they are copied to make the separation of the lath directions possible. The local directions of the grid are direction x and y . These are the directions of the sections used, which are section 0 and 1 in case of the first quadrant. Connecting the original nodes together, laths in direction x are created (Figure 6.23). This corresponds with the global direction 1. After this the laths in direction y are created (Figure 6.24), corresponding with global direction 2. These are connected to a different set of nodes by connecting the copied nodes. All elements are named after the nodes between which they are created to be able to reproduce this information. If the curvature check is desired, which was asked in the input subroutine, the subroutine "Check Angles" is executed for every created element.

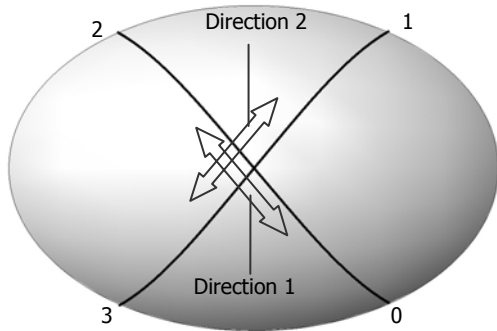


Figure 6.21: Sections 0 to 3 and global directions

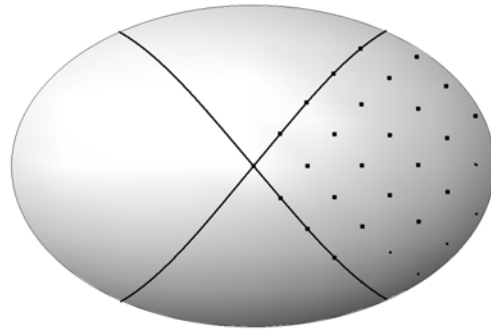


Figure 6.22: First quadrant filled with points

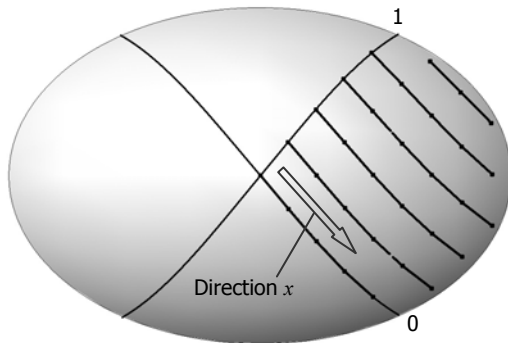


Figure 6.23: Lines in direction x (1) are drawn between the original nodes

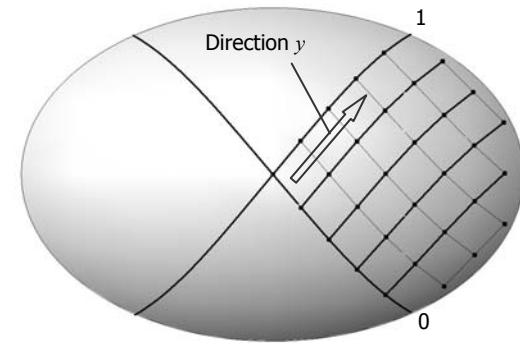


Figure 6.24: Lines in direction y (2) are drawn between the copied nodes

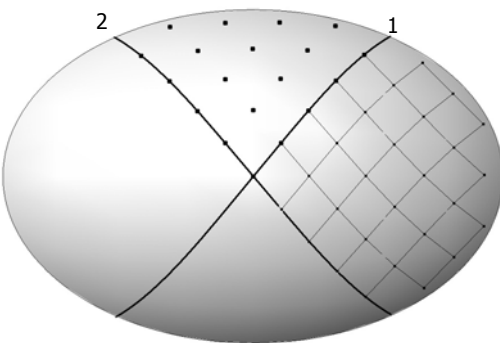


Figure 6.25: Nodes between section 1 and 2 are created

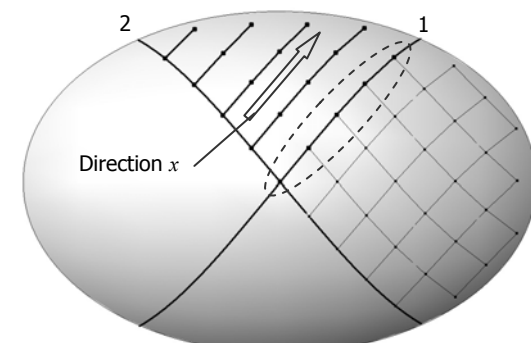


Figure 6.26: Lines in direction x (2) are drawn between the copied nodes

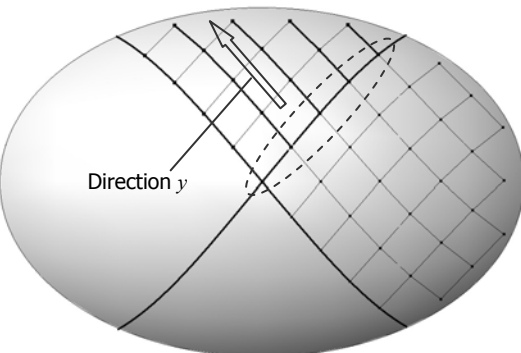


Figure 6.27: Lines in direction y (1) are drawn between the original nodes

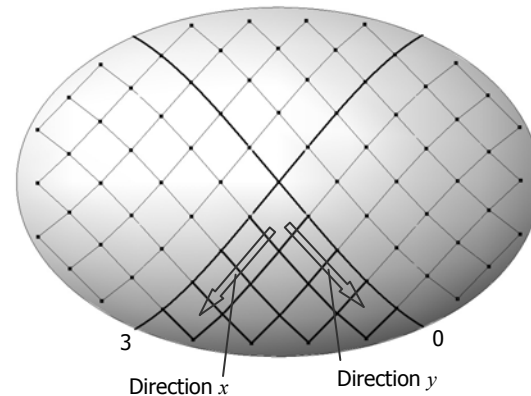


Figure 6.28: The final quadrant between section 3 and 0 is filled.

After the first quadrant is filled with nodes and elements, the quadrant between section 1 and 2 is processed. First the array of points is created (Figure 6.25). Because the process has shifted to the next quadrant, the x -direction is determined by section 1 and the y -direction by section 2. The quadrants have to connect to each other in the global directions in order to create continuous laths over the entire structure. In the first quadrant the original nodes were used to create the lines in direction x (global direction 1). The lines in direction y were connected to the copied nodes for global direction 2. For the current quadrant connecting the original nodes will create lines in the x -direction, which corresponds to global direction 2 (Figure 6.26). Creating lines with the copied nodes will create lines in the y -direction, corresponding with global direction 1 (Figure 6.27).

To connect the first and second quadrant, the points located on the adjacent section (section 1 in this case) need to be the same points for both quadrants. To connect the laths in global direction 2 (local direction x for the current quadrant), the points at the array location $(x, 0)$, encircled in Figure 6.26, need to be the same points as the copied points created at the array location $(0, y)$ in the first quadrant, which are already connected to the lines in direction 2 in that quadrant. Therefore these points are copied into the point array of the current quadrant. An equal process is performed for the lines in direction 1. The original nodes at location $(0, y)$ in the first quadrant have to be copied to the copied nodes array of the current quadrant (encircled in Figure 6.27).

The process of creating points, copying them and connecting them in the correct directions is repeated until the entire structure is processed. In the last quadrant an extra copy operation is performed. Not only the points located at the section adjacent to the previous quadrant need to be copied, but also the points located at the section between the last and the first quadrant.

When the process finishes, the lines in different directions are connected to different point sets, enabling the user to reproduce the laths as continuous in the different directions for structural analysis.

6.4.1.3 Create Grid

With the subroutine "Create Grid" the generation of the point grid is created. The process starts with checking if it is the first time a quadrant is processed. If this is true, the first section is divided by length MeshSize. If it is not the first quadrant the points located on the sections are copied to connect the adjacent quadrants, which has been explained in the previous section.

The generation of a point is processed by the subroutine "Create Points". This subroutine is repeated until the final points on the sections are used. This results in an array of points with the dimension x_{max}, y_{max} (Figure 6.29). Because this process does not fill the entire surface with points, it has to be checked if there is another point possible at the position $(x_{max}+1, i)$ or at $(j, y_{max}+1)$. This is checked by the following process.

Let's consider the check in direction y . A plane is created through points (j, y_{max}) , $(j, y_{max}-1)$ and $(j, y_{max}-2)$ (Figure 6.30 and Figure 6.31). This plane is scaled to be able to locate the intersection point(s) with the sphere intersection curve at location (j, y_{max}) (Figure 6.32). If there are two of these intersection points, the outer one is another grid point. If there is only one intersection point, no next grid point is possible at this location and the check is performed at location $(j+1, y_{max})$.

If a next grid point is located, the "Create Points" subroutine creates another row of points. When all points at the edge in y direction are checked and no additional grid points are located, the checking process is performed at the edge in x direction.

By using a plane through the three edge points to locate the next point, a next element can be created in the same plane as the preceding two elements. The new element continues the curvature of those elements.

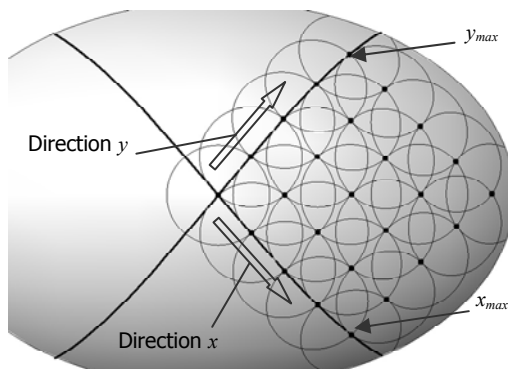


Figure 6.29: An array of dimension x_{max}, y_{max}

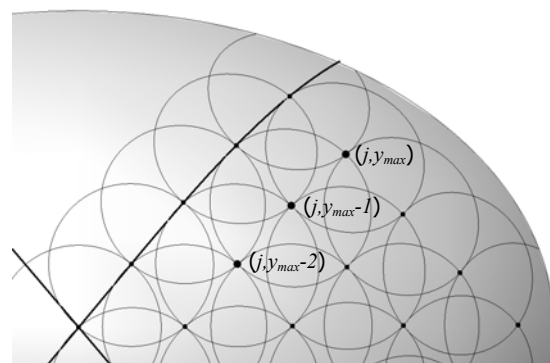


Figure 6.30: Points for creating the plane

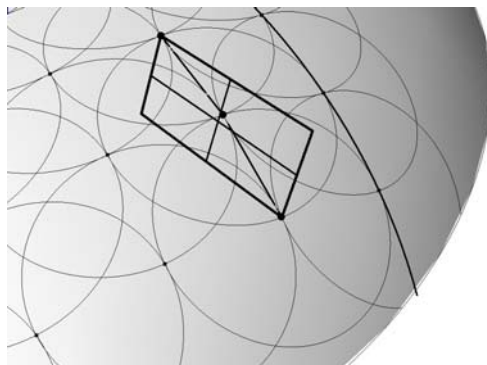


Figure 6.31: A plane through points (j, y_{max}) , $(j, y_{max}-1)$ and $(j, y_{max}-2)$ is created.

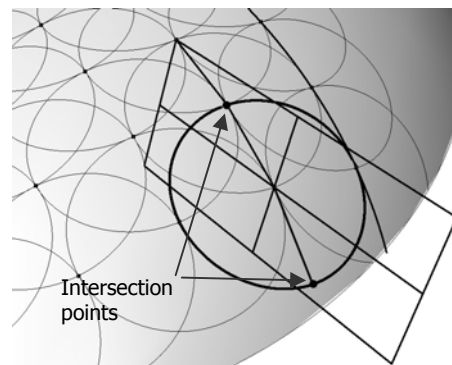


Figure 6.32: Intersection points. The bottom one is point $(j, y_{max}+1)$

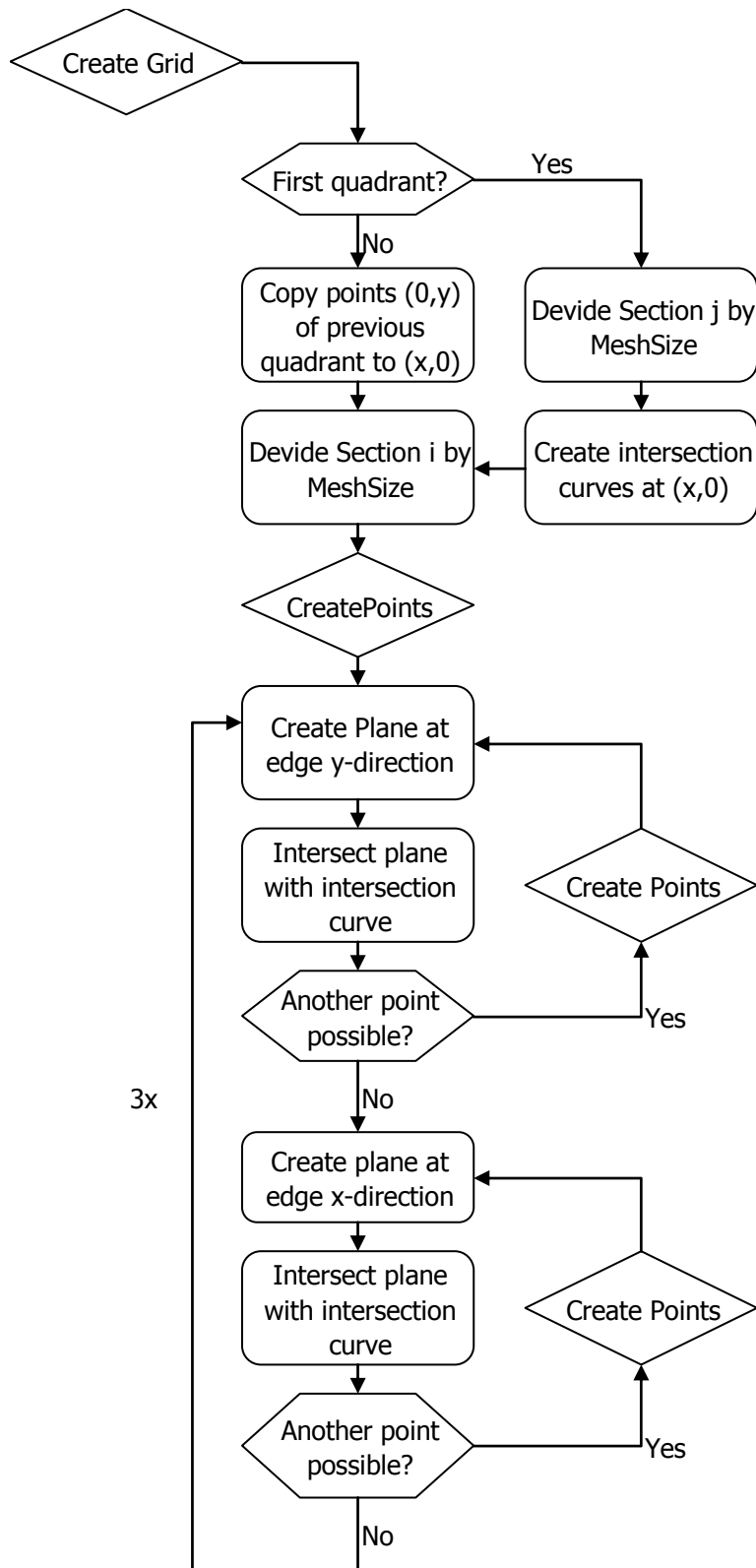


Figure 6.33: Flow chart of the "Create Grid" subroutine

6.4.1.4 Create Points

The "Create Points" subroutine is the part which locates the points on the surface with equal mesh distance. It executes the routine described in Section 6.2 in series, until all points on the sections are used and a grid array of the dimension x_{max}, y_{max} is created. When a sphere intersection curve is created, it is checked if the result of the intersection procedure is a single object and if it is a curve. It is possible that the intersection procedure creates more than one object (see Section 6.4.4). If the intersection is created with more than one curve, the parts are joined.

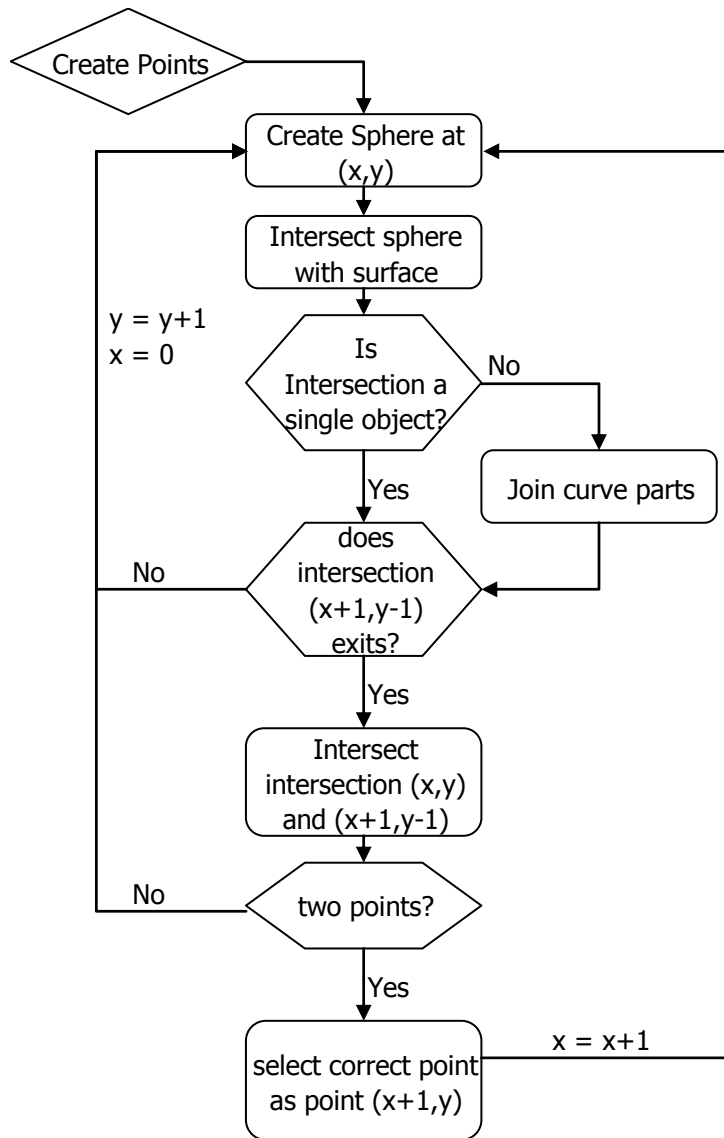


Figure 6.34: Flow chart of the "Create Point" subroutine

The points are located row for row until the outer nodes on the section is processed. Before two intersection curves are intersected to locate the grid points, it is checked if the next curve on the previous row exists (location $j+1, i-1$). If this curve does not exist, the outer node is reached and the process starts with the next row. If this curve exists, curve (j, i) and $(j+1, i-1)$ are intersected. If two intersection points are located, one of these points is the next grid point. If there is only one point, the intersection curve $(j+1, i-1)$ is located at an edge of the surface, or something went wrong with the intersection process. In either case, the process starts with a new row.

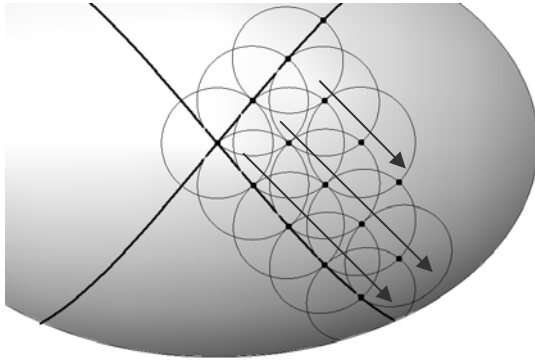


Figure 6.35: The grid is created row by row

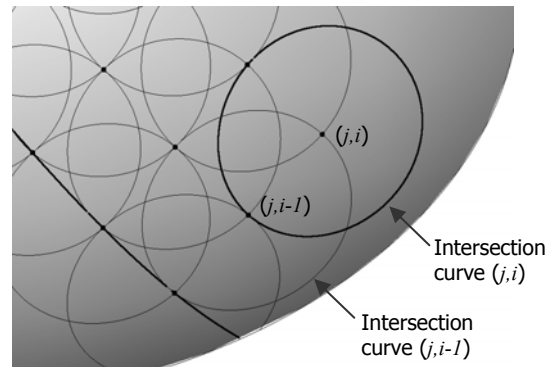


Figure 6.36: Intersection curve $(j+1, i-1)$ does not exist. The process starts with the next row

6.4.1.5 Check Angles

In the input section, the user was asked if the curvatures should be checked. If YES was answered the angle of curvature in y and z direction and the torsion angle in x direction are checked every time an element is added. The flow chart of the checking procedure is shown in Figure 6.41 and explained in this section.

The angles are determined graphically in the Rhino model. To illustrate how, let's consider two elements between the arbitrary points $j-1, j$ and $j+1$ on a surface (Figure 6.37). Angle α_y of the curvature around the y-axis between element 1 and 2 is determined with the following steps:

- At point j , the normal to the surface is created (Figure 6.38).
- A plane through this normal and element 1 is created. This is directional plane of the element. The tangent to the surface is created by creating a normal to the directional plane (Figure 6.39)
- This tangent is copied to point $j+1$ and the intersection of his copy and the directional plane is located (Figure 6.40).
- The angle of curvature around the y-axis is now defined as the angle between element 1 and the line between node j and the intersection node. This angle is called α_y .

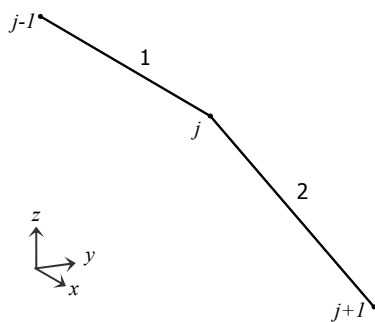


Figure 6.37: Two elements under an angle with each other

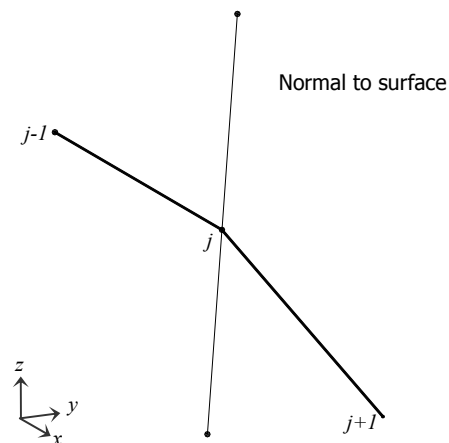


Figure 6.38: Normal to the surface created

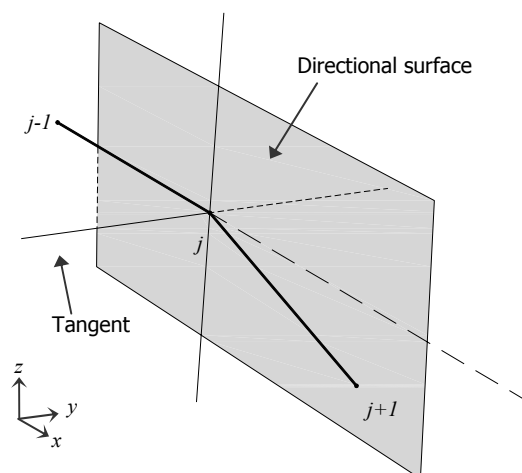


Figure 6.39: A directional plane through element 1 and normal created. The normal to this plane is tangent to the surface

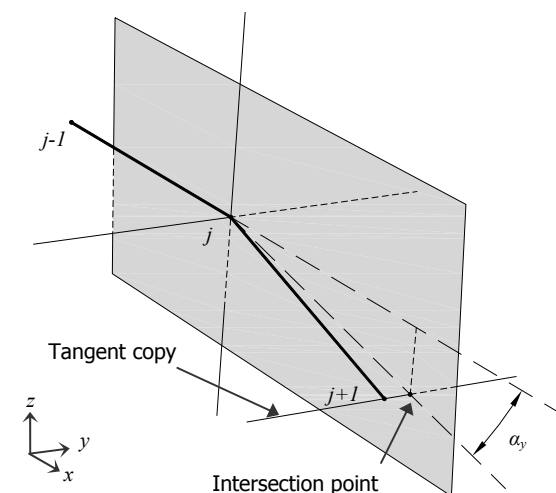


Figure 6.40: The angle α_y is determined

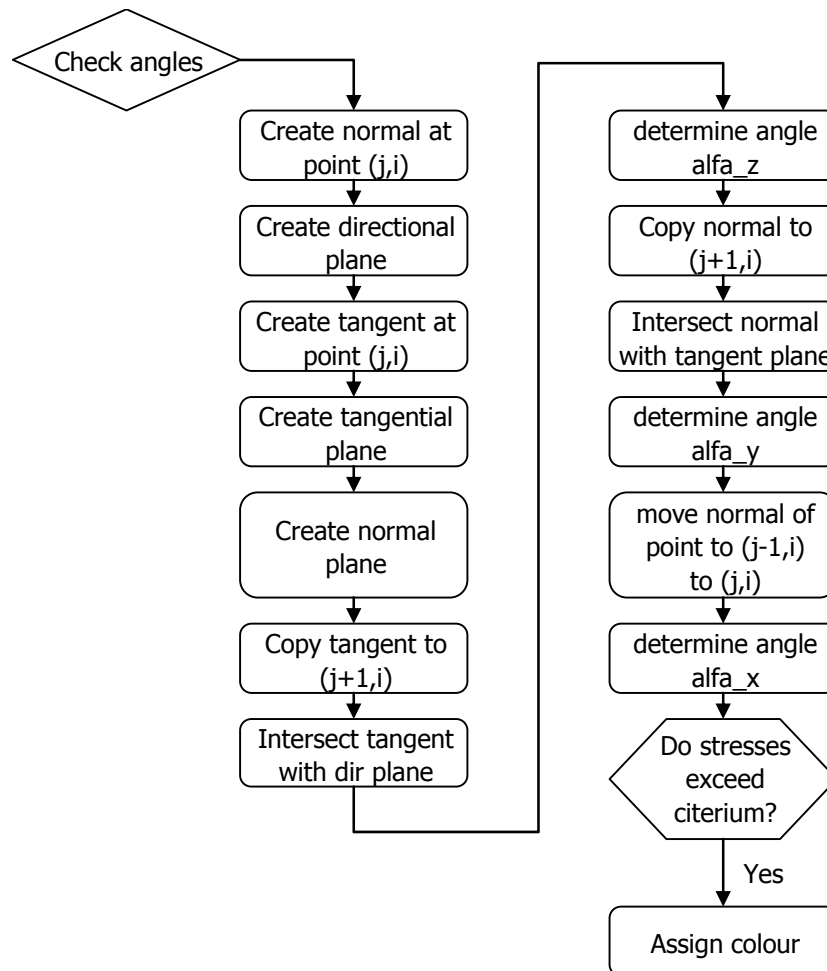
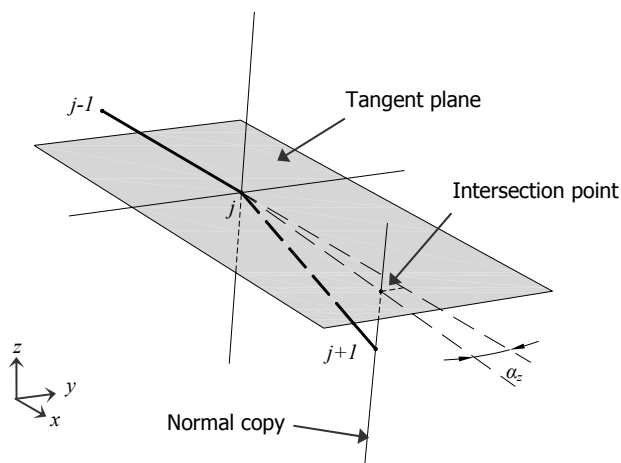


Figure 6.41: Flow chart of the "Check Angles" subroutine

Angle α_z of the curvature around the z -axis is determined in a similar way (Figure 6.42):

- The tangential plane is created through the tangent and element 1.
- The normal is copied to point $j+1$.
- The intersection point of the tangent plane and the normal copy is determined.
- The angle α_z is determined as the angle between element 1 and the line between point j and the intersection point.

Figure 6.42: Tangent plane and α_z

The determination of the angle of torsion angle α_x is determined by using the element created previous to element 1: element -1, and the normal to the surface in point $j-1$:

- The normal -1 is copied to point j .
- Then the element -1 is copied to the end of the normal -1 copy.
- The plane trough the normal and tangent of point j is created. This is called the perpendicular plane.
- The intersection of this copied element and the perpendicular plane is located
- The torsion angle is angle between the normal of point j and the line between this intersection point and point j .

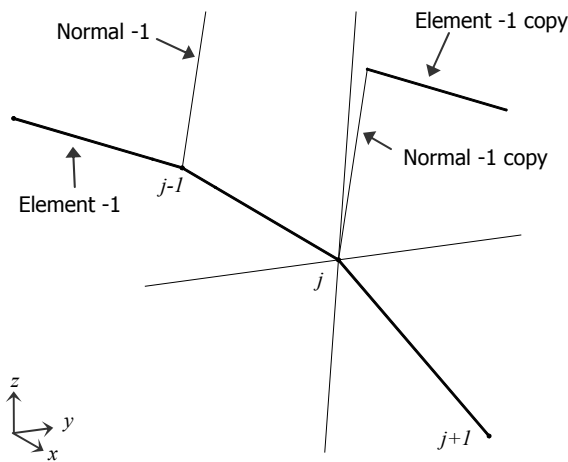


Figure 6.43: Element -1 and normal point $j-1$ are copied

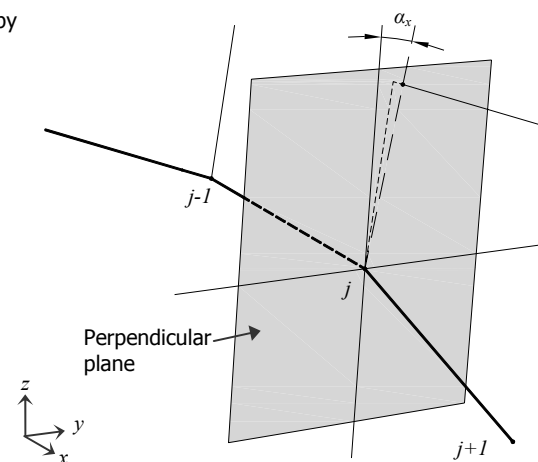


Figure 6.44: Determination of α_x

Now all angles are known, it can be checked if the stresses due to the curvatures exceed the stress criterion. The implemented criterion in the tool for the bending angles is the criterion for bending in two directions described by equations 3.17 and 3.18 in Section 3.2.4.4:

$$\frac{\sigma_{m,y,d}}{f_{m,y,d}} + k_m \frac{\sigma_{m,z,d}}{f_{m,z,d}} \leq 1 \quad (3.17)$$

$$k_m \frac{\sigma_{m,y,d}}{f_{m,y,d}} + \frac{\sigma_{m,z,d}}{f_{m,z,d}} \leq 1 \quad (3.18)$$

For this the bending stresses in different directions need to be calculated from the angles of curvature. The following equations are used for this:

The bending radius R can be calculated with equation 3.6 according to Section 3.2.4.4.

$$R = \frac{Eh}{2f_m} \quad (3.6)$$

When R is known, the current bending stress can be calculated by rewriting equation 3.6 as:

$$\sigma_m = \frac{Eh}{2R} \quad (6.1)$$

R can also be calculated with:

$$R = \frac{1}{\kappa} \quad (6.2)$$

In which curvature κ can be written as (see Appendix 1: Determination of the maximum bending radius):

$$\kappa = \frac{d\theta}{dx} \quad (6.3)$$

When for $d\theta$ the angle of curvature α is used and for dx the mesh size L is used, σ_m can be calculated with:

$$\sigma_m = \frac{Eh\alpha}{2L} \quad (6.4)$$

For torsion the check is performed by comparing the determined torsion angle with the maximum torsion angle, which is calculated according to Section 3.2.4.3, equation 3.14:

$$\alpha_{i,\max} = \frac{T_{\max} L}{KG} \quad (3.14)$$

If one of criteria in equation 3.17 and 3.18 is exceeded, or then the torsion angle between two members is larger than the maximum torsion angle, a colour is assigned to the reviewed element. This way, the curvatures of the grid are checked visually. The colours that are used are:

- red when one of the bending criteria is exceeded;
- blue when the torsion criterion is exceeded;
- green when both the bending and torsion criteria are exceeded.

6.4.2 Grid generation results

The grid generation tool creates a graphical representation of the grid structure in Rhino. All information needed for output to a structural analysis program is stored in the names of the nodes and elements and the coordinates of the nodes, as described in Section 6.4.4. Figure 6.45 and Figure 6.46 show the surface and the used sections used in this generation. Figure 6.47 and Figure 6.48 show the result of a grid generation with mesh size 2,5m in top and perspective view. With a mesh size 0,5m, which is a more realistic mesh size, the structure shows a smooth surface.

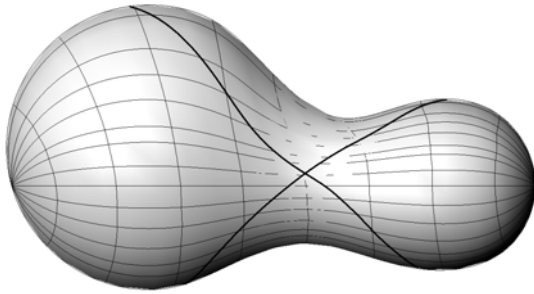


Figure 6.45: Used section curves

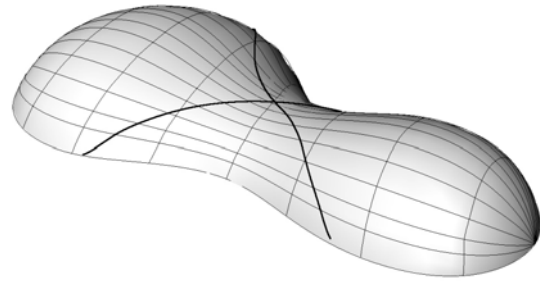


Figure 6.46: Perspective view

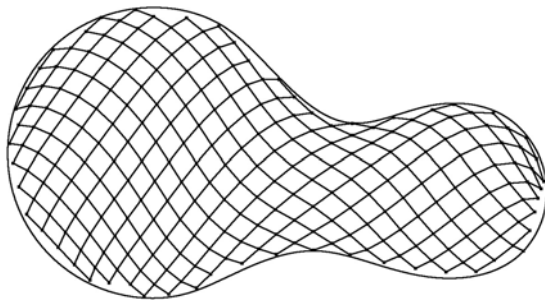


Figure 6.47: Result of the grid generation with mesh size 2,5m

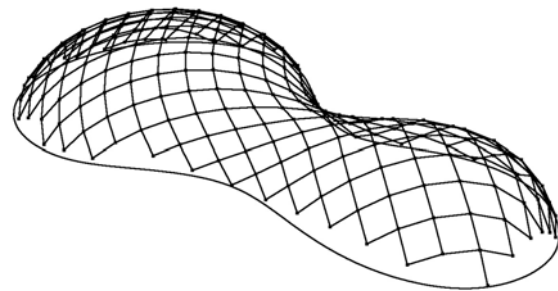


Figure 6.48: Perspective view of the result of the grid generation with mesh size 2,5m

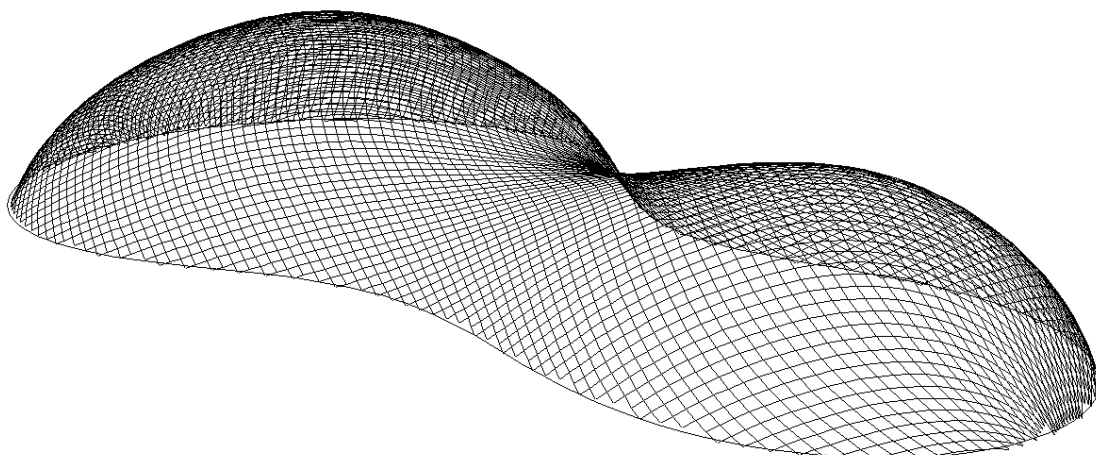


Figure 6.49: Structure with a grid with mesh size 0,5m

In Section 5.3 it was stated that an eggoid shape will be analysed to test if this shape is possible with a gridshell structure. The shape used for this analysis with the sections used is shown in Figure 6.50 and Figure 6.51. Figure 6.52 to Figure 6.54 show the result of a grid generation.

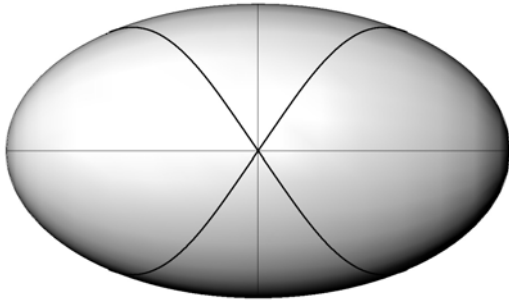


Figure 6.50: Eggoid shape top view

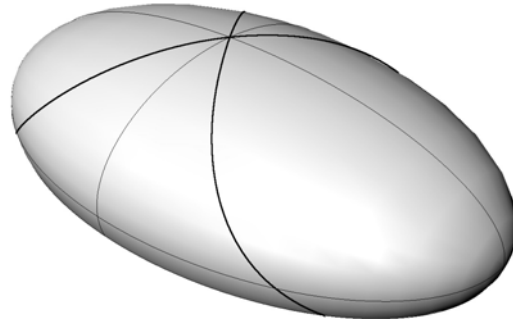


Figure 6.51: Eggoid shape perspective view

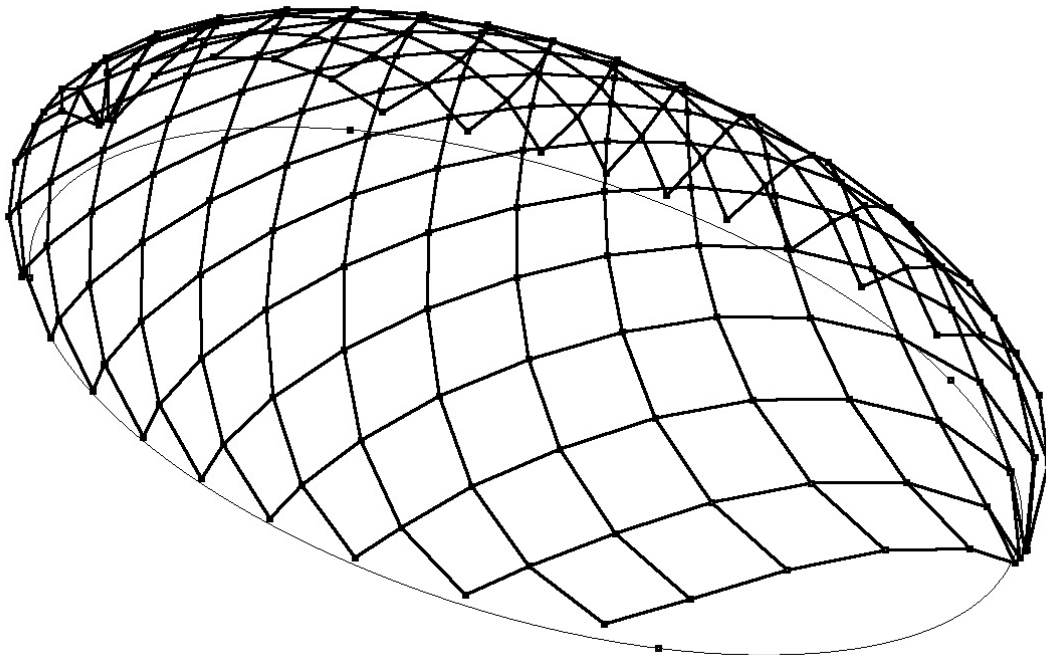


Figure 6.52: Results of grid generation with mesh size 1,5m

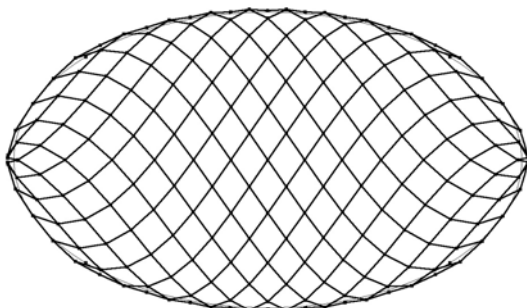


Figure 6.53: Results of grid generation with mesh size 1,5m.

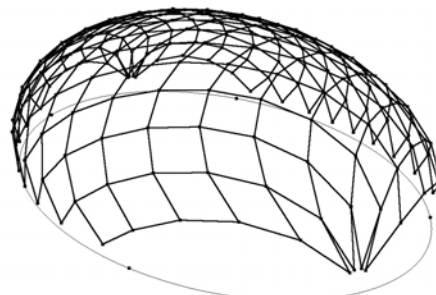


Figure 6.54: Perspective view of the eggoid

6.4.3 TrimStructure

The generation process does not create a grid which ends at the edge as it is now (Figure 6.55). The edge of the grid stays jagged because the script can not create an element if it is not between two nodes with a distance of the mesh size to each other. Of course this can be corrected by hand before exporting the structure for structural analysis, but this is not desired. This will also erase information on grid geometry that is stored in the names of the nodes and elements that will be trimmed or deleted. A solution to this problem is trimming the generated grid by a horizontal plane. This can be simply performed by hand, but when this operation is performed by a simple script, the elements and points can be named automatically to the desired format to create a correct output file.

If trimming of the shape is not desired, the surface could be extended prior to grid generation so that the grid can be trimmed back to the original shape. Figure 6.56 to Figure 6.59 show trimmed versions of the case shape and the eggoid.

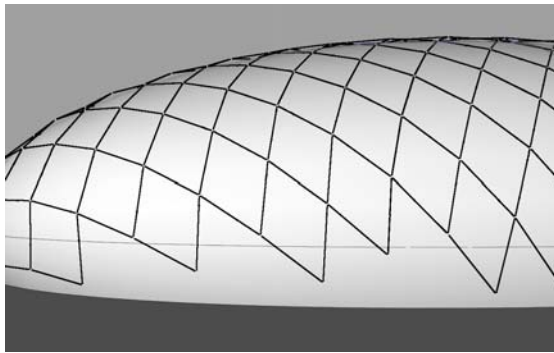


Figure 6.55: A rather jagged edge is created.

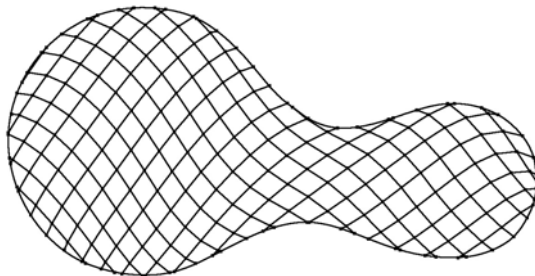


Figure 6.56: Trimmed structure top view

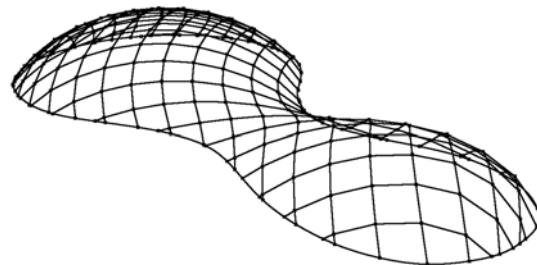


Figure 6.57: Trimmed structure perspective view

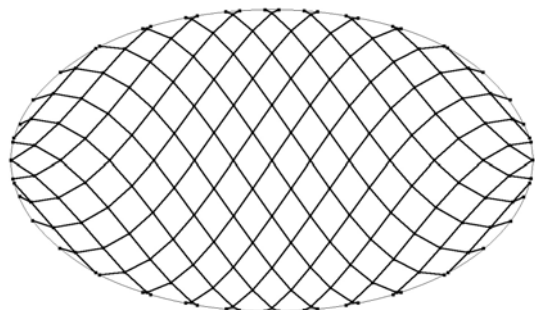


Figure 6.58: Trimmed eggoid

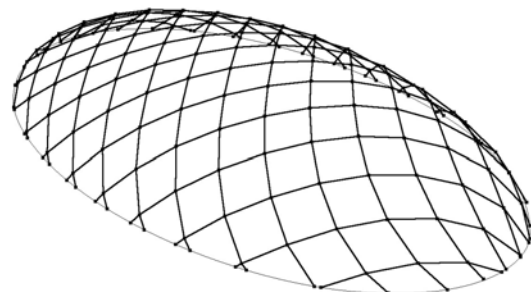


Figure 6.59: Trimmed eggoid perspective view

The trimming tool set-up is displayed in the flowchart below. The script starts with determining which elements are intersecting with a horizontal plane at the desired trimming height. When an element and the plane intersect, an intersection point is located and a new line is created between the old start point and the intersection point.

The script is set up in such a way that the naming of the elements and points stays unchanged. The newly created line and point are named after the old element and point. The output script would give an erroneous output if this was skipped. After all elements are checked, elements and points that are situated below the intersection plane are deleted.

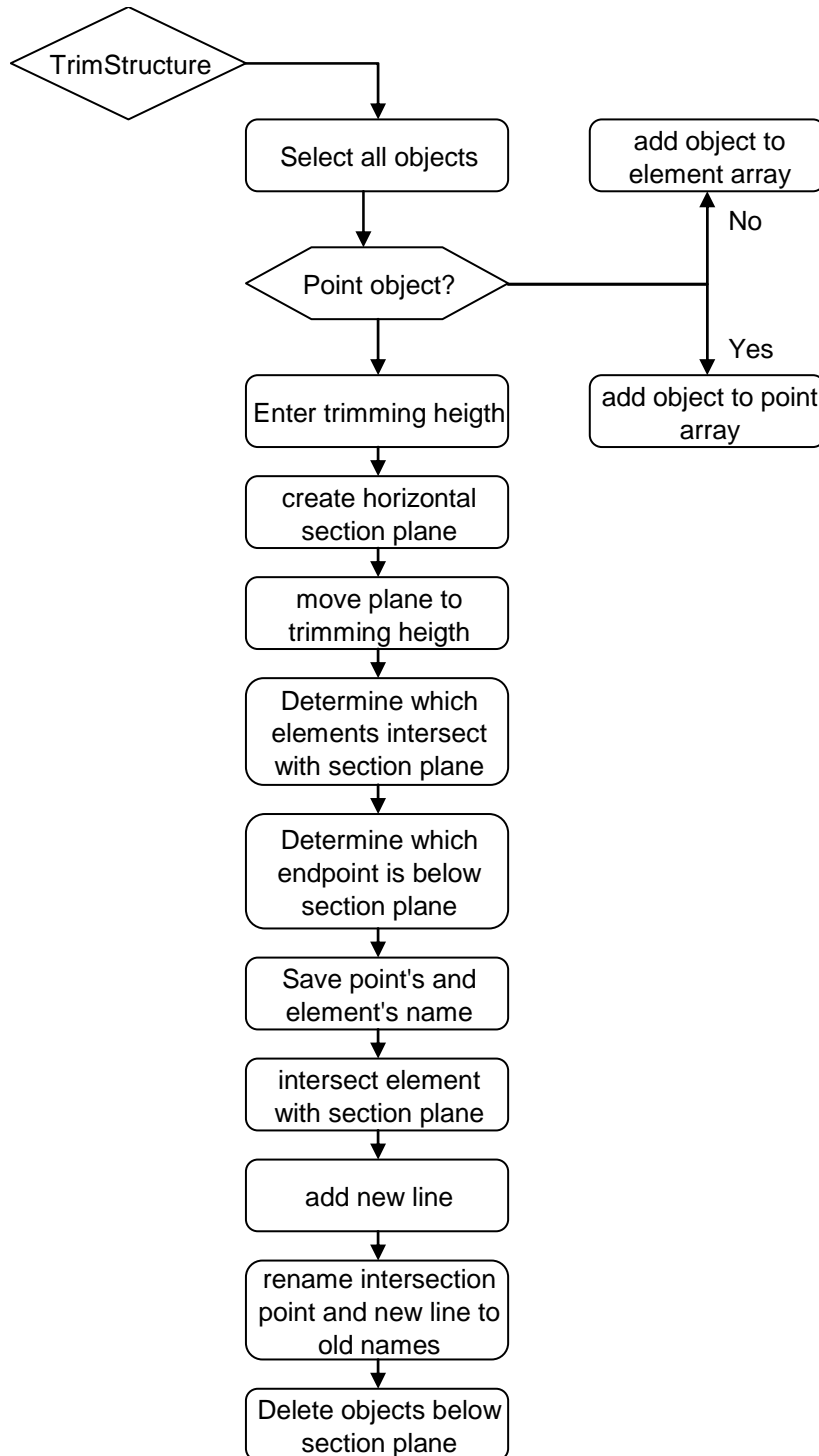


Figure 6.60: flow chart of the TrimStructure script

6.4.4 Output Script

The output of the grid generation script is the graphical representation of the points and elements, created in Rhinoceros. If it is desired to use this model in a structural analysis program, probably a compatibility problem arises. It is not possible to load the file format of Rhino in a different program. Rhinoceros provides an export feature, by which the model can be exported to the file formats of other drawing software such as AutoCad and 3Dstudio. It is also possible to create text files of the coordinates of points.

These export features exports the geometrical data of the model. The information that is needed for structural analysis is however the geometry setup data of the model, i.e. between which nodes which element is situated. This information is stored in the names of the elements by the grid generation script. All points are named by the generation script as:

"point number; base x-coordinate in the flat mat; base y-coordinate in the flat mat"

The elements are named:

"begin point; end point"

To extract this information another script is developed. This script asks the user to select all points and elements which have to be exported. The script sorts the selected objects in an element array and a point array. The user is then asked to enter a save location for the file. After this the file is opened and filled with the points names and coordinates and the element names.

The values are separated by a semicolon. The saved file is a *.txt file and has the following lay-out:

Point no.	Base X	Base Y	X	Y	Z
...
...
Element no.	Start point	End point			
...			
...			

The file can be opened with a spread sheet program to further process the data.

Unfortunately the data has to be ordered in the spread sheet. The nodes are not in ascending order and there are nodes without a number. These nodes are not part of the structure and can be neglected.

Also the node numbering needs to be restructured. The nodes are numbered by the original numbering of the script. When the model is edited, e.g. trimmed, some nodes have been deleted and new node created. When the node numbering is not restructured and copied into GSA, this software will mix up the structure because the program rennumbers the nodes, but the start and end nodes of the elements are copied in the analysis program unchanged. For example when the structure considered in Figure 6.62 is trimmed, four new nodes were created. From the trimmed structure an output is created by the output script. A list of nodes 1 to 6 is produced which are numbered {1,2,6,7,8,9} and a list of element start and end nodes. When this list is copied into GSA, this program will just number the nodes as {1,2,3,4,5,6} but not rennumbers the elements' start and end nodes. The result is that only the element between node 1 and 6 is recognized.

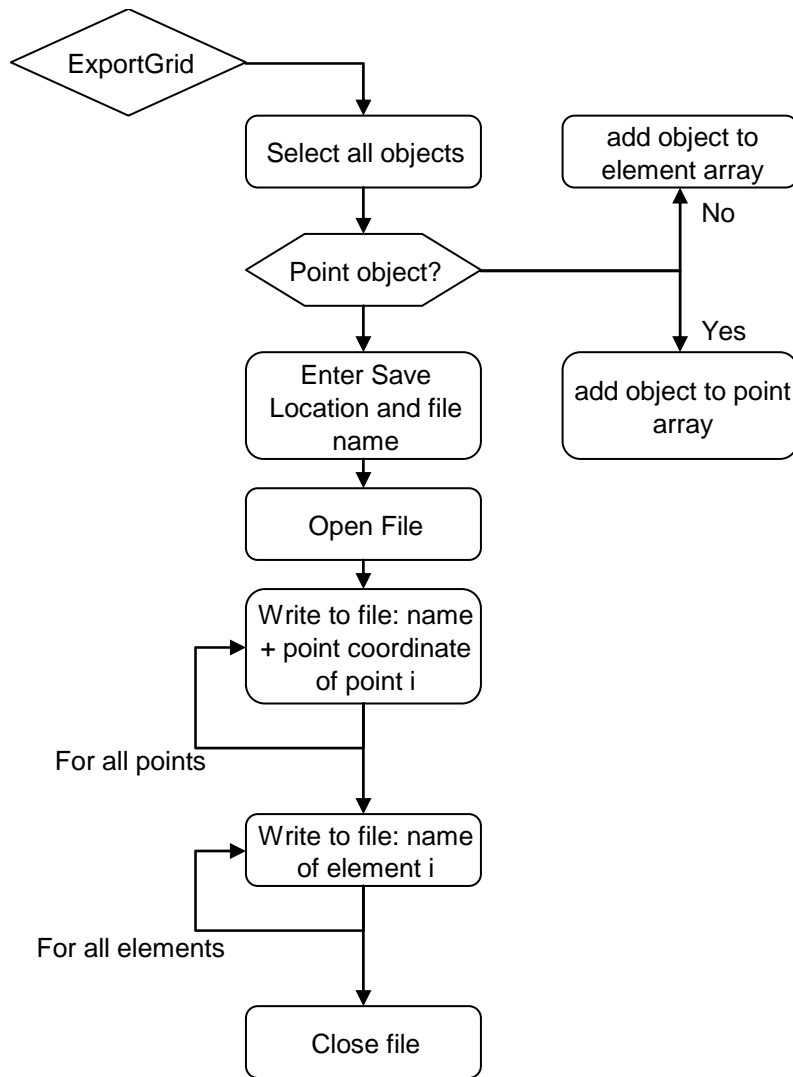


Figure 6.61: Flow chart of the Export script

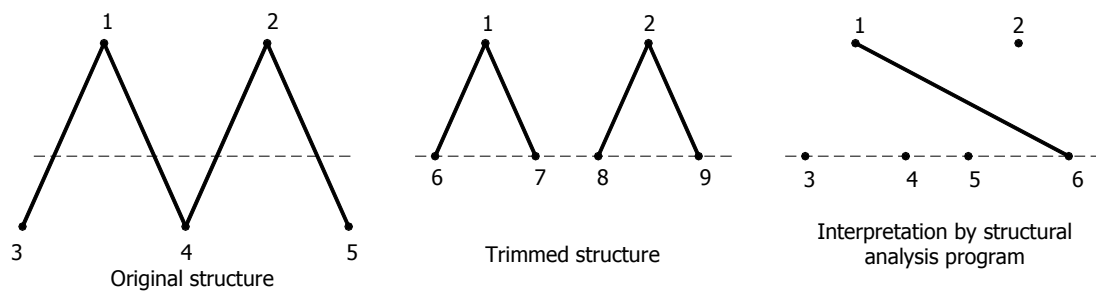


Figure 6.62: Trimmed structure and the interpretation by GSA

Nodes			Elements	
original numbering	Renumbered as		start node	End node
1	1	⇒	1	6
2	2		1	7
6	3		2	8
7	4		2	9
8	5			
9	6			

6.4.5 Grid generation with visual curve analysis

The curvature check can be executed as an option during grid generation. As stated in Section 6.4.1.5, the maximum bending stress criteria found in Section 3.2.4.4 are implemented in the grid generation tool to check the curvature of the grid members. When the maximum bending stress criteria or torsion angle criterion is exceeded, the member will change colour. The result is a generated grid with visual information on the local curvature of the laths. If the criteria are exceeded anywhere, it is necessary to adjust the structure. This adjustment can be made in a few ways. First, a smaller element height or width of the timber elements can be chosen, making a smaller radius of curvature possible. Second, timber with a smaller E/f_m ratio can be selected (see Section 3.2.4.1). Another option is to adjust the shape of the surface to a larger curvature, if this is allowed by the architect. One could say this process of adjusting the shape to the results of the grid generation is a form of backward form finding.

With the case shape, the design tool is tested with curvature check implemented. Figure 6.63 shows a grid of mesh size 2.5m, which is generated on the case shape. An element cross section of 50x50mm is used. For the modification factors $k_{mod} = 0,8$ and $\gamma_m = 1,3$ is used. The heavy printed elements are elements in which one of the bending criteria is exceeded. The dotted elements are elements where both torsion and bending criteria are exceeded. As can be seen, the radius curvature is exceeded in a large part of the surface. A modification of the structure or surface is thus needed to fulfil the demands of curvature.

First modification to the structure is reduction of the element's height. A grid is generated with cross section 35x50mm, which is shown in Figure 6.64. Still, in quite some elements, the maximum bending criteria are exceeded. Another option is to change the shape of the structure to a larger bending radius. For the grid in Figure 6.65, the curvature in the waist of the shape is lessened, resulting in a better fitting grid. One could also use different start-off sections. The sections used in Figure 6.66 have less (change of) curvature than the previous ones, resulting in a grid in which the elements are less curved.

There are still areas in the structure in Figure 6.66 where the laths of the grid cannot comply with the curvature created by the design tool. Main problem is found in the left dome, of which the curvature is the largest. To overcome this problem, the curvature of this part of the surface is decreased by scaling that part of the structure (Figure 6.67). One could also flatten the part of the surface to decrease the overall curvature in this area, but in this case the shape of the left and right part of the surface would become alike and less interesting in an architectural point of view.

The grid that is created by the design tool after this modification still shows areas in which the bending criteria are exceeded. The problem is concentrated at the ends of the structure. It seems to be problematic to create a gridshell structure for surfaces like this; that is a surface which is (semi-)spherical. The laths of the structure need to scissor and bend largely to create such surface. Additional measures such as reducing the elements' cross section in this area are needed to be able accommodate the curvature.

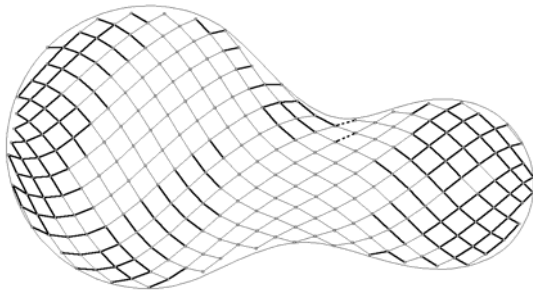


Figure 6.63: Visual curve analysis. The dark members indicate the maximum curvature is exceeded

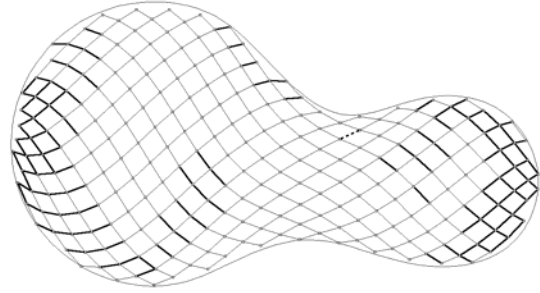


Figure 6.64: Grid generated with a smaller element height, 35mm

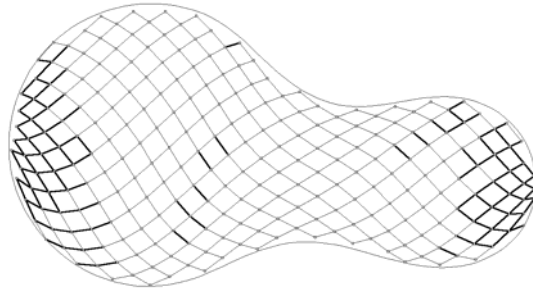


Figure 6.65: Shape with less curved waist

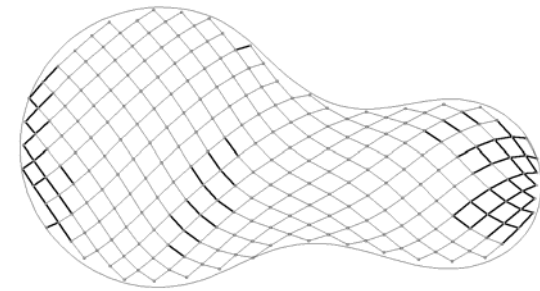


Figure 6.66: Different start-off sections

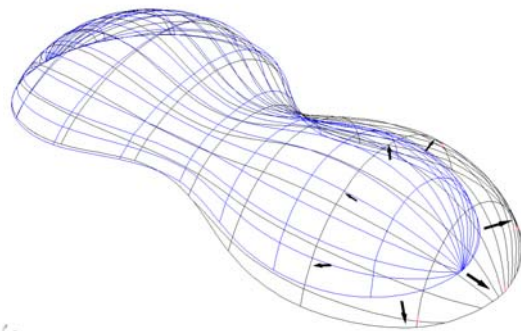


Figure 6.67: Change of the shape of the smaller dome (wire frame view of the shapes)

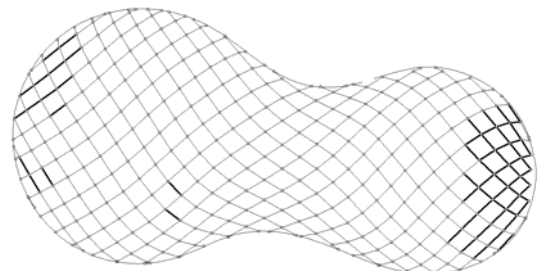


Figure 6.68: Grid generated on the shape with smaller curvatures

6.5 Results compared with reality by physical modelling

To compare the results of the grid generation tool with reality, a physical model has been constructed. This model has been created from an initially flat mat of bending members to model the shaping process during construction. The process of creating this model and an extensive comparison with the computer model can be found in Appendix 5: Physical . The result of the physical modelling is the structure shown in Figure 6.69 to Figure 6.72. Although the physical model does not resemble the computer model exactly, both models give an equal image of the structure. Similar effects in bending and scissoring of the laths have been found.

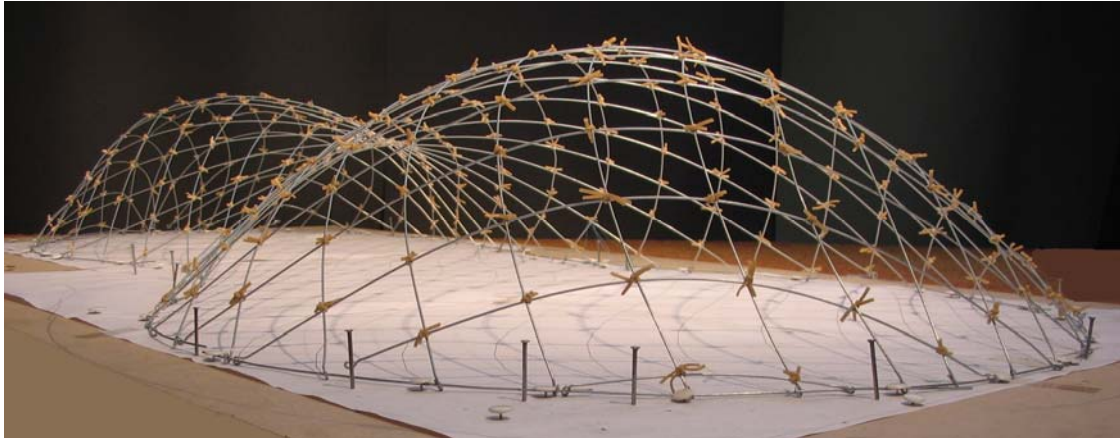


Figure 6.69: 3D view of the created model

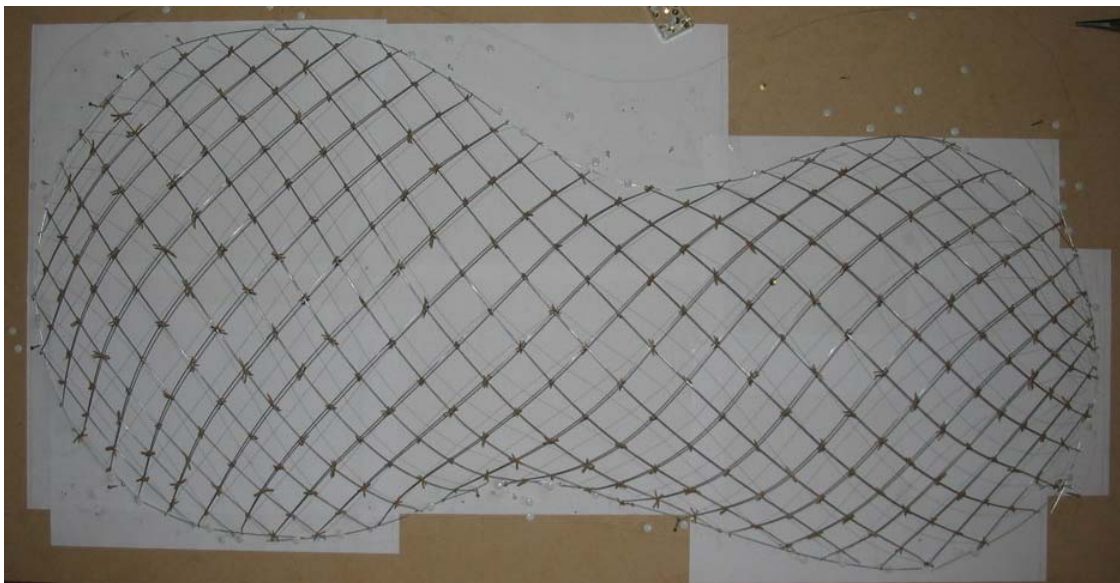


Figure 6.70: Physical model in top view.

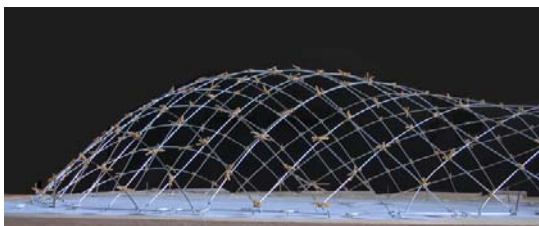


Figure 6.71: Left dome of the physical model in side view

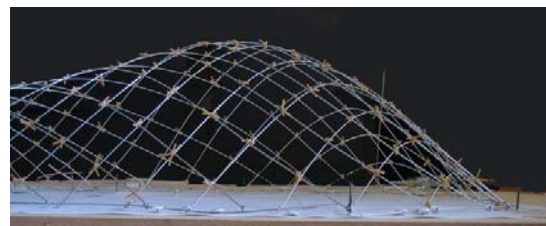


Figure 6.72: Right dome of the physical model in side view

With the grid generation tool it was found that bending curvatures become too large when the laths of the grid are bent to a (semi-)spherical surface. This problem was also found in the physical modelling process. Especially the right dome of the structure shows less scissoring and curvature in the laths as intended by the computer model (Figure 6.73). Without additional force, the structure would not achieve a position equal to the computer model. Large force was needed to pull the structure into a position, creating tension in parts of the structure (Figure 6.74). This effect can be compared with the tensioning of the fabric of a hyperbolic tent structure. Together with the results of the grid generation tool, this results show that it is hard to create a (semi-)spherical surface with a gridshell structure. It is therefore advisable to avoid such shapes when a gridshell structure is applied.

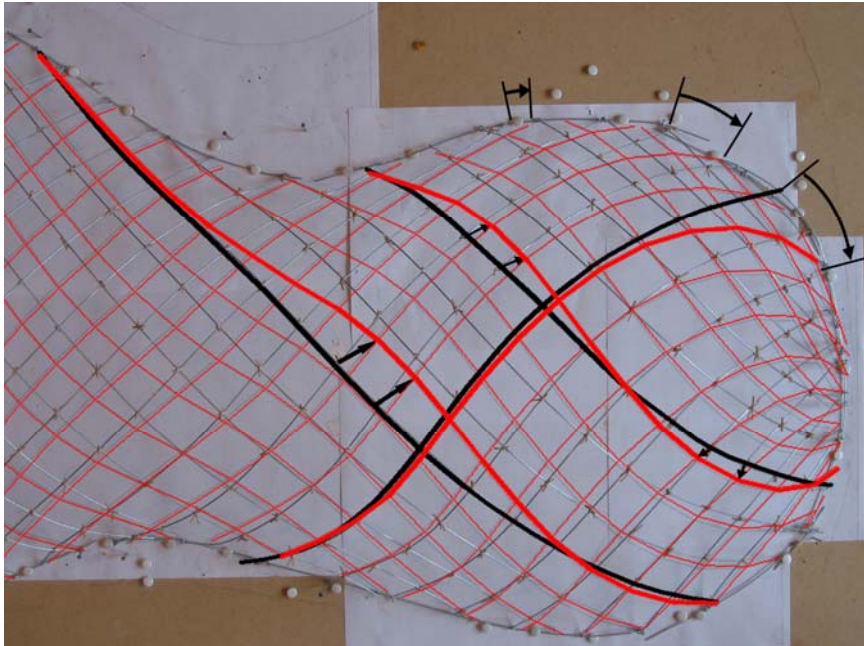


Figure 6.73: Comparison of the right dome in the two models. Moving the members in the pointed directions by force (arrows in top right) will result in a better approximation of the computer model. Some laths are printed bold for comparison. The dark and bold lines indicate the physical model. Red lines indicate the computer model.

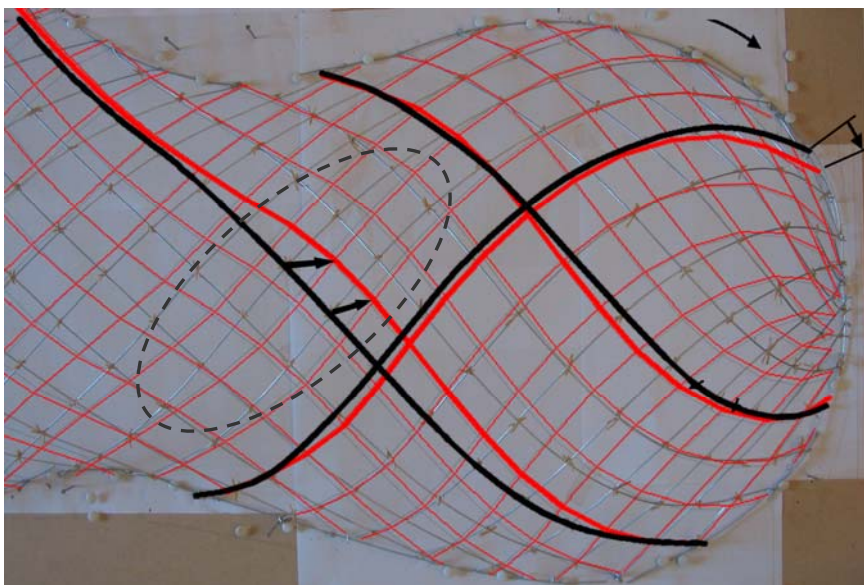


Figure 6.74: Structure, with the nodes at top right side moved in the direction of the arrow. The models resemble better, but tension exists in the encircled area.

Deviations between the two models have been found in the shape of the structure. First, the two models differ in height. The physical model has larger height than the computer model. This can be explained by the fact that the scissoring of the laths at the ends of the structure is less than in the computer model. The laths in the physical model have the same length as in the computer model however. This results in a larger height, as the laths are less curved than intended.

Second, the cross sections of the physical model show a parabolic shape, whereas the cross sections of the computer model show a more circular shape. These deviations between the two models can be well explained. The parabolic shape is generally considered as a more natural shape to divert axial forces through an arched structure. The fact that the models deviate does show that the computer model does not represent a shape that is optimized for structural behaviour. The model should be of a more parabolic shape.

Building the physical model is a type of physical form finding. Therefore the results of the physical model can be used to modify the computer model to a more optimized shape. One could say this is a reversed form finding process. In stead of first creating a shape by form finding and then creating a structure, here the structure is created first, using the grid generation script. The shape is then adjusted to a shape corresponding with the physical model. A new grid can then be generated on the adjusted, optimized shape for structural analysis.

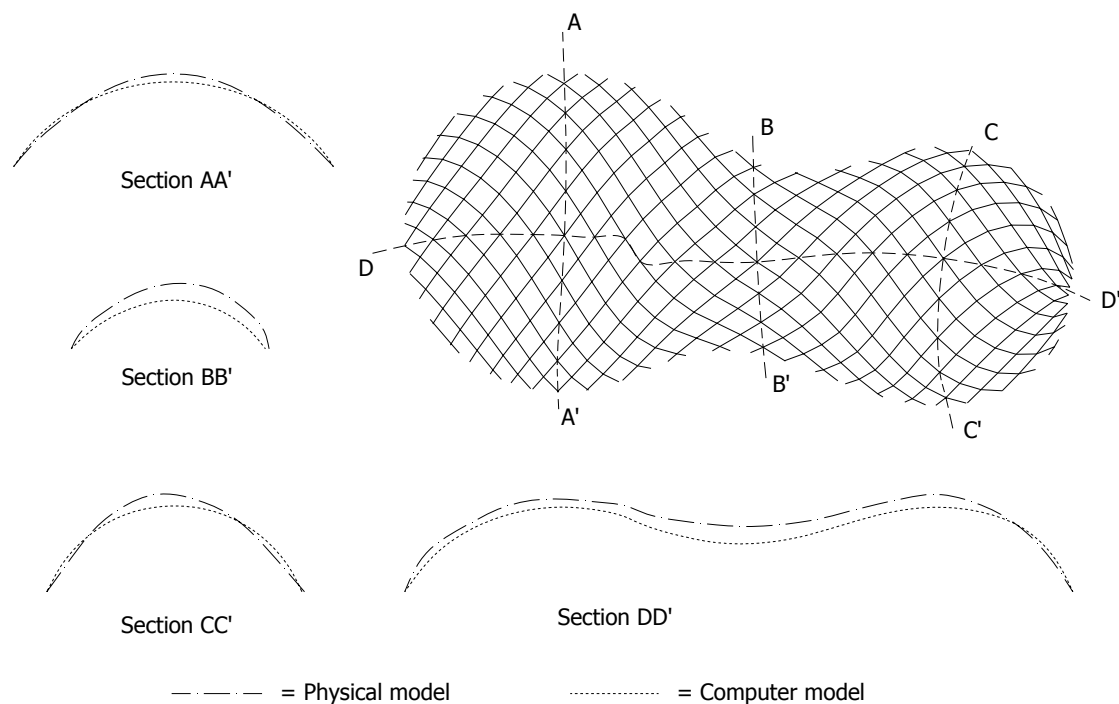


Figure 6.75: Sections of the two models

Members in bending



7.1 Introduction

The shape of a gridshell is created by applying a large deflection on the members. The laths are bent and twisted to create the desired shape with the initial flat mat of laths. The properties of timber make it possible to bend and twist the laths into shape, but also put restrictions on the shape possibilities. The material will fail when the ultimate stress capacity is exceeded. By bending and twisting of the lath, stresses are induced in the material. After construction, the formation stresses will diminish due to relaxation and approximately half of the initial stress level will remain present. On top of these residual stresses, the structure has to withstand loads like wind and snow, which desires a certain load capacity of the laths after construction. To be able to understand the behaviour of the structure and to be able to structurally analyse the gridshell structure, it is important to fully understand the behaviour of members. This is investigated in this section.

First, the question rises which stress distributions occur in a member during construction. In the form shaping sequence, the member is first bent into shape on internal supports. After pinning the structure down at the ends, the internal supports are removed. The stress distribution in the laths will probably change and thus will the shape of the structure. This behaviour will be investigated in Section 7.2 by analyzing a simple beam on two supports. This investigation will be extended to a 3D structure in Section 7.3.

For structural analysis, it is desired to take into account the formation stresses. In Section 7.4 a method to do this will be tested on a simple beam and a 3D structure. This method is based on the assumption that the bending stresses can be deduced from the angles of curvature in the members of the structure.

7.2 Stresses induced by the formation process

When a gridshell structure is erected, the members are deflected into shape by self weight and applied load. The members are supported at several points along the span. Due to the applied displacement, stresses are induced. When the shape forming process is ended, the structure is pinned or clamped at the edges and the temporary supports are removed. If the displacements applied are equal to the natural bending shape, the removal of these supports will not cause any changes. This natural bending shape is the equilibrium position which is adopted by a member by moving the ends to each other. When this is not the case, the internal stress distribution is not in equilibrium after the internal supports are removed. The beam will deflect to this equilibrium position and redistribution of the internal stresses will occur. This can be seen as a relaxation reaction of the beam. Therefore, this deflection is called the relaxation deflection. This change of shape is undesired, because it can cause unexpected and undesired change of geometry and internal stress distribution.

To understand this change of system and to be able to predict the behaviour of the structure, the different steps of the construction process are analysed. These steps are displayed in a flow chart, shown in Figure 7.1. The following steps can be distinguished:

- The first step is to lay out the laths in a flat mat on the internal supports.
- When the supports are moved, the mat will first deflect under self weight.
- The deflection by self weight only is probably not enough to create the desired shape, so force is needed to push or pull the mat into shape.
- During the formation process, the shape of the structure should be reviewed. When the resulting shape complies with the desired shape within acceptable boundaries, the structure can be pinned or clamped to the final supports. If not, additional forces are needed.
- After the formation process is ended, the internal stresses induced by the deformation should be estimated.
- It should be determined if the internal supports are removed immediately, or if these are left in place for a period of time. In case of the former, the internal stresses are probably not in equilibrium. The structure will deflect to an equilibrium position and redistribution of stresses takes place. In case of the latter, the internal stresses due to the formation process diminish in a certain extend due to relaxation of the timber, prior to the removal of the internal supports. The relaxation deflection will be smaller in this case.
- The internal supports are removed
- The relaxation deflection and corresponding stresses can be estimated.
- The structure should be re-analysed in equilibrium position.

To be able to predict the final result of the formation process, the amount of relaxation during construction should be estimated. Also the internal stress distribution after completion of the formation process and in the different steps should be estimated. To be able to make this estimation, the different steps are analysed in the next section.

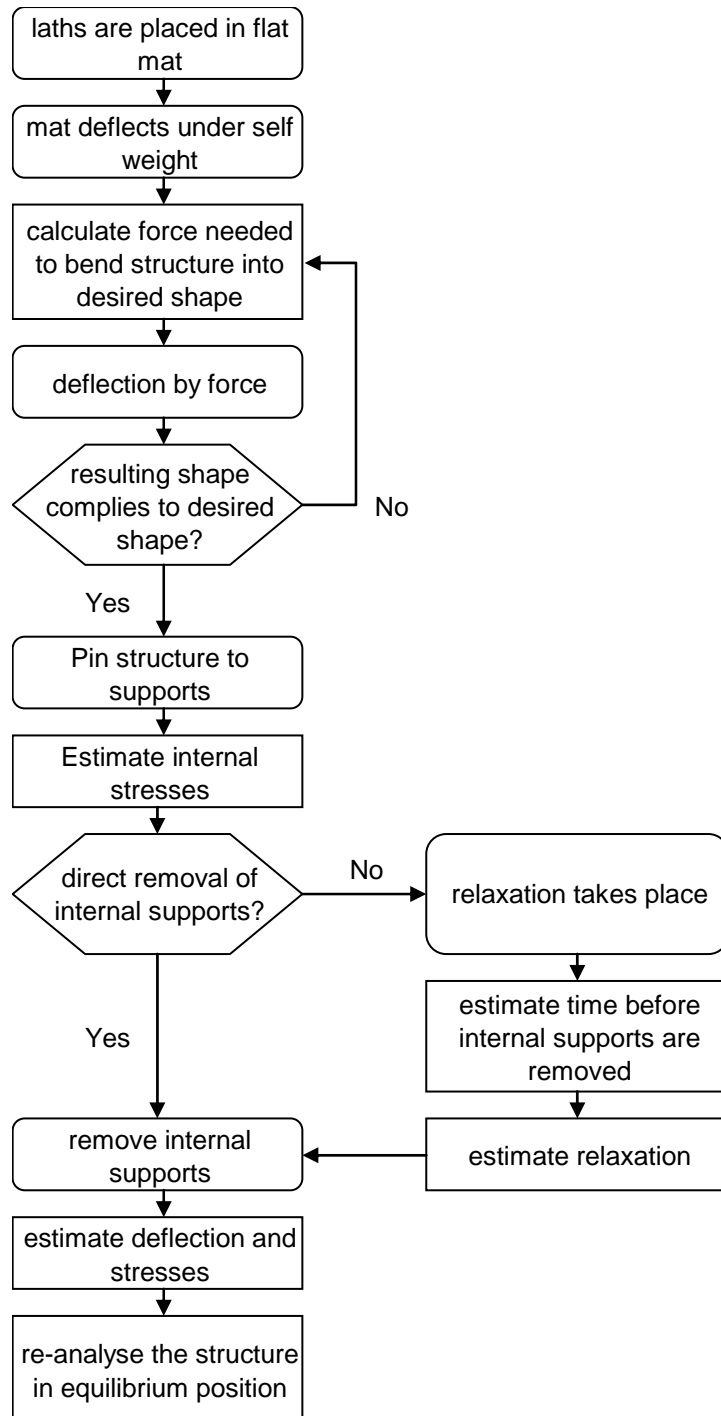


Figure 7.1: Flow chart for analysis of the construction phase

The different steps of the construction phase are analysed by studying the bending behaviour of a simple beam. This beam is a timber lath is used, 10m length with a cross section of 50x50mm and timber properties of strength class D30, supported by two pendulum columns which act as internal supports.

The formation process is modeled in the following steps (see Figure 7.2):

- The lath is first supported by two pendulum bars at 2,5 and 7,5m. For stability the lath is supported by a vertical roll at mid span.
- The lath is deformed by a vertical and/or a horizontal force at the end nodes (step 1)
- The end points are pinned at the deformed position (step 2)
- The pendulums are deleted. The lath will deflect to an equilibrium position (step 3)

These steps will be analysed in the following load cases:

- Deflection induced by vertical force at the end nodes (load A)
- Deflection induced by horizontal force at the end nodes (load B)
- Deflection induced by a combination of horizontal and vertical forces in different ratios (load C)
- Deflection induced by horizontal and/or vertical force at the end nodes, combined with self weight (load SW)

The different cases are named with a step letter and a load number, e.g. case A3 is the case with vertical load and the pendulums removed.

The analysis performed is non-linear to take into account the geometrical non-linear behaviour of the structure. A linear analysis is based on the assumption that deflections stay small. Only deflection in z direction is accounted for and displacements in x-direction stay zero. When large deflections occur, which is the case in this analysis, this assumption is no longer valid. Therefore non-linear analysis is needed.

The analysis solver for non-linear analysis in GSA is based on Dynamic Relaxation (see Section 4.2.2.2). The non-linear analysis performed by GSA is based on two different effects³³:

- Geometric non-linearity, where the load causes large deflections which must be taken into account in order to get an accurate solution.
- Material non-linearity, where the load causes material to behave in a non-linear manner, typically through yielding.

The latter is not considered here, as linear behaviour of the material itself is assumed.

³³ Help file of OASYS GSA

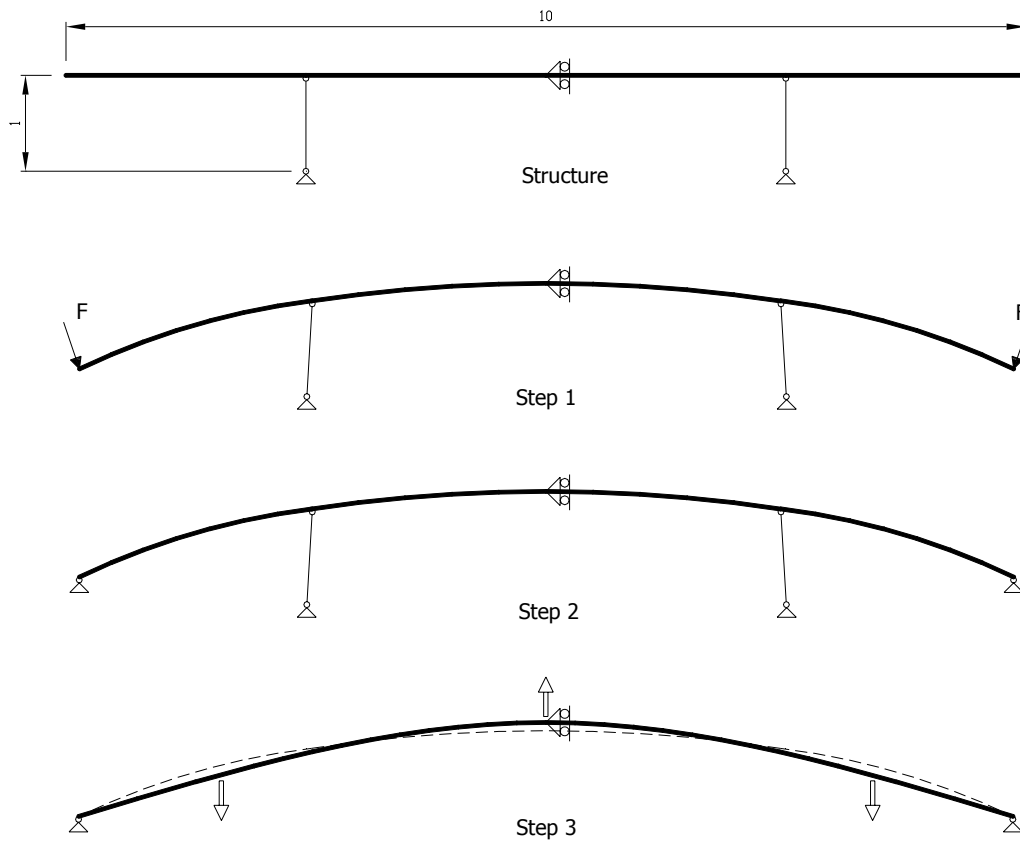


Figure 7.2: The structure is deformed in different steps

7.2.1 Load case A1

For the first load case, the slender beam is bent into shape by applying a vertical force of 100 N on both ends of the beam (Figure 7.3). Due to this load, the beam deflects to the shape shown in Figure 7.4, with a total deflection of 541mm in vertical direction. The corresponding moment, shear and axial force diagrams are shown in Figure 7.5 to Figure 7.7.

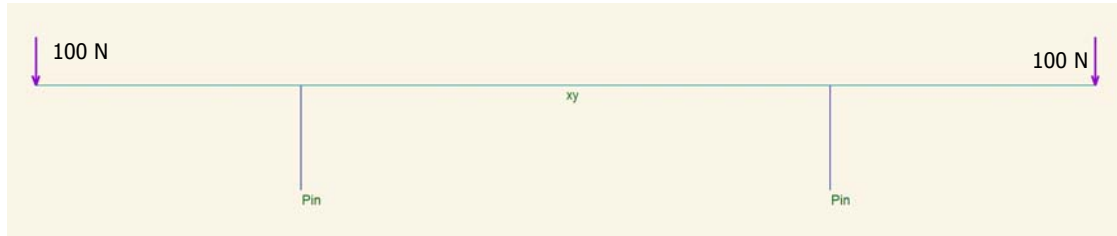


Figure 7.3: Case A1, applied force

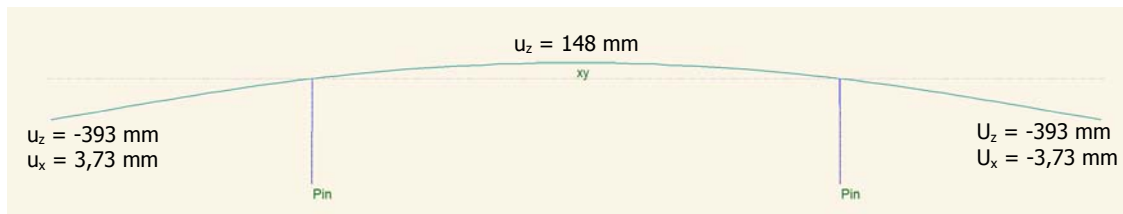


Figure 7.4: Case A1, deflection

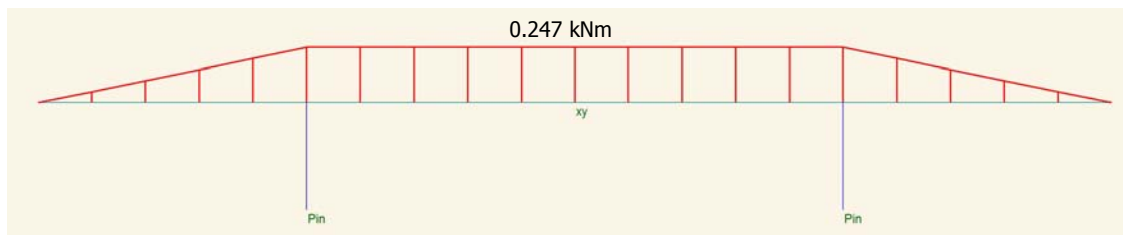


Figure 7.5: Case A1, moment line

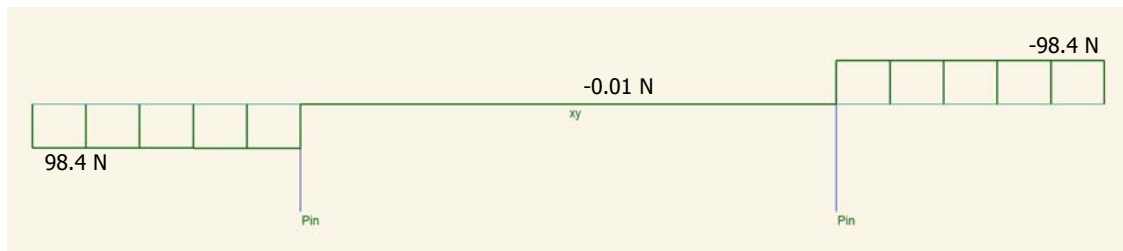


Figure 7.6: Case A1, shear force

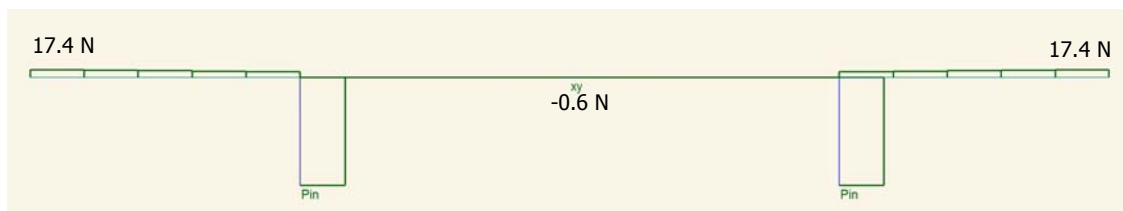


Figure 7.7: Case A1, axial force

7.2.2 Load case A2

When the structure has reached its desired shape, it is pinned to the edge supports. The deflection of the beam in case A1 is considered as this desired shape. Thus, the beam of A1 can be pinned down at this deformed position. In GSA this is implemented as an applied displacement of the end nodes, equal to the deflection of the end nodes in case A1. It is found that when the structure is pinned at the deformed position, the deflection stays equal to the case where the structure is forced down. Because all boundary conditions are equal, also the internal force distribution does not change.

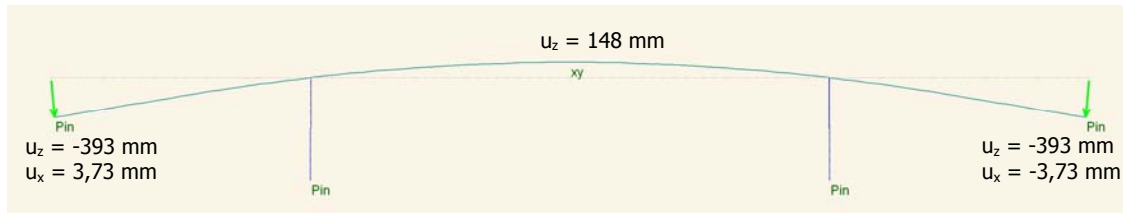


Figure 7.8: Case A2, deformation

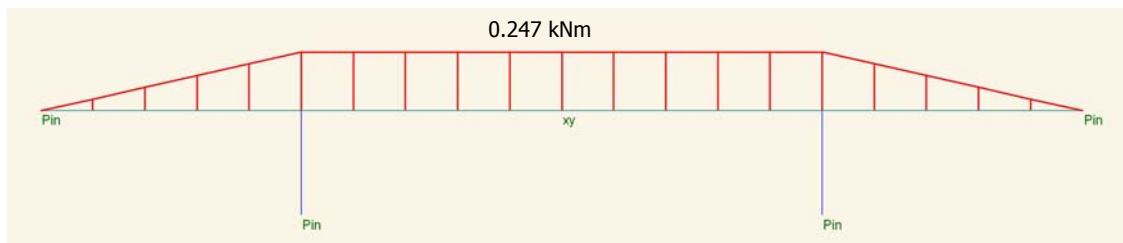


Figure 7.9: Case A2, moment line

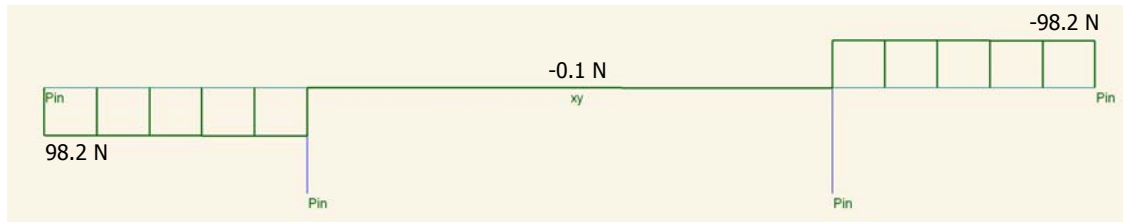


Figure 7.10: Case A2, shear force

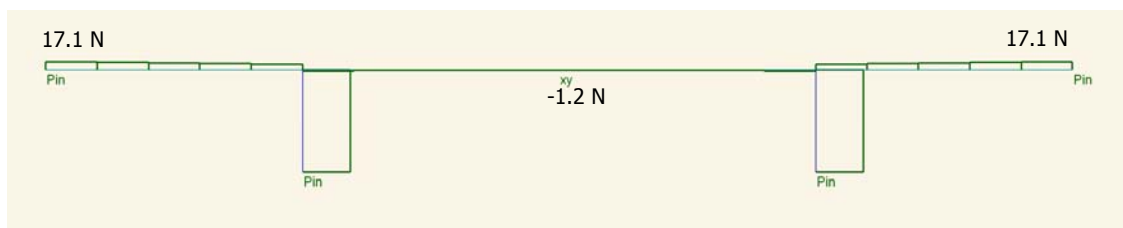


Figure 7.11: Case A2, axial force

7.2.3 Load case A3

The following step in the formation process is removing the internal supports. With this structure, this implies removing the pendulum supports. The deflection of the end nodes is kept equal and the beam can be re-analysed. This can be seen as the structure relaxing to an equilibrium position. It is found that the nodes where the pendulums were attached deflect down and the top deflects up. The bent member shifts to a more parabolic shape. This change is also seen in the moment line. The discontinuities in the moment line are disappeared, which results in a more energy efficient stress distribution. The axial force increases from approximately zero to approximately -515N (compression).

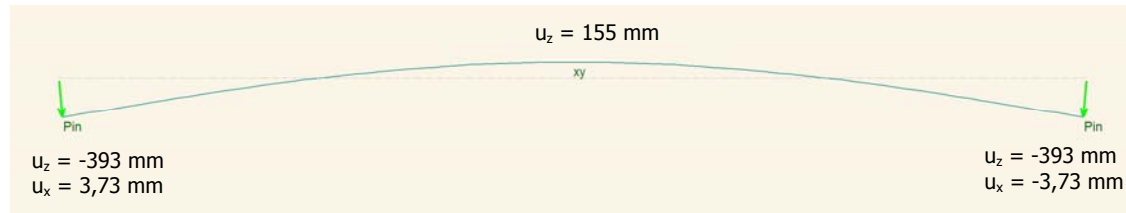


Figure 7.12: Case A3, deformation

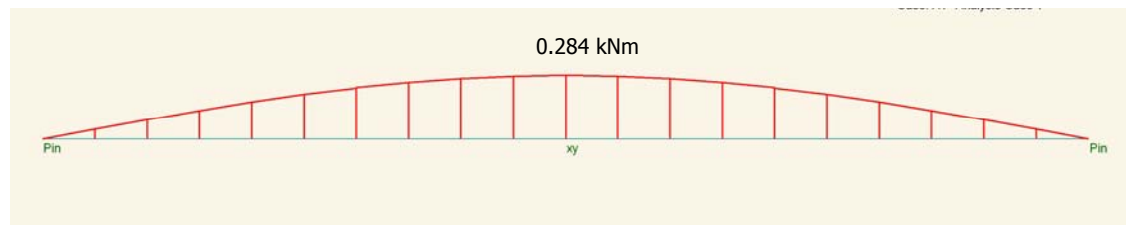


Figure 7.13: Case A3, moment Line

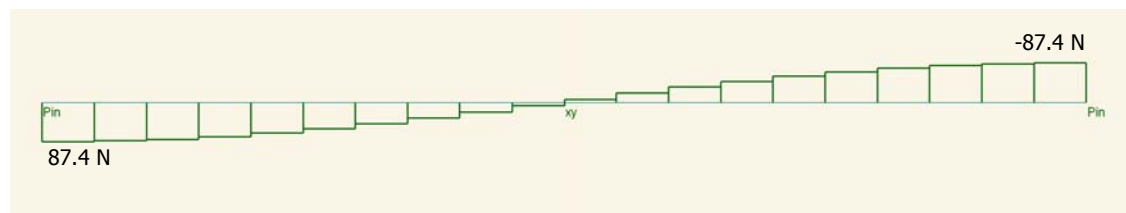


Figure 7.14: Case A3, shear force

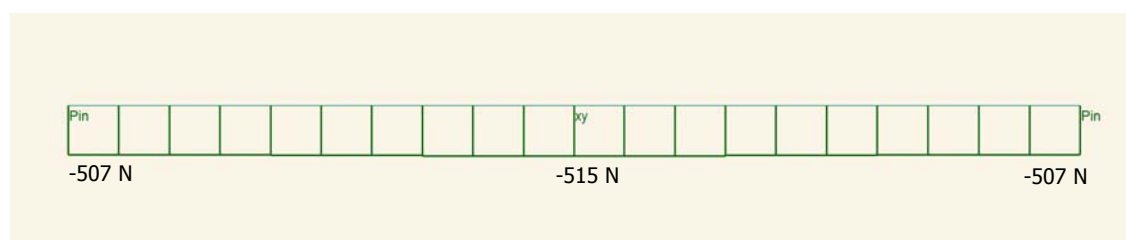


Figure 7.15: Case A3, axial force

7.2.4 Load case B1

To analyse the effect of a horizontal deformation force, this is analysed in this case. In the former load case an axial force of 515 N was found after removing the pendulums. This load is taken as the deformation force in this case. The first step in the formation process is again deforming the structure, supported by the two pendulums. A horizontal load of 515 N is applied on both ends of the member. To induce deflection in the right direction, a vertical force of 1 N is applied on the middle. It is found that the horizontal force gives a deformation approximately equal to the final step of load case A, e.g. the natural bending deflection of the beam.

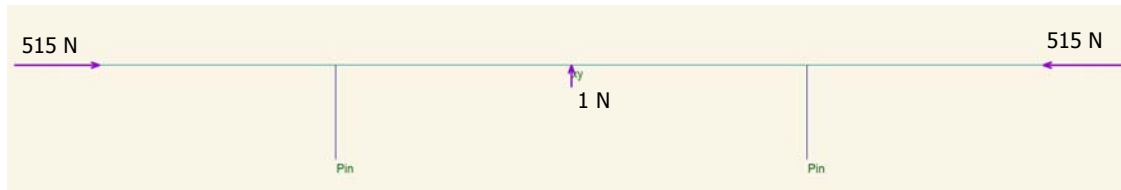


Figure 7.16: Case B1, applied forces

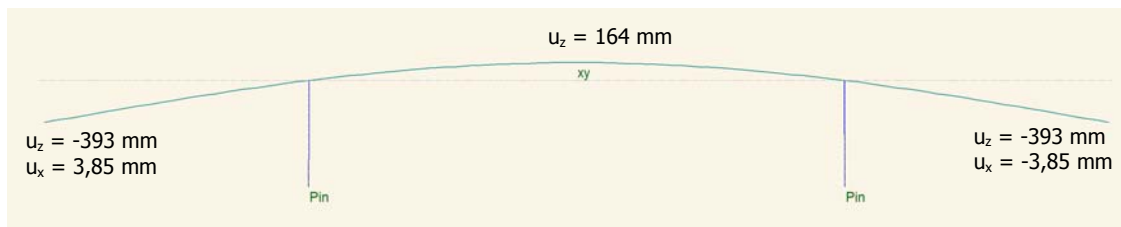


Figure 7.17: Case B1, deformation

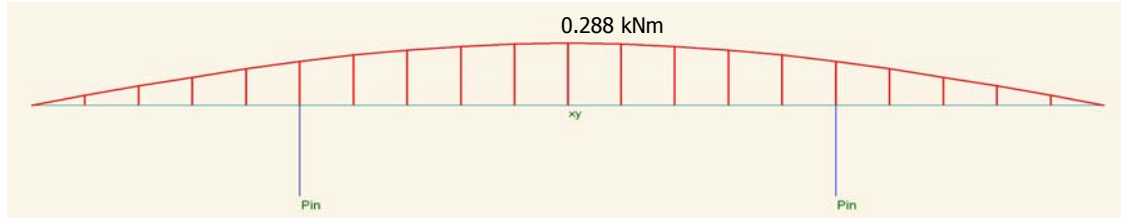


Figure 7.18: Case B1, moment line

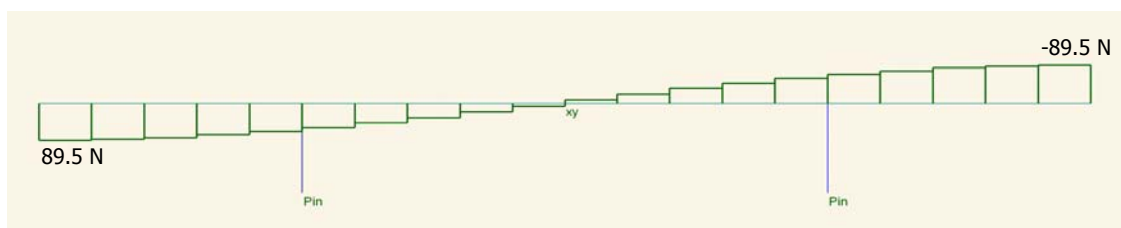


Figure 7.19: Case B1, shear force

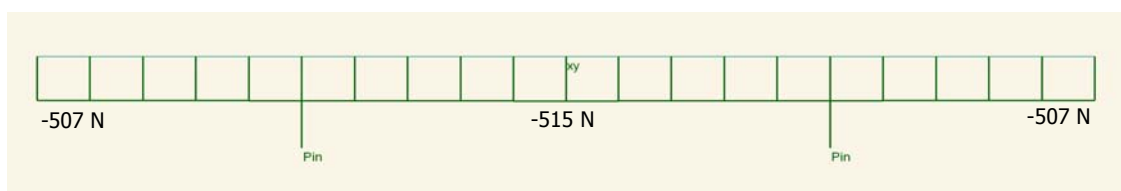


Figure 7.20: Case B1, axial force

7.2.5 Load case B2

The structure of case B1 is again pinned down at its deformed position. The deformation and moment line are displayed in the figures below. It is found that the deformation and internal force distribution is again equal to step 1, where the structure is pushed down by force.

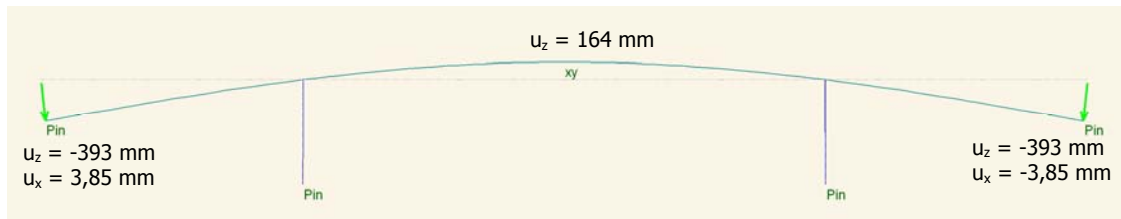


Figure 7.21: Case B2, deformation

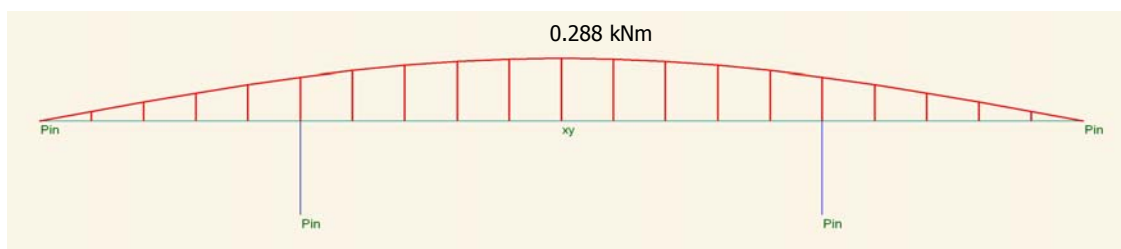


Figure 7.22: Case B2, moment line

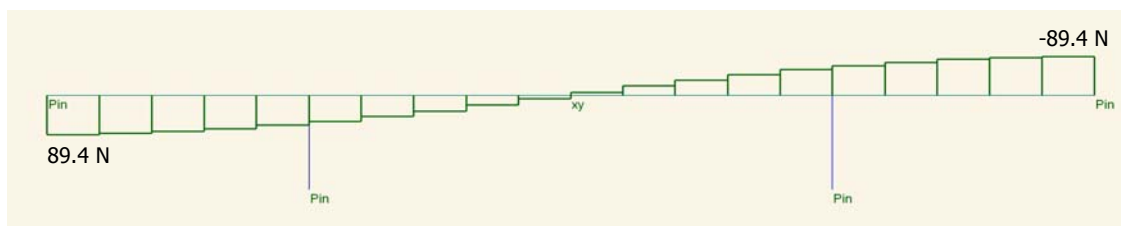


Figure 7.23: Case B2, shear force

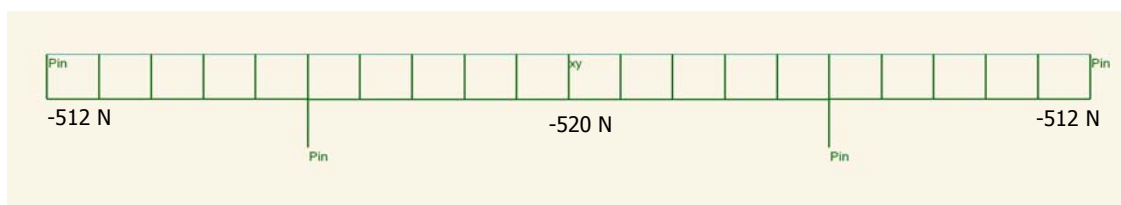


Figure 7.24: Case B2, axial force

7.2.6 Load case B3

After the structure has been pinned down, the pendulums are removed. The deformation and moment line are displayed in the figures below. It is found that the deformation and internal force distribution is equal to the begin situation, where the structure is deformed by a horizontal force and supported by pendulums. In this first step, the member already deflects to the natural equilibrium bending shape. Pushing a member into shape with a horizontal force thus approximates the natural bending shape of the pinned member

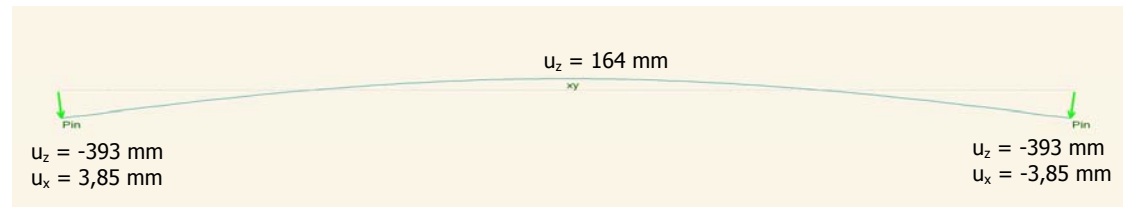


Figure 7.25: Case B3, deformation

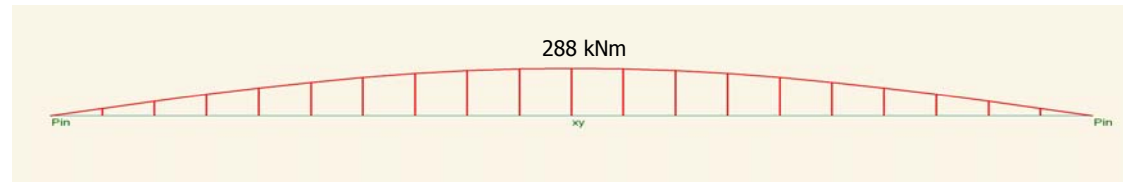


Figure 7.26: Case B3, moment line

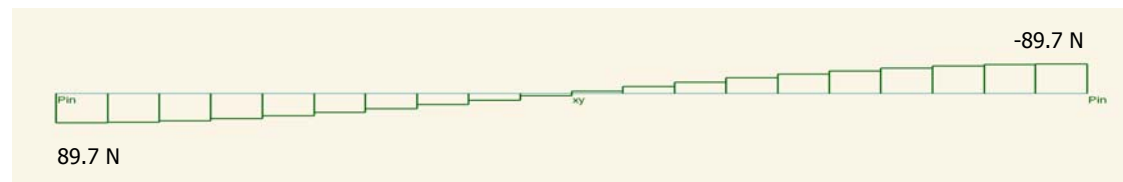


Figure 7.27: Case B3, shear force

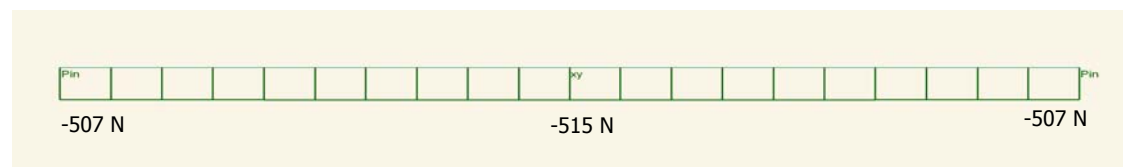


Figure 7.28: Case B3, axial force

To compare load cases A and B, the differences in deflection and stress distribution are investigated. First the different steps of analysis are reviewed. Figure 7.29 shows the difference in deflection between case A1, A2 and A3. This difference is the relaxation deflection. As can be seen pinning down the structure after pushing down (A2 - A1) has almost no effect on the deformation. Removing the pendulums does have an effect (A3 - A2). The nodes between node 8 and 14 shift up, the other nodes shift down. The maximum difference in deformation occurs at nodes 5, 11 and 17. This difference is -2,1% for node 5 and 17. In the middle this is 1,33%.

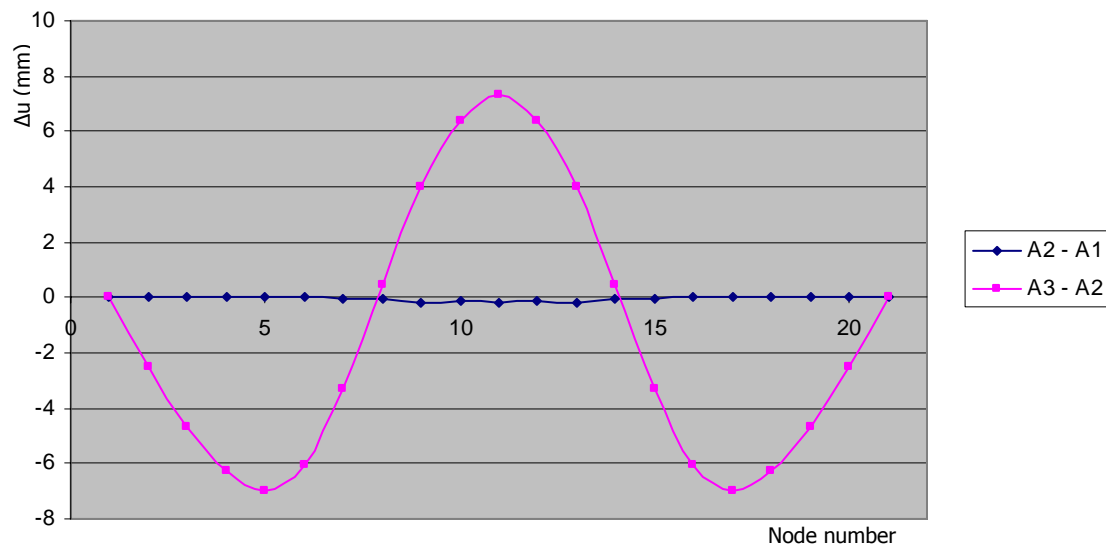


Figure 7.29: Relaxation deflection for load case A

As an example, if the structure should be 8m high, the difference after removing the internal supports is 168 mm down at $\frac{1}{4}$ and $\frac{3}{4}$ of the span and approximately 106 mm up in the middle. This is not a very large difference but it should be accounted for, e.g. when designing the facade.

When we compare case B1, B2 and B3, it is found that the difference between deformations is approximately zero. This shows that when a horizontal force is used, the deformation approximates the natural deflection. However, a much larger force is needed to induce the deformation.

It was found that when a vertical force is used, the geometry changes after removing the internal supports, although the change is not large. When the internal stress distribution is investigated, a more important effect is found. Figure 7.30 shows the moment stress distribution of the upper edge of the beams of the different cases. From case A1 to A3, the internal moment stress relaxes from a discontinuous moment to a continuous distribution. Going from B2 to B3 no difference can be seen. Figure 7.31 shows the change as a percentage of the deformation. A change of 23,8% is found for nodes 6 and 16, which are the nodes where the pendulum columns were attached. The change is 12,9% for the middle node, node 11. To avoid breakage of the laths these changes should be taken into account, especially when the laths are bent close to their ultimate bending strength.

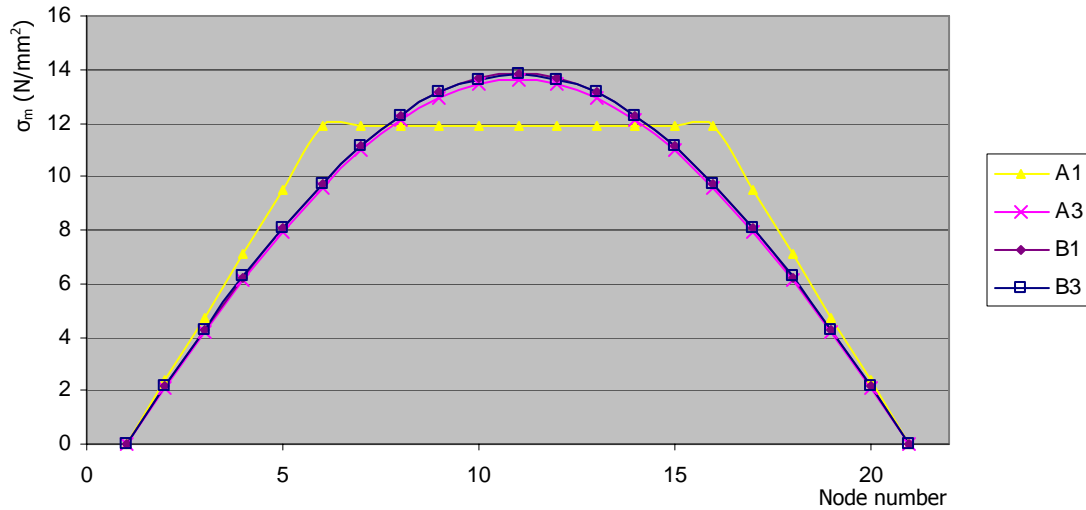


Figure 7.30: Bending stresses in the upper edge

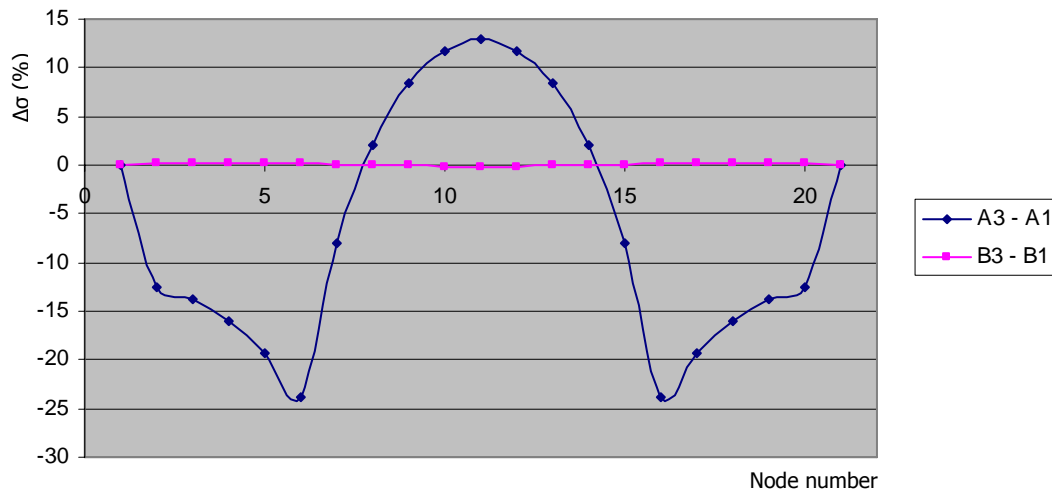


Figure 7.31: Bending stress difference in the upper edge(%)

It should also be noted that the axial stress increases going from A1 to A3, from approximately zero for case A1 to 0,206 for A3. Going from B1 to B3 however, has approximately no effect on the axial stress. In these cases, the axial stress of 0,206 N/mm² is already present due to the horizontal force.

As shown in case A2 and B2, approximately no difference occurs between step 1 and 2 (pushing or pinning the structure down). Therefore, this step is skipped in the following cases.

7.2.7 Load cases C1 and C3:

In load case A and B it is found that a horizontal force gives a much better approximation of the equilibrium bending shape of a member, than when a vertical load is applied. This suggests only horizontal force should be used to deform a grid shell. However, a much larger force is needed to reach the same deformation as with vertical forces only, which complicates the formation process. When a horizontal force is combined with a vertical force, it might be possible to reach a better approximation of the equilibrium bending shape than with a vertical force only and with less force than with a horizontal force only. This is tested by applying a load of 100 N vertical and 100 N horizontal on the beam ends (Figure 7.32).

First, the member supported by pendulums is deflected into shape. This gives the deflection and internal force distribution shown in Figure 7.33 to Figure 7.36.

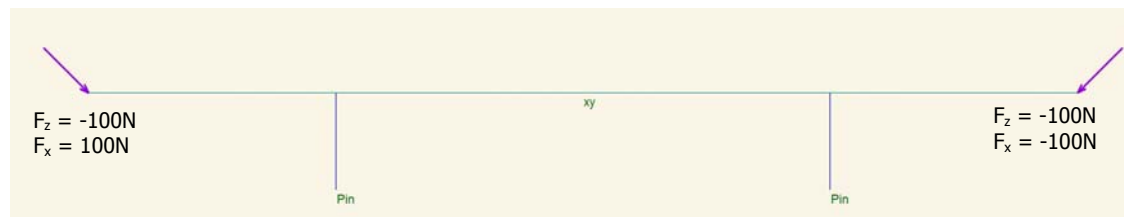


Figure 7.32: Case C1, deformation

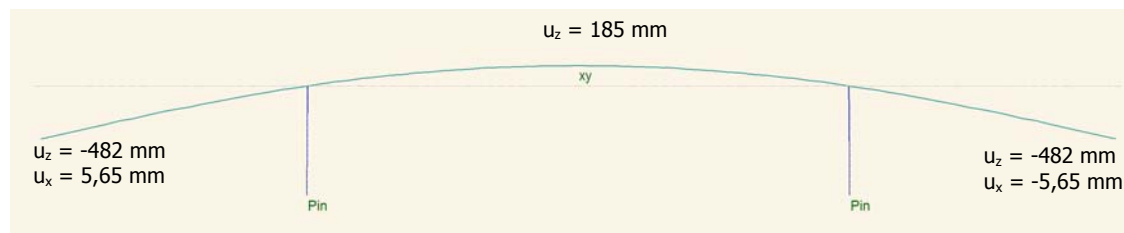


Figure 7.33: Case C1, deformation

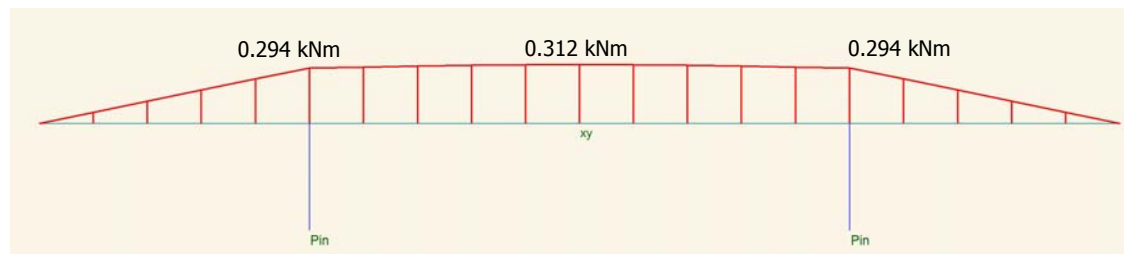


Figure 7.34: Case C1, moment line

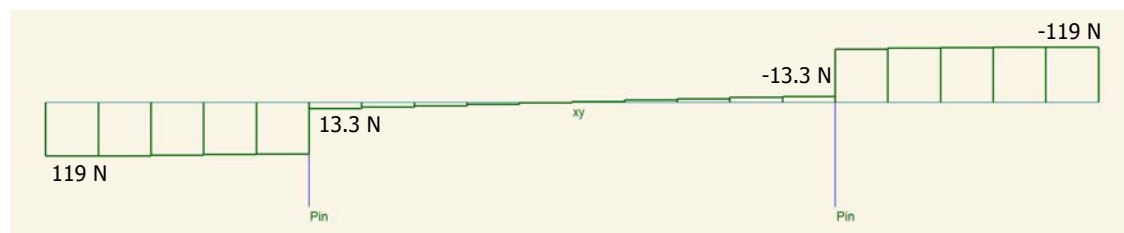


Figure 7.35: Case C1, shear force

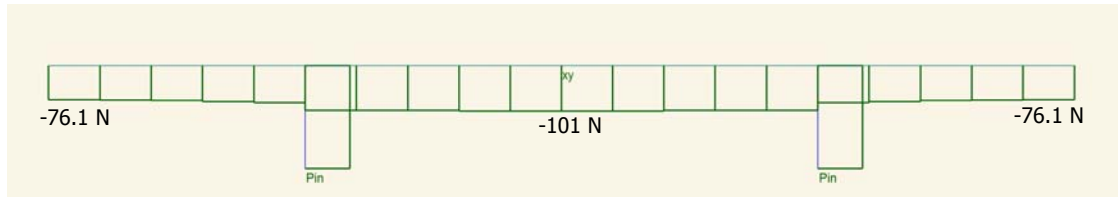


Figure 7.36: Case C1, axial force

After the deformation by force, the structure is pinned down (step 2, which is omitted here) and the pendulums are removed (step 3). The deformation and internal force distribution become:

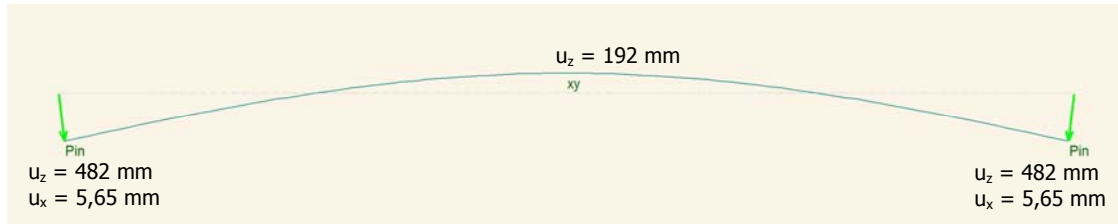


Figure 7.37: Case C3, deformation



Figure 7.38: Case C3, moment line

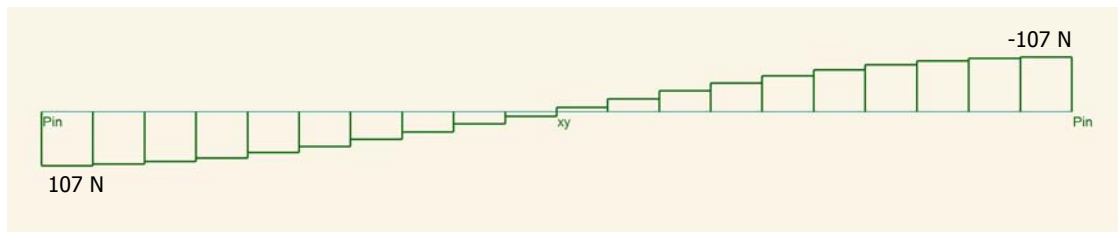


Figure 7.39: Case C3, shear force

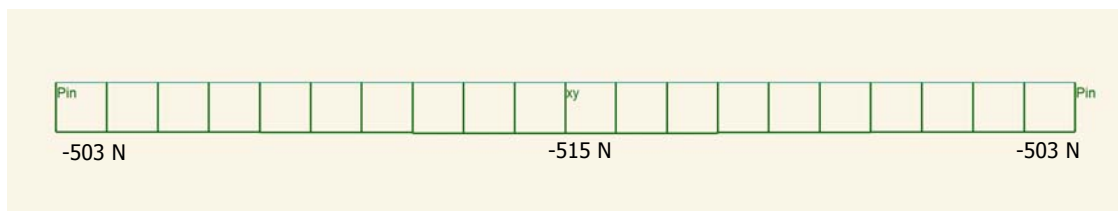


Figure 7.40: Case C3, axial force

Before the pendulums are removed, the total deflection between end points and the middle of the beam was 667mm. When the pendulums are removed, the middle of the beam deflects 7mm upward, 1,10% of the total deflection. In load case A (vertical force only) the relaxation deflection was 1,29% of the total deflection. For bending stress, the change when the pendulums are removed is also smaller: 19,1% in stead of 23,8% with vertical force only.

In load case C the ratio vertical force over horizontal force (v/h) is 1. To investigate the influence of the vertical force on the end nodes, the following cases are investigated, with and without pendulums (step 1 and 3):

- C1a and C3a: 150 N vertical, 200 horizontal force ($v/h = 0,75$)
- C1b and C3b: 100 N vertical, 200 N horizontal ($v/h = 0,5$)
- C1c and C3c: 75 N vertical, 300 N horizontal ($v/h = 0,25$)

To give an overview, the results of the deformation are put together in Figure 7.41

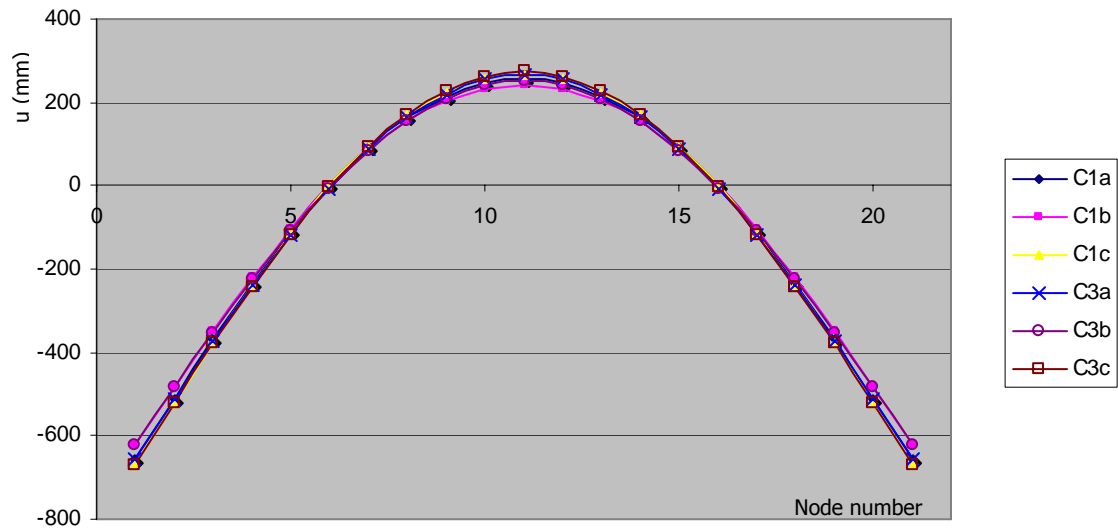


Figure 7.41: Deformation of the different cases

In the figure above the deflection of the cases with and without pendulums is plotted. The differences between step 1 and 3 are hard to see in this figure. To analyse the spring-back deflection better this difference is plotted in Figure 7.42.

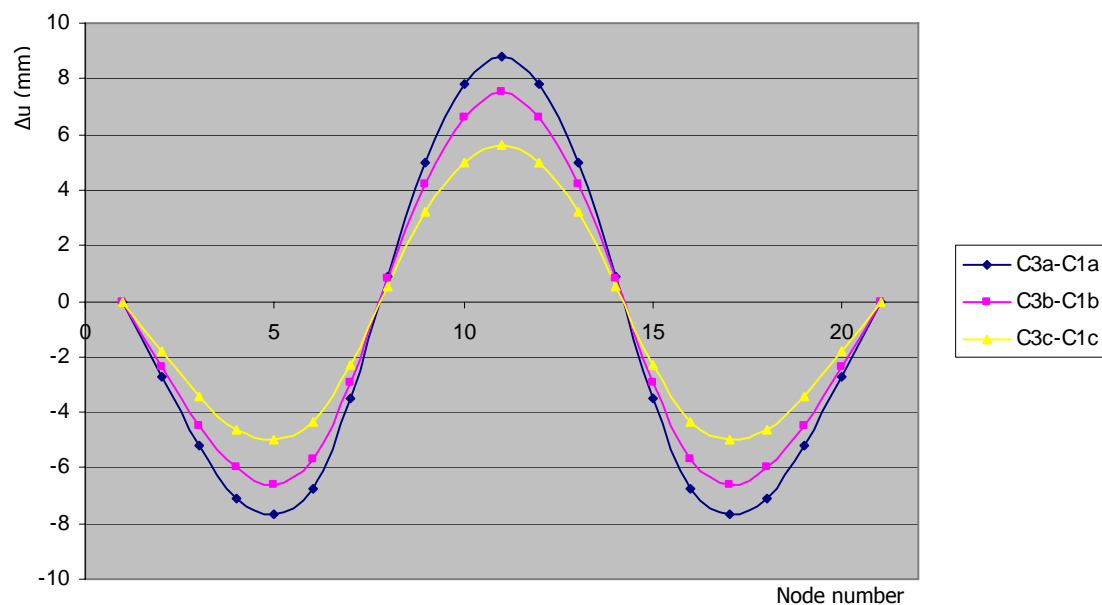


Figure 7.42: relaxation deflection load case C

7.2.8 Discussion increasing diagonal force

In the table below, the deflection results of the analysis with increasing v/h ratio are put together. This is data on deflection step 3, with the pendulums removed. To indicate the difference between the different load cases, the differences between case 3 and 1 are displayed in the same table. The change of deflection Δu is indicated for the nodes with maximum change: node 6, 11 and 16.

To analyse the relaxation deflection, this difference between the case with and without pendulums is plotted in Figure 7.43 as a percentage of the total deflection. The percentage is used because the total deflection is not equal for all cases. As can be seen, the relaxation deflection becomes relatively smaller when the horizontal force applied is made larger, going from C3 to C3a, C3b and C3c. The maximum change in percentage occurs at the nodes close to the supports. Because the absolute change is small for these nodes, this maximum is disregarded.

The ratio u_{tot}/F shown in Table 7.1 indicates the deflection in millimetres that is caused by 1 N of applied force. This ratio is the largest when only a vertical force is applied (case A3). Downside is the fact that also the relaxation deflection and change in bending stress is the largest (see Figure 7.43). Ratio u_{tot}/F is the smallest for case B3 with horizontal force only. In this case the relaxation deflection is almost zero, but for approximately every mm of deformation 1 N of force is needed.

Table 7.1: Differences in deformation between cases with and without pendulums

Case	F (N)	v/h	u_{tot} (mm)	u_{tot}/F (mm/N)	Δu (mm) node 11	Δu (mm) node 6 and 16
A3	100 v.	-	548	5,48	7,1 (1,29%)	-6,1 (1,22%)
C3	100 v 100 h	1	674	3,37	7,4 (1,10 %)	-5,8 (1,22%)
C3a	120 v 160 h.	0,75	923	3,30	8,8 (1,0%)	-6,8 (1,04%)
C3b	100 v. 200 h.	0,5	871	2,90	7,5 (0,86%)	-5,7 (0,9%)
C3c	75 v. 300 h.	0,25	942	2,51	5,6 (0,59%)	-4,4 (0,66%)
B3	515 h.	0	557	1,08	~0	~0

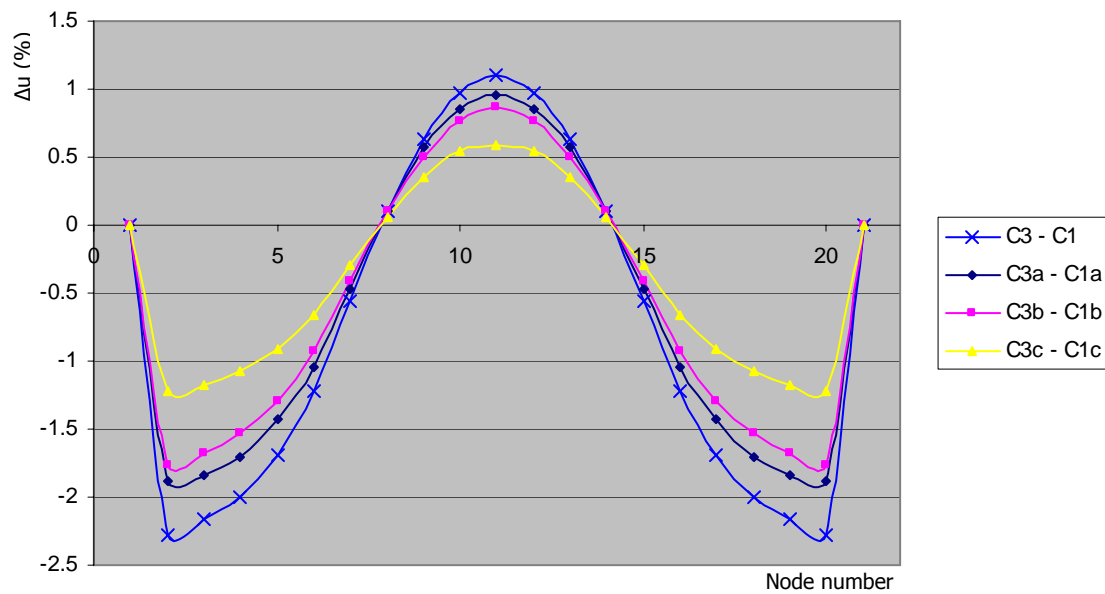


Figure 7.43: Percentage difference in deflection between pendulum cases and relaxed cases

The same effect can be seen with the bending stress. The bending stress in the upper edge is displayed in Table 7.2 for the different cases. Increasing the ratio v/h causes an increase in bending stress. The difference between the cases with and without pendulums (step 1 and 3) are displayed in Figure 7.44.

Table 7.2: Differences in bending stress between cases with and without pendulums

Case	F (N)	v/h	$\Delta\sigma_m$ (%) Node 11	$\Delta\sigma_m$ (%) Node 6 and 16
A3	100 v.	-	12,9	-23,8
C3	100 v 100 h	1	10,5	-19,1
C3a	120 v 160 h.	0,75	9,09	-16,6
C3b	100 v. 200 h.	0,5	8,14	-14,8
C3c	75 v. 300 h.	0,25	5,75	-10,3
B3	515 h.	0	0,24	0,25

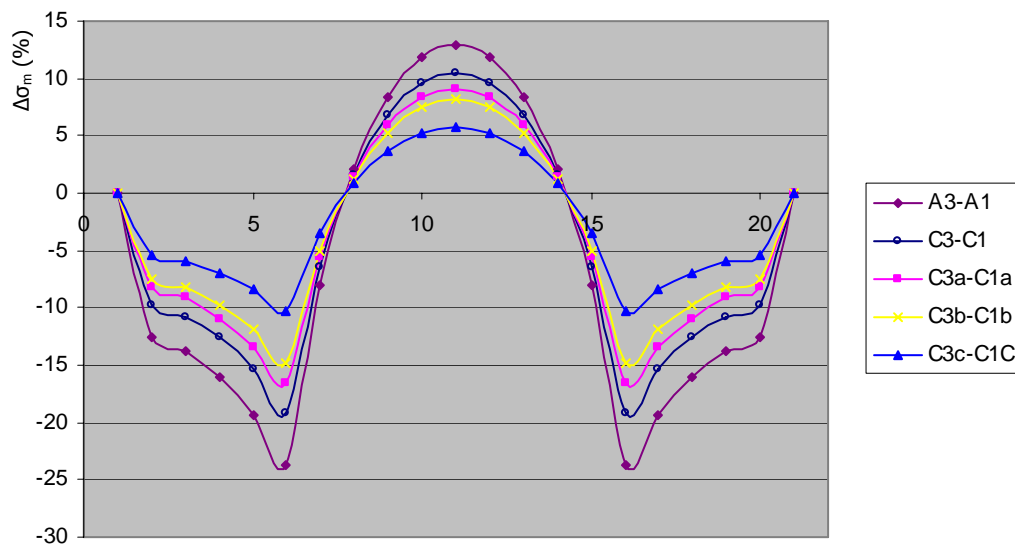


Figure 7.44: Difference in bending stresses in the upper edge (%)

The increase of the bending stress is the most important to take into account. Especially when the laths are bent close to their ultimate bending strength, the sudden increase can cause breakage of the laths.

When a choice has to be made on which forces should be applied to induce deformation, it is advisable to use a combination of horizontal and vertical force. When for example a ratio v/h of 0,5 is used, the ratio u_{tot}/F is still profitable and the spring-back deflection is already small.

The change in bending stress has to be taken into account in the design to avoid breakage. However in the test cases only two supports are used. In real, the number of supports will be larger and the shaping will be performed in a controlled manner. Therefore the effect of the increase of stresses will be less for the maxima found in this analysis.

7.2.9 Analyzing the effect of self weight

To analyse the effect of self weight on the deflection, a few cases are analysed with self weight included. First the deflection of the beam by self weight only and the moment, shear and axial force diagrams are shown in Figure 7.46 to Figure 7.49.

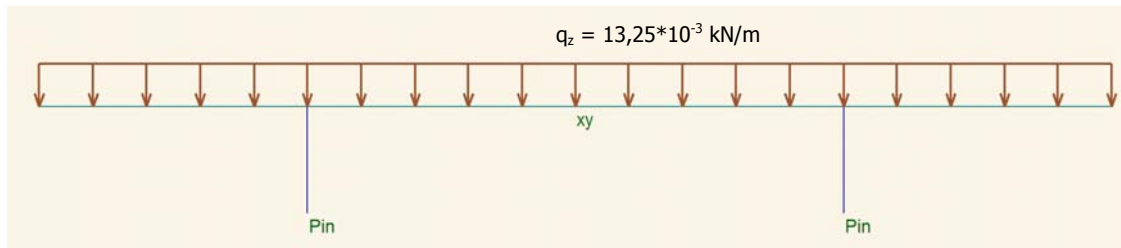


Figure 7.45: Case SW, applied load

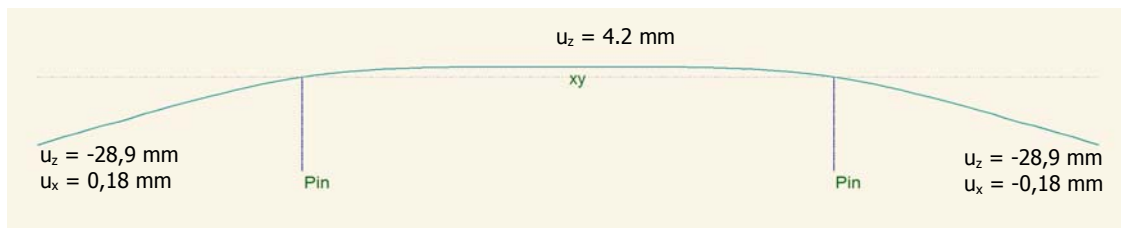


Figure 7.46: Case SW, deformation (x25)

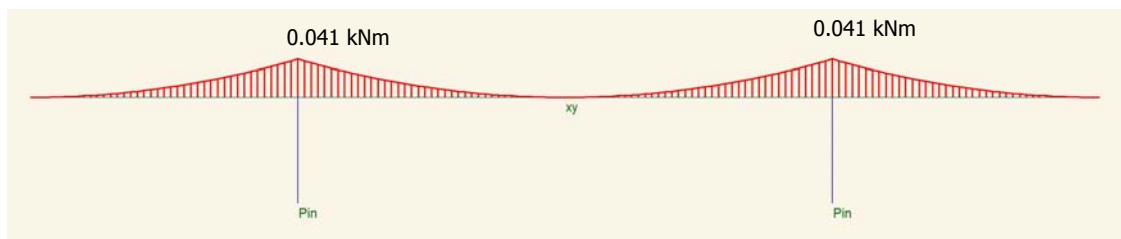


Figure 7.47: Case SW, moment line

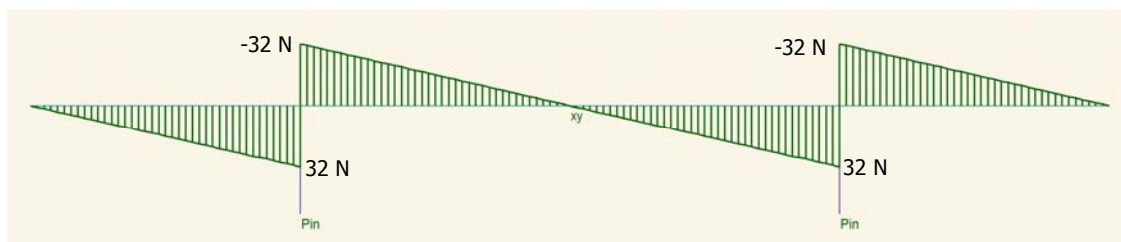


Figure 7.48: Case SW, shear force

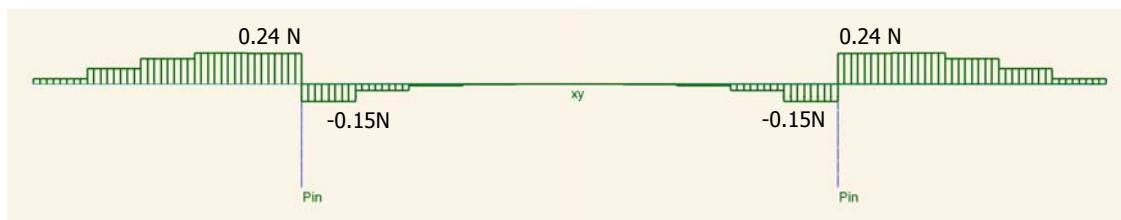


Figure 7.49: Case SW, axial force

Load cases A, B and C (vertical, horizontal and diagonal load) are analysed with self weight included to study the effect of the self weight on deflection and stress distribution. The stresses that result from the deformation by self weight are added to the stresses induced by the applied loads. Effect of the self weight is found the most prominent in stress distribution. This will be analysed in Table 7.3. The bending stress diagrams of the different cases can be found in Figure 7.50 to Figure 7.52. In these figures the bending stress in the upper edge is displayed for both the first step (supported by pendulums) and step 3 (pendulums are deleted). The deformation in the different cases increases due to the self weight, although the change is small. The change of deformation is analysed in Table 7.3 by comparing the percentage of change with and without self weight.

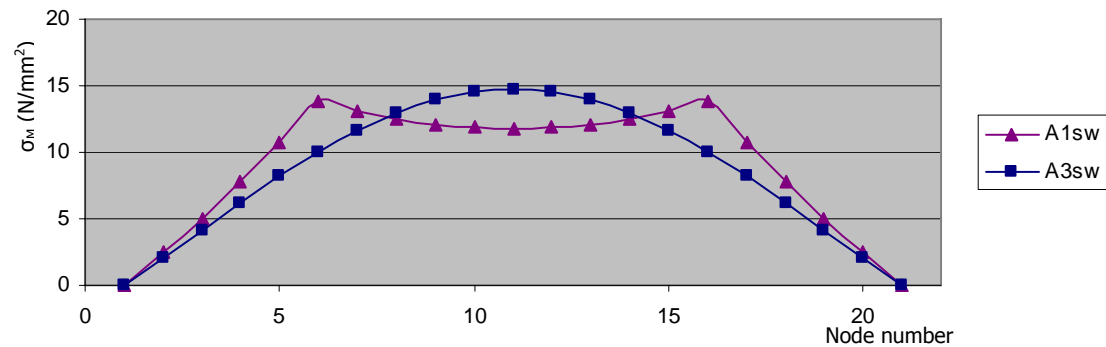


Figure 7.50: Case A1sw and A3sw (deformation by a combination of vertical force and SW), bending stress in the upper edge

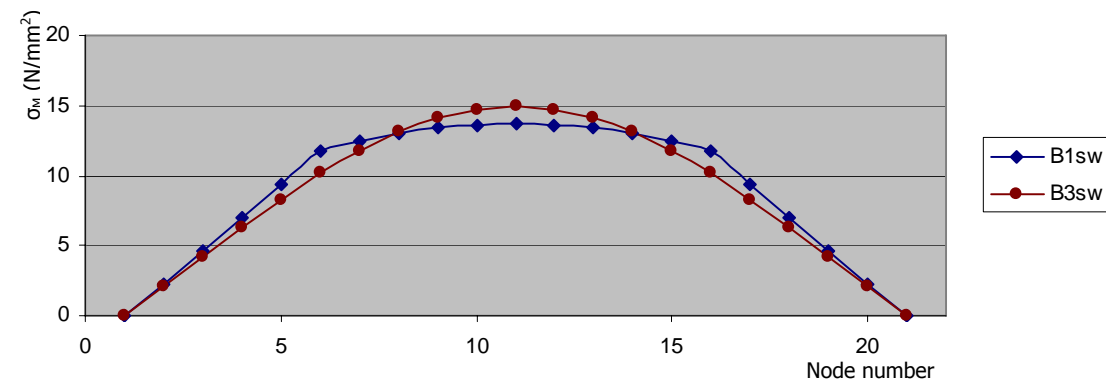


Figure 7.51: Case B1sw and B3sw (deformation by a combination of horizontal force and SW), bending stress in the upper edge

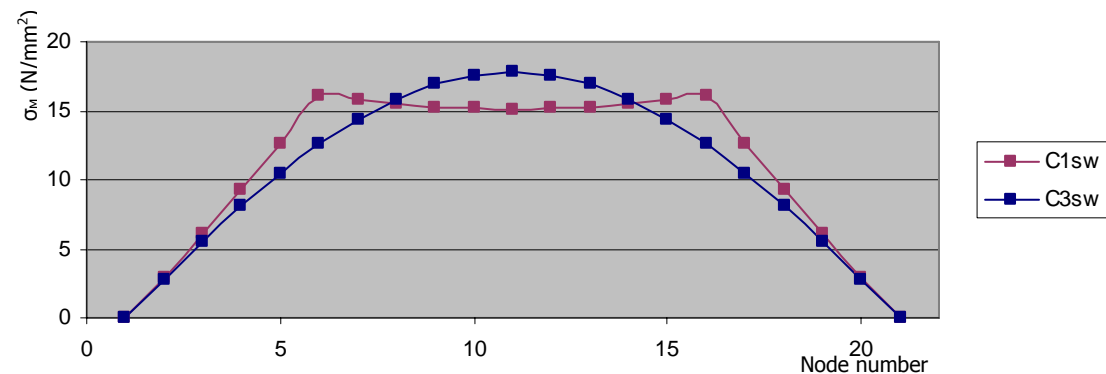


Figure 7.52: Case A3sw and C3sw (deformation by a combination of diagonal force and SW), bending stress in the upper edge

The differences between the cases with and without pendulums are presented in the table below. The differences of the cases without self weight are included to compare the different cases.

Table 7.3: Differences between cases with and without pendulums

	Δu (%) node 11		$\Delta \sigma_m$ (%) Node 11		$\Delta \sigma_m$ (%) Node 6 and 16	
	Without SW	With SW	Without SW	With SW	Without SW	With SW
A3 – A1	1,29	2,09	12,9	19,7	-23,8	-37,5
B3 – B1	0	0,86	0,24	8,4	-0,25	-15,5
C3 – C1	1,10	1,58	10,5	14,9	-19,1	-28,2

It can be seen that including self weight has an increasing effect on the differences between the cases with and without pendulums. This can be explained by two things. First the deflection by self weight and deflection by applied force have to be superimposed to acquire the total deformation and stress distribution. Second, including self weight adds to the effect of non-linear behaviour, especially for the cases with horizontal force. By the deflection due to self weight the moment arm for the horizontal force gets larger, which increases the bending moment at the supports at node 6 and 16.

As stated in Section 7.2.8, the increase in deflection and bending stresses has to be taken into account when designing a gridshell, although the effect will be less prominent when more supports are used. This is also true for the effect of self weight. When more supports are used, the weight is divided and also its influence will be less.

7.3 Interaction between the laths

To investigate the interaction between the laths, a 3D case is analysed. For this case, four equal laths are used with the same properties of the 2D case. The 3D structure, which is shown in Figure 7.53, has a middle beam of 10m in length which is supported by three similar beams at 2,5, 5,0 and 7,5 m. The middle beam is roll supported in the x direction. The transverse beams are pinned at their ends and restricted in the x direction to avoid buckling during analysis. The beams are linked together at their intersection nodes.

The interaction will be investigated by deflecting the supporting beams and analyzing the effect of their deflection on the middle beam. Two situations will be analysed: first the situation where all three supporting beams are deformed with equal deflection; second the supporting beams will be deformed by unequal deflection.

In the former cases the analysis started with a structure supported by pendulum columns, pushing the member down and then pinning it down. These first two steps will be skipped in this analysis, as the effect of these steps is already known.

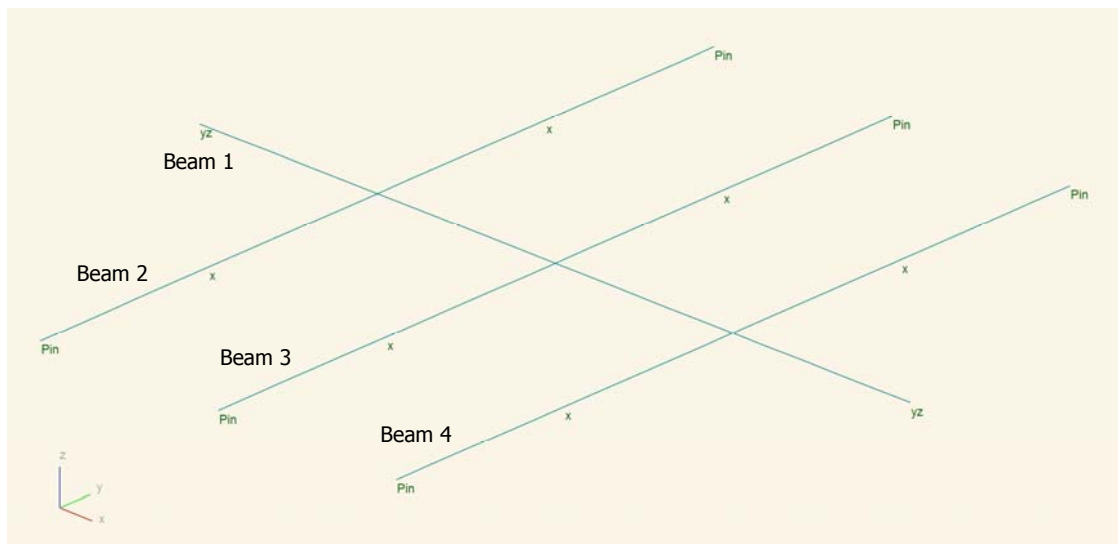


Figure 7.53: 3D structure in initial flat position

7.3.1 Supporting beams with equal deformation

In situation 1 the structure is deformed by deflecting the middle beams with deflection equal to the deflection of case C1, which was deflected by 100N vertical and 100N horizontal force. This results in the following deflection and force diagrams (Figure 7.54 to Figure 7.57):

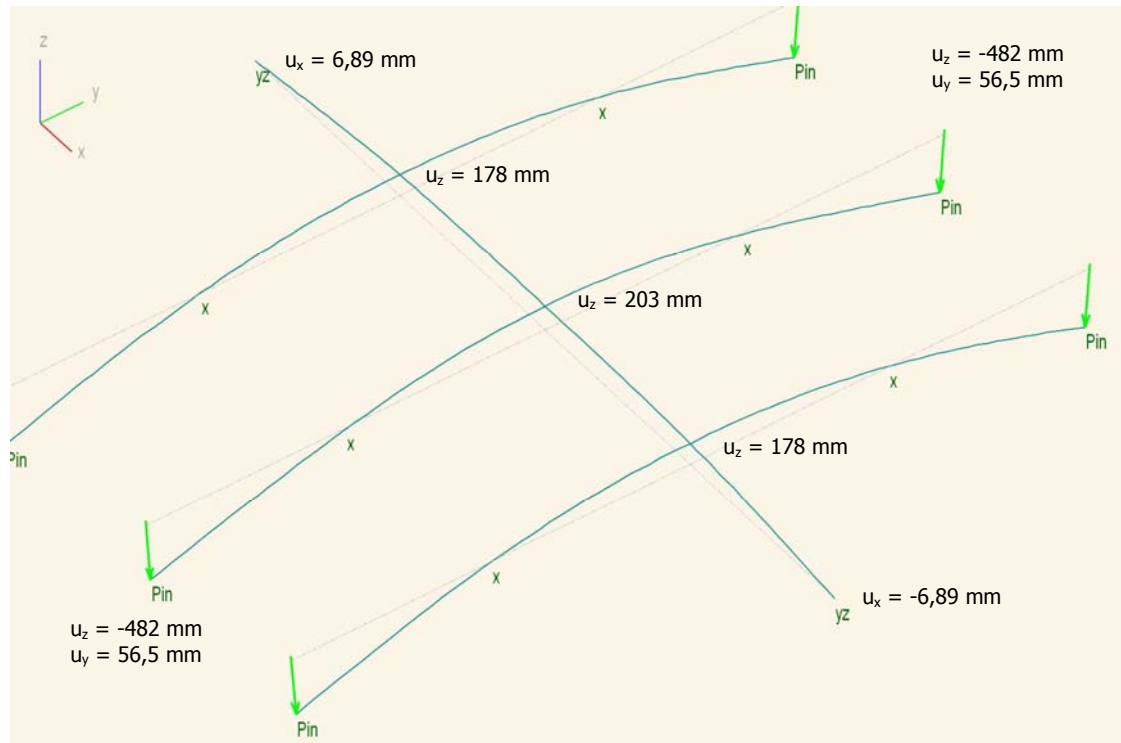


Figure 7.54: Case 3D1, deformation

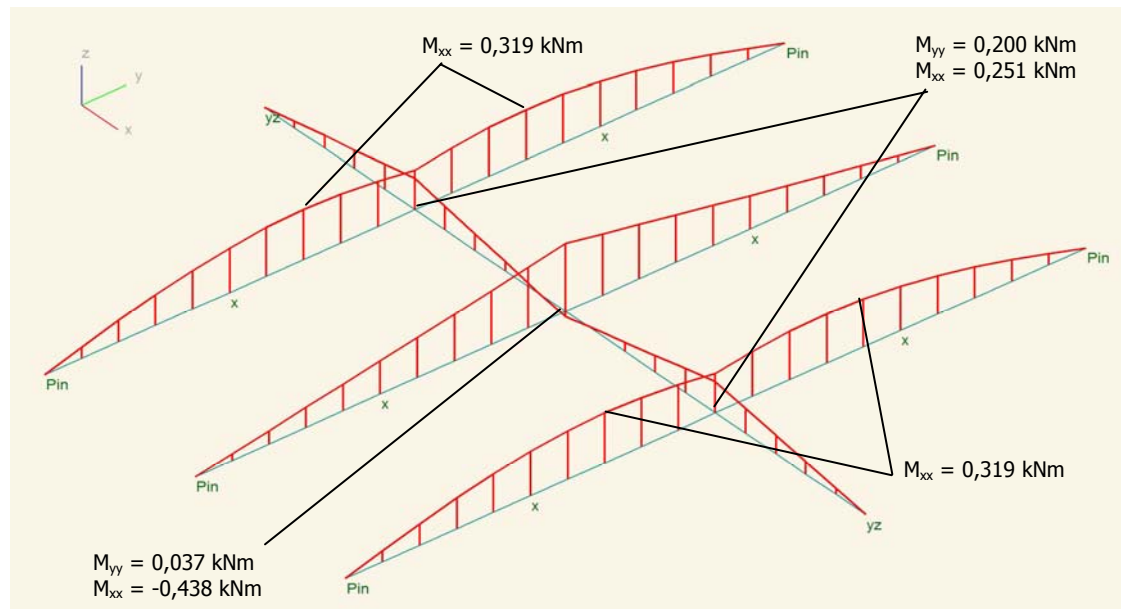


Figure 7.55: Case 3D1, moment line

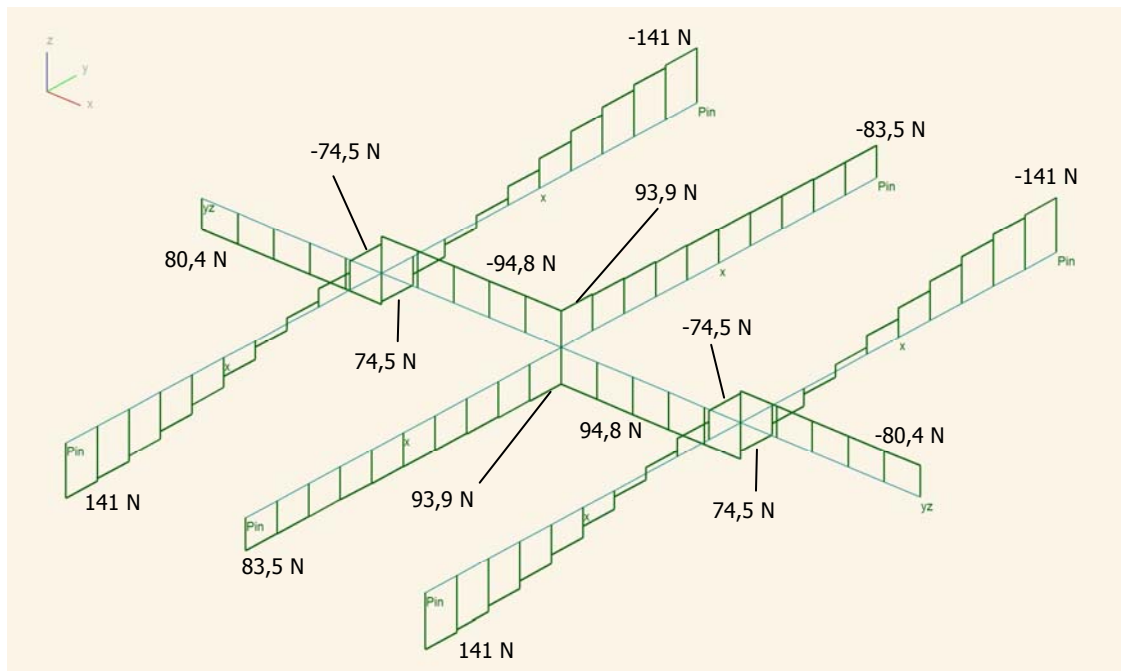


Figure 7.56: Case 3D1, shear force

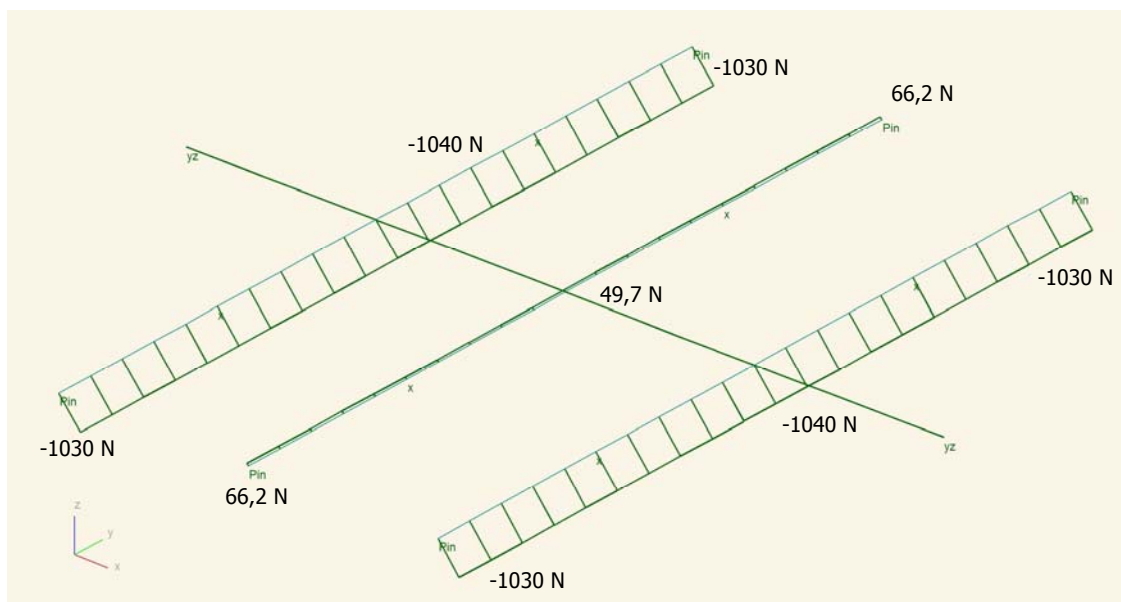


Figure 7.57: Case 3D1, axial force

7.3.2 Supporting beams with unequal deformation

In situation 2, beams 2 and 4 are deflected by a deflection equal to the deflection of case C1a, which was deflected by a horizontal force of 200N and a vertical force of 100N. The horizontal deflection of Beam 3 is kept the same as the previous situation. However, the end nodes are shifted down to the same vertical displacement of beam 2 and 4. This means that the end nodes will be at the same vertical position, which would be the case in real structure on horizontal foundations.

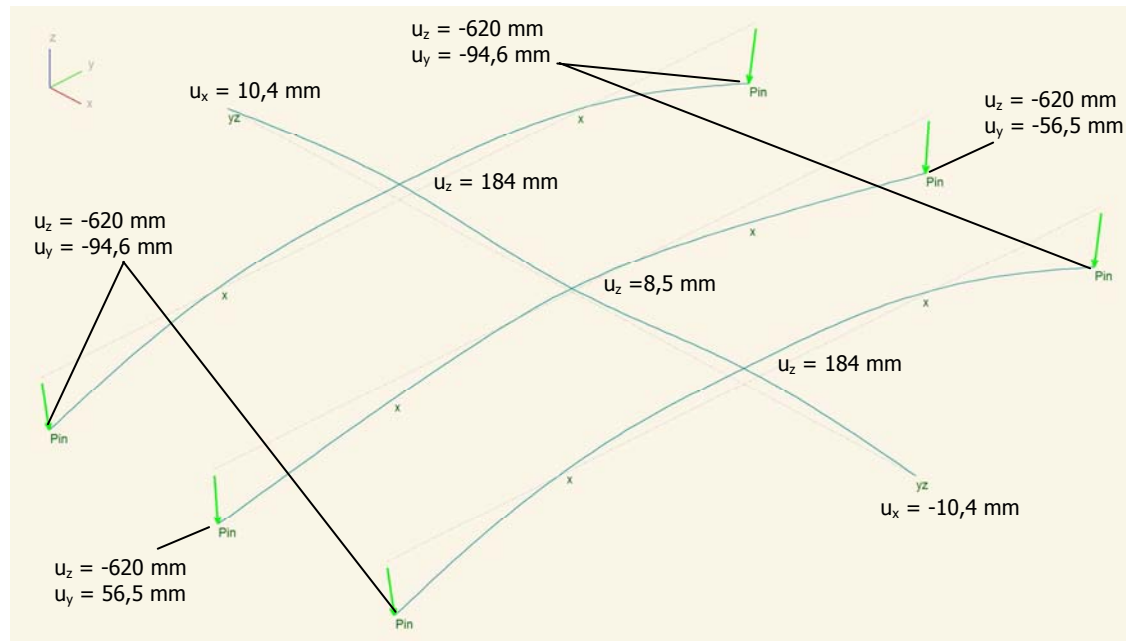


Figure 7.58: Case 3D2, deformation

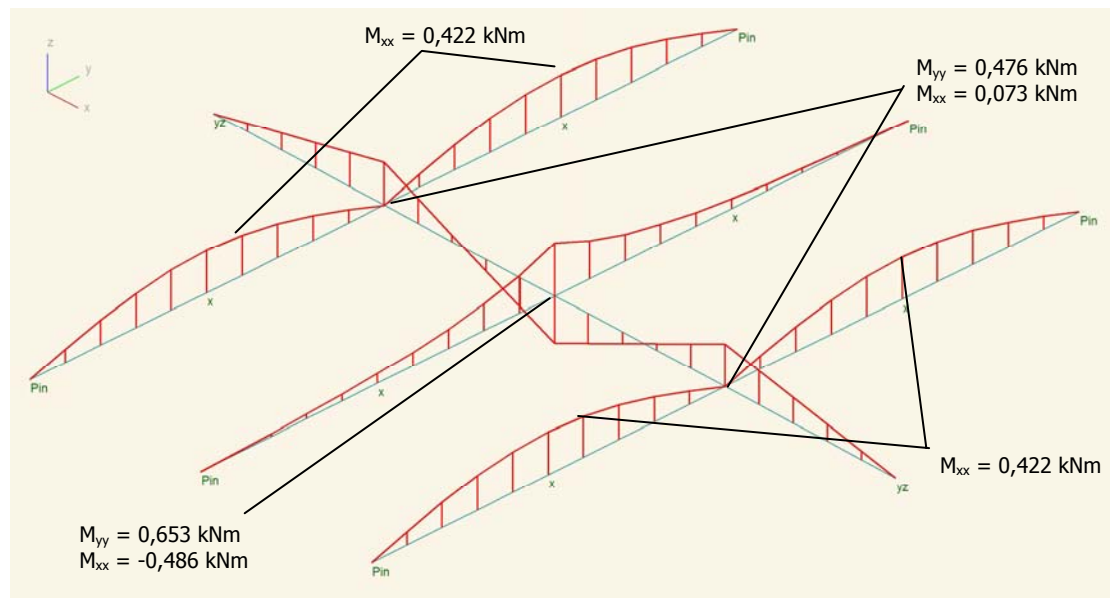


Figure 7.59: Case 3D2, moment line

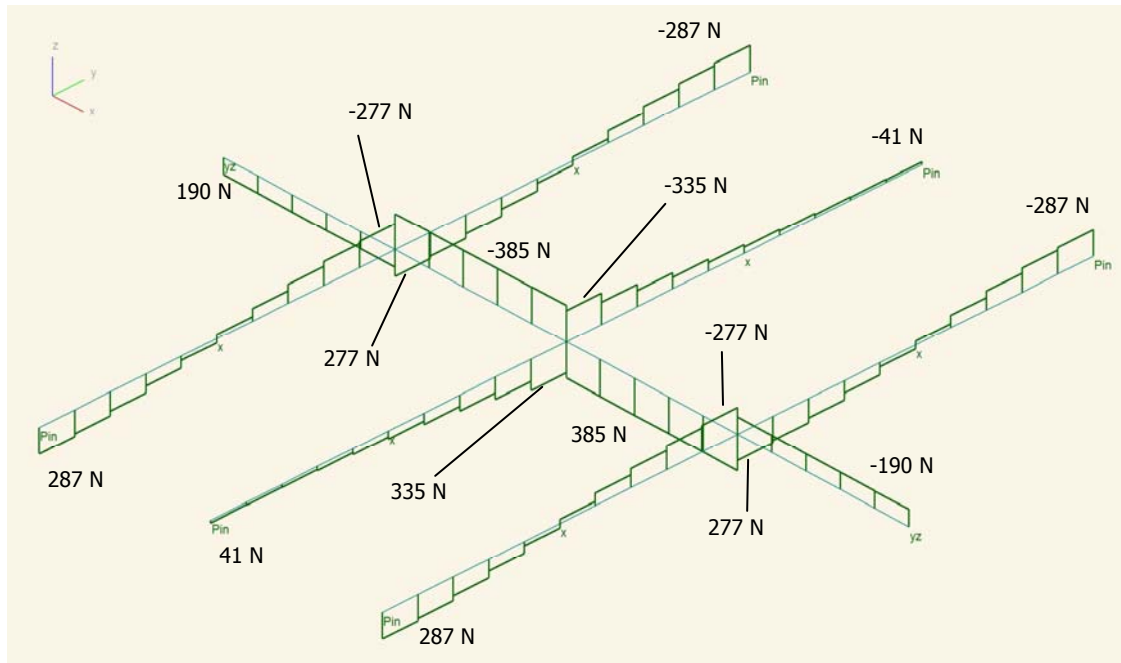


Figure 7.60: Case 3D2, shear force

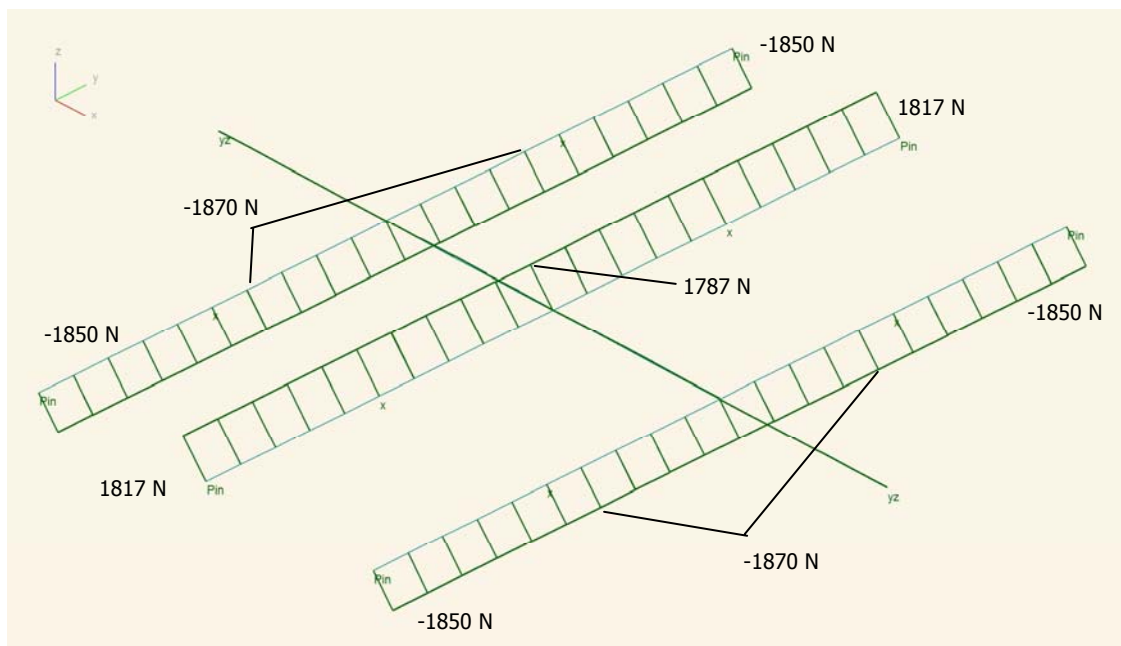


Figure 7.61: Case 3D2, axial force

7.3.3 Analyzing the interaction

By deflecting the three transverse beams, the middle beam is also deflected. The three beams interact with beam 1 and deflection of beams 2,3 and 4 cause deflection and stresses in beam 1. This interaction occurs in the links between the beams and can be translated into link forces. For situation 1 these link forces are:

- Link between beams 1-2 and 1-4: 176 N
- Link between beam 1-3: 190 N

For situation 2 the link forces are:

- Link between beams 1-2 and 1-4: 577 N
- Link between beam 1-3: 771 N

The internal stress distribution of each beam can be seen as the superposition of two load cases: the applied displacements and the link force acting on it. Due to the interaction between the beams, the internal stress distribution changes from what we have found in the analysis cases in Section 7.2 to the stress distribution found in this section.

In situation 2 the link forces are of a larger magnitude than in situation 1. This difference is the result of the difference of deflections of the transverse beams. The middle beam is pulled down by the middle transverse beam much stronger than in situation 1. This results in large compression forces in the outer transverse beams and a large tension force in the middle transverse beam (Figure 7.61). Also the moments change. From approximately zero at mid span for beam 1 in situation 1 to 0,653 kNm in situation 2. The maximum moment in beam 3 stays approximately equal, but the moment diagram does change in shape. For beam 2 and 4, the moment at the link decreases to approximately zero due to the downward force. The field moment however increases from 0,3 to 0,4 kNm. In beam 1 the moment becomes more than twice as large at the links with beam 2 and 4 and increases from 0,2 to 0,47 kNm

The link forces are shown in Figure 7.62 for situation 2. The link forces between the outer transverse beams and beam 1 are compression forces. This results in axial compression in beam 2 and 4. The compression force acts in upward direction on beam 1. The curvature of the middle beam and the outer beams are both in the same direction and when a surface is imagined over the beams, this would be a clastic surface.

The link force between beam 3 and beam 1 is a tension force, which results in an axial tension force in beam 3 and a force pulling beam 1 down at mid span. This results in an opposite curvature in beam 1 and 3. When a surface is imagined over the beams again, the surface would be anti-clastic in this area

In a larger structure, a lot more members interact with each other. The effects that members have on each other will be of the same principle with compression and tension link forces. When a clastic surface is formed, the members affect each other with compression link forces. When the shape pushed from clastic to anti-clastic, tension link forces are to be expected.

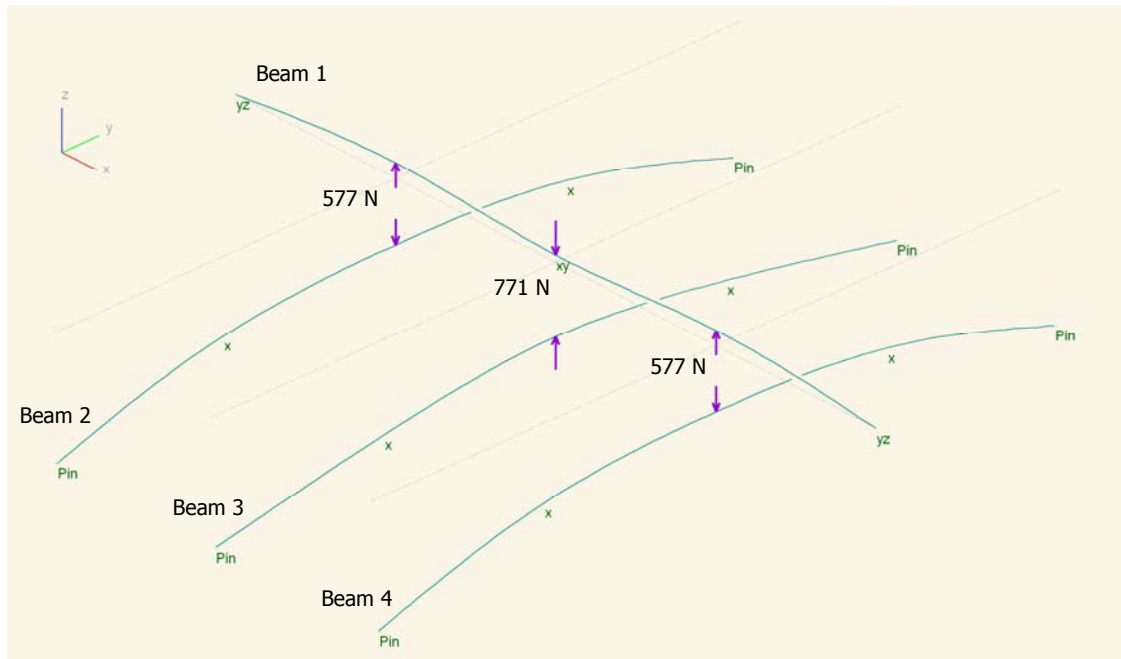


Figure 7.62: Exploded view of the structure (situation 2)

7.4 Curvature and RD-forces

As found in the previous sections, curving a lath results in a bending moment in the lath. It was also found that when a lath is curved in a shape on a series of intermediate supports, the deflected shape is probably not equal to the natural bending shape. The lath will therefore deflect back to a natural equilibrium position when the internal supports are removed: the relaxation deflection (RD).

After relaxation of the timber, approximately half of the stress level remains as residual stresses. For structural analysis, it is needed to take into account the residual formation stresses and it is therefore desired to determine these stresses. When the final geometry of the gridshell is known, the bending and torsion stresses can be calculated, using the curve angles as described in Section 3.2.4. With the gridshell design tool this becomes easy, because the angles are part of the output of the tool. By using a spreadsheet the curve stresses are quickly calculated for all nodes.

When this method is used to calculate the formation stresses, the final geometry of the structure must be known or at least a proper approximation is needed. The problem is that it is uncertain in what extent the design tool approximates the final geometry. If the generated geometry is not equal to a natural bending shape and the mat of laths is forced in this geometry during construction, a relaxation deflection will occur when the internal supports are removed, as seen in Section 7.2. To estimate the relaxation deflection, a (geometrical) non-linear analysis can be used as used in previous sections. For a simple beam this is no problem, but when a complete gridshell with a few thousand nodes and elements is to be analysed, non-linear analysis becomes time consuming. A simpler method to determine the relaxation deflection and RD-stresses would greatly help the design process of a gridshell. In this section it is researched if the curvatures of a structure can be used for this, based on the assumptions described below.

Let's consider a structure that is bent in a non-natural bending shape on internal supports. What keeps the structure in its shape prior to removing the internal supports is the reaction forces at the internal support. When the internal supports are removed, but these support reactions are kept forcing on the structure as an applied force, the structure would still keep the same shape. When equal but reversed forces are superimposed on the structure, the support reactions will be equalled out and the structure will deflect back to its natural equilibrium position. One could say that these reversed forces are the RD-forces for an asymmetric curved lath.

This theory is applied a lath curved in a non-natural way. One can simply calculate the moments that are the result of the curvature, according to Section 3.2.4.1. This curvature with its moment can be seen as the result of forces pushing the structure in a shape (Figure 7.63a and b). When the opposite of these forces is applied on the structure the structure would deflect back (Figure 7.63 c and d). These opposite forces can be calculated by translating the moment in shear forces, by taking the gradient of the moment line (Hartsuijker, 1999). When the lath is divided into discrete elements, for every element a shear force can be calculated. The difference in shear force at a node between two elements would be the RD-forces acting on this node.

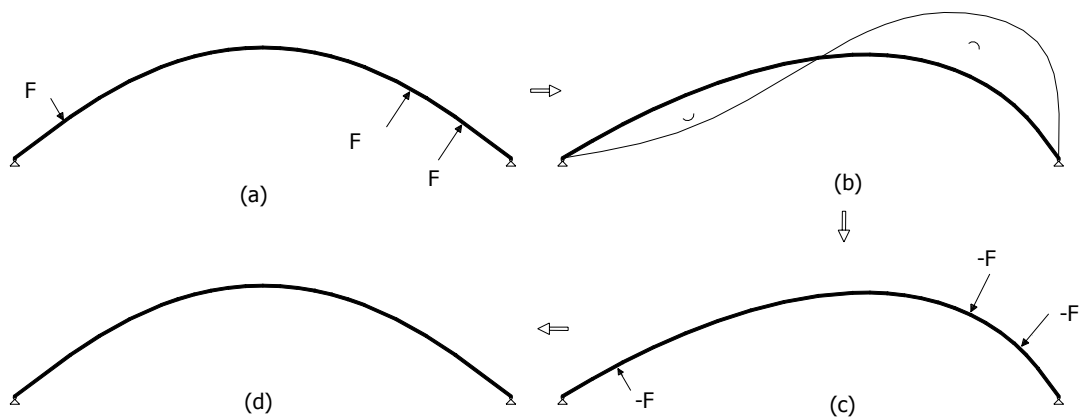


Figure 7.63: The forces F in on a natural curved beam (a) result in the moment line (b). The opposite of the forces F (c) should result in a deflection back to the natural curve (d). Deflections, forces and moment line are indicative.

Applied on a large structure which is not curved in a natural way, it would be simpler to calculate the RD-stress distribution with this method than with non-linear analysis. When all curvatures at all nodes are known, the moments due to the curvatures can be calculated and therefore also the resulting RD-forces are known. By applying these forces, a linear load case "relaxation deflection" is created. The result of this load case would be a structure deflected to the natural curved shape. One could say form-finding is applied in a very basic way.

The theory described above is tested on a simple structure as follows:

- Situation 1: a lath (lath 1) is asymmetrically curved over internal supports. The support reactions in the supports would be the inverse of the RD-forces.
- From the initially asymmetric curved lath the curve angles between segments are determined.
- These angles are translated into moments, shear forces and RD-forces;
- Situation 2: the lath is implemented in GSA with its curved geometry. This is the strainless situation.
- Situation 3: the RD-forces are applied on the structure, which results in deflections.
- Situation 4: an initial straight lath (lath 2) with a length equal to the length of lath 1 is bent up in a GSA analysis. The deflection is the natural bending curve of lath 1.
- Situation 5: the inverses of the RD-forces are applied on lath 2. This load case should be equal to situation 1 and so should be the deflections. Also the resulting moments should be equal to the moments that are derived from the curve angles.
- The different situations can be compared. The deflected shape of situation 3 should be equal to the shape in situation 4. The deflected shape of situation 5 should be equal to the shape in situation 2.

7.4.1 Initially curved beam

The theory described in the previous section is tested on a simple structure. Let's consider a lath that is bent on internal supports in a non-natural bending shape (situation 1). This lath is inputted strainless in GSA (situation 2). The lath shown in Figure 7.64 is divided into 9 elements, each 2,5m long. The angles at each node between the different elements are determined. From these angles the moments can be calculated which would have occurred when the lath would have been bent into this shape from an initial straight position. The moments can be translated into shear forces. This data is displayed in Table 7.4.

The moments at every node can be calculated using the formulas given in Appendix 1: Determination of the maximum bending radius. The next formula can be stated, which calculate the stress due to a certain bending angle:

$$\sigma_m = \frac{hE\alpha_b}{2L} \quad (7.1)$$

Where:

α_b = the bending angle
 L = the element's length

Together with

$$\sigma_m = \frac{M}{W} \quad (7.2)$$

the bending moment can be calculated.

The shear forces at each node can be calculated with:

$$F_{s,j} = \frac{M_j - M_{j-1}}{L} \quad (7.3)$$

Where:

$F_{s,j}$ = the shear force at node j
 M_j = the moment at node j

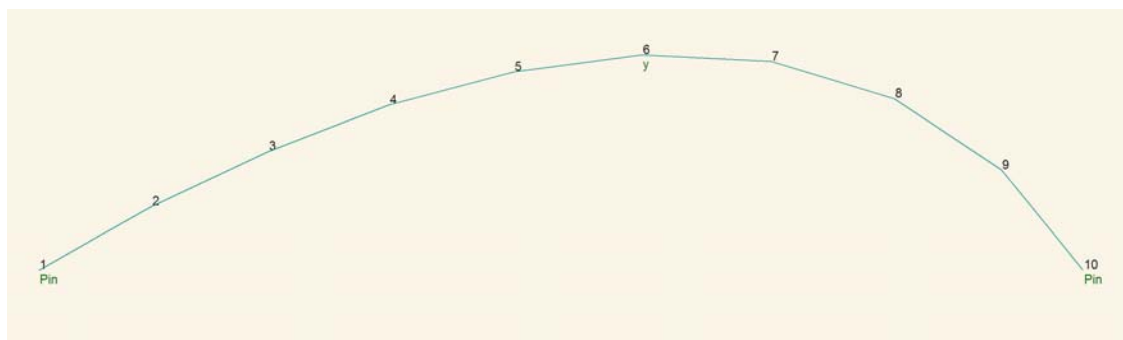


Figure 7.64: Curved beam

Table 7.4: Angles between the nodes with corresponding moments and shear forces

Node	Between elements		α	M	F_{shear}	ΔF_{shear}
			(rad)	(Nmm)	(N)	(N)
1	-	1	-	0	0	-
2	1	2	0,068	$1,42 \cdot 10^5$	56,716	-46,040
3	2	3	0,081	$1,68 \cdot 10^5$	10,676	6,230
4	3	4	0,101	$2,11 \cdot 10^5$	16,906	9,572
5	4	5	0,133	$2,77 \cdot 10^5$	26,478	13,730
6	5	6	0,181	$3,77 \cdot 10^5$	40,208	12,781
7	6	7	0,245	$5,10 \cdot 10^5$	52,988	-9,455
8	7	8	0,297	$6,19 \cdot 10^5$	43,533	-47,469
9	8	9	0,292	$6,09 \cdot 10^5$	-3,936	-239,632
10	9	-		0	-243,568	

This data can also be displayed in a moment and shear-force diagram. The moments on the structure due to curvature are:

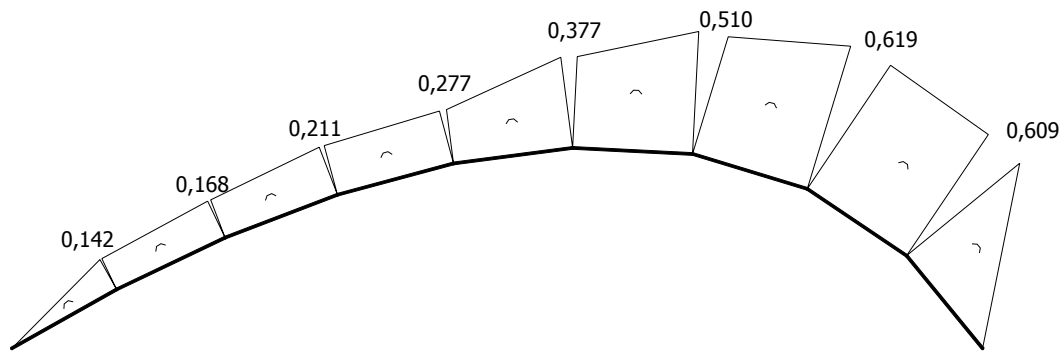


Figure 7.65: Moment due to curvature ($\times 10^6$ Nmm)

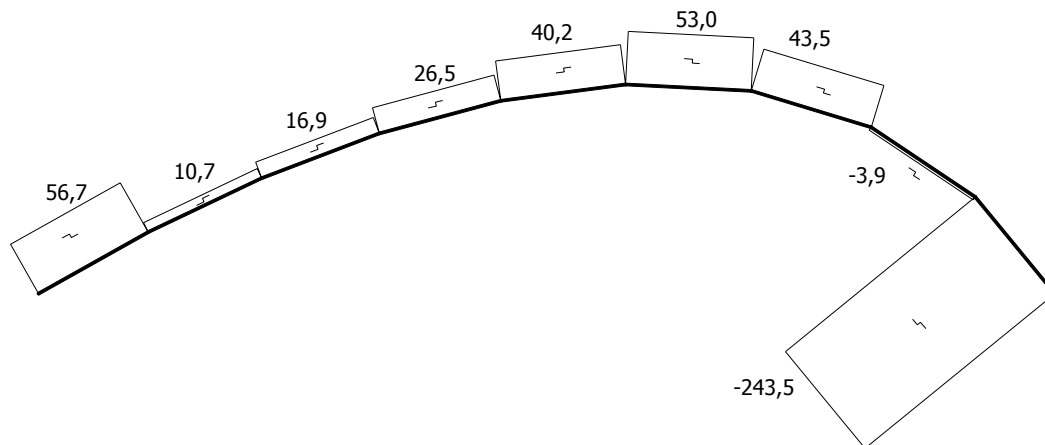


Figure 7.66: Shear forces due to curvature (N)

The difference in shear at each node results in the RD forces which are applied on the structure (situation 3). This should result in a bending shape which approximates the natural bending shape. The deflection caused by this load is shown in Figure 7.67. Corresponding moment, shear and axial force diagrams are shown in Figure 7.68 to Figure 7.70.

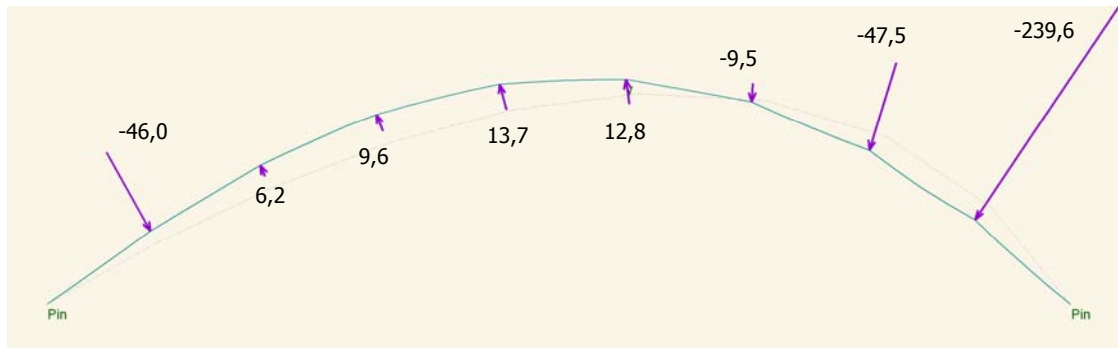


Figure 7.67: Deformation due to curvature forces (N)

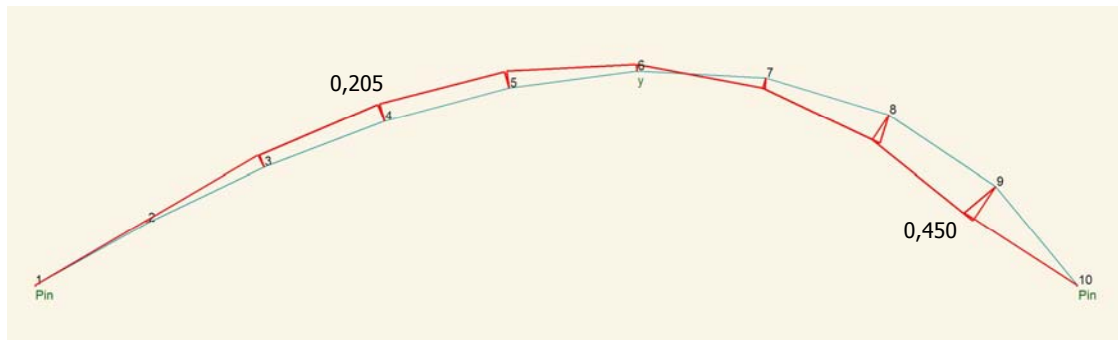


Figure 7.68: Moment line due to curvature forces (kNm)

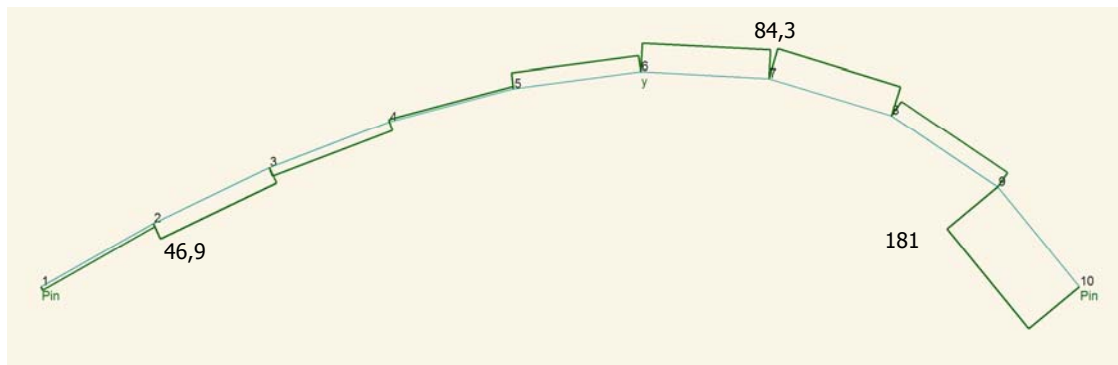


Figure 7.69: Shear forces due to curvature forces (N)

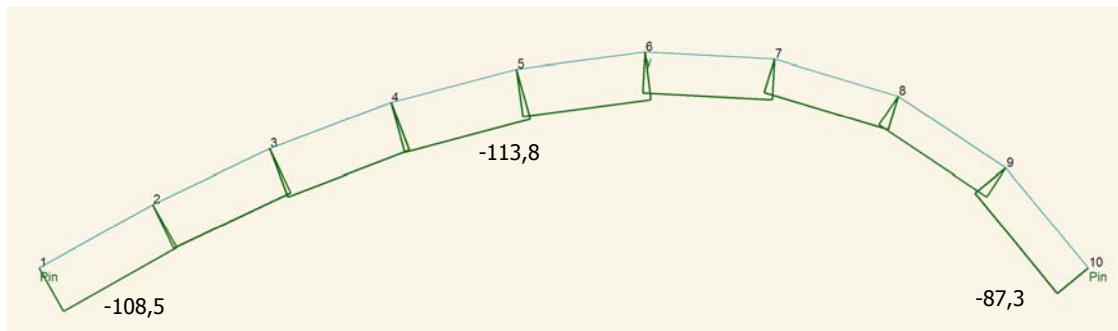


Figure 7.70: Axial forces due to curvature forces (N)

7.4.2 Comparison with a straight lath

The deformation of this asymmetric curved lath by the RD-forces (situation 3) is compared with the deformation of a straight lath which is bent up (situation 4). The deflection of this lath is the natural bending shape. The lath is deflected by moving the end nodes until the distance between the end nodes is equal to the distance of the end nodes of the curved beam. The straight lath has the same length as the curved lath of 22,5 m. the end node is moved 2,32 m. to the left. This results in the deflection shown in Figure 7.71.

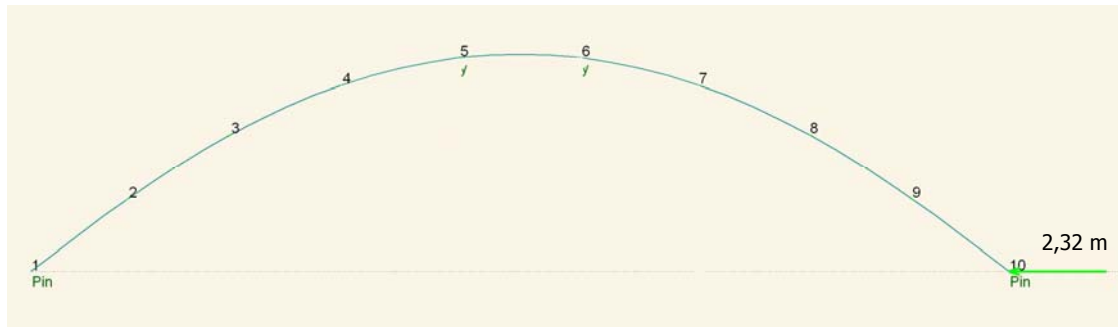


Figure 7.71: Deformation of a straight lath

To compare the deformation of the initially curved lath with the deformation of the initially straight lath, the deflections are put together in a graph (Figure 7.72). To give a complete picture, the deformations of the initial curved lath are calculated by linear and non-linear analysis. The deformation of the initial straight lath is calculated by non-linear analysis.

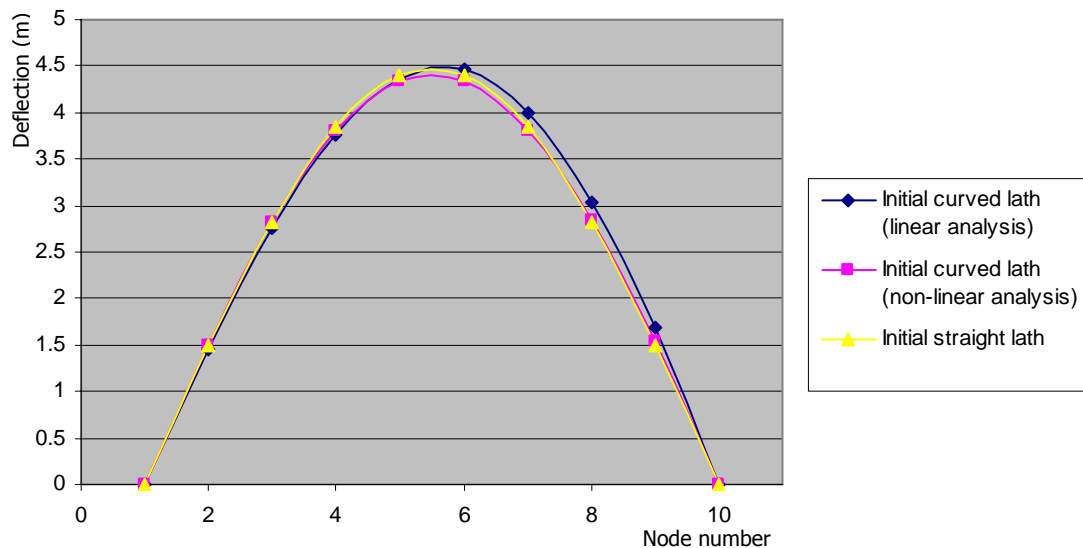


Figure 7.72: Deformation of the initial straight and initial curved lath

In the graph it can be seen that there is a small difference between the different cases. The initial straight lath bends to the natural deflection shape. Difference for the middle nodes (node 5 and 6) between the natural deflection and the deflection calculated by non-linear analysis for the initial curved lath is 60 mm downward (1,4%). With linear analysis the difference is 57mm upward for node 4 and the deformation shape keeps a small eccentricity to the right.

When this lath is loaded with the inverted RD-forces (situation 5), the deflection should become equal to the deflection of situation 2. The following results for deflection and moment are found:

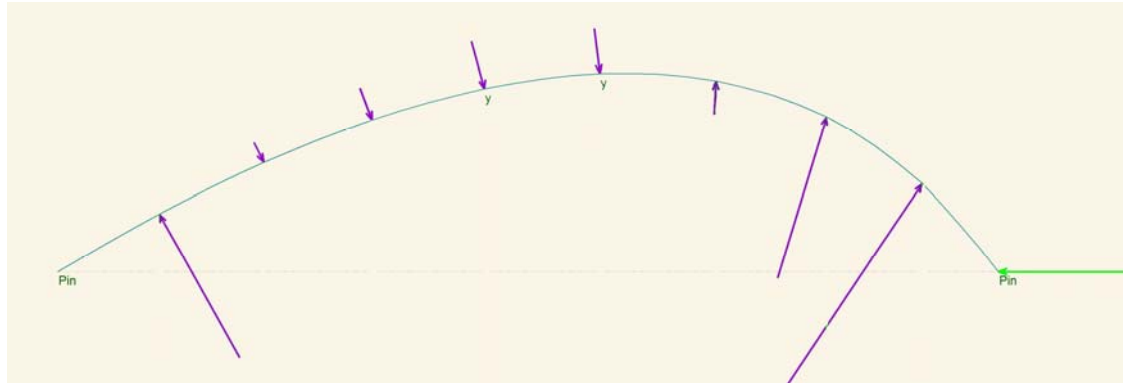


Figure 7.73: Deformation of the initial straight lath, by applied displacements and inverted RD-forces

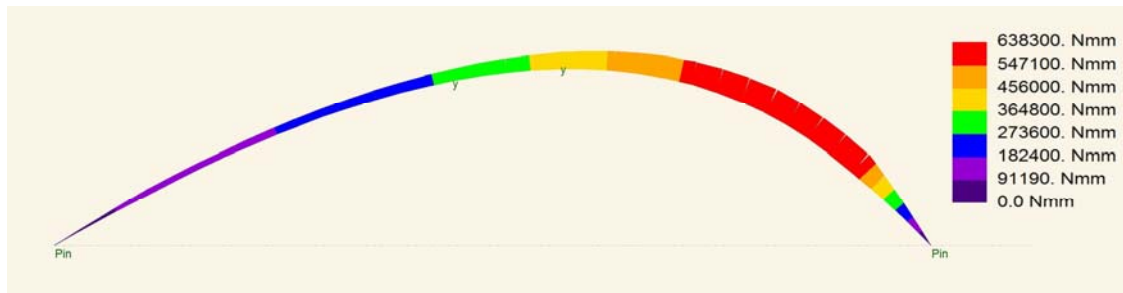


Figure 7.74: moments as result of the applied displacements and inverted RD-forces

When these results are compared with the coordinates of the initial situation (situation 2) and the moments that are calculated from the curve angles, it is found that the two situations do not differ much (Table 7.5). For the deflection a maximum difference of 2% is found. In the moments the maximum difference is 4,4%.

Table 7.5: Difference in deflection and moment between situation 2 and 5

Node	z-coordinate (m)		difference		Moment (Nmm)		difference	
	situation 5	situation 2	(m)	%	situation 5	calculated	(Nmm)	%
1	0	0	0	-	0	0	0	-
2	1.236	1.228	0.008	0.64	141200	141789	-589	-0.42
3	2.343	2.305	0.038	1.62	169100	168479	621	0.37
4	3.261	3.196	0.065	1.98	214800	210743	4057	1.89
5	3.931	3.847	0.084	2.14	286900	276938	9962	3.47
6	4.256	4.172	0.084	1.97	394900	377457	17443	4.42
7	4.102	4.045	0.057	1.38	533100	509927	23173	4.35
8	3.327	3.320	0.007	0.22	638300	618759	19541	3.06
9	1.892	1.929	-0.037	-1.95	611800	608920	2880	0.47
10	0	0	0	-	0	0	0	-

Comparing the results of situation 3 and situation 4, it can be concluded that the deflection due to the RD-forces gives an accurate result for the equilibrium position of the lath. Only a small difference is found between the results calculated with non-linear analysis and the results of the calculation with RD-forces. A non-linear analysis gives the most accurate result, so a non-linear analysis cannot be ruled out if accuracy is desired. This non-linear analysis is however much simpler than the non-linear analysis that is needed to calculate an equilibrium position for an initial flat mat of laths. In stead of calculating the deflection from initially flat to deformed, a series of forces is applied on an already curved structure and only the relaxation deflection has to be calculated.

Comparing situation 5 and situation 2, it is shown that the bending moments that can be derived from the curve angles are correct. In the analysis the derived moments only differ 4,4% with the moments calculated with the non-linear analysis.

7.4.3 RD-forces in a three dimensional grid

An equal analysis as in the previous section is performed with a 3D structure. As a test case, a shape is needed that is not symmetric. The tip of a rotated ellipsoid is chosen (Figure 7.75). Using the grid generation tool, a grid is generated with a mesh size of 2,5m, shown in Figure 7.76. This can be seen as the structure deformed on internal supports (situation 1).

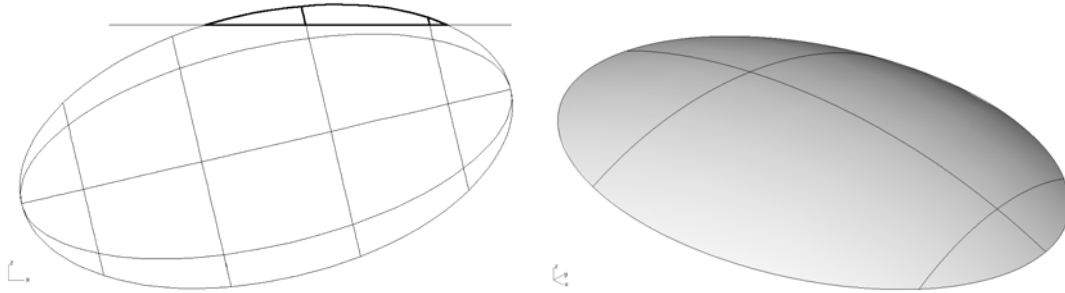


Figure 7.75: Tip of a rotated ellipsoid in side view and 3D

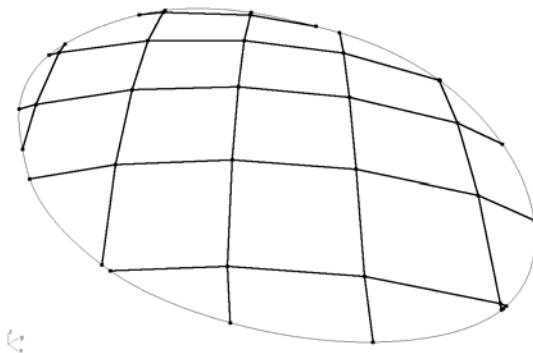


Figure 7.76: grid generated on the ellipsoid tip

The following steps are needed to perform the comparison:

- Import the structure generated by the gridshell design tool in GSA. This is the unstrained situation of the structure (situation 2).
- Calculate RD forces out of the curvatures. Curvature around the z -axis results in horizontal forces. Curvatures around the element's local y -axis result in vertical forces.
- Apply all forces on the unstrained structure. This results in the deformation of the unstrained structure (situation 3)
- Determine the natural bending shape of the grid with a non-linear analysis, by applying generated coordinates as applied displacements (situation 4)
- Compare the geometry of this strained situation with the coordinates after deformation of the unstrained structure.

The grid is generated with a lath cross section of 35mm high and 50mm wide. With the output tool the model data is exported. This data can be used to model the structure in GSA, by copying the node coordinates and the element begin- and endpoints into the program. This model is the strainless situation of the structure (situation 2). The data in the output file is ordered in such way that the laths can be implemented in GSA as continuous laths in two directions. The intersections between the laths can be implemented as link nodes, with unrestrained rotation around the z -axis.

In the output file, also the angles of curvature in x -, y - and z - direction can be found. From these angles, bending and torsion stresses can be derived for every node, in the same way as described in Section 7.4.1. These stresses can be translated in moments, and the moments in shear forces acting on every element. The difference between the shear forces at every node are the RD forces. These can be applied on the strainless structure (situation 3). If the assumption made in this section is correct, this should result in a shape similar to the natural bending shape.

The deflected shape of the strainless structure should be compared with the natural bending shape. This natural bending shape can be determined with a non-linear analysis in GSA. With a relatively small structure as this, a non-linear analysis is quickly performed. This analysis starts with an initially flat mat of laths. As with the cases in Section 7.2, applied displacements are enforced on all nodes of the structure to deform the structure to a curved shape. The applied displacements in x , y and z direction are equal to the x , y and z -coordinates of the nodes that are generated by the design tool. It should be noticed that a permanent applied displacement can only be enforced on a node which has a support. The applied displacements that are enforced on the nodes that do not have an edge support are used to push the structure in an initial shape. In the non-linear analysis iterates to an equilibrium position and what is left is the applied displacements of the supported edge nodes and the equilibrium displacements of the other nodes.

Because a non-linear analysis iterates to a situation in which the structure is in equilibrium, this shape should be the natural bending shape of the grid (situation 4), complying with the applied displacements of the supports. Now this shape is known, the deflections of the unstrained structure can be compared with the natural bending shape.

First, the unstrained structure is implemented in GSA (Figure 7.77). This structure is then loaded by the RD-forces in horizontal and vertical direction (Figure 7.78 and Figure 7.79). Results will be displayed on the points indicated by their node number in Figure 7.77, the loads are displayed. The resulting deflection is shown in Figure 7.80 with a magnification of 20.

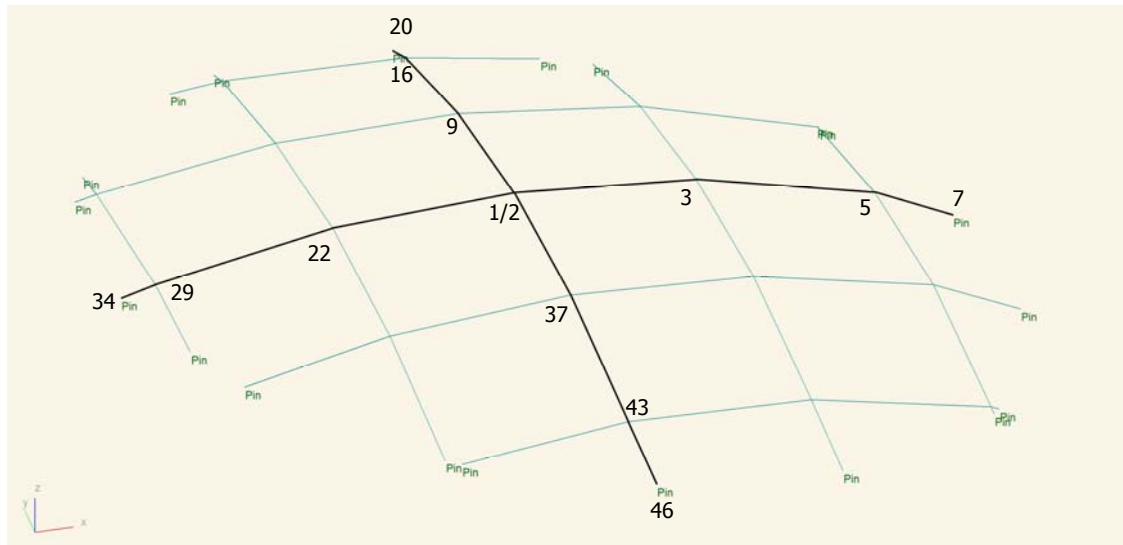


Figure 7.77: Unstrained structure in GSA (with node numbers for indicative sections)

Table 7.6: Angles of curvature at nodes, with corresponding moments, shear forces and RD-forces

Node number	α_{yy} (rad)	α_{zz} (rad)	σ_{yy} (N/mm ²)	σ_{zz} (N/mm ²)	M_{yy} (Nmm)	M_{zz} (Nmm)	τ_{xz} (N)	τ_{xy} (N)	RD forces (N)	RD forces (N)
34	0	0	0	0	0	0	-	-	-	-
29	0.138	0.026	9.687	1.799	98891	53528	39.556	21.411	-39.223	-41.933
22	0.140	0.001	9.769	0.075	99724	2225	0.333	-20.521	2.431	30.359
1	0.149	0.013	10.446	0.901	106635	26819	2.765	9.838	3.280	-5.142
3	0.170	0.019	11.926	1.296	121746	38558	6.044	4.695	5.745	-3.072
5	0.212	0.020	14.813	1.432	151217	42617	11.789	1.624	-72.275	-18.671
7	0	0	0	0	0	0	-	-	-	-
20	0	0	0	0	0	0	-	-	-	-
16	0.141	0.016	9.864	1.133	33723	5584	40.278	13.489	-40.349	-16.128
9	0.141	0.013	9.847	0.911	27125	5283	-0.071	-2.639	2.528	-6.250
2	0.149	0.002	10.448	0.165	4904	5192	2.456	-8.889	3.428	10.625
37	0.170	0.004	11.889	0.311	9245	5221	5.884	1.736	5.713	29.471
43	0.210	0.042	14.729	2.932	87262	5330	11.597	31.207	-71.741	-66.112
46	0	0	0	0	0	0	-	-	-	-

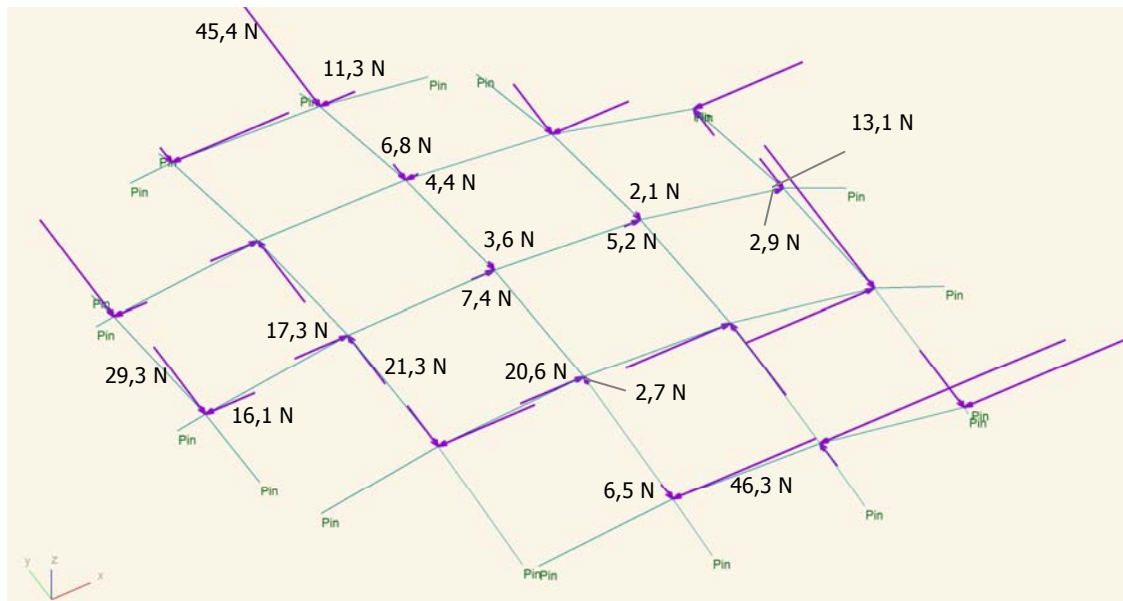


Figure 7.78: Horizontal RD-force, which result from bending around the z-axis (N) (figures are the sum of two nodes in an intersection and therefore not equal to the figures in Table 7.6)

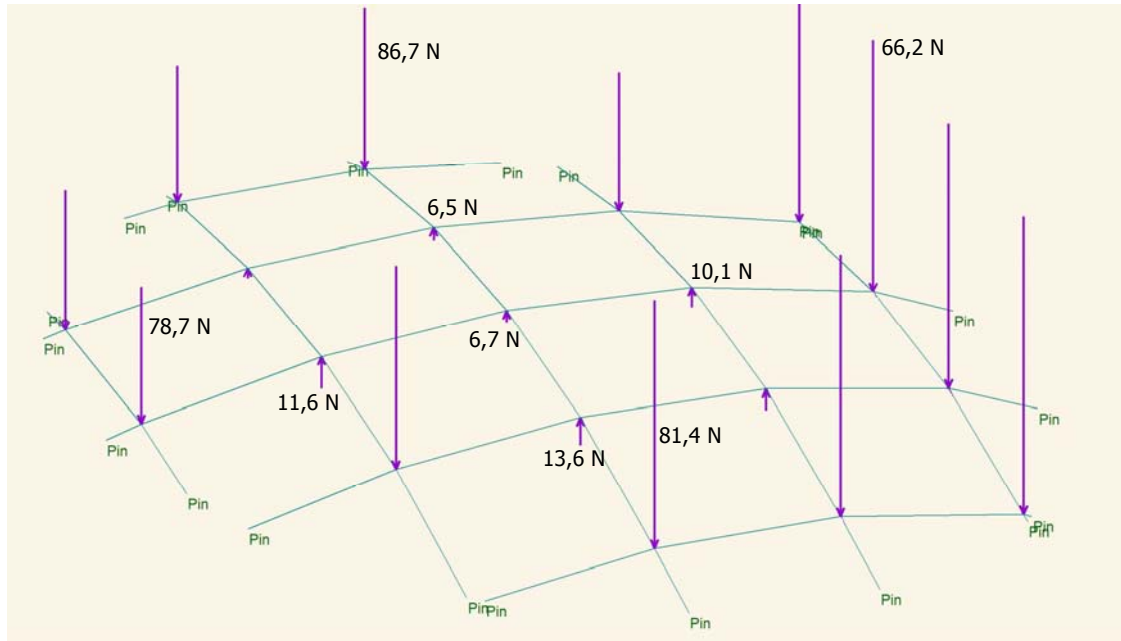


Figure 7.79: Vertical RD-forces, resulting from bending around the (local) y -axis (N) (figures are the sum of two nodes in an intersection and therefore not equal to the figures in Table 7.6)

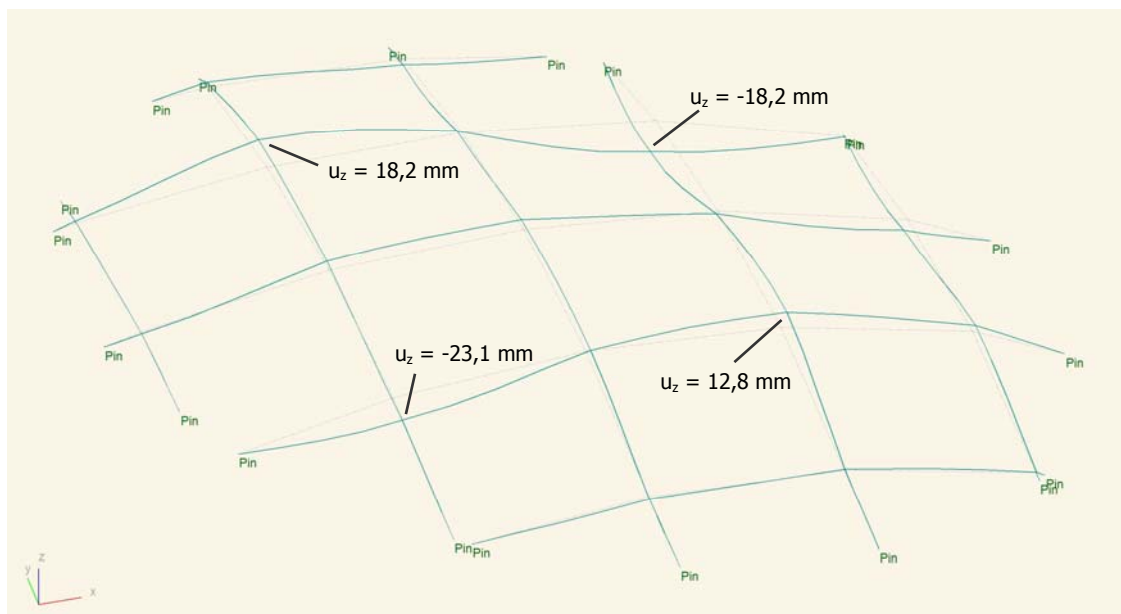


Figure 7.80: Deformation by the RD forces (magnified 20x) (mm)

For the non-linear analysis, the structure is first implemented as a flat mat (Figure 7.81). The structure is then deformed by applied displacements. The results of the non-linear analysis are displayed in Figure 7.82.

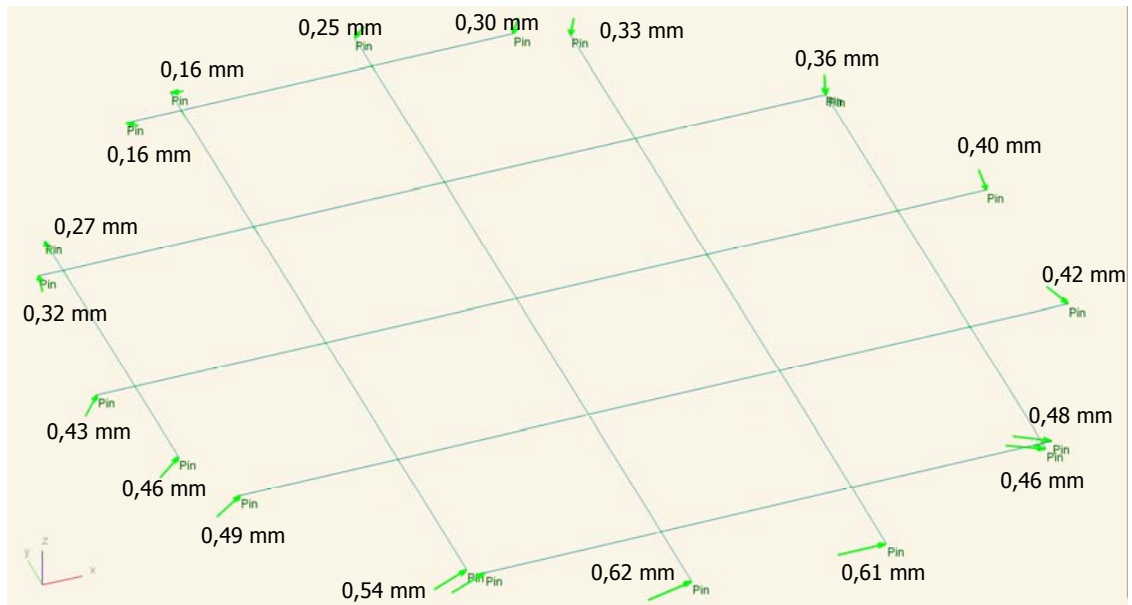


Figure 7.81: Undeformed mat of laths with applied displacements of the support nodes (m)

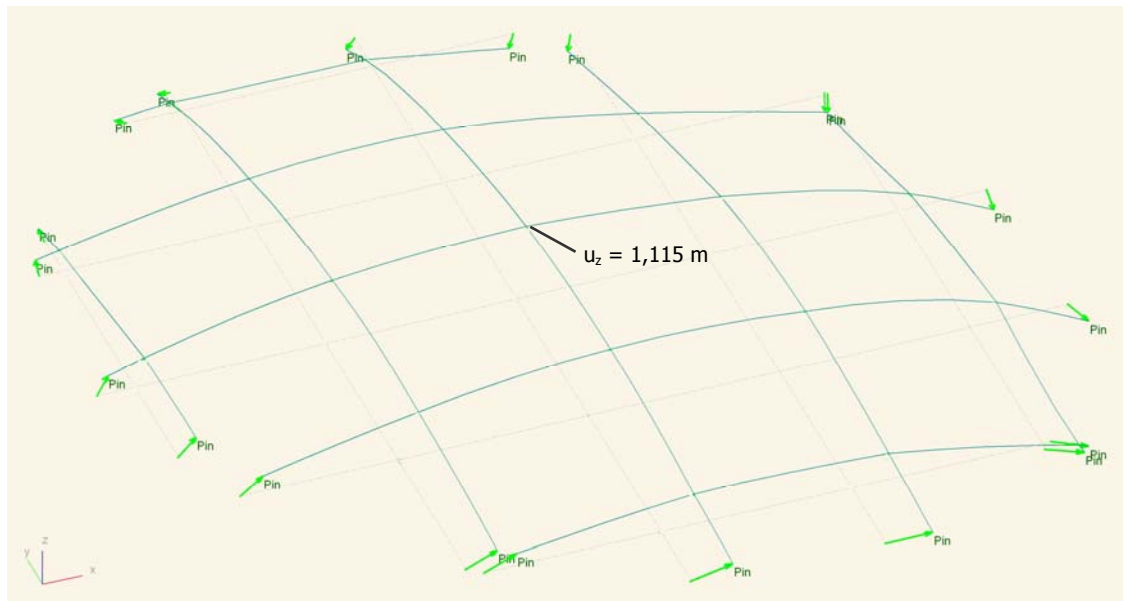


Figure 7.82: Deformed structure, by non-linear analysis

Now the results are known, the structures can be compared. Two sections are reviewed, displayed in Figure 7.83. The coordinates of the nodes on these sections are displayed in the graphs in Figure 7.84 and Figure 7.85.

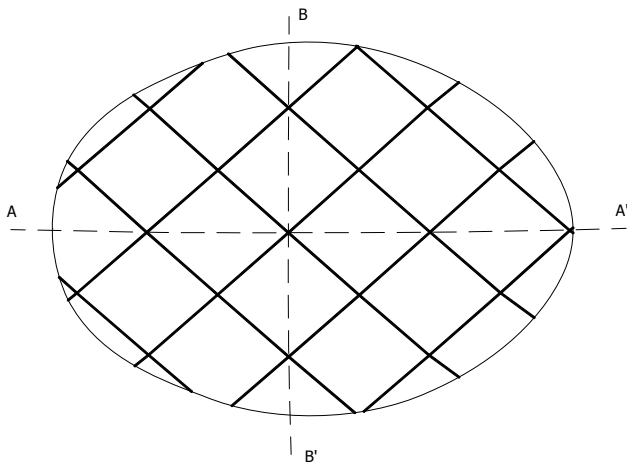


Figure 7.83: Sections AA' and BB'

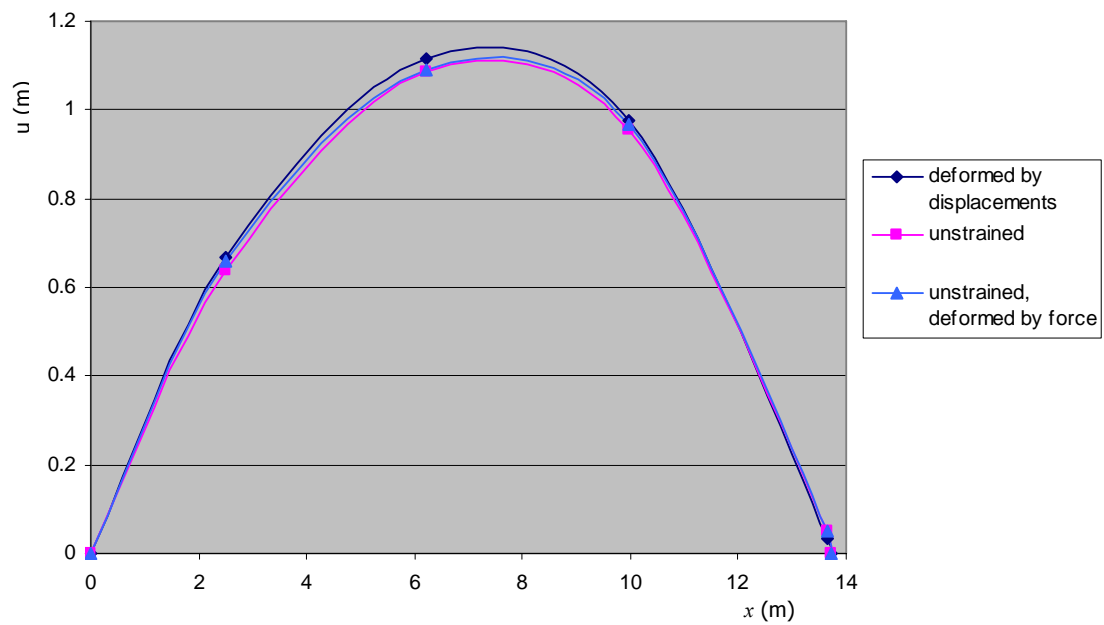


Figure 7.84: Section AA' over the different structures

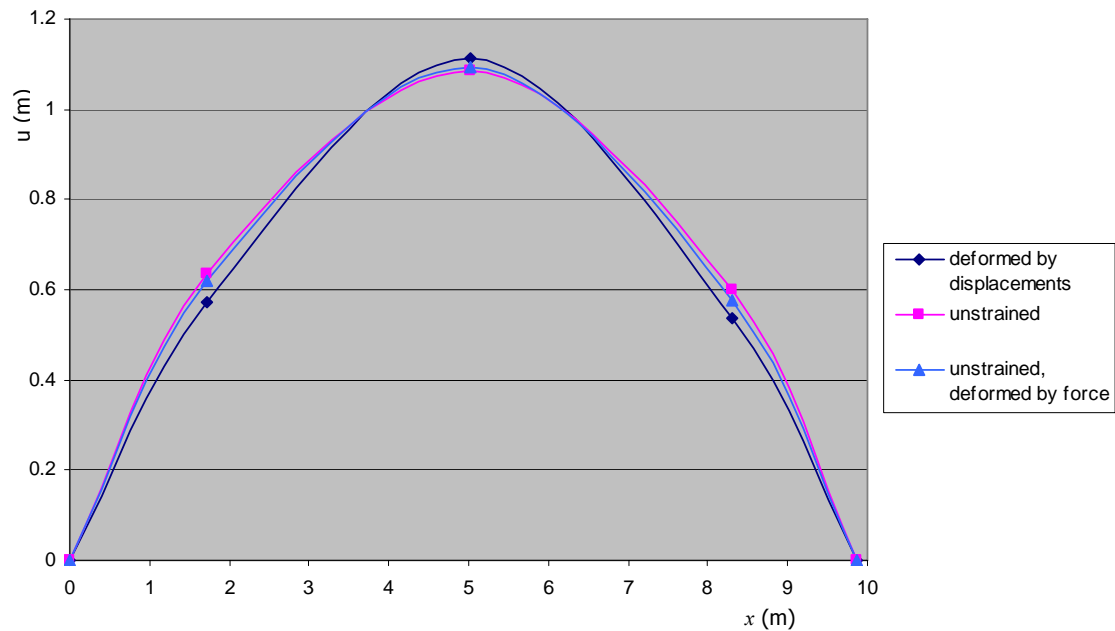


Figure 7.85: Section BB' over the different structures

As can be seen, the shape that is determined by non-linear analysis by applied displacements shows a different shape than the unstrained structure, which is equal to the original surface. This deformed shows a more parabolic shape. The difference between the form found structure and the unstrained structure is 30,3mm in vertical direction, which is 2,8% of the total deflection. When the RD forces are applied, this is reduced to 23,5mm (2,1%)

When the RD forces are applied on the unstrained structure, the structure does deflect toward the form found shape, but not much. With the single lath, applying the RD-forces gives a deflection back to the natural bending shape of the lath. With this 3D structure, less resemblance is found. This is probably due to the fact that a 3D structure reacts more stiff to applied loads than a single element.

From this analysis it cannot be concluded that the RD-forces can be used as a load case in structural analysis to implement the stresses due to the formation process of the shape. With a single lath the results look promising, so more research with 3D structures could prove the method usable.

7.4.4 Stress level derived from curve angles

Another option to implement the formation stresses is to use the stresses calculated from the curvatures of the generated grid as a superposition load case. Load cases like snow and wind can be analysed in a structural analysis program. By adding the formation stress manually, the structure can be checked for the combination of stresses.

To analyse the usability of these stresses, they are compared with the stresses that are found in GSA in the form found structure.

For the comparison, the two laths are reviewed that are indicated by node numbers in Figure 7.77. The bending stress resulting from bending around the y -axis can be calculated from the curve angles and is displayed in the Table 7.7. The results from the non-linear analysis are less straight forward. Due to the interaction between laths, there is not one bending stress for every node, but it can differ for each element attached to the node. In Figure 7.86 the moment lines of the moment around the y -axis is displayed. This clearly shows jumps in the moment at certain nodes.

In Table 7.7, the bending stress for the elements left and right to the node (element 1 and element 2) is displayed, as well as the average of the two. These stresses are compared with the calculated stress. The difference is displayed as percentage of the calculated stress.

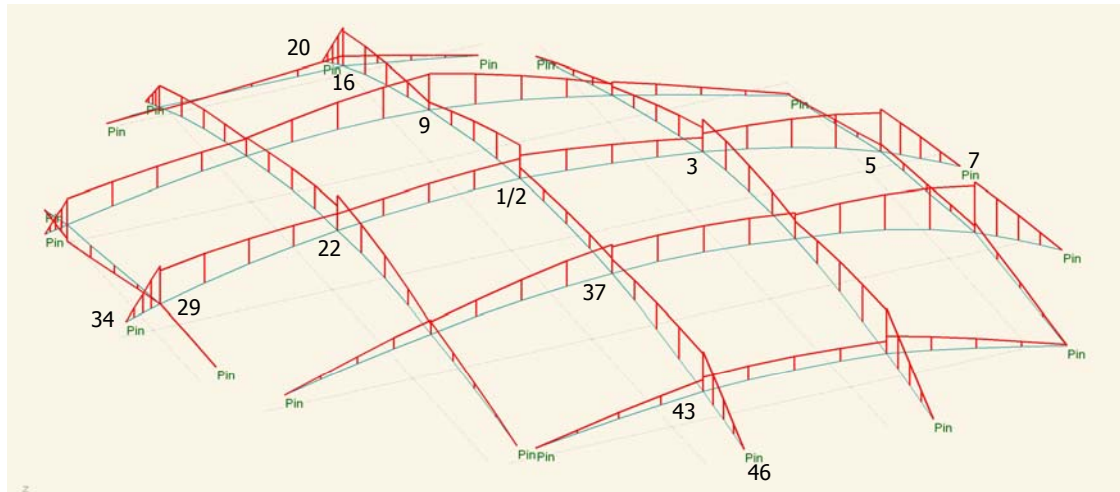


Figure 7.86: Moment lines on the form-found structure (numbers indicate the reviewed nodes)

Table 7.7: Bending stress in the upper edge of the elements

	element1	element2	average	calculated	% diff 1	% diff 2	% diff av.
Node	(N/mm ²)	(N/mm ²)	(N/mm ²)	(N/mm ²)	(%)	(%)	(%)
34	-	0	0	0	0	0	0
29	20.07	17.63	18.85	9.687	107.18	81.99	94.58
22	8.936	8.948	8.942	9.769	-8.53	-8.40	-8.46
1	10.2	11.86	11.03	10.446	-2.35	13.54	5.59
3	6.76	8.52	7.64	11.926	-43.32	-28.56	-35.94
5	23.32	25.59	24.455	14.813	57.43	72.75	65.09
7	0	0	0	0	0	0	0
20	-	0	0	0	0	0	0
16	20.49	18.33	19.41	9.864	107.72	85.83	96.78
9	5.808	5.813	5.8105	9.847	-41.01	-40.96	-40.99
2	17.22	6.34	11.78	10.448	64.82	-39.32	12.75
37	7.803	7.165	7.484	11.889	-34.37	-39.73	-37.05
43	22.59	24.42	23.505	14.729	53.37	65.79	59.58
46	0	-	0	0	0	0	0

When the difference between the average of the bending stress from the GSA analysis and the bending stress calculated from the curve angles is reviewed, it is noticed that the difference in the outer nodes differ largely. Moving to the middle of the structure, the difference becomes smaller. For the middle nodes, node 1 and 2, the difference is 5,6 and 12,7 respectively.

The large difference between the analysed stress and the calculated stress can be explained by the fact that in GSA the supports are modelled as pin supports. The bending stress therefore has to increase from zero in the support to a bending moment corresponding with the bending radius. The stresses calculated from the bending angles provided by the design tool are based on a continuous curve and therefore a more uniform stress distribution.

The stresses in the middle nodes differ less with each other than the outer nodes. The edge disturbance has less influence on the stress level when the distance to the edge becomes larger. Also this analysis is performed with a mesh size of 2,5m. In reality the mesh size will be smaller, e.g. 0,5m or 1,0m. The peaks in moment found in the form-found structure will be also smaller, because the edge disturbance is spread over more elements.

It can therefore be assumed that in a larger structure, a better resemblance can be found between the stresses provided by GSA and the calculated stresses. In a larger structure the edge moments will settle to a more uniform stress distribution within the first few elements.

To give an indicative view on the level of stress that is caused by the formation process, the stress level in the two reviewed laths is checked with the stress criterion stated in 3.2.4.4. The combination of stresses in the formation process should comply with:

$$\left(\frac{\sigma_{m,d}}{f_{m,d}}\right)^2 + \left(\frac{\tau_{v,d}}{f_{v,d}}\right)^2 + \left(\frac{\sigma_{c/t,0,d}}{f_{c/t,0,d}}\right)^2 \leq 1 \quad (7.4)$$

in which:

$$\sigma_{m,d} = \sigma_{m,y,d} + \sigma_{m,z,d}$$

$$\tau_{v,d} = \tau_{xy,d} + \tau_{tor,d}$$

This is first checked for the calculated stress level. Using the curve angles, stress levels for moment in two directions, shear and torsion can be determined. Moment and torsion is determined according to Sections 3.2.4.1 and 3.2.4.3 respectively. Shear stress can be calculated by deriving shear forces from the bending moments as described in Section 7.4.1. The shear stress can be calculated with:

$$\tau_{xy} = \frac{3 V_d}{2 A} \quad (7.5)$$

In which:

V_d = the shear force

A = the cross section of the element

It is not possible to determine levels for axial stress, so this is left out. This results in the stresses displayed in Table 7.8.

For the structure analysed with GSA, the stress levels can be collected from the output tables. First the results that are found by GSA for bending and shear stress in two directions and axial stress is displayed in the figures below:

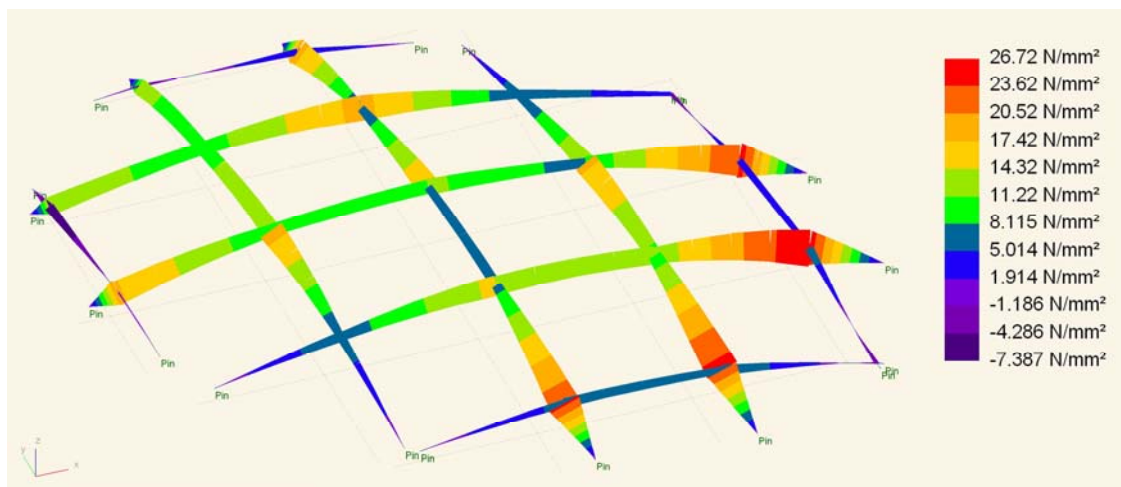


Figure 7.87: Bending around the elements' y-axis, M_{yy}

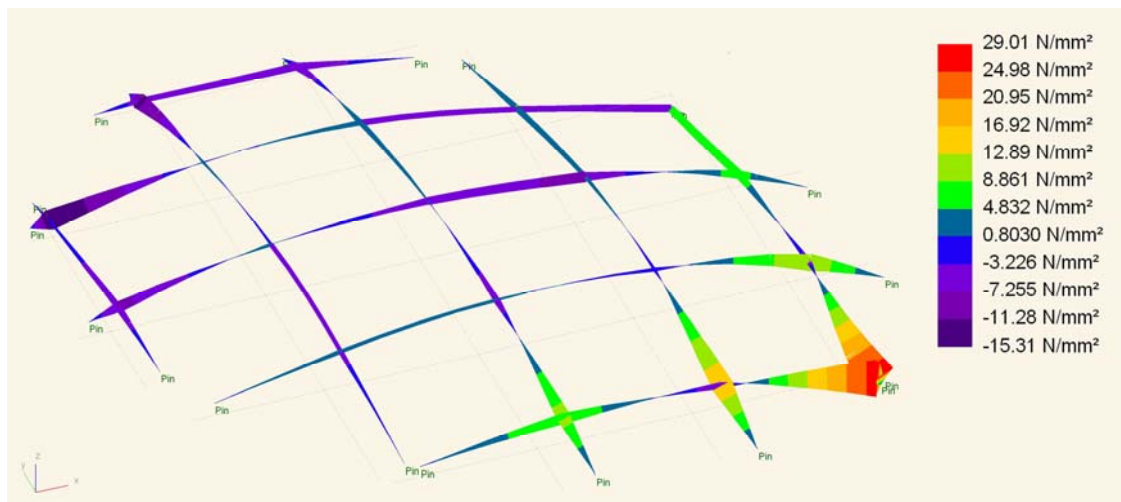


Figure 7.88: Bending around the elements' z-axis, M_{zz}

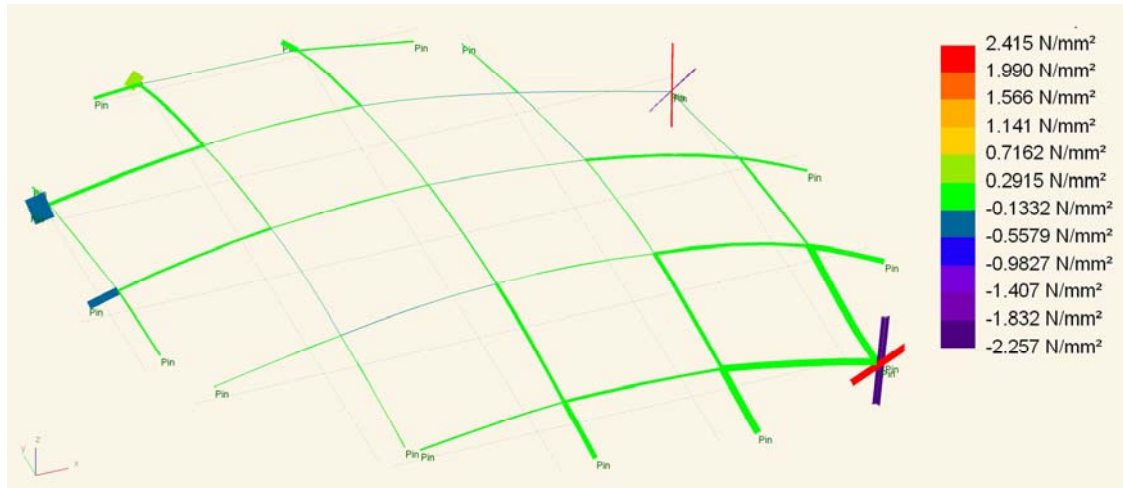


Figure 7.89: Shear stress in the elements' y-direction, τ_{xy}



Figure 7.90: Shear stress in the elements' z-direction, τ_{xz}

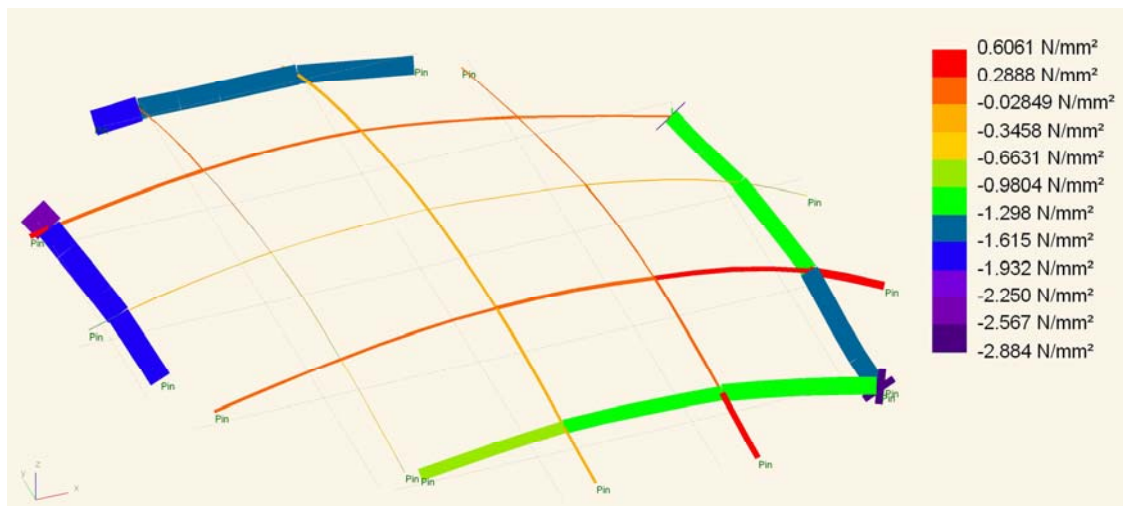


Figure 7.91: Axial stress in the elements, σ_{xx}

The stress levels from the both cases can be displayed in tables with the result for the stress combination criterion. For the stresses calculated from the curvature angles, this is displayed in Table 7.8. The stress levels that are collected from the GSA output for the analysed structure are displayed in Table 7.9. If stress levels at both sides of a node differ, the maximum stress level is used.

When the calculated stresses are used to check the stress level, all elements comply with the criterion. The stress level is 0,32 to 0,97 times the maximum allowed stress combination. When the stresses found by GSA are checked, it is found that in the nodes attached to the edge elements, the stress combination criterion is exceeded. This resembles with the findings that in these nodes a much larger bending moment exists. The other nodes comply with the criterion within a range of 0,31 to 0,99, which resembles the results of the calculated stresses. If the peaks in moment are neglected, based on the assumptions made on page 166, it can be stated that stress levels found by using the curve angles give a usable approximation for superposition in structural analysis.

Table 7.8: Stress levels calculated from curve angles

	σ_{yy}	σ_{zz}	τ_{xx}	τ_{xz}	τ_{xy}	
Node	(N/mm ²)	Criterion				
34	0	0	0	-	-	-
29	9.69	1.80	0.40	0.03	0.02	0.45
22	9.77	0.07	0.38	0.00	-0.02	0.32
1	10.45	0.90	0.38	0.00	0.01	0.42
3	11.93	1.30	0.37	0.01	0.00	0.56
5	14.81	1.43	0.38	0.01	0.00	0.82
7	0	0	0	-	-	-
20	0	0	0	-	-	-
16	9.86	1.13	0.40	0.03	0.01	0.41
9	9.85	0.91	0.38	0.00	0.00	0.38
2	10.45	0.16	0.37	0.00	-0.01	0.37
37	11.89	0.31	0.37	0.01	0.00	0.48
43	14.73	2.93	0.38	0.01	0.03	0.97
46	0	0	0	-	-	-

Table 7.9: Stress levels found by GSA in the structure

	σ_{yy}	σ_{zz}	τ_{xx}	τ_{xy}	τ_{xz}	σ_{xx}	
Node	(N/mm ²)	Criterion					
34	0.00	0.00	0.00	-0.15	0.28	0.01	0.01
29	20.07	7.45	0.00	-0.15	0.28	0.01	2.23
22	8.94	2.82	-0.09	0.04	-0.02	-0.07	0.41
1	11.86	5.84	0.40	-0.01	-0.01	-0.06	0.96
3	8.52	6.58	-0.05	0.05	0.04	-0.08	0.67
5	25.59	5.81	0.00	-0.05	-0.15	-0.04	2.90
7	0.00	0.00	0.00	-0.05	-0.15	-0.04	0.01
20	0.00	0.00	0.00	0.10	-0.24	-0.14	0.01
16	20.49	5.84	0.00	0.10	-0.24	-0.14	2.04
9	5.81	4.42	0.07	-0.04	0.04	-0.22	0.31
2	17.01	1.38	0.03	0.01	-0.03	-0.19	0.99
37	7.80	4.67	0.08	0.02	0.00	-0.19	0.46
43	24.42	10.17	0.00	0.10	0.16	-0.22	3.53
46	0.00	0.00	0.00	0.10	0.16	-0.22	0.02

7.5 Conclusions

From the analysis performed on members in bending a few conclusions can be drawn. On the subject of maximum curvature the analysis showed that it is beneficial to select timber with a low E/f_m ratio. This will result in a small maximum bending radius and thus large curvatures can be reached prior to failure. This is also true for the torsion angle. It would be interesting to look at E/f_m of green timber. By applying green timber, a larger curvature should be possible. Proper property information however is scarcely available. With the Weald and Downland gridshell green timber was applied. Extensive bending testing proved the timber to have sufficiently moment and bending capacity.

On the subject of the formation stresses, the analysis showed that care should be taken when deforming the laths over internal supports. When the deflection does not approximate the natural equilibrium deflection, the structure will deflect to its equilibrium position after removal of the internal supports. This results in a change of geometry and a change in stress distribution. When this is left unaccounted for, breakage of the laths can occur. The analysis showed that the deflection by applying a horizontal force approximates the equilibrium shape best. A large force is needed however to reach the desired deflection. A combination of horizontal and vertical forces gives a larger deflection with less applied force and an acceptable difference from the equilibrium shape.

In the 3D analysis, it was found that the laths in a 3D structure influence each other by interaction in the nodes. Link forces act on the laths in the nodes and can be seen as forces superimposed on the applied deflection.

The assumption that from the curvature of a curved member relaxation deflection forces can be derived is also tested and the results look promising. When the RD-forces are applied on the curved member, the member deflects to a shape that approximates the equilibrium position of a bent lath. This can be seen as a form finding process, as the structure's equilibrium position is approximated. However, for the 3D structure analysed, the results are less accurate. This is probably due to the fact that a 3D structure reacts much stiffer to a load due to the 3D force flow. More research is needed to validate the use of the RD-forces to determine the equilibrium position.

When the bending stress from the formation process is calculated by using the curve angles, the results are accurate when the single lath is reviewed. This method thus is correct. However, in the 3D structure, the interaction between the laths disturb the moments that would be the result of curvature only. The difference that is found between the stress in the form found structure and the generated structure is 6% for the top node to 60-97% for the edge nodes. It is assumed that edge disturbances are the cause for the large difference at the edges. In the middle of the structure, the edge disturbances have less influence on the stress distribution. In a larger structure with smaller mesh size this will result in a more continuous stress flow. It is therefore assumed that the curve angles can be used for structural analysis for large part of the structure, to give an indicative stress level. Because of the possible differences one should be conservative in using the calculated bending stress level. When for example a relaxation factor of 0,7 is applied in stead of 0,5, the calculation will give a safe solution for the bending stress level after relaxation of the timber.

Conclusions and recommendations



8.1 Introduction

In this Master's thesis, a study has been performed into the applicability of a design tool based on the main geometrical property of the gridshell. This is the equal distance between the mesh nodes in a quadrangle grid. This method has been implemented in a design tool. With the design tool, a gridshell grid can be generated on an arbitrary surface. The resulting model contains all geometrical information which is needed for exporting the geometry to a third party structural analysis software package. The output data also contains angles of curvatures of the members in different directions. These can be used to determine the bending stress levels resulting from the form shaping process.

The findings of this Master's thesis research will be stated here as conclusions and recommendations for further research.

8.2 Conclusions

- The grid generation method proposed in this thesis can be used to determine the geometry for the grid of a gridshell. The method has been implemented in a design tool. This design tool can be used for determining the grid geometry. An output can be created, which can be processed further for structural analysis. The created geometry is not necessarily correct. A large amount of experience is still required to review and analyse the created geometry.
- The use of start-off sections provides a method for determining a grid with user determined directions of the laths. This makes testing of different grid directions possible.
- The resemblance between the physical model and the computer model show that the grid generation technique creates geometry that approximates reality.
- It is uncertain whether the start-off sections as created in Rhino represent the directions that will occur in reality when shaping a gridshell.
- The script can be set-up with a sequence that checks stress levels based on the curve angles in the grid members that will occur when the laths are bent to the curvatures needed.
- The curve check in the design tool shows that a (semi-)spherical surface is hard to create from an initial straight mat of laths. The laths need to curve and scissor largely to comply with the surface. This was also shown in the physical form finding of the gridshell.
- An iterative design process is needed to adjust the initial surface to a surface which is optimized for a gridshell grid. The graphical setup of the design tool provides information on whether the maximum bending stress is exceeded in the members. This gives quick insight in the fitness of the shape for application to a gridshell.
- The use of internal supports to create the desired shape can result in undesired changes in shape and stress levels in the elements when the internal supports are removed. If the intended shape is not equal to the natural equilibrium shape of the grid, the structure will deflect to this equilibrium position when the internal supports are removed.

Changes in stress level up to 23% have been found in this research. Change of shape is less prominent. Changes of 1,3% or less have been found.

- Stress levels that can be calculated using the angles of curvatures can be used to estimate the residual stress levels due to the bending of the laths during the formation of the shape. These stress levels can be used in structural analysis by superposition to other load cases.
- It is hard to estimate the relaxation deflection by using the difference in shear force that can be determined by using the bending stresses corresponding to the curve angles. For a single lath applying these forces as relaxation deflection forces gives a deflection corresponding to the natural bending shape of a lath. For a 3D structure, less correspondence was found.

8.3 Recommendations

- It would be largely beneficial if the script could approximate the input surface, complying with the maximum angles. The way the design tool has been set up now, the grid generation process does not take account of the properties of the timber when creating the grid points. The curvature has been checked after the structure has been created. The shape of the surface has to be adjusted after the grid generation will have been completed, if maximum curvature angles are exceeded. Form finding has to be performed by hand. Automatic form finding would enhance the design tool.
- Further testing is advisable to verify the use of the correctness of the start-off sections. The correctness of the generated grid depends on the correct input of these start-off sections.
- It is advised to avoid surfaces with an angle of attack on the horizontal larger than approximately 30 degrees. The results of the design tool and the physical modelling show that such surfaces are difficult to create using a gridshell structure.
- The output of the design tool should be enhanced. In the current output the nodes and elements are not ordered well. Especially when the structure is trimmed to remove the jagged edge, the output becomes discontinuous. The output file then needs processing before it can be used in a structural analysis program.
- The design tool should be optimized to save computer time. Especially the graphical determination of the curve angles takes relatively much time. An analytical determination might save time.
- Further research should be performed to determine a correct load factor on the initial bending stress resulting from the formation process, by checking the stress level after relaxation of the timber.
- Further research should be performed on the applicability of the stresses that can be derived from the angles of curvature, provided by the design tool. Especially the differences in stress level at the edge nodes that were found in this thesis should be analysed.

8.4 Evaluation of the gridshell design tool

From the results of the grid generation tool, the conclusion has been drawn that the proposed grid generation method can be used for the determination of the geometry of a gridshell grid. The gridshell design tool as it is created for this Master's thesis thus complies with the demands stated in this thesis. The results of the grid generation look promising. The created grid is not necessarily correct however. This is dependent on the correctness of the start-off sections. When the created grid was reviewed, it can be stated that a structure was created that flowed smoothly over the surface. When a physical model was created based on the generated geometry, similar results were found.

One result found both by physical modelling and the design tool was the difficulties in forming a (semi-)spherical shape by means of a grid shell structure. The laths could not bend and twist enough to comply with the curvature needed to form the shape. Because the two models show similar results, the assumption can be that the use of the start-off sections is legitimate. However the method is used depends on the correctness of these sections, as the generated grid is based on this. Further testing is needed to verify the usability of the sections created by Rhino.

Also deviations have been found between the two models. The shapes of the two models differed in height and cross sectional shape. The physical model assumed a more parabolic shape in cross section than the computer model. This can be explained by the fact that a parabolic shape is a more natural bending shape for a bending member to take on. Similar effect can also be found with form finding techniques. The parabolic shape can be compared with the catenary line which is assumed by a chain hanging between supports. In the design process of a gridshell, the design tool can contribute to the conceptual design stage. First the tool is used to check if a gridshell is possible in the initially desired shape. When the tool shows that the maximum stress criteria are exceeded, the shape needs to be adjusted. Also by adjusting the section curves, an optimal direction for the laths can be searched. When adjusting the surface, one should also take account of physical form finding principles. It is therefore advised to determine the shape with a shape optimization software tool.

When a gridshell is deformed into shape, bending and torsion stresses occur in the members. Due to relaxation of the timber the stress levels will diminish approximately by factor 0,5. When structurally analysing a gridshell, these stresses should be taken into account. The bending stresses in the members can be derived from the curve angles in structure. These angles are part of the design tool output and can therefore be utilized easily. The use of the bending stresses as an implemented load case has been analysed. This analysis shows that this is hard to achieve. The theory of deriving relaxation deflection forces from the bending stresses gives accurate results for a single member, but when a 3D structure is analysed the results are less accurate. This is probably due to the fact that a 3D structure reacts much stiffer to an applied load.

It is easier to use the formation stresses as a superposition load case after analysis in GSA. The stress levels (reduced for relaxation) can be added to the stress levels that will be found by analysis of load cases like wind and snow loads. A problem is that in a 3D structure a complex member interaction takes place. When an element rotates around its y -axis, this results in a torsion moment in an element perpendicular to it, and vice versa. This results in jumps in the stress levels. This behaviour is hard to implement when using the curve angles to determine the stress levels. In the elements close to the edge supports, large deviations between the stress levels analysed by GSA and the stress levels calculated with the curve angles have been found. For nodes closer to the middle of the structure, a better resemblance has been found. Therefore the assumption is that the use of the curve angles to determine the stress levels can be applied in structural analysis. To take account of deviations from reality, a reduction factor which gives conservative results is advised. Further research should estimate this reduction factor.

What also should be taken into account are the relaxation deflection and the related change in stress distribution. When the gridshell is shaped on internal supports and the shape is not

equal to the natural equilibrium position of the deformed structure, the structure will deflect when the internal supports are removed. In the analysis a maximum change of 23% in stress level was found. If this is neglected, breakages can occur during construction. It was tried to estimate the relaxation deflection using the relaxation deflection forces, derived from the curve angles, but this result was not found accurate enough.

If the general use of gridshell structures is reviewed, it can be stated that this type of structure has high potential. Recently built structures prove the gridshell to be a worthy addition to prestigious structures. The waving shapes that are possible add architectural value to the building. It is also possible to design the structure as a sustainable building. Using timber from sustainable sources make sure the building has highly sustainable value, as timber is renewable material. Also the fact that the structure is a shell, which has efficient use of material related to the span, adds to the minimization of material use.

The power of the gridshell is the result of the construction method. From an initial flat mat of laths a continuous shell structure can be created. A 2D surface can be transformed to 3D, without disconnecting the elements. In the different grid shell examples, different construction methods were used. The simplest one was used in the Savill Garden gridshell. Here, the laths were just simply placed into position lath by lath on formwork. If this is also the most economic one can be questioned, because this method is labour intensive. On the other hand, in the other gridshells all laths had to be placed into position in the flat mat and connected to each other too. An advantage is that this can be performed on a flat working area. The building method also depends on the size of the structure. The Savill Garden gridshell is four times as large as the Weald and Downland Gridshell. For large surfaces it is probably a lot more difficult to deform the entire surface into the desired shape at once.

It is shown in this thesis that not every shape is possible using a gridshell structure. Especially (semi-)spherical surfaces are problematic. The laths that are connected to each other in the nodes need to bend and scissor beyond their minimum bending radius to create such a surface. The structure is constrained in shaping by the timber properties and by the fact that the elements are connected to each other. When the constraint of the attached nodes is released, it might be possible to create different surfaces. If a mat of laths is imagined where the laths are only connected to each other in parts of the structure, e.g. in the parts which would be the tops of anti-clastic parts, different geometry might be created. If the laths at the edges are free to move in plane of the surface, this might make other geometries possible. This would be possible by using a modified version of the connector used in the Weald and Downland gridshell. In the current structure, a pin restrains the middle laths from moving. If this pin is omitted, the constraint of equal distance between the nodes is released and the nodes are free to move within certain boundaries.

References

- Barnes, M.R. 1999, 'Form Finding and Analysis of Tension Structures by Dynamic Relaxation', *International Journal of Space Structures*, Vol. 14, No. 2, 1999
- Blass, H.J. Aune, P., Choo, B.S., Görlacher, R., Griffiths, D.R., Hilson, B.O., Steck, G. (eds) 1995, *Timber engineering STEP 1: basis of design, material properties, structural components and joints*, Centrum Hout, Almere.
- Boer, S. & Oosterhuis, K. 2002, *Architectural Parametric Design and Mass Customization* available at http://www.oosterhuis.nl/quickstart/fileadmin/Projects/129%20the%20web%20of%20north%20holland/02_Papers/000-040603-ECPPM.pdf
- Booth, L.G. 1964, 'The strength testing of timber during the 17th and 18th centuries' in YEOMANS, D (ed.) 1999, *The Development of Timber as a Structural Material*, Ashgate Publishing Limited, Hampshire, pp. 211-236.
- Booth, L.G. 1971, 'The development of laminated timber arch structures in Bavaria, France and England in the early nineteenth century' in Yeomans, D (ed.) 1999, *The Development of Timber as a Structural Material*, Ashgate Publishing Limited, Hampshire, pp. 291-304.
- Burkhardt, B. et al. (eds) 1978, *IL13: Multihalle Mannheim*, Institut für leichte Flächentragwerke, Stuttgart.
- Coenders, J.L. 2004, 'Structural Form Finding and Structural Optimization Techniques', in *Form Finding and Structural Optimization*, MSc thesis, Delft University of Technology
- Courtenay, L. & Mark, R. 1987, 'The Westminster Hall roof: a historiographic and structural study' in Yeomans, D. (ed.) 1999, *The Development of Timber as a Structural Material*, Ashgate Publishing Limited, Hampshire, pp. 127-150.
- GeoDomeDesign, '*Planetarium Artis*', [brochure]
- Groot, de, H. 2007, 'Rechthoekig Gebogen, Savill Garden Visitor Centre, Windsor Great Park London' in *Het Houtblad*, jaargang 19, nummer 2, Het Houtblad BV, Almere
- Holzbau Konstruktionen, *Hölzernes Hängedach Bundesgartenschau in Dortmund*, [Brochure], Sonderdruck für die Arbeitsgemeinschaft Holz e.V. aus DETAIL, Zeitschrift für Architektur + Baudetail.
- Happold, E & Liddell, W.I. 1975, Timber lattice roof for the Mannheim Bundesgartenschau, *The Structural Engineer*, No. 3, Volume 53, March 1975
- Harris, R. & Kelly, O., 'The structural engineering of the Downland gridshell' in Parke, G.A.R. & Disney, P. (eds) 2002, *Space Structures 5 volume 1*, Thomas Telford, London
- Harris, R., Romer, O., Kelly, O. & Johnson, S. 2003, 'Design and Construction of the Downland Gridshell' in *Building Research and Information*, Volume 31, Number 6, pp. 427-454, Routledge, part of the Taylor & Francis Group
- Hartsuijker, C. 1996, *Mechanica van Constructies 1b, deel 2*, Reader TU Delft

- Hartsuijker, C. 1999, *Toegepaste Mechanica deel 1, Evenwicht*, Academic Service, Schoonhoven
- Heymans, J. 1967, 'Westminster Hall roof', in Yeomans, D. (ed.) 1999, *The Development of Timber as a Structural Material*, Ashgate Publishing Limited, Hampshire, pp. 151-176.
- Hoefakker, J.H. & Blaauwendraad, J. 2005, *Theory of Shells, Course CT5143*, Delft University of Technology, Delft
- Horn, C. & W. 1973, 'The cruck-built barn of Leigh Court, Worcestershire, England' in Yeomans, D. (ed.) 1999, *The Development of Timber as a Structural Material*, Ashgate Publishing Limited, Hampshire, pp. 1-25.
- Jensen, F. 2000, *Erection Procedure for the Downland Gridshell*, MSc thesis, University of Bath
- Kelly, O.J. 2003, Harris, R.J.L., Dickson, M.G.T. & Rowe, J.A. 2001, 'Construction of the Downland Gridshell', *The Structural Engineer*, No. 17, Volume 79, September 2001
- Kuilen, van de, J.W.G & Vries, de, P.A. 2005, *CT3051A Constructieleer 3A*, Reader, Delft Technical University
- Leupi, J. 2002, 'Parametric design for the structural elements of timber rib shells', *Space Structures 5 volume 1*, Thomas Telford, London
- Lewis, W.J., *Tension Structures, form and behaviour*, Thomas Telford, London.
- Müller, C. 2000, *Holzleimbau, Laminated Timber Construction*, Birkhäuser, Basel; Berlin; Boston.
- Otto, F. et al. 1982, *Natürliche Konstruktionen*, Deutsche Verlags-Anstalt, Stuttgart
- Pestman, J.H., *Vormgeving in hout*, C.A. Spin en Zoon N.V., Amsterdam
- Ross, P. 2002, *Appraisal and Repair of Timber Structures*, Thomas Telford Publishing, London.
- Thelandersson, S. & Larsen, H.J. (eds) 2003, *Timber Engineering*, John Wiley & Sons, LTD, Chichester.
- Van Drenth Groep, *Uit het juiste hout gesnede* [Brochure]
- Wilhelm, K. 1985, *Architekten heute, Frei Otto*, Quadriga-Verlag Severin, Berlin.
- Yeomans, D (ed.) 1999, *The Development of Timber as a Structural Material*, Ashgate Publishing Limited, Hampshire.
- Young, W.C. & Budynas, R.G. 2002, *Roark's Formulas for Stress and Strain*, 7th edn, McGraw-Hill, New York

List of symbols

κ	= curvature of the beam;
κ_1	= first principle curvature;
κ_2	= second principle curvature;
κ_g	= Gaussian curvature;
σ_n	= normal stress;
σ_m	= bending stress;
f_u	= ultimate stress strength;
$\sigma_{m,d}$	= the design bending stress
$f_{m,d}$	= the design bending strength
$\sigma_{m,y/z,d}$	= the design bending stress in the y or z direction;
$f_{m,y/z,d}$	= the design bending strength in the y or z direction;
$\sigma_{c/t,90,d}$	= the design compression/tension stress perpendicular to the grain;
$f_{c/t,90,d}$	= the design compression/tension strength perpendicular to the grain.
$\sigma_{c/t,0,d}$	= the design compression/tension stress parallel to the grain;
$f_{c/t,0,d}$	= the design compression/tension strength parallel to the grain;
σ_o	= stress level at the outer edge of a curved beam;
σ_i	= stress level at the inner edge of a curved beam;
M	= bending moment;
E	= modulus of elasticity;
I	= moment of inertia;
W	= moment of resistance;
R	= radius of curvature;
R_{in}	= the inside radius of a beam;
l_o	= outer length of a curved beam;
Δl_o	= change of outer length of a curved beam;
l_i	= inner length of a curved beam;
$M_{ap,d}$	= the design moment in the apex zone;
b	= width of the member;
h	= height of the member;
h_{ap}	= height of the beam in the apex zone;
α_{ap}	= angle of taper;
k_l	= reduction factor for design bending stress in curved beams;
k_r	= a reduction factor which takes into account the bending stresses in the laminates of curved glued laminated timber due to production;
k_m	= factor which makes allowance for re-distribution of stresses and the effect of inhomogeneities of the material in a cross section;
t	= thickness of a laminate;
c	= constant by which the minimum radius can be estimated;
V_d	= the shear force;
A	= the cross section of the element;

Appendices

Appendix 1: Determination of the maximum bending radius

To analyse bending behaviour, a segment of a member is considered shown in Figure A.1. The member is subjected to a bending moment, which results in internal stresses, deformation and deflection.

First let's consider the kinematics relations, linking deformations and displacement (Hartsuijker, 1996)

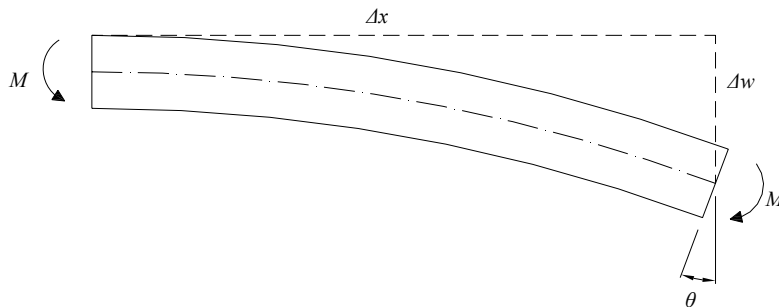


Figure A.1: Bending member

According to the hypothesis of Bernoulli, if deflections are considered to be small sections perpendicular to the member's axis stay perpendicular when the member deforms. For the angle of rotation of the section we can thus write:

$$\theta = -\frac{dw}{dx} \quad (\text{A.1})$$

where:

- θ = rotation of the section about the y -axis
- w = displacement in the z -direction
- x = distance along the x -axis

The angle θ is also the angle of the strain diagram. The strain in the fibres due to deformation can be written as:

$$\varepsilon(z) = \kappa_z z \quad (\text{A.2})$$

with:

$$\kappa = \frac{d\theta}{dx} \quad (\text{A.3})$$

where:

- κ = gradient of the strain diagram
- $\varepsilon(z)$ = strain over the height of the beam
- z = distance from the member axis to the outer fibres

κ can also be defined as the curvature of a curve. Mathematically this is defined as the change of direction angle of the tangent per curve length:

$$\kappa = \lim_{\Delta s \rightarrow 0} \frac{\Delta \theta}{\Delta s} = \frac{d\theta}{ds} \quad (\text{A.4})$$

where:

κ = curvature
 s = curve length

The curve length s of a fibre in a beam is dependent on the strain of that fibre (equation A.4). Therefore also s is dependent on z , which is the distance from the referred fibre to the member axis. When the strains are considered small ($\varepsilon(z) \ll 1$), it can be neglected that the strain that the strain differs over the height of the beam and s can be considered equal over the height of the member. Equation A.4 can then be written as:

$$\kappa_z = \lim_{\Delta s \rightarrow 0} \frac{\Delta \theta}{\Delta s} = \lim_{\Delta x \rightarrow 0} \frac{\Delta \theta}{\Delta x} = \frac{d\theta}{dx} \quad (\text{A.5})$$

This shows that the curvature of the beam is equal to the gradient of the strain diagram. The absolute value of the curvature reciprocal is the curve radius R :

$$R = \frac{1}{|\kappa|} \quad (\text{A.6})$$

Next, constitutive relations are considered which link the section forces to the deformation. Together with Hook's law and equation A.2 the curvature can be calculated as a function of the bending stress:

$$\sigma_m = E\varepsilon = E\kappa_z z \quad \rightarrow \quad \kappa = \frac{\sigma_m}{Ez} \quad (\text{A.7})$$

When equation A.7 is substituted in equation A.6, the bending radius of the member can be calculated as a function of the bending stress. By using the maximum bending stress of the material f_m , the minimum bending radius of the member can be calculated:

$$R_m = \frac{zE}{f_m} \quad (\text{A.8})$$

Combining equation A.1, A.6 and A.8, the maximum angle of curvature becomes:

$$\theta_{\max} = \frac{x f_m}{zE} \quad (\text{A.9})$$

When this is re-written to $R_m = c * d$, R_m can be calculated by multiplying the height of the beam $d (=2 * z)$ by a constant c :

$$c = \frac{E}{2f_M} \quad (\text{A.10})$$

For timber class C and D these values can be calculated:

C24:	$R_0 = 229d$	D30:	$R_0 = 167d$
C27:	$R_0 = 213d$	D35:	$R_0 = 143d$
C30:	$R_0 = 200d$	D40:	$R_0 = 138d$
C35:	$R_0 = 186d$	D50:	$R_0 = 140d$
C40:	$R_0 = 175d$	D60:	$R_0 = 142d$

As a rule-of-thumb, the average of c can be used. For C-class timber this is 200. For D-class this is 145. This average value can be used for checking the preliminary design. The final design has to be checked with the corresponding strength value of the timber used.

For use in a gridshell, a timber grade is desired which is able to bend to the smallest curvature needed to accomplish the desired shape without breaking. This can be translated in a ratio E/f_m as low as possible, i.e. a low bending stiffness combined with a high bending strength.

To analyse the influence of the E/f_m ratio, this ratio can be compared with the maximum possible bending radius. For this analysis, the timber strength classes with corresponding material properties are used according to the code EN338. This calculation is made for timber of class C24 to D60. The results are plotted to the corresponding class ultimate bending strength in Figure A.2.

The use of properties according to timber strength classes can be questioned, as the properties of a timber beam do not have to be equal to values of its assigned strength class. A timber population is assigned to a strength class, when its characteristic values of bending strength, modulus of elasticity and density are equal to or greater than the corresponding values of the related strength class. These characteristic values are determined as the weighted means of the lower 5-percentiles for strength properties and density, and as the weighted mean for modulus of Elasticity (Blass et al, 1995).

Therefore, the values of the properties of a beam are likely to be different than the values of its assigned strength class. However, in this analysis the values of the different grades are used to give an insight in the bending behaviour related to the material properties.

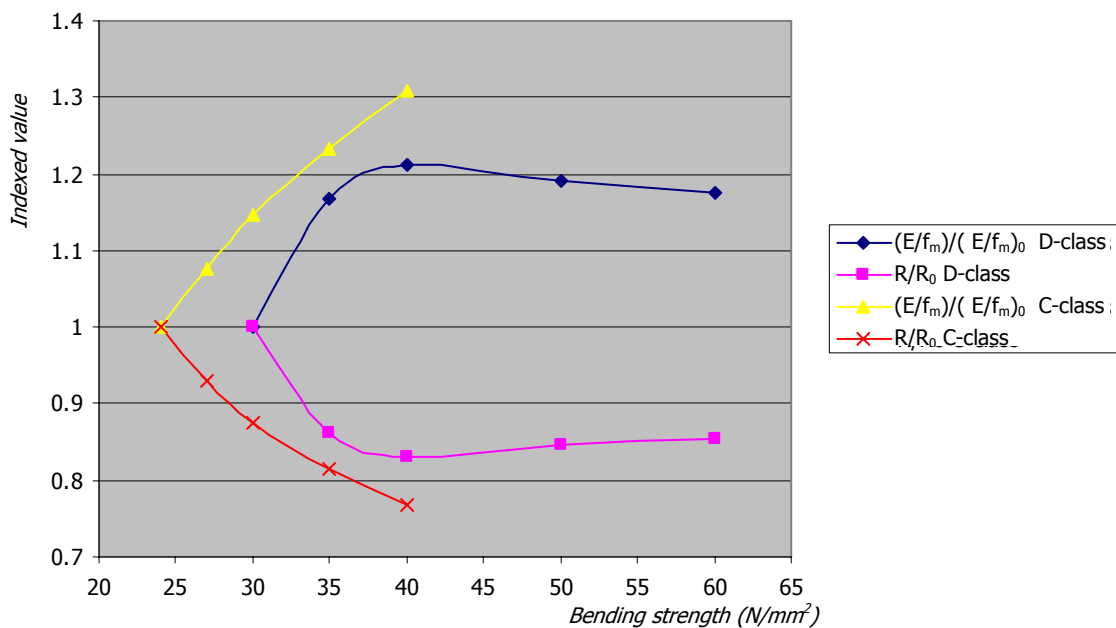


Figure A.2: E/f_m ratio and R , indexed to the values of timber class C24 for C-class timber and to the values of D30 for D-class timber, plotted to the corresponding grade ultimate bending stress.

To compare the moment needed to accomplish the maximum bending radius for different timber grades, the maximum radius R and the maximum moment M for timber of class C24 to D60 are plotted to the corresponding class ultimate bending strength in Figure A.3. The values are indexed again to the values of C24 for the C-class timber and to the values of D30 for D-class timber.

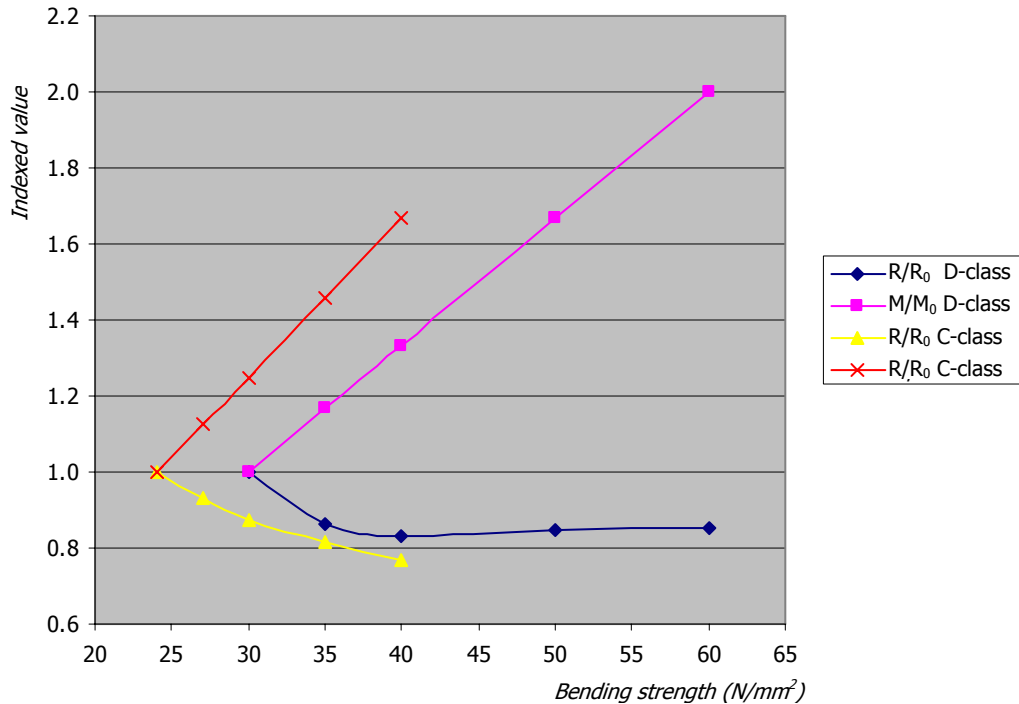


Figure A.3: R_0 and M_{ur} indexed to the values of timber class C24 for C-class timber and to the values of D30 for D-class timber, plotted to the corresponding grade ultimate bending stress.

From these figures it can be concluded that for timber of coniferous species (C-class), it is beneficial to choose a timber quality with high bending strength with respect to the curvature. Figure A.3 shows a moment M increasing proportionally to the bending strength f_m and a maximum curvature radius R decreasing disproportionately to f_m . A higher bending strength corresponds with a lower modulus of elasticity and therefore a lower maximum radius is possible. This allows a stronger curved surface.

Reviewing deciduous species (D-class), Figure A.2 shows an optimum of the smallest bending radius, coinciding with the optimum of the highest f_m/E ratio. This optimum corresponds with a timber strength class D40. For timber of deciduous species it can be concluded that choosing timber with material properties corresponding to a higher bending strength than class D40 is not beneficial. A higher strength class will not lead to a decreasing bending radius, due to the fact that the f_m/E ratio does not increase. This can also be seen in Figure A.3. A higher bending strength implies a higher maximum bending moment, but the minimum bending radius does not decrease above class D40.

The maximum torsion angle can be calculated with the formula in 3.2.4.3. This is performed with the timber properties corresponding with timber class C24 to D60. These are plotted to the corresponding strength class in Figure A.4. The figure shows that an increasing timber class does not necessarily imply a larger torsion capacity. With D-class timber, there is a maximum at strength class D40 of 0.16 rad. This coincides with the optimum of the f_m/E ratio (Figure A.2).

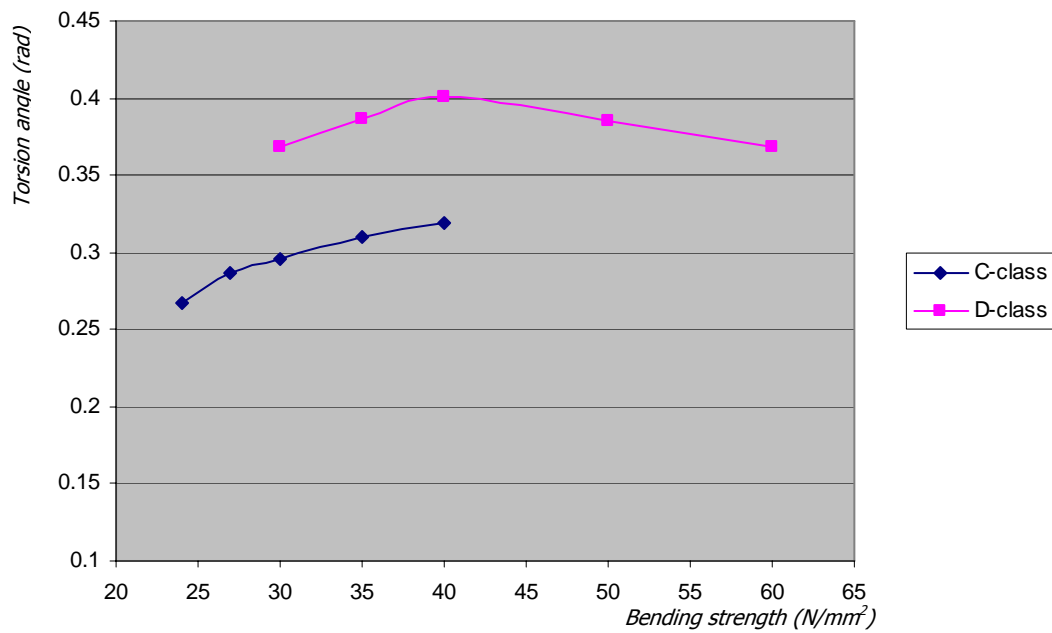


Figure A.4: Maximum torsion angle plotted to the bending strength

Appendix 2: GenerativeComponents

GenerativeComponents is a parametric associative design system, which combines direct interactive manipulation of design methods with visual and traditional programming techniques³⁴. GC is a plug-in for Bentley System's Microstation and it was still a Beta version at the time of use for this Master's thesis. The consequence of this is that there are bugs in the program to be expected. A big disadvantage is the lack of a user guide, which means everything has to be learnt from other users' experiences and trial and error. The high potential of the software makes it attractive to use however.

With GC, it is possible to create your design based on adjustable parameters by using built in features. For example, when designing an office building, Storey height could be assigned as a parameter. By simply adjusting this parameter, your design is adjusted to the new storey height. It is also possible to build your own features. For example, it is possible to create a 'Storey' feature consisting of an entire storey including columns, façade, ceiling etc., and attach a parameter 'number of floors' to it. By simply changing this parameter, more storeys will be added to your design.

For this thesis, using a parametric setup for the structural grid is a great advantage. The mesh size of the grid is a key parameter for this model. The idea is to set up the model with a few other parameters as well. By using the dome height and radius, the design can be adjusted in size and height. The angle between the horizontal plane and the tangent to the bottom of the surface can be a parameter, so more complex shapes can be reviewed. Furthermore, the base angle between the grid elements can be variable as well, to be able to experiment with different starting angles of the grid.

The declared parameters can be adjusted by moving sliders between user defined intervals (Figure A.5). The graphics update themselves in real time. Figure A.6 to Figure A.9 show the changing graphics when parameters are changed.

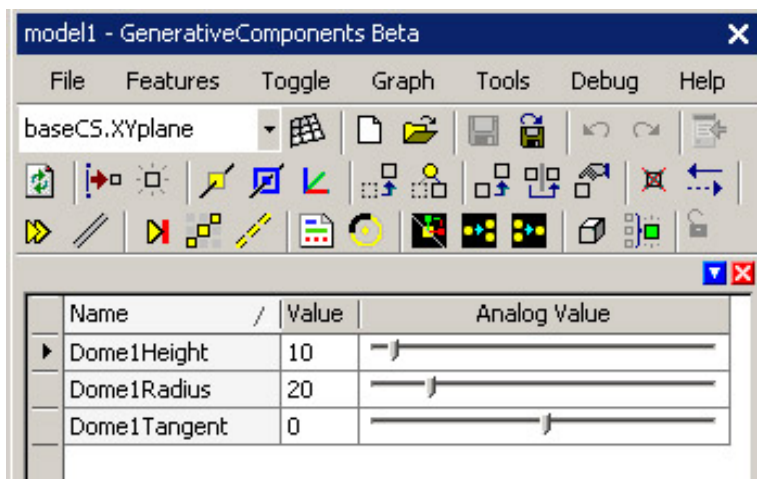


Figure A.5: Graph variables user interface. Parameters can be adjusted by moving sliders.

³⁴ <http://www.smartgeometry.com/tech.htm> accessed 10-10-06

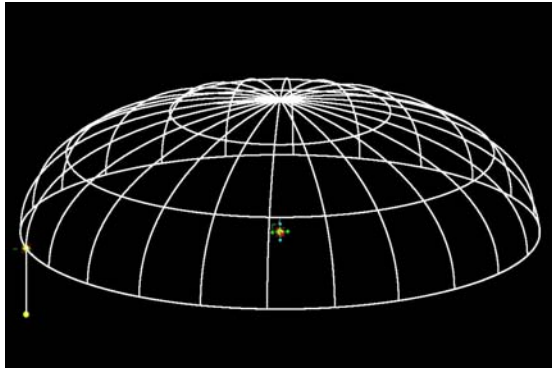


Figure A.6: Start position.

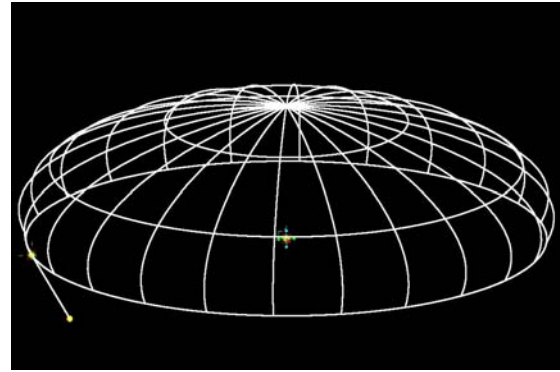


Figure A.7: changing ground tangent.

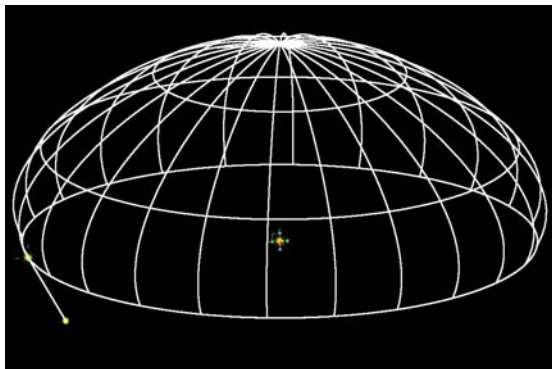


Figure A.8: Changing dome height.

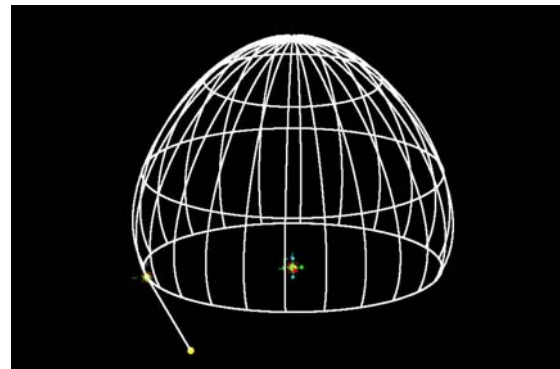


Figure A.9: Changing dome radius.

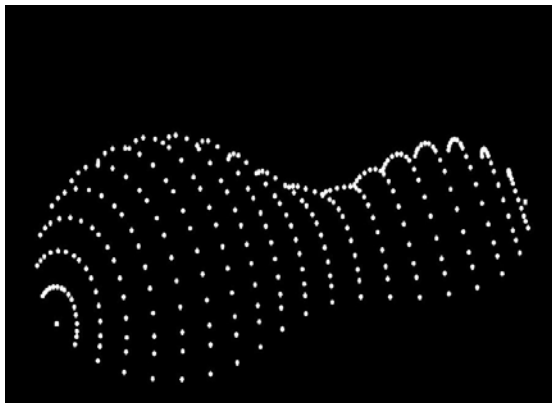


Figure A.10: Imported points.

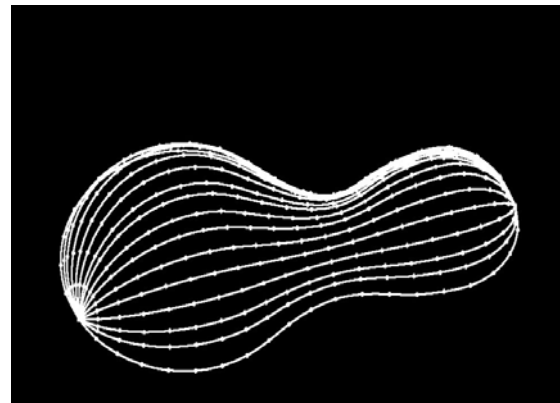


Figure A.11: Curves trough points.

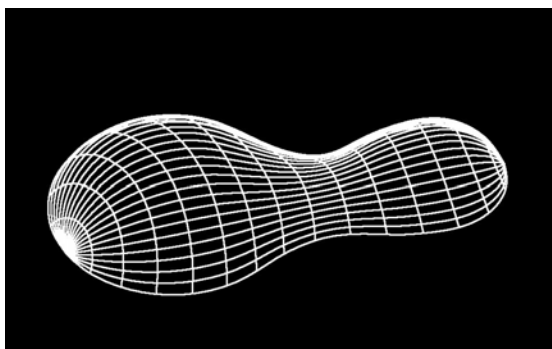


Figure A.12: Surface trough curves.

After exploring the possibilities of GC, the aimed design should be imported into the application for processing. A compatibility problem with Rhinoceros raises, as it is not possible to import the Rhino model into GC. To be able to do this, the following steps were necessary. First, in Rhino sections have to be made of the model. Then, a series of points has to be created on each section and these have to be exported to a text file. By importing these text files, the sections can be redrawn GC. The surface can be recreated by lofting a surface through these sections. Figure A.10 to Figure A.12 show the created surface in GC.

The way the sections are created is also of importance. The proceeding points on each section have to be in the same direction; otherwise the lofting process will produce a distorted surface. Also discontinuity in a section is not wanted, as the curve through the imported points needs to be continuous for the lofting process. The tube-like entrance in the design is such discontinuity, as it is not possible to create continuous sections through the shape. As stated in Section 5.3, the entrance is left out for analysis.

Next step is to project the grid points on the surface. The variable grid angle is to be implemented in this step. A first try-out is projecting the intersection points of a horizontal grid on the surface. This horizontal grid is changeable in angles by moving one of the two pivot points (Figure A.13 & Figure A.14).

Because this projection method does not create the wanted grid with uniform element length, the sphere method is tested in GC. Two spheres with radius x are created with their centre on the surface (Figure A.15). The intersection curves of the spheres with the surface are needed to locate the two wanted intersection points of the spheres and the surface. The software was unable to do this however, creating a problem for this grid generation technique. A different way of creating the surface is tested. By using standard elements, like parts of spheres, the surface should be easier to process (Figure A.16). At the same time, by using standard elements implementing the variables like dome height and tangent angle should be possible. However, using a simpler surface does not solve the problem.

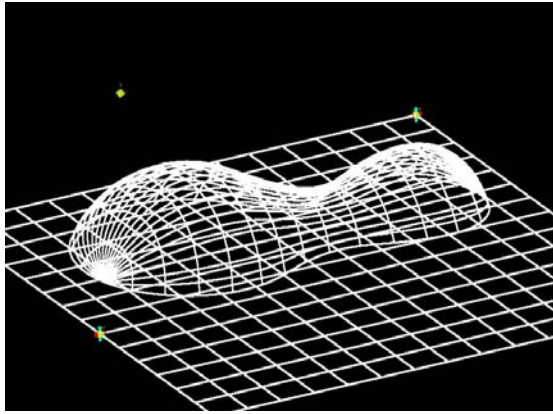


Figure A.13: Changeable grid.

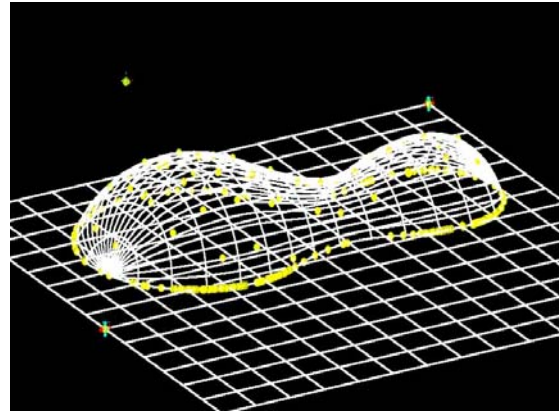


Figure A.14: Points projected on surface.

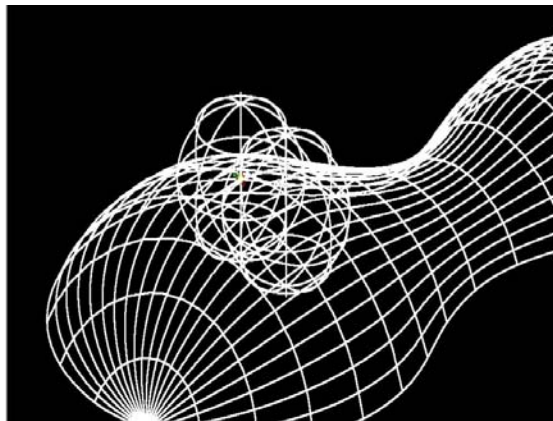


Figure A.15: Spheres on surface.

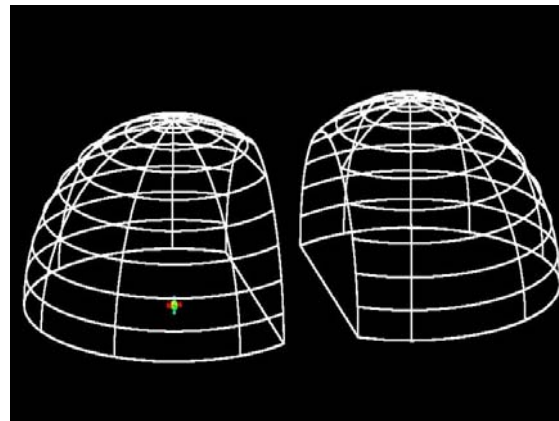


Figure A.16: Parts of domes.

Review GC

GenerativeComponents is a promising software application with a lot of possibilities. The parametric set up makes it possible to change your design easily, even when it is in a developed state. When changing a parameter, the 3D view is updated in real-time so the changes are visible immediately. Also the possibility of creating your own feature gives the designer a powerful tool in CAD.

However, the problems with surface modelling and surface processing which the author ran into during the stage of study and try-out are a major obstacle for the grid development process. The Beta status of the application is probably the cause of the problems found, as there are probably still bugs in the software which makes it hard to process complex surfaces. Also the lack of a users guide does not ease the use of the application. Because of these problems, it is decided to stop using GC and to switch to Rhinoceros.

Appendix 3: Proof of $R \gg$ mesh size

The assumption that the difference in length between the curved element and the straight line can be neglected is proved by the following calculation:

When a timber lath of 50*50mm with timber grade D30 is assumed, the minimum bending radius R is $167*50= 8,35$ m, according to Section 3.2.4.1. The mesh size is assumed to be 500mm.

The length s of a curve can be calculated with:

$$\theta = \sin^{-1}\left(\frac{l}{R}\right)$$

$$s = \theta R$$

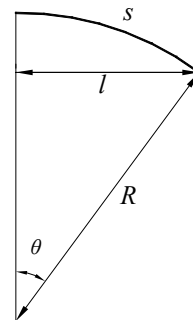
Where:

s = curve length

l = mesh size

R = Curve radius

θ = angle of curvature



With $l = 500\text{mm}$ and $R = 8,35\text{m}$, s becomes:

$$s = \sin^{-1}\left(\frac{500}{8350}\right) * 8350 = 500,299\text{mm}$$

The difference between mesh size l and curve length s is 0,299mm. This difference is 0,06% and is small enough to be neglected.

Appendix 4: Problems encountered in developing the grid generation tool

Different problems are encountered developing the scripts. The problems encountered are on one hand related to the scripting itself and on the other hand related to the way Rhino handles the surfaces creates intersections. The script related problems are about finding the right VBScript or RhinoScript command. A lot of registered commands that can be used in Rhino at the command prompt are implemented in RhinoScript as standard features, but not all. Commands that are not available as a feature can be executed by using the "Rhino.Command" command. This runs a registered Rhino command as if it has been typed in the command prompt³⁵. The example below uses a standard feature and the Rhino.Command to create an intersection between a sphere and a surface. The sphere and the surface have already been identified by the script as "arrSphere(j,i)", which is the sphere at array position (j,i), and "Surface". "Rhino.SelectObject" selects the sphere and the surface. The intersection is created by adding the Rhino command "Intersect" to the RhinoScript command "Rhino.Command". "Intersect" is now executed with the two selected objects.

```
Rhino.SelectObject arrSphere(j,i)
Rhino.SelectObject Surface
Rhino.Command ("Intersect")
```

The problem of this method is what is returned in the script as result. Rhino.Command returns a Boolean, true or false, indicating success or failure of the command. What is needed however to be able to use the intersection created in Rhino, is the identifier of the created object. In most cases it is sufficient to select the last created object, but here a problem arises in the way Rhino handles surfaces and creates intersections.

When the intersection curve between a sphere and the surface is made, Rhino creates one closed curve in most cases. The single object can be identified and used by the script. In some cases however, this process creates more than one object. If the last created object is selected for further processing, the wrong object is probably used. The next problems are encountered with the intersection procedure:

- When a sphere is intersected by a discontinuity in the surface, like the edge of two different surface parts, Rhino encounters problems with the intersection process (Figure A.17). The created intersection is not continuous and can consist of several open curves. These curves need to be joined to create a closed curve (Figure A.18).
- Close to a discontinuity, the intersection is not created as a closed curve.
- Close to a discontinuity a curve is created with a loop. Until this problem was met, the curves were selected by open or closed status. The loop creates two closed curves, one of them being very small (Figure A.19). This creates a selection problem, as both curves are closed.

³⁵ RhinoScript Help file

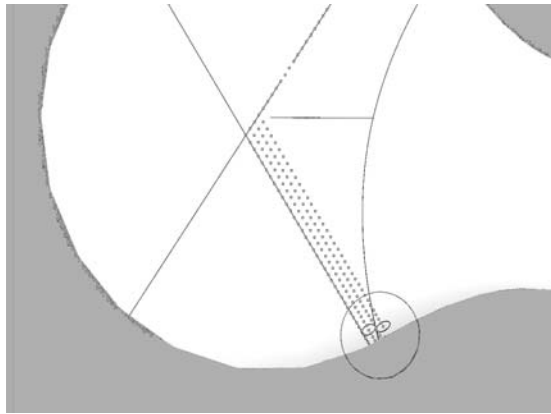


Figure A.17: Intersection problems occur at discontinuities in the surface

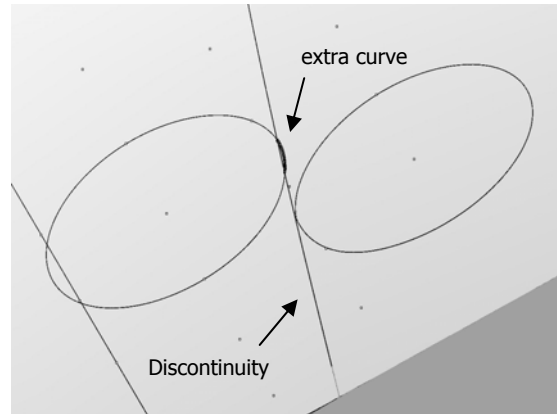


Figure A.18: At the left two intersection parts are created: a closed curve and an extra curve right to the discontinuity.

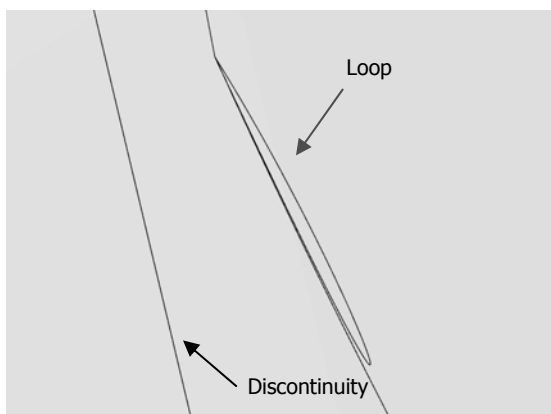


Figure A.19: Zooming in on the right intersection curve of Figure A.18, near the discontinuity. A loop is created to close the curve.

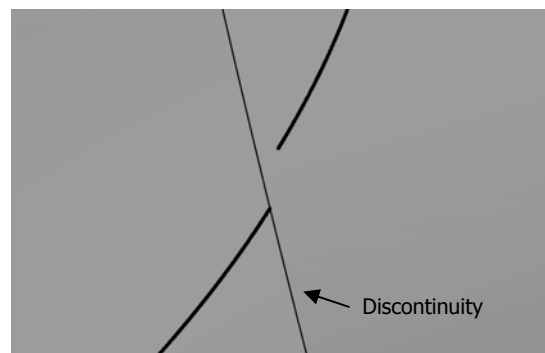


Figure A.20: An open curve is created caused by the discontinuity in the surface

Also problems were encountered creating the intersections between two curves. The result of this operation should be two intersection points. This is not always the case. The following problems were found:

- One or more small curves are created in stead of a point. This is a problem related to the discontinuity of the surface.
- More than two points are created. During one test runs, more than 10 points were created at one intersection. This is probably an error in the intersection process.

These unexpected intersection problems lead to a trial and error approach to filter out all options and slow down the process of developing the script. For every newly found error, the script has to be modified to rule out all incorrect options. This also makes the selection procedure difficult. If more than one object is created, it is not possible to simply select the object created last. Every object created in one command has to be checked.

The main reason for a lot of problems is discontinuities in the surface. The shape which has been used to test the script contains quite some discontinuities when it is used as a poly surface (see Section 5.3). When the surface is simplified and recreated as a single NURBS surface, a lot of intersection problems can be obviated.

Appendix 5: Physical modeling

1. Introduction

Building a physical model in an early stage of design provides insight in shape, possibilities and structural behaviour. The later is most important when it concerns a structure with complicated structural behaviour such as a gridshell structure. With the gridshell, also the construction phases can be modelled and reviewed, as the same building method is used for a real size gridshell as for the model.

This model described here is intended as a geometrical model. It will be used to compare the results of the computer model with reality. Deviations are to be expected between the computer model and the physical model. These will be caused by inaccuracies of the physical model and, probably more important, because the shape of the physical model will be dictated by laws of nature and not by the constraints of the computer model. The shape of the physical model is therefore unlikely to coincide precisely with the computer model, which is a 3D representation of the shape desired by the architect. Building the model is therefore also physical form finding. The results of the physical model can be used to adjust the computer model to a more natural shape. This will result in a more efficient structural behaviour.

In this chapter the process of creating a physical model is described. The geometry of the adjusted structure of Section 6.4.5 is used to create the model and the physical model will be compared with the geometry of this model.

The materials which are used for the model are discussed first after which the building process is described in Section 3. Third the observations made are described. After the conclusions are presented in Section 5, the chapter is ended with the description of the conceptual model for the eggoid shaped gridshell.

2. Materials

To reach a desired accuracy and correct modelling of the structure, materials have to be selected with care. The properties that have to be modelled correct:

- scissoring of the laths: flexible nodes are needed
- mat layout: continuous members are to be used
- building method: initial mat has to be flat
- bending: the bending behaviour of the modelled members should be approximately the same as the members in real. This implies bending resistance of equal magnitude in the two directions perpendicular to the member axis and similar torsion behaviour
- bending strength: model members need to be able to bend to the desired scaled curvature without breakage or plastic deformation

For a geometrical model it is less important to scale all the characteristics of the structure in a correct way, since there is no intention to measure deflection or forces.

The following materials have been used to build the model (Figure A.22):

- For the members a steel welding rod of 1mm diameter is selected. This material has adequate bending behaviour. The rods can bend without breakage, but care has to be taken for yielding. A simple bending test proved that the desired curvature can be reached without yielding, so no problems are to be expected. Downside of this material is that the circular cross section has equal bending stiffness in every direction in stead of just y and z direction. The difference between I_{yy} of a square cross section and I of a circular cross section of equal size is 5,5% (see Figure A.21). It is assumed that the bending behaviour of a square cross section with torsion capacity is approximated sufficiently by the bending behaviour of a circular cross section.
- A flexible node can be created by rubber bands. A simple double knot, firmly tightened, provides the desired flexibility of the mat of rods. The materials roughness provides enough resistance against slipping if tightened sufficiently.
- As a base, MDF of 12 mm thick is selected. This material provides a smooth and flat surface and is very suitable for pinning the structure down with nails or pins.
- Nails and pins, for pinning down the structure at the edges

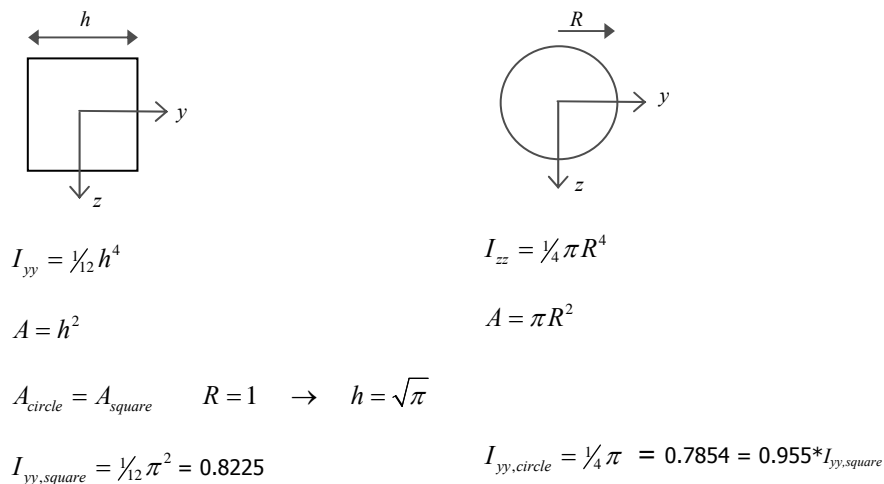


Figure A.21: difference in I_{yy} between a square and circular rod of equal cross section in size

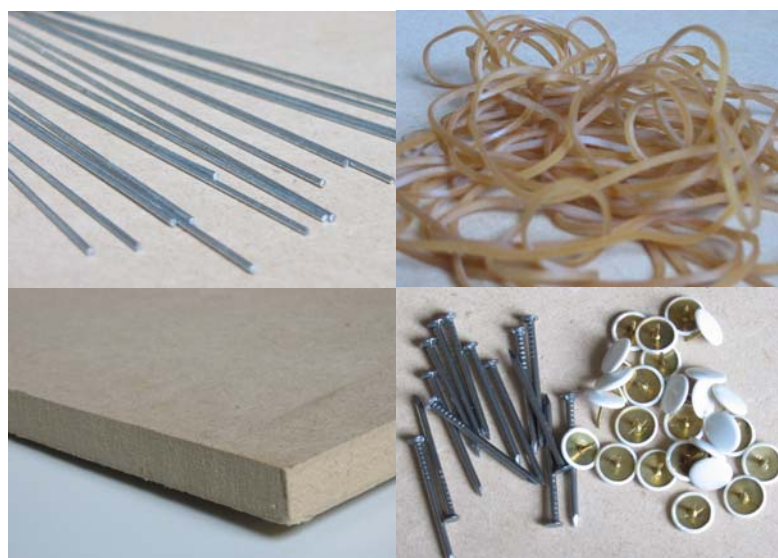


Figure A.22: Materials used for geometrical model

3. Formation process

In this section the formation process is illustrated in steps.

- A mat of steel rods is tied with rubber bands. The dimensions of the mat and lengths of the rods are determined by using a template print-out of the flat structure (Figure A.23). This template is created by using data generated by the generation script. Using the base coordinates which are in the output text file, the lengths and layout of the flat mat can be plotted. By placing the rods on the template print-out, the rods can be tied at the correct position and equal distance from each other (Figure A.25).
- The rods are cut to the correct length.
- The ends are bent into eyes for ease moving and positioning of the members.
- Rubber bands are tightened and cut short.
- The mat is placed on the MDF base and on a top view template (Figure A.24 and Figure A.25) of the structure in final position. By using the template, the end position of the member ends is determined. Also a visual check of the curve of the members can be performed after the formation process.
- Rods are placed through the end eyes, divided in sections of 10 to 20 cm. By doing this, not every node itself has to be moved and pinned (Figure A.26).
- On the long side, the mat is pinned at two points which are into place already (Figure A.26).
- The structure is tensioned by pinning down the edges on the short sides and then pushing inward from the free long edge (Figure A.27). A relatively large force is needed to create an initial curvature. This is due to the fact that the members have to buckle into shape.

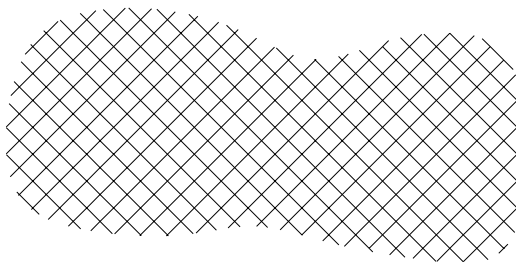


Figure A.23: Template of the flat mat

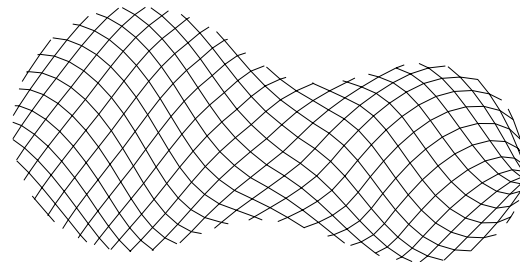


Figure A.24: Template of the deformed structure

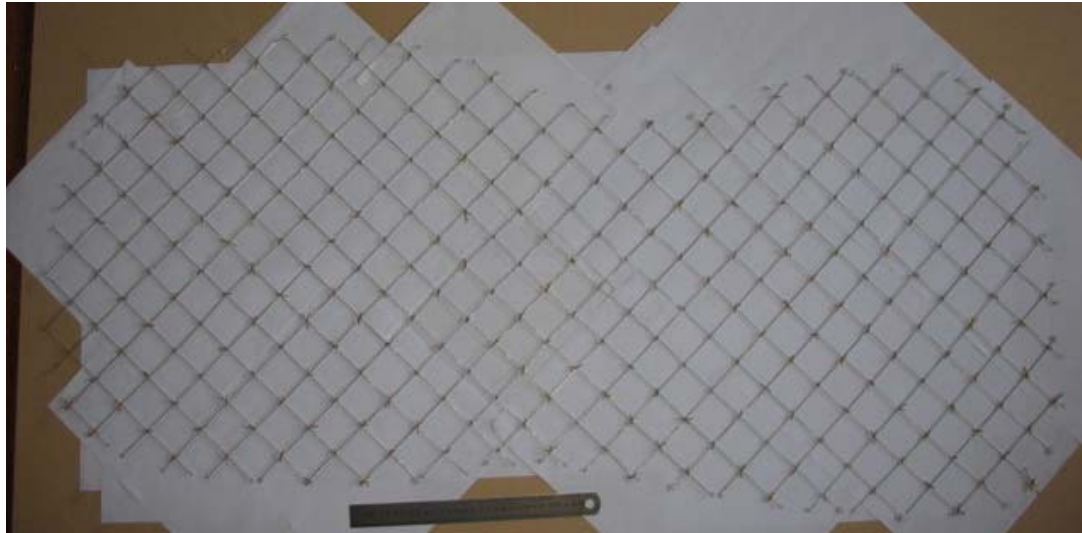


Figure A.25: Flat mat of rods is laid out on a template print-out

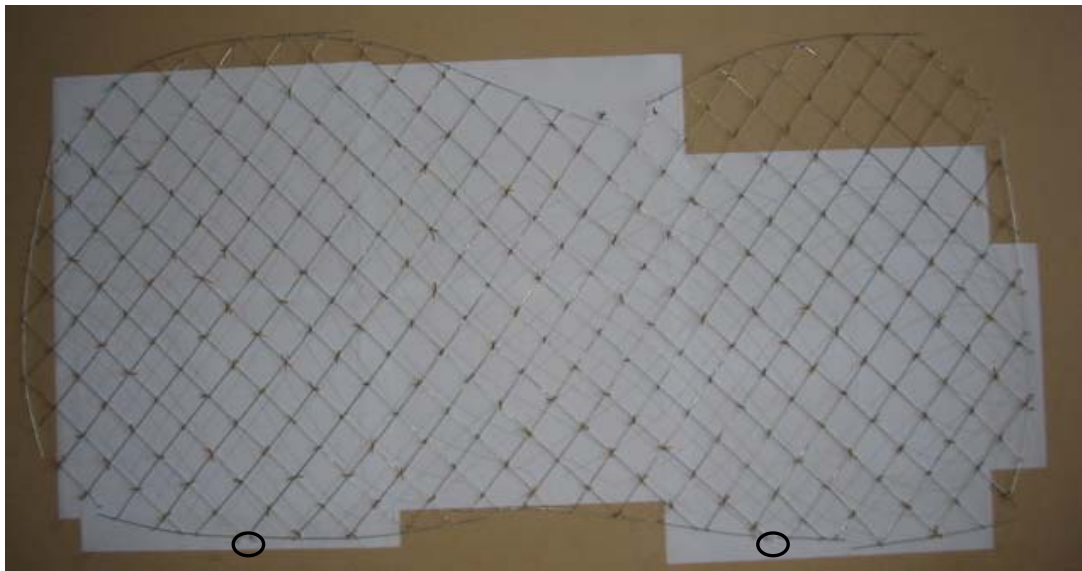


Figure A.26: Edge rods are added. The structure is pinned at two points which are already on their final location..



Figure A.27: The structure is tensioned by pushing on the long edge and preventing movement at the short edges.

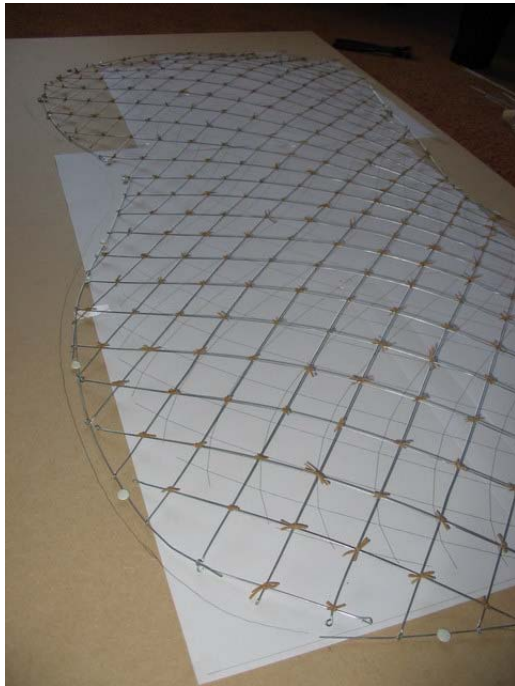


Figure A.28: A vaulted shape is formed.



Figure A.29: By pushing from the sides, domes are shaped.

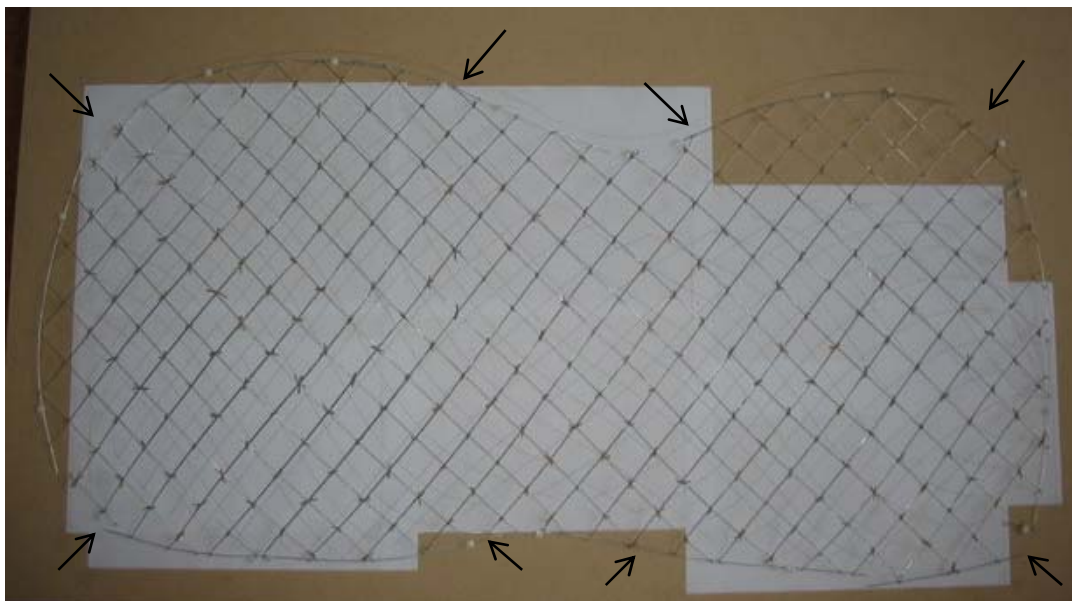


Figure A.30: Pushing from the sides to form domes

- The structure is further tensioned by pushing the long edge inward. A shallow vaulted shape is created (Figure A.28).
- The structure is now properly tensioned for the further forming process. First the domes are formed by pushing in diagonal direction (Figure A.29 and Figure A.30).
- By going in circles around the structure, pushing inward bit by bit, the curvature of the structure gets larger in a controlled manner (Figure A.31, Figure A.32 and Figure A.33). It is found that pushing inward perpendicular to the length axis of the structure is relatively easy. The formation of the domes requires larger force.
- On the edge which was pinned in the beginning, all the edge sections reach their final position quite soon in the formation process. The anti-clastic part can now begin to form properly (Figure A.31).
- An intermediate assessment shows that the left dome is almost finished in terms of position of the edges. The right dome needs to move inward further (Figure A.34). Also a larger curvature is needed going down to the edge supports (Figure A.36). The saddle between the two domes also needs a larger curvature and is already in too high position (Figure A.35 and Figure A.36).
- Slowly pushing the edges of the domes to their intended end position the curvature gets larger. The left dome reaches its final position without much trouble. For the right dome it takes quite a lot more force however to reach the desired curvature and to push the edges to their intended final position. The final shape is shown in Figure A.37 to Figure A.39.

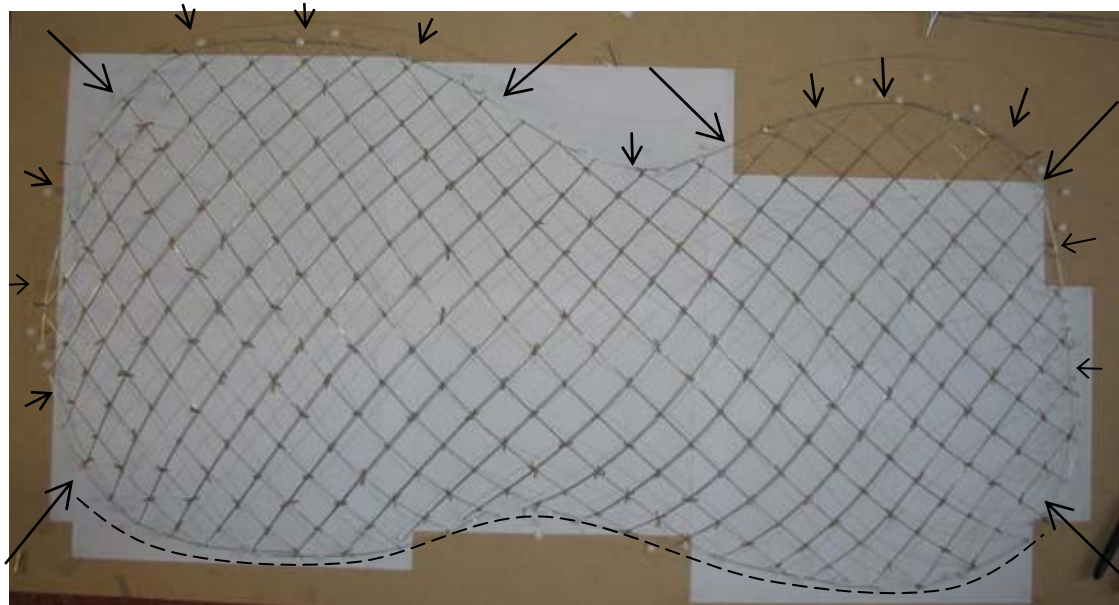


Figure A.31: Pushing the edges inward going around in circles shapes the structure. At one edge the final position is reached quite soon (dashed line). The curved S-shape of the members becomes visible.



Figure A.32: Domes and saddle are shaped

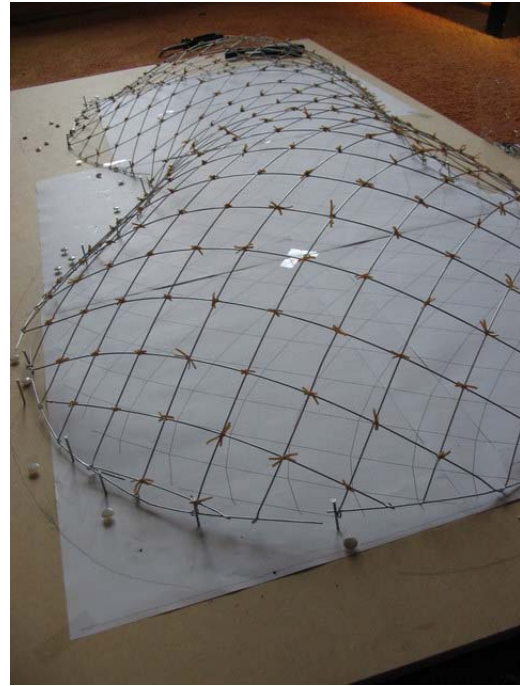


Figure A.33: Further shaping of the structure



Figure A.34: Shallow dome (left) formation is almost finished. The formation of the stronger curved dome (right) needs to move upward to reach the desired height.

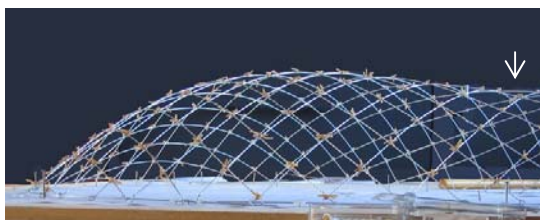


Figure A.35: Left dome approaches final shape, although the saddle is too high

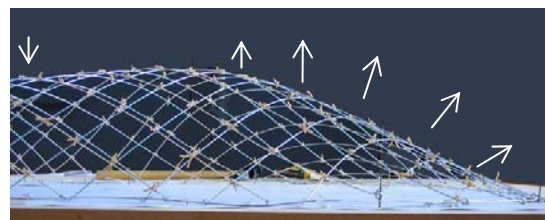


Figure A.36: Right dome must become higher and curved stronger. The saddle is already too high.

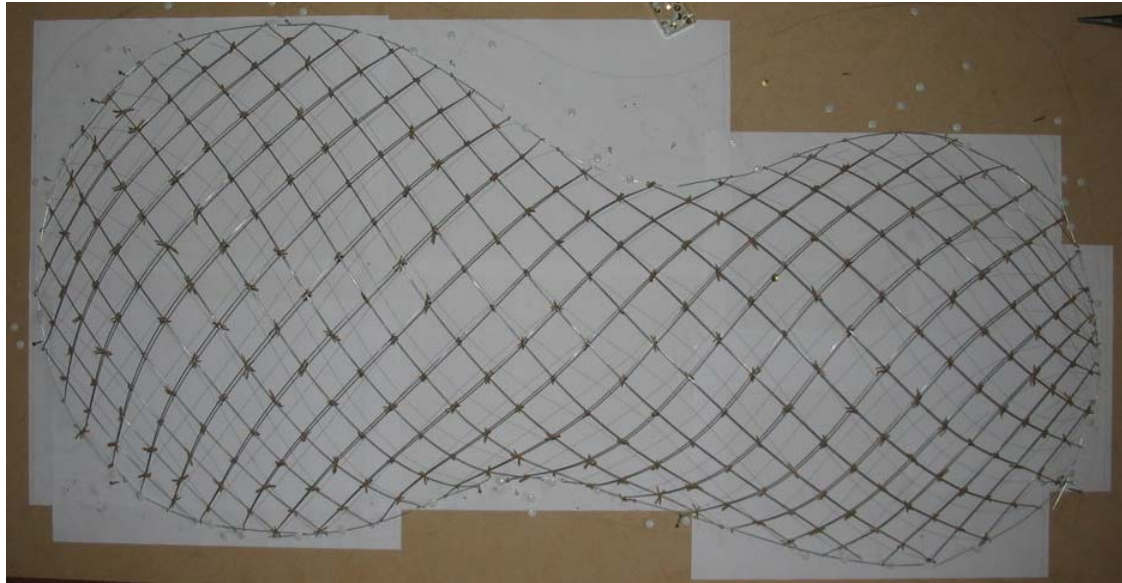


Figure A.37: After further pushing the edges inward, the edges reach final position.

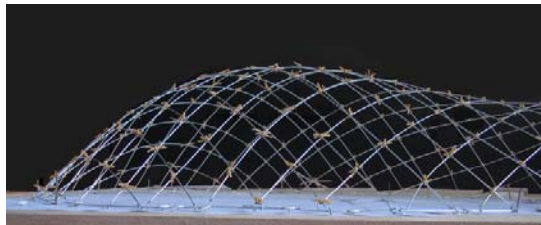


Figure A.38: Left dome with edges near final position

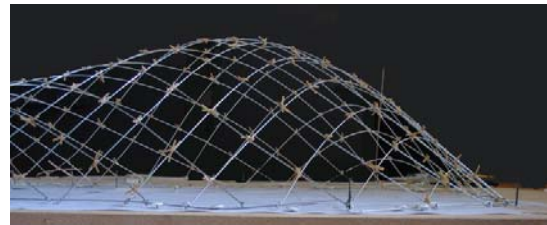


Figure A.39: Right dome with edges near final position

4. Observations

Shape

First, the computer model and the physical model are compared in terms of shape. The height and position of nodes in the physical model are measured at normative sections shown in Figure A.41. The height of the nodes' position is determined by using a plummet to determine the length of the plumb line. The horizontal location along the section line is measured by the distance of the base of the plumb line to the edge of the structure (Figure A.40). From these measurements and the coordinates of the corresponding nodes from the computer model, the sections shown in Figure A.41 are created. This shows that the physical model has too much height compared to the computer model. Section AA' over the shallow left dome shows that in this section the two models coincide quite well. The physical model is slightly higher and shows a more parabolic curve, whereas the computer model shows a circular arched cross section.

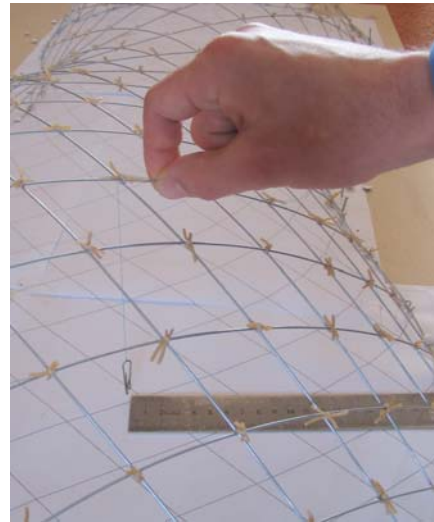


Figure A.40: Measuring the plummet line

Looking at section CC' a larger deviation is shown. The computer model shows a circular arched cross section of a smaller radius than cross section AA'. The physical model shows a parabolic shape again, but the deviation from the computer model is larger. It should also be noticed that there is also a horizontal deviation. The top of the parabola is situated more to the left than the top of the arc and the right side of parabola is more flattened than the left. This is also shown in the longitudinal section DD', where the right end side has a more flattened shape than the section of the computer model. Figure A.42 shows the difference between the two models.

As a result of the parabolic shape and larger height of the structure, also section BB' is higher than the computer model. Section BB' also shows a different shape. At the right side the section approaches the support with a larger curvature and touches down at the support with an almost vertical angle.

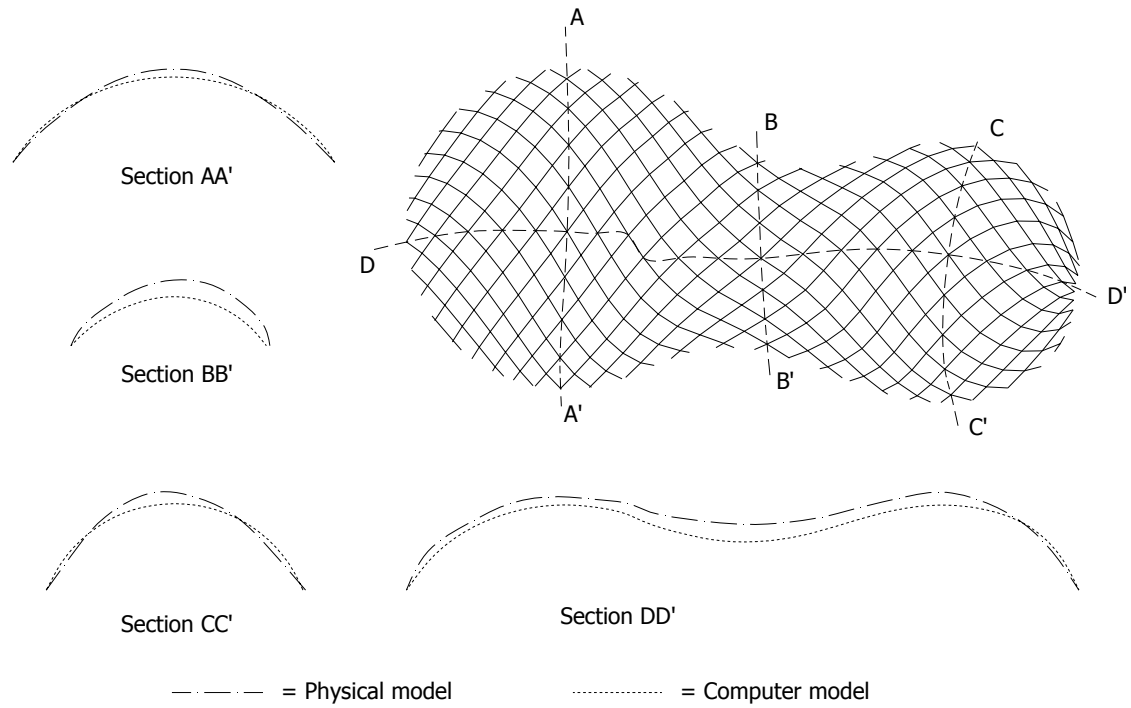


Figure A.41: Sections of the two models

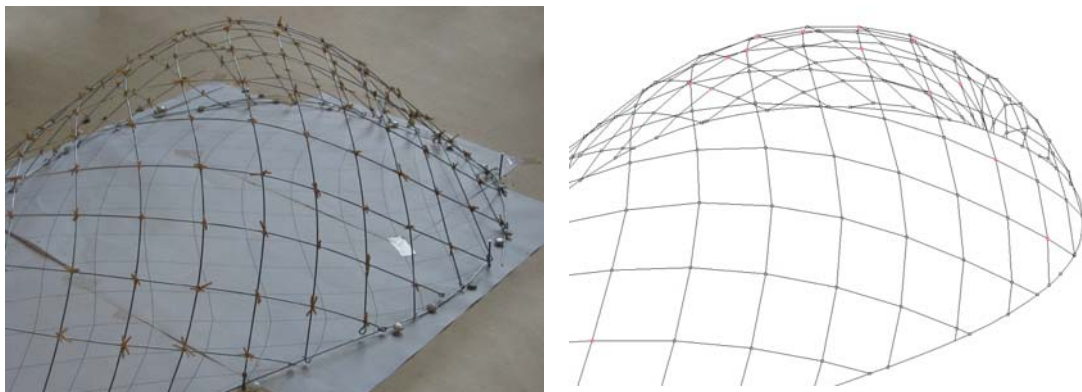


Figure A.42: Difference in curvature between the physical model and the computer model in the right dome.

Curvature

Second, the curvature of the individual members is reviewed. For the two domes different observations are made. First the shallow dome is reviewed (Figure A.43). The computer model of this part of the structure coincides with the physical model within acceptable accuracy, corresponding with the observations of the shape. Seen in top view, the members of the physical model have only a small deviation from the computer model. The moderate S shape of the members which is seen in the computer model also occurs in the physical model. Also the end points of the member coincide with their position in the computer model. Moving to the right of the structure, the deviation between the computer model (grey line) and the physical model (black line) becomes larger. This also corresponds with the shape observations, as the deviation in shape from the computer model was already found to differ more as we move to the right part of the structure. In these figures an inaccuracy must be taken into account, because of the difference between the perspective view of the photo and the isometric computer plot.

When the smaller dome is reviewed, a larger deviation is noticed (Figure A.44). This corresponds with the shape analysis of the models. Especially in the transition zone between anti-clastic and clastic shape, the members of the physical model show less curvature in horizontal direction than the members of the computer model. This relates especially for the members which run from top left to bottom right in Figure A.44. More to the right in the structure the curvature of the members in the model coincides better again.

This difference in curvature and also the difference in height and shape of the dome can be explained as follows. First, the member ends do not coincide with the support positions of the computer model. This is relates especially for the members ending in the top right of Figure A.44. As the length of the rods is bent with a smaller distance between the end nodes, the arcs become higher. Second, the cross section in the anti-clastic part has a much steeper angle with the base, as the computer model does (see Figure A.41). This has the effect that the nodes in the transition zone are shifted in horizontal direction.

What is also found in the grid generation using the curvature check, is the difficulties in the ends of the structure. According to the script, the members cannot meet with the curvature needed to create the semi-spherical shape. This is also shown in the deviations between the computer and the physical model. Especially in the smaller dome, the laths have difficulties bending and scissoring to the desired end position.

It is possible to approximate the shape of the computer model with a better fit. The physical model can be modified by moving the ends of the members closer to their desired end position by force (see Figure A.45). All nodes then shift to a position fitting better with the computer model. The force needed to pull the nodes into position results in a tension force which extends over the structure in diagonal direction. This is the encircled region in Figure A.45. This results in a lower shape and a member curvature corresponding better with the computer models height and shape. Especially in the anti-clastic zone, the structure is pulled down by the tension in the rods. However, by doing this the members are forced to a position which exceeds the maximum curvature.

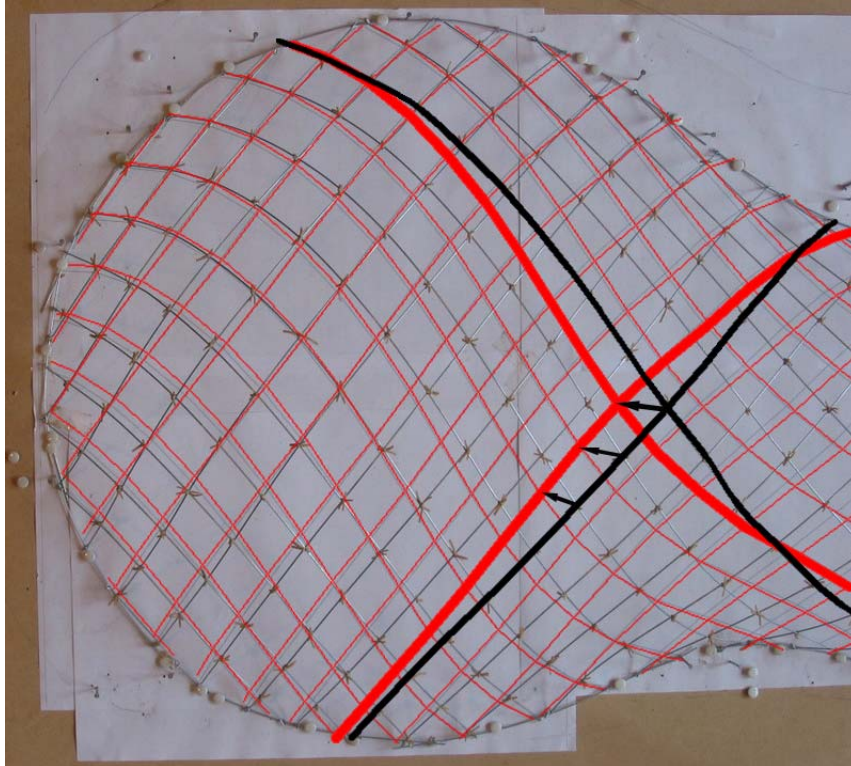


Figure A.43: Comparison of the left dome in the two models. The grey lines indicate the computer model

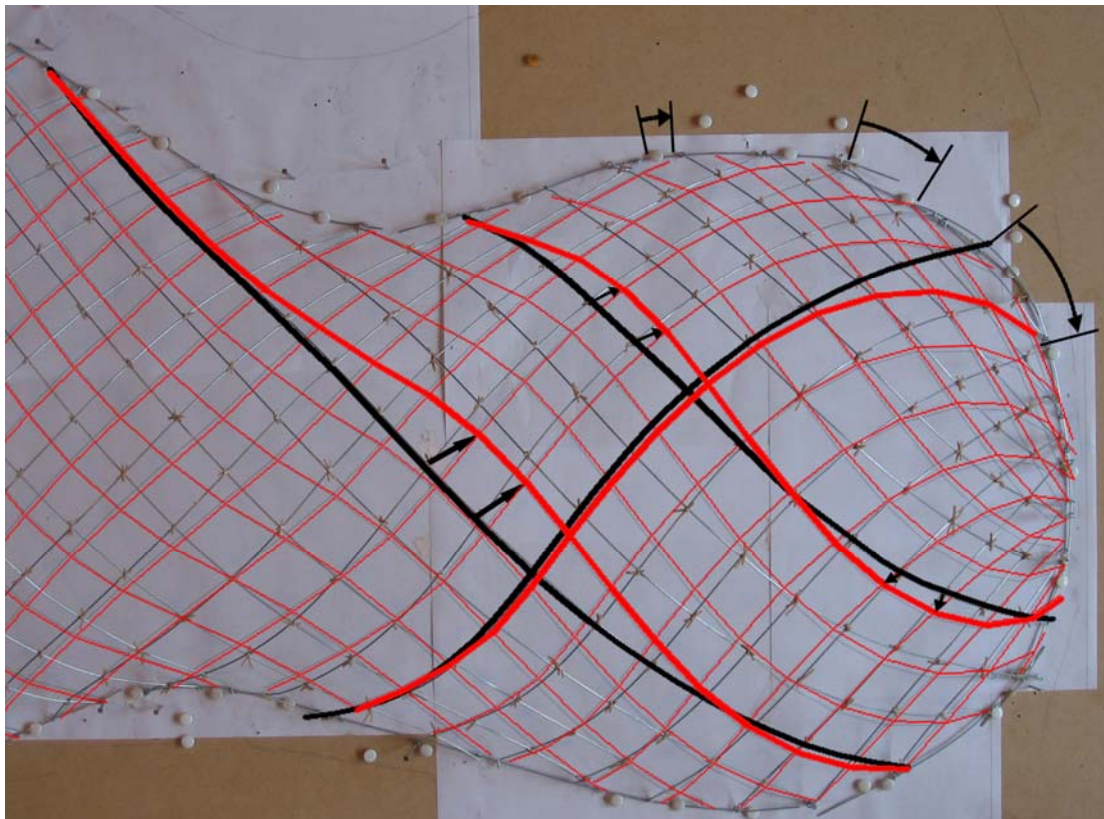


Figure A.44: Comparison of the right dome in the two models. Moving the members in the pointed directions (arrows in top right) will result in a better approximation of the computer model.

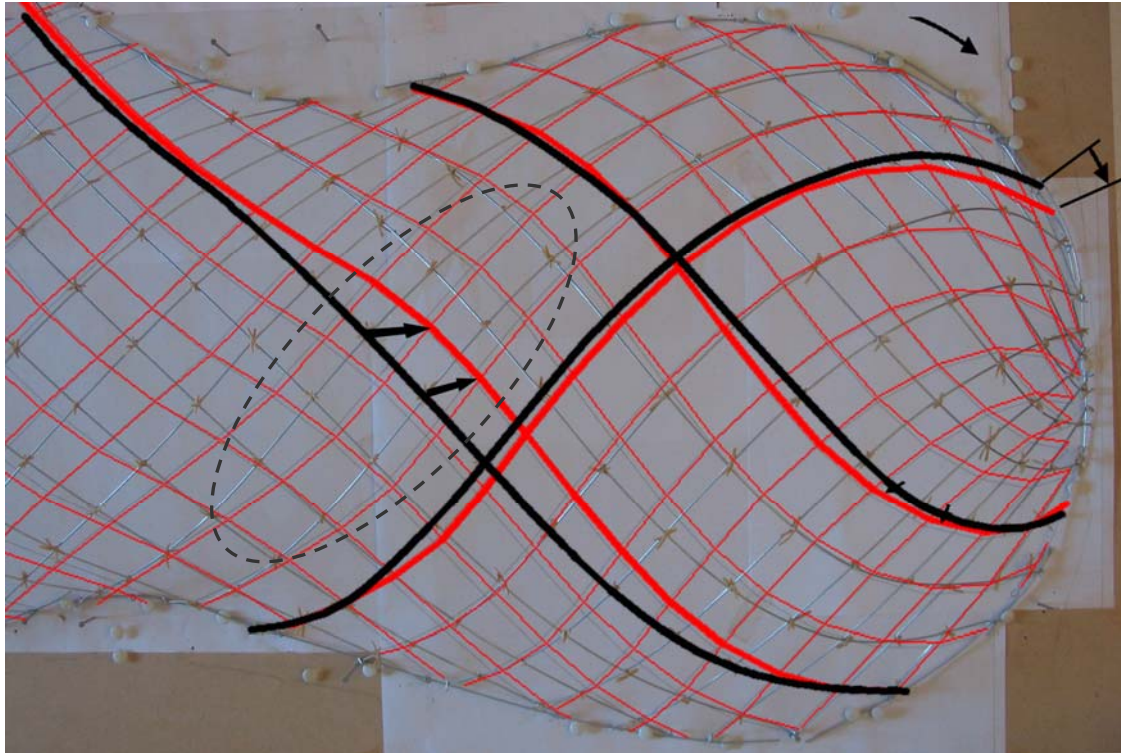


Figure A.45: Structure, with the nodes at top right side moved in the direction of the arrow. Tension exists in the encircled area.

5. Conclusions

The deviations found between the computer and physical model can be well explained. The cross sections deviate from circular arc to more parabolic shape. This shape is generally considered as a more natural shape to divert axial forces through an arched structure. Because of this tendency to parabolic shapes, the horizontal S-shape in the members is less prominent and as a result of this the physical model has larger height as intended.

Although the physical model deviates from the computer model, this does not mean that the computer script creates a grid which is incorrect. By moving the members ends to their computed position the shape and curvature of the computer model is approximated better. However to do this force is needed to pull the members in position and tension is created in the members which cross the anti-clastic part of the structure. This can be compared with the tensioning of the fabric of a hyperbolic tent structure.

The fact that the models deviate does show that the computer model does not represent a shape that is optimized in structural behaviour. The model should be of a more parabolic shape. As stated in the introduction of this chapter, building the physical model is a type of physical form finding. Therefore the results of the physical model can be used to modify the computer model to a more optimized shape. One could say this is a reversed form finding process. Instead of first creating a shape by form finding and then creating a structure, here the structure is created first by the grid generation script. The shape is then adjusted to a shape corresponding with the physical model. A new grid can then be generated on the adjusted, optimized shape for structural analysis.

With the grid generation tool it was found that bending curvatures become too large when the laths of the grid are bent to a (semi-)spherical surface. This problem is also found in the physical modelling process. It is therefore advisable to avoid such shapes or to take additional measures, such as applying members with a smaller cross section in the problematic area.

6. Conceptual model of the Eggoid

As stated in section 5.3 it is interesting to investigate the possibilities of an eggoid shaped gridshell. To do this a conceptual model is built. The materials used for this model are:

- For the grid members strips of VIVAK are cut. VIVAK is a plastic material which has a high bending capacity around its weak axis before failure. Therefore it is very suitable for testing different geometries. Downside is that the difference between bending capacity in different directions is large, due to the rectangular cross section.
- To create flexible nodes, binding wire is tied through holes in the VIVAK (Figure A.46). With a hot needle these holes are easily pierced in the strips.
- As a base a rigid cardboard box is used. An ellipse is cut out of the base, to act as an edge boundary template.
- Needles are used to pin down the structure.

Some interesting observations are made creating the model. First the bending behaviour of the grid is observed with respect to the direction of the members. The mat is supported in the middle and deflects under self weight. When the members intersect at a small angle, the stiffness of the mat is generally directed in one direction and the weight of the members is carried in that direction (Figure A.47). When the members are moved apart, the number of members per unit of surface becomes smaller in one direction and larger in the other direction. The stiffness of the structure is now divides itself between the two principle directions (Figure A.48). When the members are moved apart further, the stiffness in the first direction becomes too small and the structure snaps through its balance point (Figure A.49).

By doing this simple experiment, it is physically experienced what the influence of the direction of the member has on the structural behaviour of the mat. Obviously, there is an optimum in angle between the members. An angle too small makes the structure too stiff and all load transfer only takes place in one direction. An angle too large gives an inefficient structural behaviour. To use the structures in an optimal way the optimal direction should be estimated to fully use the bi-directional character of the structure.



Figure A.46: The grid is tied with binding wire

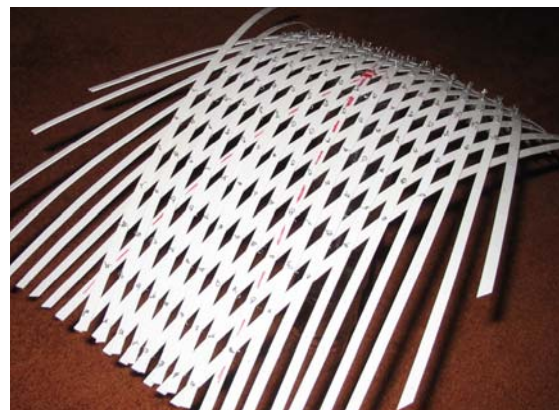


Figure A.47: Load carried in one direction

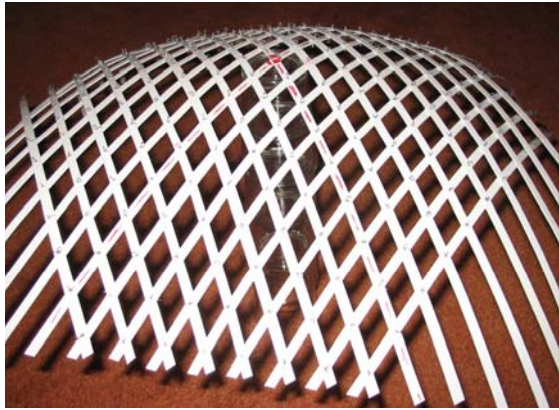


Figure A.48: Load carried in two directions at an angle close to the structures snap-through point

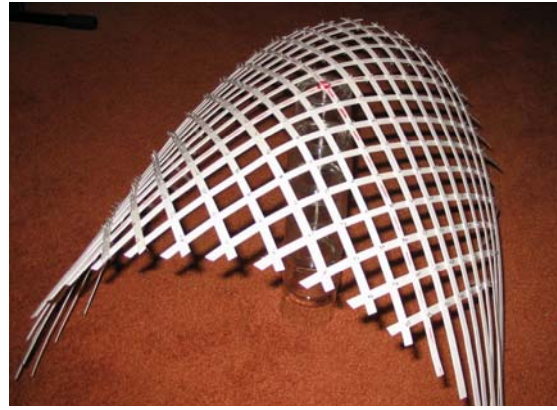


Figure A.49: The structure as snapped though its ultimate point of balance.

The experiences of previous experiment are used when creating the model. First the mat is orientated at an angle slightly orientated in one direction, at an angle of 60 degrees between the members. The mat is carefully pushed down in the boundary template. Soon the curvature becomes too large. The members cannot bend to the curvature needed and buckle inward (Figure A.51 and Figure A.52)

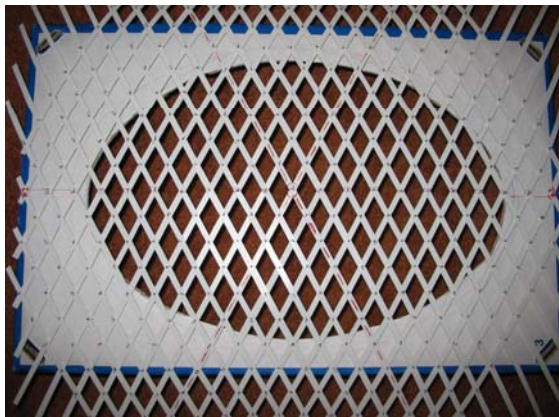


Figure A.50: Flat mat orientated with an angle of approximately. 60 degrees

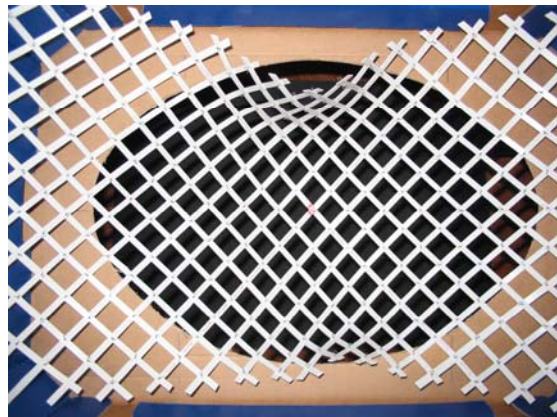


Figure A.51: The mat is pushed into shape, but buckles quite soon at the long edge.



Figure A.52: Edge buckling

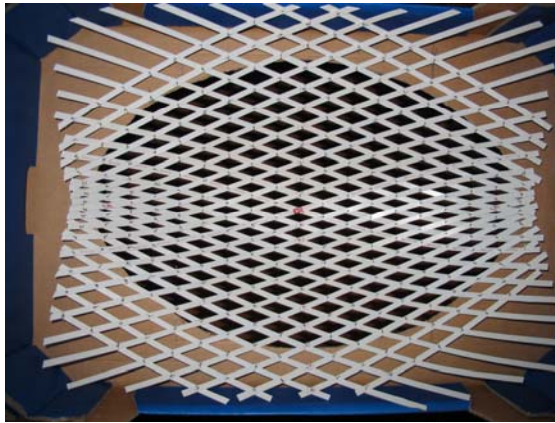


Figure A.53: Mat orientated at approximately 140 degrees.

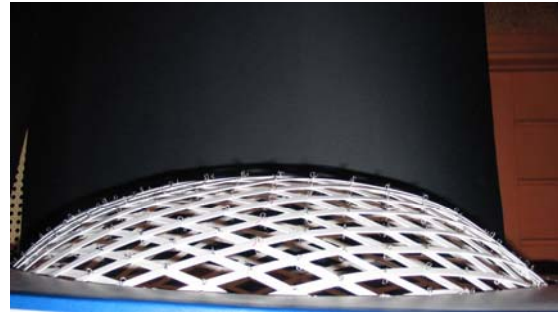


Figure A.54: curvature of the structure with a member orientation 140 degrees

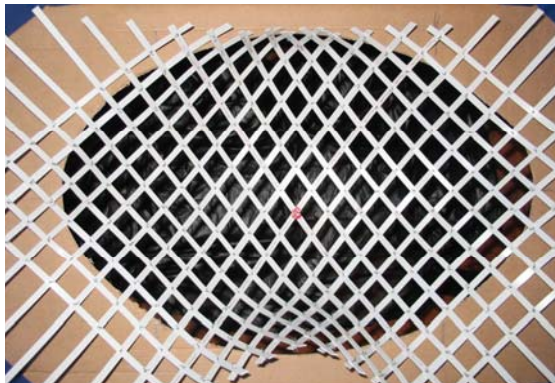


Figure A.55: Mat orientated at approximately 80 degrees

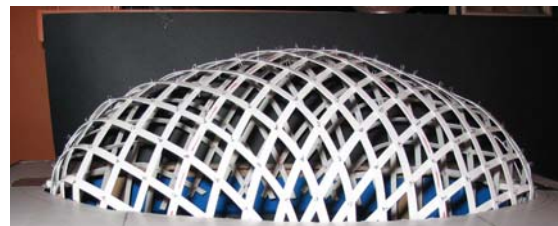


Figure A.56: A large curvature is possible, but at the narrow sides buckling occurs

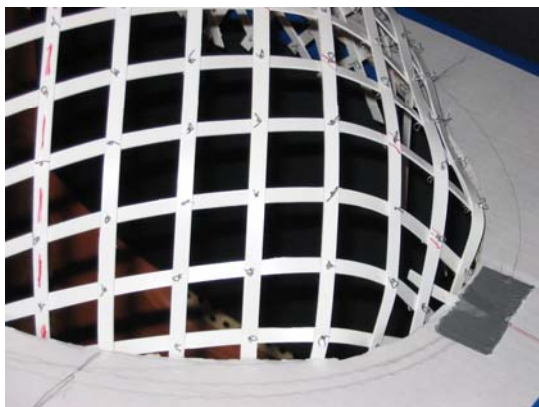


Figure A.57: Buckling of the structure at the small end.

When the mat is orientated mainly in the other direction (Figure A.53), the members come very close to each other at the narrow sides when the mat is pushed into shape. This effect is already seen in the free form shape in the small dome with large curvature, but here the effect becomes extreme. The curvature cannot be made very large before the mat starts buckling and resisting at these edges (Figure A.54).

At an orientation of approximately 80 degrees the mat lets itself being pushed into shape more easily and to a larger curvature (Figure A.55 and Figure A.56). However, again at the narrow sides of the ellipse the members start buckling. When the mat is being pushed further into the desired eggoid shape, the members are buckling and twisting (Figure A.57). This is due to the fact that the members cannot bend enough due to the relatively large bending stiffness in the stiff direction, in combination with a large curvature of the shape.

The structure is finished with an angle between the members of approximately 80 degrees and a moderate curvature (Figure A.58 and Figure A.59). This results in a smooth surface without buckling. To compare the model with a computer model a grid is generated on a similar eggoid shape (Figure A.60 and Figure A.61). This also shows the members scissoring to each other at the narrow ends. When the generated grid is trimmed at the same height as the physical model, the two models coincide.

The most important observation made while creating this model is the member behaviour with large curvatures. A large curvature forces the members to scissor to each other and to a large curvature of the individual members. If the bending and rotation capacity of the members is insufficient, the members will buckle and twist. It is therefore advisable to limit the curvature if possible.



Figure A.58: Final structure with moderate curvature

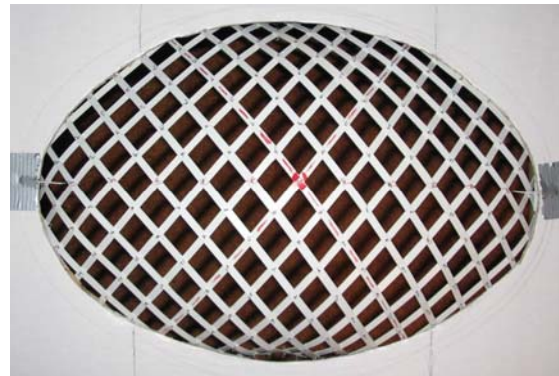


Figure A.59: Final structure with an angle of approximately 80 degrees

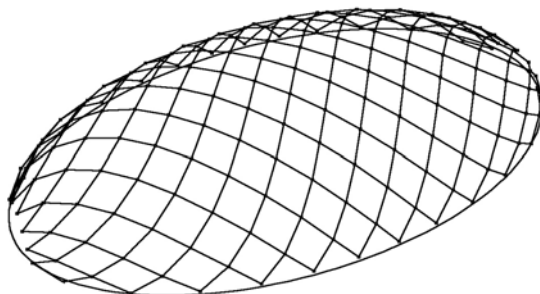


Figure A.60: Computer model of the eggoid (untrimmed). Scissoring is clearly visible.

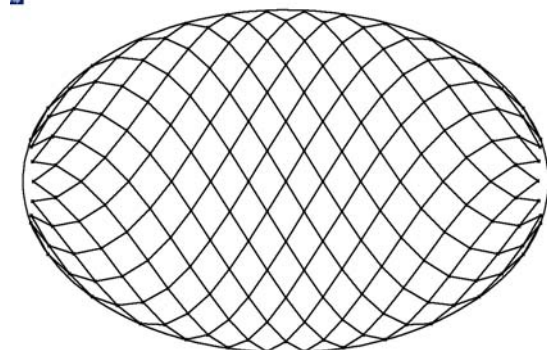


Figure A.61: top view of the computer model (untrimmed)

Appendix 6: Contact information

Contact information student:

Name: Matthijs Toussaint
Student no.: 9840294
Address: Vlierboomstraat 445, 2564JD DEN HAAG, The Netherlands
Phone: 06-14348691
E-mail: mhtoussaint@gmail.com

Contact information graduation committee:

Prof. Ir. L.A.G. Wagemans

Organisation: Delft University of Technology
Faculty: Civil Engineering and Geosciences
Section: Structural and Building Engineering
Address: Stevinweg 1, 2628 CN Delft
Room no.: ST II 1.59
Telephone: 015 - 27 84752
E-mail: L.A.G.Wagemans@TUDelft.nl

Ir. J.L. Coenders

Organisation: Delft University of Technology
Faculty: Civil Engineering and Geosciences
Section: Structural and Building Engineering
Address: Stevinweg 1, 2628 CN Delft
Room no.: ST II 1.58
Telephone: 015 - 27 85711
E-mail: J.L.Coenders@TUDelft.nl

Dr.ir. P.C.J. Hoogenboom

Organisation: Delft University of Technology
Faculty: Civil Engineering and Geosciences
Section: Structural Mechanics
Address: Stevinweg 1, 2628 CN Delft
Room no.: OG 6.48
Telephone: 015-2788081
E-mail: P.C.J.Hoogenboom@TUDelft.nl

Dr.ir. J.W.G. van de Kuilen

Organisation: Delft University of Technology
Faculty: Civil Engineering and Geosciences
Section: Structural and Building Engineering
Address: Stevinweg 1, 2628 CN Delft
Room no.: ST II 2.56
Telephone: 015-2782322
E-mail: J.W.G.vandeKuilen@TUDelft.nl